HIGH REPETITION RATE CONTINUOUSLY TUNABLE CO_2 LASER SYSTEM INVESTIGATION.

by

LOURENS RASMUS BOTHA

Submitted in partial fulfilment of the requirements

for the degree of Doctor of Philosophy

in the

Department of Physics, University of Natal.

Durban

December 1990

PREFACE

The work described in this thesis was carried out at the Atomic Energy Corporation of South Africa in Pretoria as well as at the Department of Physics, University of Natal in Durban, from March 1989 to August 1990 under the supervision of Prof M M Michaelis.

These studies represent original work by this author and have not been submitted in any form to another University. Where use was made of the work of others it has been duly acknowledged in the text.

ACKNOWLEDGMENTS

I would like to extend my sincere thanks to the following people, who contributed in no small measure to this thesis in one way or another.

M M Michaelis

my supervisor for his guidance and encouragement.

R N Campbell

for his enthusiastic support and practical suggestions.

E R Ronander

for his support and encouragement.

My wife Erna

for her support, tolerance and encouragement.

H J du Toit

my technical assistant,without whom this would not have been possible.

My parents

for their support through all these years.

My colleagues at the AEC,

for stimulating discussions and a pleasant working environment.

Finally I would like to thank the Atomic Energy Corporation for the opportunity to use their facilities for a part of this thesis.

soli DEO gloria

ABSTRACT

The purpose of this thesis was to investigate certain factors important for the operation of a high repetition rate continuously tunable CO_2 laser. The tuning range of specific importance for this research program was the R30 region within the ten micron band, since this frequency is of great importance for the laser isotope separation of uranium. This research program focused on:

(i)Lowering the pressure at which viable continuous tunability could be achieved.

(ii)Resonator design and analysis.

(iii)Investigating the feasibility of using water capacitors in a high repetition rate laser system.

A theoretical as well as an experimental investigation was done into the use of CO_2 isotopes to lower the pressure at which continuous tunability in the R30, ten micron band could be achieved.

A theoretical analysis was done into the use of a three mirror resonator with an etalon and a grating to ensure single longitudinal mode tuning in the R30 region. Such a resonator was designed and experimental results obtained were compared

with those predicted by the theoretical analysis.

A study was done into the use of water as a dielectric medium in a high repetition rate pulse power supply. A mathematical model, describing the electric breakdown of water,was developed. This was compared with published experimental results. Certain parameters important for the design of a water capacitor were experimentally measured. These include the intrinsic time constant,dielectric constant and resistivity of the water. A design proposal as well as a comparison between a water capacitor and other capacitor technologies are presented.

TABLE OF CONTENTS

CHAPTER 1.

INTRODUCTION.

1.1 SCOPE AND PURPOSE OF THIS THESIS.

The purpose of this thesis was to investigate certain factors important for the operation of a high repetition rate continuously tunable single longitudinal mode CO_2 laser. The tuning range of specific importance for this research program is the R30 region within the 10 μm band since this frequency is of great importance for the laser isotope separation of uranium.The major problems identified in operating such laser systems are the following:

(i) High pressure, which implies the use of high voltage.

(ii) Switch operation and lifetime.

(iii) Capacitor lifetime.

(iv) Resonator design.

(v) Power supply.

This research program focused on:

(i) Lowering the pressure at which viable continuous tunability could be achieved.

(ii)Resonator design and analysis.

(iii) Investigating the feasibility of using water capacitors in a high repetition rate laser system.

1.2 GENERAL BACKGROUND.

1.2.1 MIXED ISOTOPE CO_2 LASERS.

Continuous tunability of a CO_2 laser can be achieved by utilizing the pressure broadening of the CO_2 lines. For a single isotope CO_2 laser, continuous tunability in the R28 to R32 region requires pressures of typically greater than 10 atmospheres. Such continuously tunable high pressure systems have been widely reported in the literature [1..9]. There are a number of technical problems associated with high pressure CO_2 laser system design and operation; the most obvious of these are:

(i) The design and manufacturing of the pressure vessel.

(ii) The difficulty of obtaining a stable discharge.

(iii) The high voltage requirements(typically 10 kV/cm.atm [10]).

(iv) Pumping the high pressure gas.

The energy and power requirements of high pressure systems are

generally considerably larger than that required for low pressure systems. The pump power requirement is directly proportional to the operating pressure.Thus it would be easier as well as cheaper to operate at a low pressure. The problem is to generate acceptable continuous tunability at these reduced pressures (since the pressure broadening is much less). A solution could be to use CO_2 isotope mixtures as the lasing medium. Gibson,Boyer and Javan [11] investigated an isotopic mixture of $^{12}C^{16}O_2$, $^{12}C^{18}O_2$, $^{12}C^{16}O^{18}O$ and reported continuous tunability at pressures of a half to a quarter of that of a single isotope CO_2 laser. The advantage of using an asymmetric isotope like $^{12}C^{16}O^{18}O$ is that it possesses both odd and even rotational transitions, thus doubling the number of lines available. A theoretical investigation into such a system was reported by Shimada et al. [12] and they predicted that continuous tunability of an isotopic mixture of CO_2 could be achieved at 4 atm. They reported no experimental results. In this research program we were particularly interested in the minimum pressure at which continuous tuning in the R28– R32 region could be achieved.

1.2.2 RESONATOR DESIGN.

Considerable work has been done on resonators to provide single longitudinal mode continuous tunability of high pressure CO_2 lasers [13–20]. Such a resonator must provide tunability over a

broad range; a narrow band width; frequency stability and protection of sensitive optical elements such as the grating and the etalon. Such a resonator was designed and tested. A thermal analysis as well as a mode discrimination analysis of this resonator, concentrating on the R30 10μm line, were also done. Using this analysis the maximum expected R30 pulse energies were calculated by solving the CO_2 laser rate equations. These calculated values were compared with the experimentally measured values.

1.2.3 WATER CAPACITORS.

The feasibility of using a water capacitor in a high repetition rate laser system has been investigated. Water has often been used as a dielectric medium in transmission line type pulsers, where the water pulse forming line is used as an intermediate energy storage element as well as a pulse forming element [21–26]. The use of water capacitors in a high repetition laser pulse power supply is not that common. Cirkel et al. [27] reported a 40 Hz excimer laser using water capacitors with a solid state pulse charging circuit and a multi–channel pseudo–spark switch. No literature on the use of water in high repetition rate systems was found. The breakdown of water under microsecond charging times was investigated and a theoretical breakdown model is presented.

1.3 STRUCTURE OF THIS THESIS.

This thesis is divided into three main parts:

(i) The investigation of a mixed isotope CO_2 laser .

(ii) The resonator design and analysis.

(iii) The investigation into the feasibility of using water capacitors in a high repetition rate laser system.

Chapter two contains basic CO_2 laser theory as well as the theoretically calculated gain curves for mixed isotope lasing media. Chapter three contains the design of a three atmosphere CO_2 laser using a C–C transfer circuit and a surface discharge UV pre–ionization scheme. Also included in this chapter are the experimental results obtained with this laser and isotopic mixtures.The resonator design and analysis are presented in chapter four and the experimental results obtained with this resonator, mounted on a commercial high pressure CO_2 laser, in chapter five.The water capacitor investigation is presented in chapter six and seven and a conclusion in chapter eight.

CHAPTER 2

BASIC LASER THEORY APPLIED TO A CO_2 LASER.

2.1 THE STRUCTURE OF LASER THEORY.

Lasers are devices that generate or amplify light. "Light" must be understood broadly since lasers with wavelengths ranging from the infrared to the X–ray are available. The essential elements of a laser are :

(i) A laser medium.
(ii) A pumping process to excite the medium.
(iii) A suitable optical feedback system.

Laser light is generated by stimulated emission. Stimulated and spontaneous emission of light are typical quantum mechanical processes. A proper laser theory must thus be a quantum mechanical theory. Realistic quantum mechanical laser theories are in general quite complicated. A number of features of laser behaviour can be understood by simpler theories. It all depends on the questions one wants answered. If the question is : "Under what conditions does laser action occur and what is the intensity of the laser light ? ", then a simple rate equation model is sufficient. If the actual frequency of the light is required or if processes such as phase locking and ultra short

pulses are investigated then a semiclassical approach is required. If phenomena such as coherence and linewidth intensity fluctuations are investigated a complete quantum mechanical theory is required. A review of the three theories is given by Haken [28]. In this thesis a summary of the semiclassical theory is given.

2.2 SEMICLASSICAL LASER THEORY.

2.2.1 INTERACTION OF RADIATION AND ATOMIC/MOLECULAR SYSTEMS: THE FIELD EQUATIONS.

In semiclassical laser theory the radiation is treated classically and the atomic/molecular system is treated quantum mechanically. The radiation is thus governed by the four Maxwell equations as can be found in any text book on electrodynamics . The Maxwell equations in rationalized MKSA units are given by:

$$\overline{\nabla}.\overline{D}=\rho \qquad 2.1$$

$$\overline{\nabla}.\overline{B}=0 \qquad 2.2$$

$$\overline{\nabla}x\overline{H}=\overline{J}+\frac{\partial\overline{D}}{\partial t} \qquad 2.3$$

$$\overline{\nabla}x\overline{E}=-\frac{\partial\overline{B}}{\partial t} \qquad 2.4$$

It is assumed that the material is homogeneous, non–magnetic, non–conducting and that there are no free charges. The displacement vector $\overline{D}$ can be written as :

$$\overline{D} = \epsilon_0\overline{E} + \overline{P} \qquad 2.5$$

$\overline{P}$ is the polarization which can be divided into its linear (L) and non–linear (NL) components. ϵ_0 is the permittivity of free space.

$$\overline{P} = \overline{P}_L + \overline{P}_{NL}$$

Take the curl of equation (2.4) and use the vector identity $\overline{\nabla}x\overline{\nabla}x\overline{A} = \overline{\nabla}(\overline{\nabla}.\overline{A})-\nabla^2\overline{A}$. Then the following equation is obtained:

$$\nabla^2\overline{E} - \mu_0\epsilon \frac{\partial^2\overline{E}}{\partial t^2} = \mu_0 \frac{\partial^2\overline{P}_{NL}}{\partial t^2} \qquad 2.6$$

ϵ is the linear medium permittivity and μ_0 is the permeability of free space. Equation (2.6) is the nonlinear wave equation . It shows how an electric field evolves in the presence of a nonlinear polarization. In the absence of a nonlinear polarization, the right–hand side is zero, and this wave equation reduces to the standard linear wave equation, in which many waves simultaneously present in an unbounded material, pass through each other without any mutual influence and without generating any new waves. Coupling between waves can only come about through an interaction that creates a nonlinear polarization.

For notational simplicity all electric fields and polarizations are assumed to be plane polarized. This allows the vector notation to be dropped.The field dependant polarization of the material

can be re–written in terms of the field–dependant susceptibility χ of a material.

$$P(E)=E\chi(E)=\chi^{(1)}E+\chi^{(2)}E^2+\chi^{(3)}E^3 + \ldots \qquad 2.7$$

The χ's are in general complex terms. The $\chi^{(1)}$ term corresponds to linear optical properties including index of refraction, absorption, gain , and birefringence. The $\chi^{(2)}$ term corresponds to second order non–linear effects which , in general, can be called three wave mixing. These effects are for example, second–harmonic generation, parametric mixing and the Pockels effect. The $\chi^{(3)}$ term corresponds to third order non–linear effects such as stimulated Raman and Brillouin scattering and optical phase conjugation. When interaction of radiation and the lasing medium is investigated the parameter of interest is the gain of the medium; thus the $\chi^{(1)}$ term. In semiclassical laser theory this $\chi^{(1)}$ term is calculated quantum mechanically and this will be done in the next section. In most lasers the gain medium is a small portion of the atoms or molecules present. These host materials, in the absence of the laser atoms/molecules, are transparent dielectric materials that are nearly lossless at laser wavelengths, but have a relative dielectric constant ϵ that is usually greater than unity.These materials will therefore possess a large non–resonant linear electric polarization P_{host}. The displacement vector could thus be written as :

$$D = \epsilon_0 E + P_{host}+P_{trans} \qquad 2.8$$

In this equation P_{host} refers to the large, broadband, linear nonresonant polarization associated with the host material ; whereas P_{trans} refers to the narrowband, linear resonant polarization produced by the atomic/molecular transitions. In general P_{host} is much larger than P_{trans}. P_{host} can be written as :

$$P_{host}=\chi^{(1)}_{host}\epsilon_0 E \qquad 2.9$$

Using this equation the displacement vector can be written as :

$$D=\epsilon_0[1+\chi^{(1)}_{host}]E+\chi^{(1)}_{trans}\epsilon_0 E \qquad 2.10$$

Using the usual definition for the relative dielectric constant (see Jackson [29]) this can be written as :

$$D=\epsilon E+\epsilon_0\chi^{(1)}_{trans}E=\epsilon[1+\frac{\epsilon_0}{\epsilon}\chi^{(1)}_{trans}]E=\epsilon'(\omega)E \qquad 2.11$$

With:

$$\epsilon'=\epsilon[1+\frac{\epsilon_0}{\epsilon}\chi^{(1)}_{trans}] \qquad 2.12$$

The susceptibility χ_{trans} is the susceptibility of interest for laser action.The subscript "trans" will be dropped from this stage onwards.As will be shown in the next section the susceptibility

$\chi^{(1)}$ is frequency dependant. The significance of $\chi^{(1)}(\nu)$ can be understood in the following manner: Consider a plane electro–magnetic wave propagating through a medium with a susceptibility $\chi^{(1)}(\nu)$. The plane wave can be written in the following manner [30]:

$$E(z,t)=Re[Ee^{i(\omega t-k'z)}] \qquad 2.13$$

where:

$$k'=\omega\sqrt{\mu\epsilon}'=\omega\sqrt{\mu\epsilon}[1+\frac{\epsilon_0}{\epsilon}\chi^{(1)}(\nu)]^{1/2} \qquad 2.14$$

ω is the radial frequency of the EM wave and μ is the permeability of free space.Since χ' is generally much smaller than one, k' can be expanded in a Taylor series and can be approximated as :

$$k'=k(1+\frac{\epsilon_0}{2\epsilon}\chi^{(1)}) \qquad 2.15$$

With:

$$k = \omega\sqrt{\mu\epsilon}$$

Since the susceptibility $\chi^{(1)}(\nu)$ is complex, as will be shown later , it can be written as :

$$\chi^{(1)}(\nu)=\chi^{'(1)}(\nu)+i\chi^{''(1)} \qquad 2.16$$

Thus the wave vector k' can be written as :

$$k'=k[1+\frac{\chi'(\nu)}{2n^2}]-ik\frac{\chi''(\nu)}{2n^2} \qquad 2.17$$

Where $n = (\epsilon/\epsilon_0)^{1/2}$ is the index of refraction of the medium far from resonance. Thus the wave propagates according to :

$$E(z,t)=Re[Ee^{i\omega t-i(k+\Delta k)z+(\gamma/2)z}] \qquad 2.18$$

Thus the result of the atomic/molecular polarization is to change the phase delay per unit length from k to $k+\Delta k$ where:

$$\Delta k=\frac{k\chi'(\nu)}{2n^2} \qquad 2.19$$

A further consequence of the polarization is to cause the amplitude to vary exponentially with distance according to $e^{(\gamma/2)z}$ where:

$$\gamma(\nu)=-\frac{k\chi''(\nu)}{n^2} \qquad 2.20$$

$\gamma(\nu)$ is the so–called small signal gain and was first derived by

Einstein [31] in 1917 using transition rates.This can be written as [30]:

$$\gamma(\nu)=\frac{(N_2 - (g_2/g_1)N_1)\lambda^2}{t_{spont}\,8\pi n^2}g(\nu) \qquad 2.21$$

With:

N_2 : population of the upper laser level.

N_1 : population of lower laser level.

g_1 : degeneracy of lower laser level.

g_2 : degeneracy of upper laser level.

λ : wavelength of electromagnetic radiation.

$g(\nu)$: Lorenzian lineshape function given by:

$$g(\nu) = \frac{(\Delta\nu/2\pi)}{(\nu-\nu_0)^2-(\Delta\nu/2)^2} \qquad 2.22$$

t_{spont} : spontaneous emission lifetime of the atomic or molecular transition.

n : index of refraction.

Einstein derived these equations using classical arguments where he assumed induced transition rates proportional to the energy density per unit frequency. These proportionality constants are the so–called Einstein A and B constants.

2.2.2 QUANTUM MECHANICAL ENSEMBLE THEORY : THE DENSITY MATRIX.

In treating quantum mechanical systems it is necessary to deal with two types of uncertainty. The first type of uncertainty is due to the probabilistic interpretation of the wave function $\Psi(\overline{r},t)$ and is manifested in the Heisenberg uncertainty principle. The second type of uncertainty occurs because of the statistical nature of the system due to the large amount of molecules/atoms present.

Consider an ensemble of N identical systems where N >> 1. These systems are characterized by a common Hamiltonian, which may be denoted by an operator H, the physical states of the various systems will be characterized by the wave function $\Psi(\overline{r}_i,t)$ where $\overline{r}_i$ denotes the position coordinates relevant to the systems under study.Let $\Psi^k(\overline{r}_i,t)$ denote the normalized wave function characterizing the physical state in which the k th system of the ensemble happens to be at time t with k=1,2,..N. The time variation of the function Ψ^k will be determined by the Schrodinger equation:

$$H\Psi^k(t)=ih\dot{\Psi}^k(t) \qquad 2.23$$

Introducing a complete set of orthonormal functions u_k the wave function may be written as [32]:

$$\Psi^k(t)=\Sigma_n c_n^k(t)u_k \qquad 2.24$$

Where

$$c_n^k(t)=\int u_n^* \Psi^k(t)d\tau \qquad 2.25$$

The physical significance of the coefficients c_n^k is evident from equation (2.24). They are the probability amplitudes for the k th system of the ensemble to be in the respective states u_k. The number $|c_n^k(t)|$ represents the probability that a measurement at time t finds the k th system of the ensemble to be in the particular state u_k. The density operator $\rho(t)$ can now be introduced as defined by the matrix elements [32]:

$$\rho_{mn}(t)=\frac{1}{N}\sum_{k=1}^{N} c_m^k(t)c_n^{k^*}(t) \qquad 2.26$$

The matrix elements $\rho_{mn}(t)$ are the ensemble average of the quantity $c_m(t)c_n^*(t)$. In particular the diagonal elements $\rho_{nn}(t)$ is the ensemble average of the probability $|c_n(t)^2|$. The quantity $\rho_{nn}(t)$ now represents the probability that a system, chosen at random from the ensemble at time t, is found to be in state u_n.A matrix will be denoted with bold letters.The equation of motion for the density matrix is given by :

$$i\hbar\dot{\rho}=[H,\rho] \qquad 2.27$$

Finally the expectation value of a physical quantity A which is represented by an operator A is given by[32]:

$$\langle A\rangle=\mathrm{Trace}(\rho A) \qquad 2.28$$

2.2.3 INTERACTION OF RADIATION AND ATOMIC/MOLECULAR SYSTEMS: THE MATERIAL EQUATIONS.

Most atoms/molecules respond to the electric field of an applied electro–magnetic signal rather than the magnetic field. The strongest atomic/molecular transitions , and those most important for laser action, are usually of the type known as electric dipole transitions.There do exist other types of atomic transitions including some laser transitions, that are classified as magnetic dipole, electric quadropole or even higher order [33]. For this derivation an electric dipole transition has been assumed. A further assumption is made that only two levels with energies E_1 and E_2 are involved in the interaction. This assumption can be made if the frequency of the field satisfies the relation:

$$\omega=(E_2-E_1)/h \qquad 2.29$$

Since the system can now take on only two eigenvalues E_1 and E_2 the density matrix ρ now reduces to a 2x2 matrix. Since electric dipole transitions are considered the interaction Hamiltonian can be written as :

$$H'(t)=-\mu_d E(t) \qquad 2.30$$

Where μ_d is the component of the dipole operator in the

direction of the field E(t). Since this is the semiclassical approach the field will be considered as a classical variable. Since the time dependence of the diagonal elements of the ensemble averages μ_{d11} and μ_{d22} (see equation (2.26)) cancel out, these diagonal elements represent the ensemble average of the permanent dipole moments[35] . For this derivation it has been assumed that the atoms/molecules have no permanent dipole moment, thus the diagonal elements of the matrix μ_d vanishes.

$$\mu_{d11}=\mu_{d22}=0 \qquad 2.31$$

The off diagonal elements correspond to the transitions from state 1 to 2. Thus according to equation (2.26) the transition probability is proportional to the square of the time–dependant off diagonal elements[34] . It was assumed that the transition probability from level 1 to 2 is the same as that from level 2 to 1, thus:

$$\mu_{d21}=\mu_{d12}=\mu_d \qquad 2.32$$

The total Hamiltonian of the system is given by:

$$\mathbf{H_{total}}=\mathbf{H}+\mathbf{H}' \qquad 2.33$$

To calculate the material polarization caused by the applied field it is necessary to calculate the ensemble average of the dipole

moment $<\mu_d>$, since $P=N<\mu_d>$ where N is the atomic/molecular number density, and this is, according to equation (2.28), given by:

$$<\mu_d>=tr(\rho\mu_d) \qquad 2.34$$

Using equations (2.31) and (2.32) this can be written as :

$$<\mu_d>=\mu(\rho_{d12}+\rho_{d21}) \qquad 2.35$$

$<\mu_d>$ is in general a function of time. It is thus necessary to know how ρ_{12} and ρ_{21} change with time.Since ρ_{ii} is the probability of finding an atom in the i'th state and if N is the density of atoms then $N(\rho_{11}-\rho_{22})$ is equivalent to ΔN, the average population difference between two levels. Thus to understand how the population difference changes with time it is necessary to calculate $\frac{d}{dt}(\rho_{11}-\rho_{22})$.If use is made of equation (2.27) and of the eigenfunctions Ψ^k of the unperturbed Hamiltonian, then $\mathbf{H}\Psi^k = \mathbf{E}\Psi^k$, and defining the resonance frequency as $\omega_0=(E_2-E_1)/h$, $\frac{d\rho_{21}}{dt}$ can be written as :

$$\frac{d\rho_{21}}{dt}=-i\omega_0\rho_{21}+i\frac{\mu_d}{h}E(t)(\rho_{11}-\rho_{22}) \qquad 2.36$$

In a similar manner $\frac{d\rho_{22}}{dt}$ can be written as :

$$\frac{d\rho_{22}}{dt}=-i\frac{\mu_d}{h}E(t)(\rho_{21}-\rho_{21}^{*})' \qquad 2.37$$

And thus :

$$\frac{d}{dt}(\rho_{11}-\rho_{22})=2i\frac{\mu_d}{h}E(t)(\rho_{21}-\rho_{21}^{*}) \qquad 2.38$$

Up to now it has been assumed that a specific phase relationship exists between the wave functions of the molecules/atoms in the ensemble. The macroscopic polarization, when all molecules/atoms are oscillating in phase with each other, may be rather large in practical situations. The dipoles are then said to be oscillating coherently with each other. This is not the case in a practical laser system. There are almost always perturbation effects, or dephasing effects. These effects will scramble or randomize the time–phases of the individual wave functions which cause the macroscopic polarization to become much smaller.Examples of these effects are spontaneous transitions and collisions between the atoms/molecules. These collisions are characterized by the fact that they conserve the average energy but cause a loss of ensemble information involving the phase in the wave function.

A simple model [33] can illuminate the way in which a macroscopic polarization P can be destroyed by random dephasing events. Suppose that the dephasing events for individual dipoles happen randomly in their times of occurrence

and in the phase changes they produce. Let there be some large number N_0 of dipoles in a unit volume, all initially oscillating in phase, so that the initial polarization at a starting time t_0 is:

$$P=N_0<\mu_d> \qquad 2.39$$

At any time $t > t_0$ these N_0 dipoles can be divided into : (a) a decreasing number of dipoles $N_d(t)$ that have not yet suffered any collisions at all, and (b) an increasing number $N_0 - N_d(t)$ of dipoles that have suffered at least one collision. The $N_d(t)$ dipoles that have not undergone any collisions or dephasing events will continue to oscillate in phase producing a polarization:

$$P(t)=N_d(t)<\mu_d> \qquad 2.40$$

Those dipoles that have suffered at least one collision will have phases that are completely random. It must be emphasized that the collisions under consideration here are completely elastic collisions. Hence these dipoles will add up to produce no coherent polarization at all.Suppose that the collisions occur at a random rate $1/T_2$ collisions per atom/molecule per second. Then the total number of collisions dN that the members of the uncollided group will undergo in a time interval dt around a time t will be given by :

$$dN_d(t) = -\frac{N_d(t)}{T_2}dt \qquad 2.41$$

Thus the polarization would decrease at a rate which is proportional to the number of in–phase dipoles. The ensemble average of the polarization is given by the sum of ρ_{12} and ρ_{21}. Thus the ensemble average of the polarization will decrease with the same proportionality constant as N_d, thus the rate of decrease in ρ_{12} caused by the collisions will be given by:

$$\frac{d\rho_{12}}{dt} = -\frac{\rho_{12}}{T_2} \qquad 2.42$$

Thus this term must be added to equation 2.36 to compensate for the loss of phase caused by the elastic collisions between molecules. For the same reason a term $\frac{(\rho_{11} - \rho_{22}) - (\rho_{11} - \rho_{22})_0}{\tau}$ must be subtracted from equation 2.38 to compensate for the loss of phase caused by inelastic collisions. The subscript 0 indicates the equilibrium [E(t) = 0] value.If the special case of a time harmonic perturbing field E(t),as is found in a laser cavity, is considered :

$$E(t) = \frac{E_0}{2}(e^{i\omega t} + e^{-i\omega t}) \qquad 2.43$$

Then according to Yariv [30] page 158, the expectation value of the dipole moment in this periodic driving field , is given by :

$$<\mu_d(t)>=2\mu[\mathrm{Re}\sigma_{21}(t)\cos\omega t+\mathrm{Im}\sigma_{21}(t)\sin\omega t] \qquad 2.44$$

With:

$$\mathrm{Im}\sigma_{21}=\frac{\Omega T_2(\rho_{11}-\rho_{22})_0}{1+(\omega-\omega_0)^2T_2^2+4\Omega^2T_2\tau} \qquad 2.45$$

$$\mathrm{Re}\sigma_{21}=\frac{(\omega_0-\omega)T_2^2\Omega(\rho_{11}-\rho_{22})_0}{1+(\omega-\omega_0)^2T_2^2+4\Omega^2T_2\tau} \qquad 2.46$$

$$(\rho_{11}-\rho_{22})=(\rho_{11}-\rho_{22})_0\frac{1+(\omega-\omega_0)^2T_2^2}{1+(\omega-\omega_0)^2T_2^2+4\Omega^2T_2\tau} \qquad 2.47$$

With :

$$\Omega=\mu_d E_0/2h \qquad 2.48$$

The macroscopic oscillating polarization ,$P=N<\mu_d>$, is thus :

$$P=\frac{\mu_d^2\Delta N_0 T_2}{h}E_0\left[\frac{\sin\omega t+(\omega_0-\omega)T_2\cos\omega t}{1+(\omega-\omega_0)^2T_2^2+4\Omega^2T_2\tau}\right] \qquad 2.49$$

The population difference per unit volume is :

$$\Delta N=\Delta N_0\frac{1+(\omega-\omega_0)^2T_2^2}{1+(\omega-\omega_0)^2T_2^2+4\Omega^2T_2\tau} \qquad 2.50$$

Where :

$\Delta N_0 = N(\rho_{11}-\rho_{22})_0$ is the population difference at zero field. If the atomic susceptibility is now defined as :

$$\chi^{(1)}=\chi^{(1)'}-i\chi^{(1)''} \qquad 2.51$$

Then:

$$P(t)=Re(\epsilon_0\chi^{(1)}E_0e^{i\omega t})=E_0(\epsilon_0\chi^{(1)'}\cos\omega t+\epsilon_0\chi^{(1)''}\sin\omega t) \qquad 2.52$$

Using equation (1.42), $\chi^{(1)'}$ and $\chi^{(1)''}$ can be written as :

$$\chi^{(1)''}(\omega)=\frac{\mu^2}{2\epsilon_0 h}\Delta Ng(\nu) \qquad 2.53$$

$$\chi^{(1)'}(\omega)=\frac{\mu^2(\omega_0-\omega)T_2}{2\epsilon_0 h}\Delta Ng(\nu) \qquad 2.54$$

$g(\nu)$ is the normalized lineshape function and is given by:

$$g(\nu)=\frac{\Delta\nu/2\pi}{(\nu-\nu_0)^2+(\Delta\nu/2)^2} \qquad 2.55$$

With:

ν_0 the frequency at line center and:

$$\Delta\nu=(\pi T_2)^{-1} \qquad 2.56$$

This is referred to as the normalized Lorentzian lineshape function and is characteristic of collision (τ, T_2) dominated transitions. According to this analysis the full width at half maximum $\Delta\nu$ is determined by the term T_2 only. T_2 is the time constant characterizing the loss of phase coherence caused by elastic collisions, as was shown previously. This is not entirely true since the full width at half maximum is the sum of this term and intrinsic atomic/molecular linewidth. This intrinsic linewidth is the spontaneous emission linewidth of the atom/molecule. This linewidth is determined by the lifetime of the transition as can be seen from Heisenberg's uncertainty relation:

$$\Delta E\Delta t \geq h \qquad 2.57$$

Where ΔE is the uncertainty in energy and Δt is the lifetime of the specific level. At higher gas pressures the pressure broadening term completely dominates the intrinsic linewidth

term. The reason why this term does not manifest itself in the semiclassical analysis is that the semiclassical approach is sufficient in treating the coherent interaction of atoms/molecules with a strong electromagnetic field [30]. To treat spontaneous emission, a complete quantum mechanical approach is required. This broadening mechanism is typical of so–called homogeneous broadening terms. This means that the dephasing mechanism acts on all the dipoles in the same way so that the response of each individual oscillator in the collection is broadened in the same fashion.

In an inhomogeneously broadened system, different atoms in a collection of nominally identical atoms have slightly different resonant frequencies. Thus the resonant frequencies for different atoms are randomly shifted by small but different amounts for each atom/molecule in the ensemble. An applied signal passing through a collection of atoms/molecules will only see a total response due to all the atoms/molecules. It will have no way of picking out only those atoms/molecules with specific frequency shifts. If the random shifting of the individual center frequencies is sizable compared to the linewidth of each individual response, any measurement of the overall response of all the atoms in the collection will then give a broadened summation of the randomly shifted response of the collection of atoms. Thus the overall response of the collection of atoms/molecules will be substantially broadened and the response at line center will be substantially reduced in amplitude.

There are several causes for the random shifting of resonance frequency and thus of inhomogeneous broadening [33]. Since a gas laser is investigated in this thesis, only the mechanism responsible for inhomogeneous broadening in a gas laser will be mentioned. In gases different atoms have different kinetic velocities . This motion produces a doppler shift in the frequencies of an applied signal as seen by the atom/molecule, or alternatively a doppler shift in the apparent resonance frequency of the atoms/molecules as seen by the applied signal.

2.2.4 LASER OSCILLATION CONDITION.

A semiclassical analysis of an inhomogeneous laser is done in Yariv[30]. He considered a model of a generalized resonator that contained an inverted medium. It is assumed that some mode l of the resonator is oscillating. This mode with electric field $\overline{E}_l(\overline{r},t)$ induces a coherent polarization field $\overline{P}_l(\overline{r},t) = \epsilon_0 \chi \overline{E}_l(\overline{r},t)$ where the susceptibility χ is given by equation (1.46) and (1.47). The circle is completed by requiring that $\overline{P}_l(\overline{r},t)$, acting as a driving source, gives rise to an oscillating field $\overline{E}_l(\overline{r},t)$. The results obtained using this approach is equivalent to those obtained when a Gaussian beam is assumed to exist in the resonator . In this case the laser oscillation condition is obtained by requiring that the Gaussian beam reproduces itself in shape, phase and amplitude after each round trip in the resonator.Using this condition a laser oscillation condition can be derived. This will be done in chapter 3.

2.3. THE PHYSICS OF THE CO_2 MOLECULE

Molecules have certain symmetry characteristics. If the symmetry of a molecule is known then it is frequently possible to draw conclusions about the spectrum of the molecule. By the symmetry of a molecule is meant the symmetry of the configuration of its nuclei. A molecule may have several symmetry elements such as a plane of symmetry and an axis of symmetry. To each symmetry element corresponds a symmetry operation – a coordinate transformation that will produce a configuration of nuclei indistinguishable from the original one [35].

It can be shown that some combinations of symmetry elements form a mathematical group [35].This means that if the 'product' of two symmetry elements of the same combination is taken, the result will also be a member of the same combination. Thus the combination of symmetry elements is closed with respect to the product operation. By 'product' is meant that the two symmetry operations are performed sequentially. Further requirements are that there must be an identity element in the combination, an inverse element and that the associative law is valid [36]. In molecular physics these groups are usually called point groups.

The $C^{16}O_2$ and $C^{18}O_2$ molecules have the point group $D_{\infty h}$

[35]. This means that the molecule has an axis about which the molecule can be rotated $360^0/\infty$ to leave a configuration indistinguishable from the previous one (an axis C_∞). It also has an infinite number of axes perpendicular to the previous axis about which the molecule can be rotated $360^0/2$ to leave a configuration indistinguishable from the previous one(an axis C_2). The final symmetry element that it possesses is a plane of symmetry(σ_h) perpendicular to the first mentioned axis.

The molecule $^{16}O^{12}C^{18}O$ has the point group $C_{\infty\nu}$. This means that it has an axis C_∞ and an infinite number of vertical planes of symmetry (σ_ν) leaving the molecule indistinguishable if it is reflected through a vertical plane.

2.3.1 THE ROTATIONAL LEVELS

The rotational levels of a linear polyatomic molecule are called positive or negative, depending on whether the total eigenfunction Ψ of the molecule remains unaltered or changes its sign by reflection of all particles. It can be shown [35] that even rotational levels are positive and odd ones are negative. If the molecule has the point group $D_{\infty h}$ ($C^{16}O_2$ or $C^{18}O_2$) there is in addition to the property positive–negative, the property symmetric or anti–symmetric with respect to an exchange of the identical nuclei, again the even rotational levels are symmetric and the odd levels are anti–symmetric.

Pauli's exclusion principle can be applied to the molecules $C^{16}O_2$ and $C^{18}O_2$. Pauli's exclusion principle states; if n particles of a system are identical, then the wave function must be symmetric with respect to the interchange of particles, if the particles have integral spin (Bosons), and anti–symmetric if the particles have half integral spin (Fermions) [37]. If the oxygen atoms in $^{16}O^{12}C^{16}O$ or $^{18}O^{12}C^{18}O$ are interchanged and if it is assumed that ^{16}O and ^{18}O are Bosons, then the wave function must be symmetric with respect to an interchange of the oxygen atoms. This can only happen if the odd rotational levels for these two molecules are absent. This is observed experimentally and it can thus be assumed that ^{16}O is a Boson. This argument does not apply to $^{18}O^{12}C^{16}O$ since the two

oxygen molecules are not identical and thus Pauli's exclusion principle is not applicable to this particular molecule. Thus the odd and even rotational levels are present in this molecule.

The statistical weight of a rotational level j is given by the number of possible orientations of j in a magnetic field specifically; –j..0..j possible orientations and thus in number (2j+1).

2.3.2 THE VIBRATIONAL LEVELS

The CO_2 molecule has 3 normal modes of vibration, the ν_1,ν_2 and ν_3 modes. The ν_2 mode is doubly degenerate [35]. The three normal modes of vibration are shown in figure 2.1.A linear combination of the two degenerate vibrations of the ν_2 mode causes the so–called vibrational angular momentum. l is the vibrational angular momentum quantum number.

Because a molecule has symmetry the normal vibrations and vibrational eigenfunctions also have certain symmetry properties. These symmetry properties form a symmetry species. For the point group $C_{\infty\nu}$ there are only two species of non–degenerate vibrations. Both are symmetric with respect to C_∞; one is symmetric with respect to the plane σ_ν and the other is anti–symmetric. These two species are designated Σ^+ and Σ^- respectively. Since these levels are non–degenerate the quantum number $l = 0$. The degenerate specie l=2 is indicated by Π. The species for the point group $D_{\infty\nu}$ is similar to the previous one with the only difference being subscripts g and u which are used to indicate symmetric and anti–symmetric with respect to the center of symmetry.

2.3.3 VIBRATIONAL INFRARED SPECTRUM.

Any motion of an atomic system that is connected with a change of its dipole moment leads to an emission or absorption of radiation. During the vibrational motion of a molecule the charge distribution undergoes a periodic change and therefore the dipole moment changes periodically. Since in the harmonic oscillator model the vibration of a molecule may be resolved into a sum of normal vibrations with appropriate amplitudes and since normal vibrations are simple periodic motion, the normal frequencies are the frequencies that are emitted or absorbed by the molecule.

Normal vibrations that are connected with a change in dipole moment and therefore appear in the infrared, are called infrared active . Vibrations for which the change in charge distribution is such that no change of dipole moment arises and which therefore do not appear in the infrared, are called infrared inactive. For CO_2 the modes ν_2 and ν_3 are infrared active while ν_1 is infrared inactive.

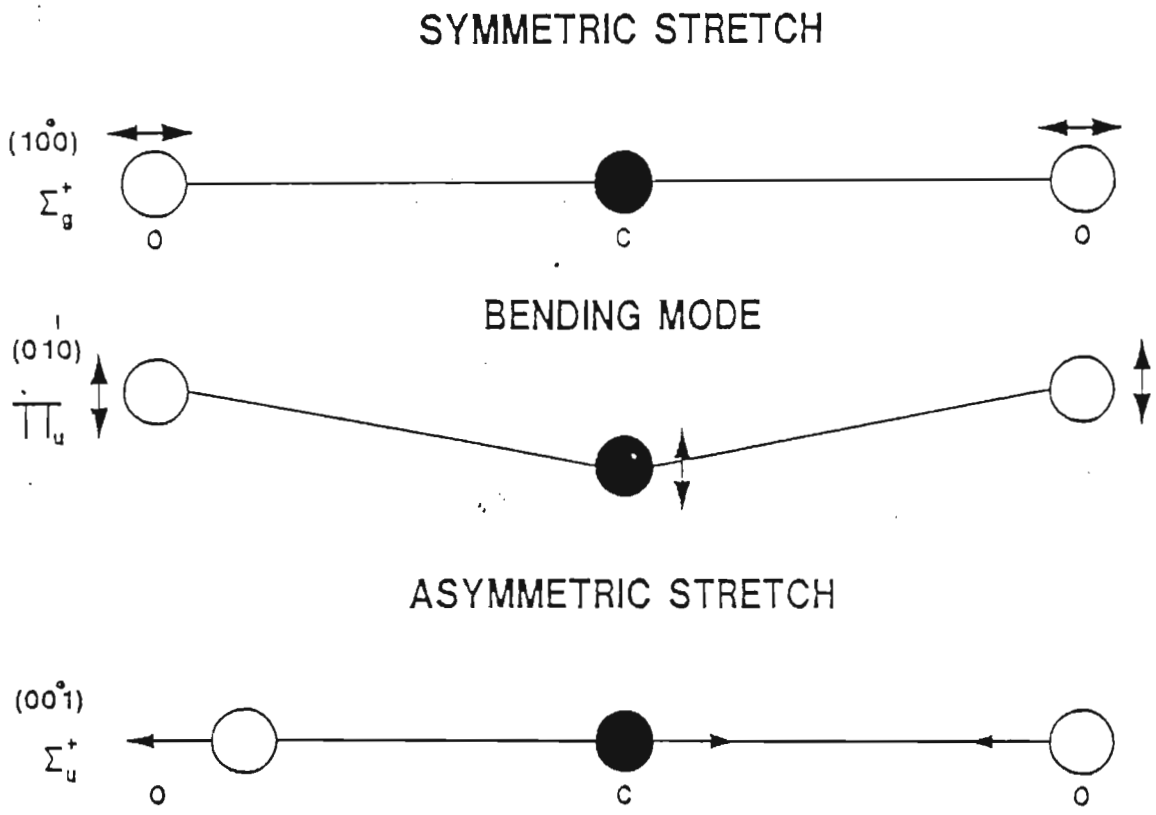

Figure 2.1. The vibrational modes of a CO_2 molecule.

2.3.4 ROTATION–VIBRATION SELECTION RULES

Rigorous vibration–rotation selection rules for $C^{16}O_2$, $C^{18}O_2$ and $C^{16}O^{18}O$,thus for the point groups $D_{\infty h}$ and $C_{\infty v}$ respectively, were derived by Herzberg [35] and are given below. Only those vibrational transitions occur for which:

$\Delta l = 0,\pm 1,\ \Sigma^+ <\!\!-\!\!+\!\!-\!\!> \Sigma^-,\ g <\!\!-\!\!+\!\!-\!\!> g,\ u <\!\!-\!\!+\!\!-\!\!> u$

And only those rotational transitions for which:

$\Delta j = 0,\pm 1,\ (j=0 <\!\!-\!\!+\!\!-\!\!> j=0),\ + <\!\!-\!\!-\!\!> -,\ s <\!\!-\!\!+\!\!-\!\!> a$

According to the above selection rules the following three types of infrared bands of linear molecules can occur:

(i) Transitions for which l=0 in both the upper and lower state (Σ–Σ). For these bands only $\Delta j=\pm 1$ can occur. Thus they have only one P ($\Delta j=+1$)and one R ($\Delta j=-1$) branch but no Q branch.

(ii) Transitions for which $\Delta l=\pm 1$ (Π–Σ). For these bands Δj =0 as well as $\Delta j=\pm 1$ are possible and therefore P($\Delta j=+1$),Q($\Delta j=0$), and R($\Delta j=-1$) branches are possible. The Q branch is stronger than either the P or R branches.

(iii) Transitions for which $\Delta l=0$ but $l \neq 0$ ($\Pi-\Pi$). For these bands $\Delta j=0,\pm 1$ is possible and therefore P,Q,and R branches are possible. In this instance the Q branch is much weaker than either the P or R branches.

2.4 THE USE OF ISOTOPES IN A CO_2 LASER

2.4.1 THE PULSED CO_2 LASER

The CO_2 laser is representative of the so–called molecular lasers in which the energy levels of concern involve the internal vibration of the molecule. The atomic electrons remain in their lowest energetic states and their degree of excitation is not affected.As was mentioned, the CO_2 molecule has three normal modes of vibration: (i) Symmetric stretch, ν_1= $(1,0^0,0)$ (ii) Bending, ν_2= $(0,1^0,0)$ and (iii) Asymmetric stretch, ν_3= $(0,0^0,1)$. These modes are shown in figure 2.1

As can be seen from figure 2.2 the CO_2 laser transitions are Σ–Σ transitions. Thus only P and R branches are possible. The Q branch is absent in these transitions.

A convenient method of exciting a CO_2 laser is to use a self sustained volume discharge initiated by a homogeneous electron avalanche. Methods of obtaining such a discharge will be discussed in the following chapter. In this method an electric field is suddenly applied to the gas in the discharge gap. This causes the initially low level of ionization in the discharge gap to grow exponentially via the electron avalanche process until the plasma impedance becomes limited by the output impedance of the driving circuit[38].

Patel[39] demonstrated that optimal CO_2 laser operation was obtainable with a mixture of CO_2,He, and N_2. The two principal pumping mechanisms in a CO_2 laser are:

(i) Direct electron impact.

(ii) Resonance transfer of energy between $N_2(\nu=1)$ and $CO_2(00^01)$.

Because N_2 is a linear diatomic molecule with no permanent dipole moment[35], transitions from one vibrational state to another in the same electronic state are forbidden.The cross–section for electron impact excitation to the first excited vibrational state is considerably higher than the cross sections for the higher vibrational states so that population tends to build up in the first excited level. The energy discrepancy between the first excited level and the (00^01) level of CO_2 is only 18 cm^{-1} so that resonant energy transfer is very efficient.

The cross–section for inelastic scattering of CO_2 molecules by electrons is roughly the same for all the vibrational modes, thus the (00^01) level is not populated preferentially by electron impact. It is the different decay times of the various levels that give rise to a population inversion between the lasing levels. The lifetime for spontaneous radiative decay of the (00^01) upper laser level to the (02^00) and (10^00) states is 4.2 seconds. The lifetime

against decay by collisions is pressure dependant but at atmospheric pressure is approximately 17 microseconds. On the other hand the lifetime for radiative decay of the (10^00) and (02^00) laser levels to the (01^00) level is very short, approximately a few tens of nanoseconds. A bottleneck tends to build up on the (01^00) level as it has a long lifetime (0.5 microseconds) for decay to the ground state, but the addition of helium to the lasing gas tends to cool this level faster than other levels (since kT at room temperature is approximately 210 cm^{-1} and this level has an energy of 667 cm^{-1}, while the energy of all the other levels is at least double this) and helps lasing action considerably.

Nighan and Bonnet [40] calculated the fractional power transferred to the appropriate upper vibrational levels of N_2 and CO_2. This is shown in figure 2.3. As can be seen for an E/N value of approximately $10^{-16}Vcm^2$, approximately 45% of the electron energy goes directly into CO_2 and slightly in excess of 40% goes into the (ν=1 to 8) vibrational levels of N_2.

The role of the Helium gas in the mixture is to cool the gas by aiding in the depopulation of the lower CO_2 vibrational level that acts as a bottleneck for transferring the molecules down to the ground state. In addition He plays an equally important role, as the main discharge carrier,in maintaining the quasi–stable E/N value in the proper range for more efficient excitation of the CO_2 molecules refer, to figure 2.3. Denes and Lowke [41]

did an experimental study of the V–I characteristics of pulsed CO_2 discharges. They found that in each mixture the E/N value stabilizes at the same quasi–stable value. The values they measured are given in table 2.1. Wiederhold et al. [42] executed a theoretical investigation of the discharge excitation. Their model predicted comparable E/N values to those measured by Denes and Lowke[41]. Wiederholdt et al found that the E/N value was mainly determined by the Helium concentration.

The quantum efficiency of CO_2 can be calculated from figure 2.2 The quantum efficiency for the 10.6 μm branch is 41%. According to figure 2.3 for the typical discharge with an E/N value of $2.0 \times 10^{-16} V.cm^2$ the fraction of the power transformed to the coupled CO_2 and N_2 system is approximately 70%. Thus the theoretical maximum total efficiency of a CO_2 laser is approximately 30%.

Mixture CO_2:N_2:He	1:0:9	1:7:30	1:1:8	1:2:3	1:2:1
E/N(10^{-16}Vcm^2)	1.7	2.6	2.7	4.8	6.7
kV/cm.atm	4.1	6.3	6.5	11.7	16.3

Table 2.1 Measured values of the self–sustained discharge parameter for representative CO_2 laser mixtures. From Denes and Lowke [41].

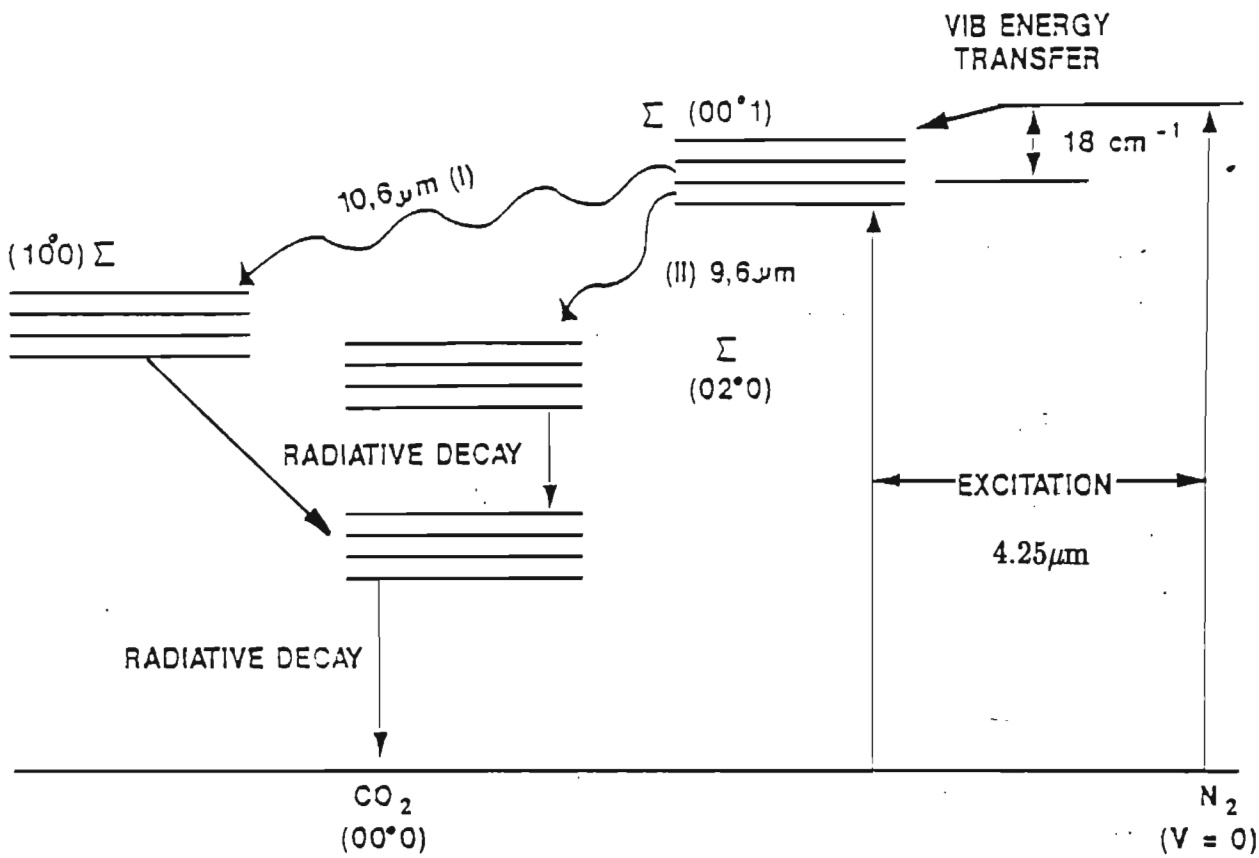

Figure 2.2. The pumping mechanism of a CO_2 laser.

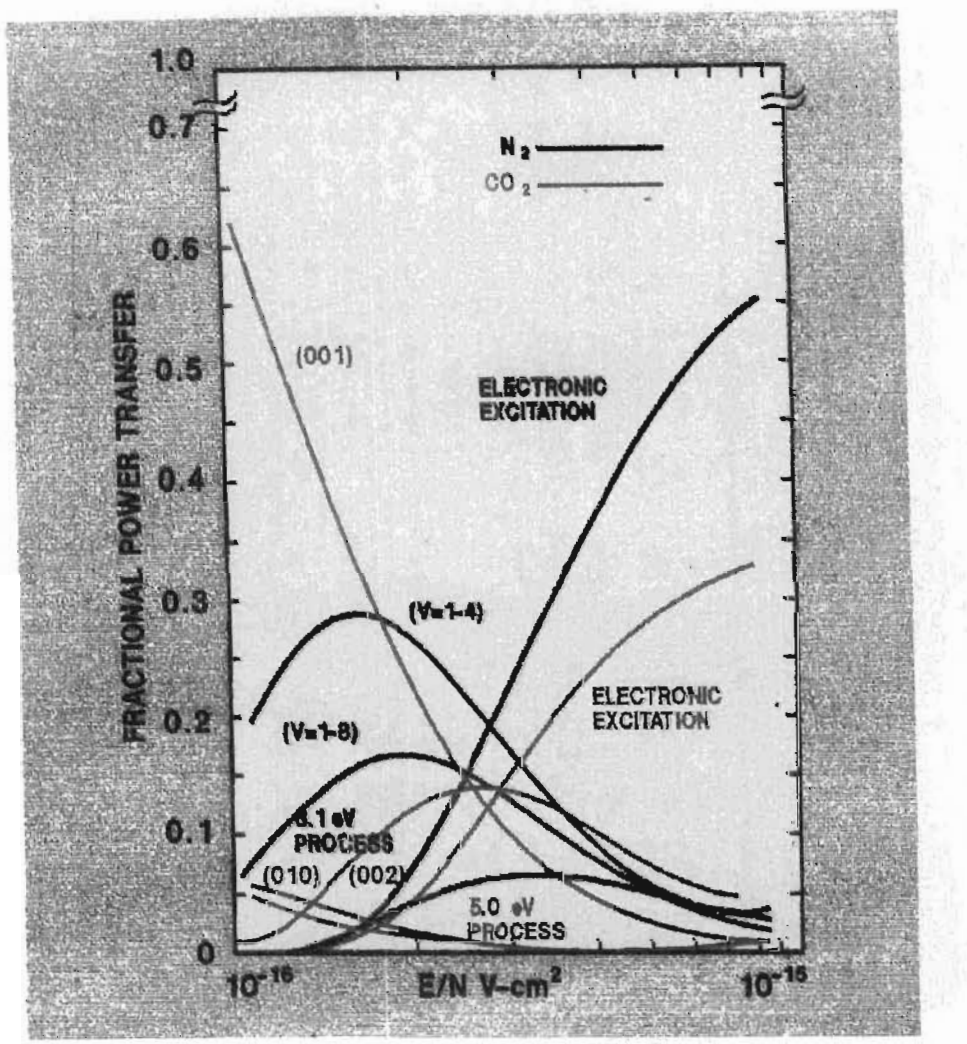

Figure 2.3. The fractional power transferred to the appropriate vibrational levels of N_2 and CO_2[40].

2.4.2 THE GAIN OF A MULTI–ISOTOPE CO_2 LASER.

CO_2 isotopes can extend the frequency range of a CO_2 laser. Laser action in the 8.9 μm to 12.3 μm region have been demonstrated using CO_2 isotopes [43]. These isotope shifts are a direct result of the mass dependence of the vibrational and rotational constants and depend on , self evidently, the masses of the individual atoms which form the molecule.

The first rare isotope laser was reported by Wieder and Mc Curdy [44]. They used $^{12}C^{18}O_2$. Jacobs and Bowers [45] reported $^{13}C^{16}O_2$ laser action in 1967 . Siddoway[46] reported $^{14}C^{16}O_2$ laser action in 1968. The main interest in CO_2 isotope lasers has been their extended frequency range which was used in high resolution laser spectroscopy [47], and using rare isotopes in a CO_2 laser radar [48,49]. Rare isotope CO_2 lasers provide improved performance when used in CO_2 laser radars relative to normal CO_2. $^{13}C^{16}O_2$ is typically used in this application, due to its virtual lack of attenuation from atmospheric CO_2.

The basis of investigation into CO_2 isotopes in this thesis was lowering the pressure at which continuous tunability could be achieved. Gibson, Boyer and Javan [11] reported a mixed isotope multi–atmosphere CO_2 laser using $^{12}C^{18}O_2$, $^{12}C^{18}O^{16}O$, and $^{12}C^{16}O_2$. They achieved the same continuous tunability, with this mixture, at pressures of a half to a quarter of that achieved when using normal CO_2. Shimada et al [12] did

theoretical calculations of the gain profile of a similar mixed isotope CO_2 laser . They predicted that continuous tuning at a pressure of 4 atm would be possible with this mixture and it would offer the same tunability as a 10 atm $C^{16}O_2$ laser.. They planned to use such a laser to generate ultra short pulses. The purpose of this research presented here was to determine, both theoretically as well as experimentally, the minimum pressure at which continuous tuning in the R28 to R30,10μm region could be achieved.

According to equation (2.21) the small signal gain, of a specific vibration–rotation transition, of a monochromatic wave travelling through a medium (a monochromatic wave can be used since it is assumed that a high pressure CO_2 laser is homogeneously broadened) in an excited state multiplied by the intensity I_ν is given by:

$$\frac{\text{Power}}{\text{Volume}} = \left[N_{2j} - \frac{g_2}{g_1} N_{1j}\right] \frac{\lambda^2 g(\nu) I_\nu}{8\pi n^2 t_{spont}} \qquad 2.58$$

Here g_2 and g_1 are the respective degeneracies.λ is the wavelength.$g(\nu)$ is the normalized lineshape function.t_{spont} is the spontaneous lifetime of level 2.n is the index of refraction of the lasing medium.N_{2j} and N_{1j} are the respective population densities of the upper and lower level rotational lines.

At high pressures, pressure broadening, as discussed in section

2.2.2, causes the overlap of neighbouring rotational lines. The total gain at a specific frequency is thus given by the collective sum of the contributions of the various rotational lines at that frequency because of the overlap of rotational lines caused by the pressure broadening $g(\nu)$. The total small signal gain coefficient at a specific frequency can thus be written as :

$$\gamma(\nu)=\sum_{j}\left[N_{2j}-N_{1j}\frac{g_{2j}}{g_{1j}}\right]\frac{\lambda^2 g(\nu)}{8\pi n^2 t_{spont}} \qquad 2.59$$

As has been discussed in the previous section for the case of the symmetrical CO_2 molecules $C^{16}O_2$ and $C^{18}O_2$, the summation is only over the even values of j. For the unsymmetrical molecule $C^{18}O^{16}O$ summation over both the odd and even values of j are appropriate. Assuming vibrational populations of N_2 and N_1 respectively and assuming that the rotational line populations are in thermal equilibrium the population of an individual rotational line is given by:

$$N_{2j} = Z_{2j}N_2 \qquad 2.60$$

With Z_{2j} the Boltzman factor, given by :

$$Z_{2j}=(1/Q)g_{2j}e^{-\frac{hcB_2}{KT}j(j+1)} \qquad 2.61$$

Where B_2 is the rotational constant, j is the rotational quantum

number, K is Boltzmann's constant, T is the temperature and Q is the partition function given by:

$$Q=\sum_{j} g_{2j} e^{-\frac{h c B_2}{KT} j(j+1)} \qquad 2.62$$

The degeneracy g_{2j} is, according to section 2.2.2, given by:

$$g_{2j}=(2j+1) \qquad 2.63$$

Thus the small signal gain coefficient,equation (2.59), can be written as:

$$\gamma(\nu)=N_{2j}\sum_{j}\left[Z_{2j}-\frac{N_{1j}}{N_{2j}}Z_{1j}\frac{g_j}{g_j}\pm 1\right]\frac{\lambda^2 g(\nu)}{8\pi n^2 t_{spont}} \qquad 2.64$$

g_{j+1} corresponds to the R branch and g_{j-1} corresponds to the P branch.As shown in equation (2.55) ,$g(\nu)$ is the Lorentzian lineshape function given by:

$$g(\nu)=\frac{\Delta\nu/2\pi}{(\nu-\nu_j)^2-(\Delta\nu/2)^2} \qquad 2.65$$

$\Delta\nu$ is the full width at half maximum (FWHM) of the specific rotational transition and has been experimentally determined by Abrahams [50] and is given by:

$$\Delta\nu = \beta_{CO_2} P_{CO_2} + \beta_{N_2} P_{N_2} + \beta_{He} P_{He} \qquad 2.66$$

With P_{CO_2} , P_{N_2}, P_{He} the partial pressures of CO_2, N_2 and He respectively, and:

$$\beta_{CO_2} = 5.79 \times 10^9 \text{ Hz / atm}$$
$$\beta_{N_2} = 4.23 \times 10^9 \text{ Hz / atm}$$
$$\beta_{He} = 3.72 \times 10^9 \text{ Hz / atm.}$$

According to Yariv[30] the spontaneous lifetime of a specific vibrational level can be written as:

$$t_{spont} = \frac{G_{12}(j+1/2 \pm 1/2)}{\lambda^3 g_j} \qquad 2.67$$

With G_{12} a constant that depends only on the vibrational quantum numbers [30].Thus for a specific vibrational level,with C a constant, the gain can be re–written as:

$$\gamma(\nu) = C \sum_j \left[\left[Z_{2j} - \frac{N_1}{N_2} Z_{1j} \frac{g_j}{g_{j\pm1}} \right] \frac{1}{(j + \frac{1}{2} \pm \frac{1}{2})} \frac{\Delta\nu / 2\pi}{(\nu_j - \nu_0)^2 - (\Delta\nu/2)^2} \right] \qquad 2.68$$

Thus the relative gain is given by:

$$\gamma_r(\nu)=\sum_j\left[\left[Z_{2j}-\frac{N_1}{N_2}Z_{1j}\frac{g_j}{g_{j\pm1}}\right]\frac{1}{(j+\frac{1}{2}\pm\frac{1}{2})}\frac{\Delta\nu/2\pi}{(\nu_j-\nu_0)^2-(\Delta\nu/2)^2}\right] \qquad 2.69$$

Where ν_j is the frequency of a specific rotational–vibrational transition and was calculated using the following equations and the constants listed in table 2.2.

The P and R lines are given by [35]:

$$P(j)= \nu_0-(B'+B'')j-(B'-B'')j^2 \qquad 2.70$$

$$R(j)= \nu_0+2B'+(3B'-B'')j+(B'-B'')j^2 \qquad 2.71$$

The spectroscopic data used was those reported by Bradley, Soohoo, and Freed [51] and a summary of the data is given in table 2.2. The unit used is vacuum wavenumbers.

Equation (2.69), together with equations (2.70) and (2.71), were used to calculate the relative gain curves of different isotopic mixtures of CO_2.A PASCAL program was set–up to execute this calculation. The program is given in appendix 1. Since the spectral region of interest lay in the 10 μm R28 to R30 region of the gain curve, only the 10 μm R branch is presented in the

following figures.

Figure 2.4 gives the 5 atm gain curves of the $^{12}C^{16}O_2$ and $^{12}C^{18}O_2$ 10 μm R branch . The isotopic shift can clearly be seen as well as the fact that the peak gain values are considerably greater than the intra–peak values.Continuous tunability at this pressure might be possible, but the laser energy would be significantly higher on the peaks than the off peak value. Figure 2.5 gives the 10 atm 10R gain curve for$^{12}C^{16}O_2$. As can be seen this is a much smoother curve than the previous one. It is evident that continuous tuning at this pressure should be possible. The 5 atm $^{12}C^{16}O_2$ and $^{12}C^{16}O^{18}O$ 10R gains are shown in figure 2.6. Again the isotope shift is clearly noticeable. Another significant observation is the fact that the 5 atm gain curve of $^{12}C^{16}O^{18}O$ is as smooth as the 10 atm $^{12}C^{16}O_2$ curve. The reason for this is because the dual labeled isotope has twice as many rotational transitions.

Figures 2.7 and 2.8 are the 4 and 3 atm gain curves of isotopic mixtures respectively. The mixtures used were 25% $^{12}C^{16}O_2$, 50% $^{12}C^{16}O^{18}O$ and 25% $^{12}C^{18}O_2$. The 4 atm isotopic gain curve is almost the same as the 10 atmosphere gain curve of figure 2.5, although it is slightly less smooth. The 3 atm gain curve shown in figure 2.8 is significantly less smooth than the 10 atm curve of figure 2.5. It might still be possible to achieve continuous tunability at this pressure with this isotopic mixture but the off–line–center energies might be significantly less than

the line–center values.

It thus seems that the most favorable isotope to use to achieve low pressure continuous tunability would be the dual labeled isotope. There is, however, a problem associated with the use of a dual labeled isotope in a closed loop laser system. Indeed a closed loop laser system is essential by virtue of the high cost of the CO_2 isotopes. In a CO_2 laser system a small percentage of the CO_2 is dissociated into CO and O_2. If a laser is operated in a closed loop gasflow system, impurity gases will build up and with that, the laser energy will decrease [52]. A further problem associated with these impurities (0.1–0.5%) is the destabilization of the gas discharge. For these reasons catalysts are used to catalytically recombine the CO and O_2 to form CO_2. A problem with the catalytic recombination is that isotopic scrambling might occur. That is, a ^{16}O may combine with a $C^{18}O$ to form $C^{18}O^{16}O$ or ^{16}O might recombine with $C^{16}O$ to form $C^{16}O_2$. Through many cycles of dissociation and recombination the mixture would eventually reach the equilibrium mixture 1:2:1 for $C^{16}O_2$,$C^{18}O^{16}O$, and $C^{18}O_2$. This is an advantageous ratio since the gain of $C^{18}O^{16}O$ is half that of single isotope CO_2.Stable operation using a catalyst has been reported for up to 10^6 shots at 10 Hz with no degradation in the laser pulse energy [52]. These tests were stopped after 10^6shots thus stable operation for many more shots might be possible.

Experimental results obtained with different isotope mixtures at different pressures will be presented in chapter 3.

	$C^{16}O_2$	$C^{18}O_2$	$C^{16}O^{18}O$
ν_0[001–I]	960.934	966.705	966.019
ν_0[001–II]	1067.257	1083.695	1072.660
B'	0.386	0.344	0.365
B"	0.390	0.347	0.368

TABLE 2.2 Spectroscopic constants of different CO_2 isotopes All values are in vacuum wave numbers.

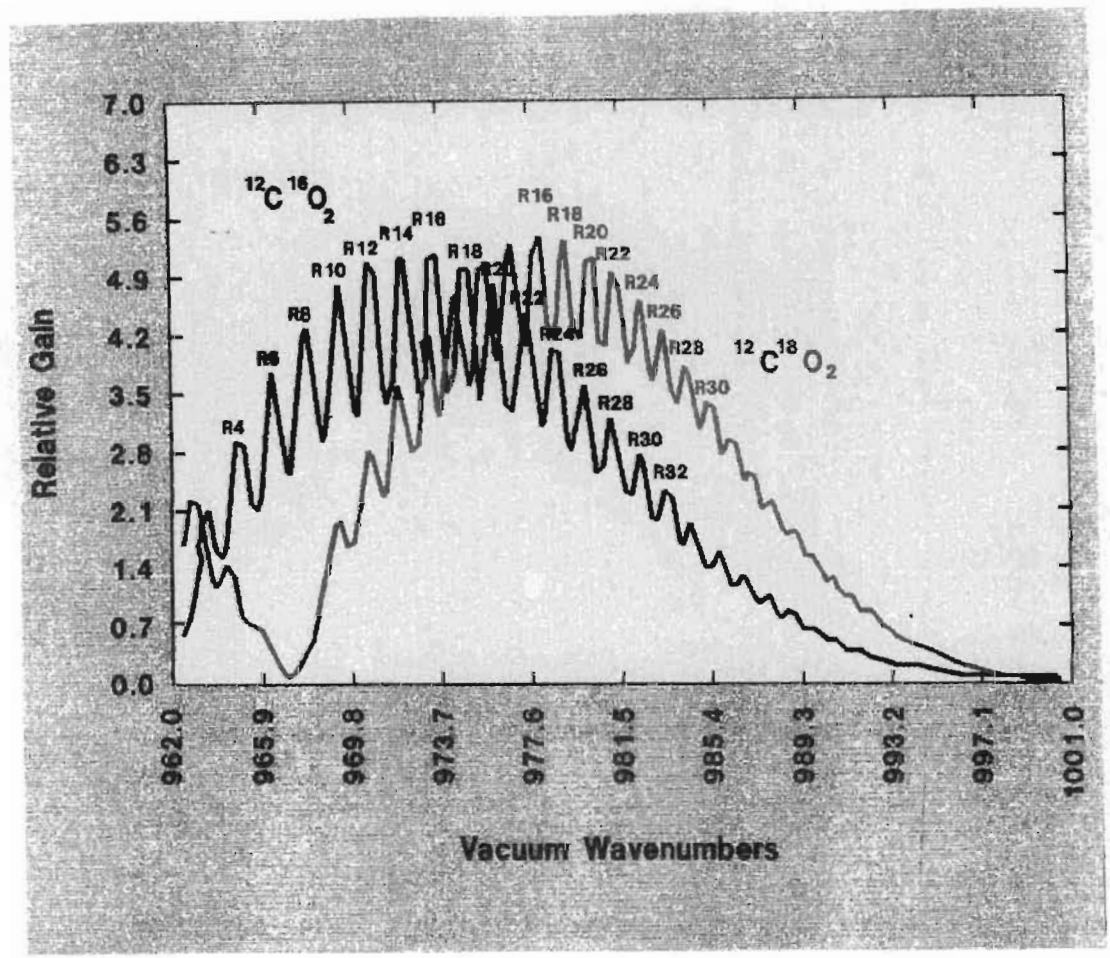

Figure 2.4. The 5 atm gain curves of $^{12}C^{16}O_2$ and $^{12}C^{18}O_2$. The 10 μm R branch is shown.

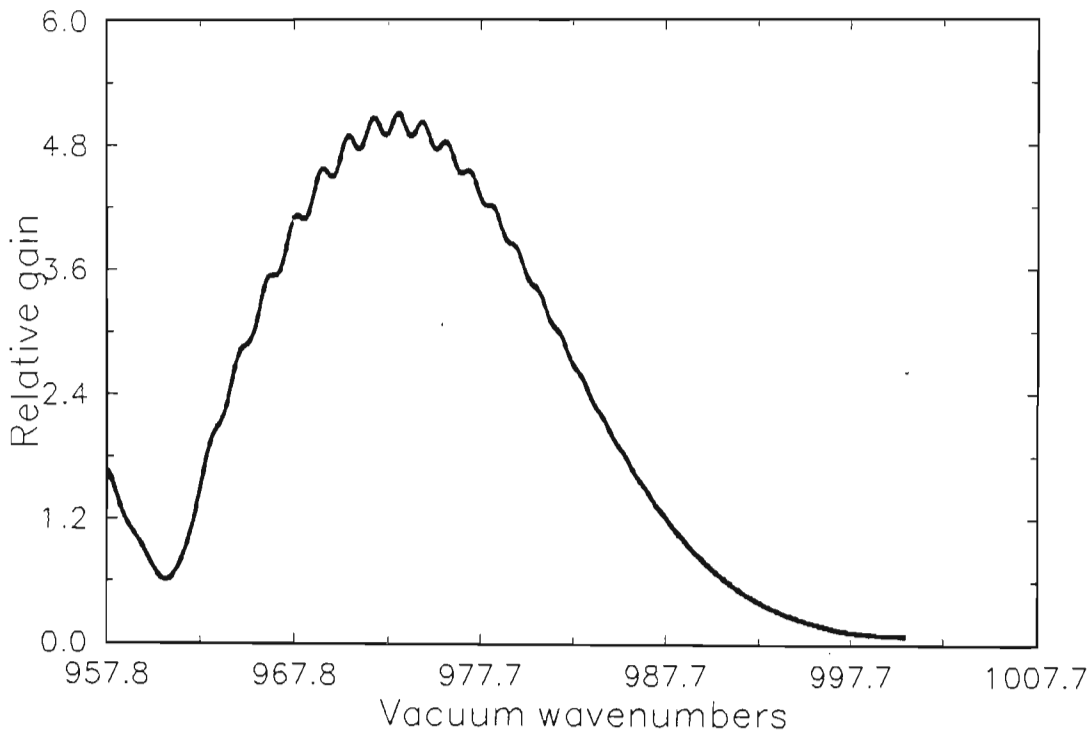

Figure 2.5. The 10 atm gain curve of $^{12}C^{16}O_2$. The 10 μm R branch is shown.

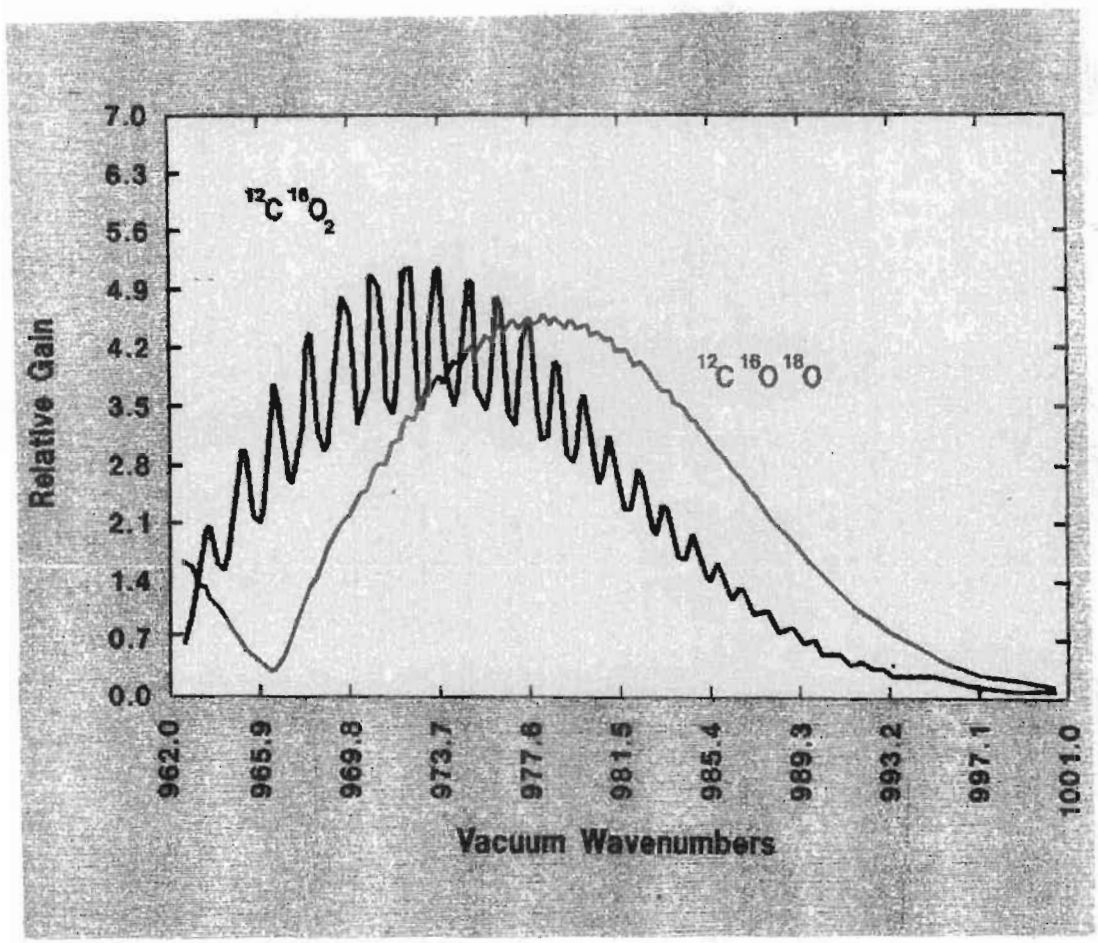

Figure 2.6 The 5 atm gain curve of $^{12}C^{16}O_2$ and $^{12}C^{18}O^{16}O$. The 10 μm R branch is shown.

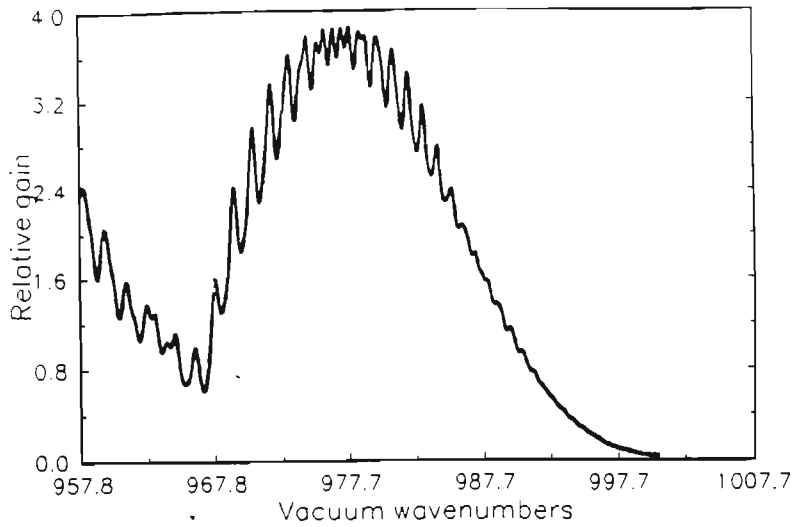

Figure 2.7. The 4 atm gain curve of a mixture of 25% $^{12}C^{16}O_2$, 50% $^{12}C^{18}O^{16}O$ and 25% $^{12}C^{18}O_2$. The 10 μm R branch is shown.

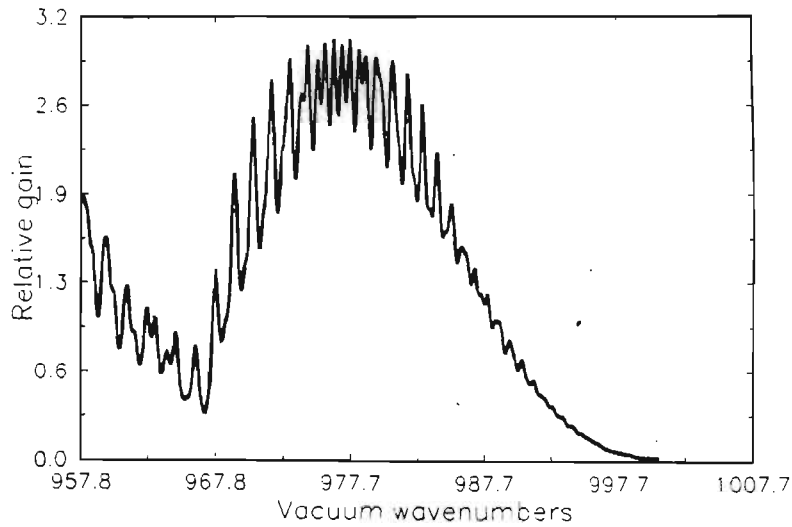

Figure 2.8. The 3 atm gain curve of a mixture of 25% $^{12}C^{16}O_2$, 50% $^{12}C^{18}O^{16}O$ and 25% $^{12}C^{18}O_2$. The 10 μm R branch is shown.

CHAPTER 3

EXPERIMENTAL INVESTIGATION OF A MIXED ISOTOPE LASER.

3.1 EXPERIMENTAL PROCEDURE

3.1.1 LASER USED IN THE EXPERIMENT

3.1.1.1 GAS DISCHARGE EXCITATION OF A CO_2 LASER.

There are three main methods of pumping a high–pressure gas laser:

(i) direct e–beam (high energy electron beam) pumping[53].
(ii) e–beam sustained discharge [54].
(iii) pre–ionized avalanche/self–sustained discharges [55].

In this investigation a pre–ionized self sustained discharge was used. In this method an electric field is suddenly applied to the gas in the laser. The electric field is usually considerably higher than the breakdown threshold across the discharge gap and causes the initially low level of ionization in the discharge gap to grow exponentially, via the electron avalanche process until the plasma impedance becomes limited by the output impedance of the driving circuit[25].

It has been found [56] that the high voltage pulse creating the electron

multiplication in the laser gas must have a very fast rise time and a relatively short duration ($<10^{-8}$S) in order to avoid the formation of filamentary arcs within the discharge volume.Efficient laser pumping in the presence of arcs is impossible due to the inadequate excitation rates in the areas of high current density caused by the rapid thermal equilibration rate. This tends to destroy the population inversion in this region. In addition the resultant non–uniform distribution of refractive index within the inhomogeneously excited medium makes the formation of high optical quality laser beams difficult. A further problem associated with severe arcing is the very low plasma resistivity in the concentrated arcs. The sudden decrease in the plasma resistivity with rapidly increasing local current densities may cause the total load resistance across the gap to collapse momentarily to values far below that of the driving circuit impedance [56]. When this occurs, the discharge will either self–terminate or go into a self oscillatory arc discharge mode, depending on the characteristics of the driving circuit and the extent of the impedance mismatch [56]. This self oscillatory behaviour or ringing can be extremely harmful to some of the PFN elements like the thyratron and capacitors.

There are two types of electrical breakdown that can convert an initially non–conducting high–pressure gas between two parallel electrodes into a highly conducting plasma upon the application of a high voltage pulse. One is the classical Townsend breakdown [57], and the other is the so–called plasma streamer breakdown [58]. The basic process for electron multiplication is due to electron avalanche in both processes. The conditions for occurrence and applicable range of field

strength to gas density ratio E/n are different [56].

Townsend or Pashen breakdown is characterized by a large number of successive electron avalanches that originate from secondary electron generation. The space charge field caused by differential motion between the electrons and positive ions is assumed to be so weak as to be completely negligible. Streamer breakdown in contrast to the Townsend breakdown occurs as a result of a large space–charge field, that develops from a single electron avalanche. This transforms an otherwise orderly avalanche into a rapidly propagating plasma streamer. The large space charge fields that develop are due to the relatively low mobility of the positive ions as compared to that of the electrons. On the timescale of interest, in a typical short duration pulsed discharge, the electrons are free to move towards the anode while the ions are essentially frozen in space. The avalanche head can be idealized as a negatively charged sphere behind which is the positive space charge, refer to figure 3.1 [59]. The shape of the avalanche head is determined by electron diffusion.

According to the streamer breakdown model, breakdown will occur whenever a single primary electron avalanche is allowed to develop to the critical point of streamer initiation [56]. The applied electrical field for the initiation of a Townsend–type breakdown is generally much weaker than that required for streamer breakdown [56]. However streamer type breakdown can take place in a time much shorter than the characteristic time,

$$\tau_e = \frac{d}{\nu} \qquad 3.1$$

for the single transit of a primary electron from the cathode to the anode, a distance d apart with a constant electron drift velocity of ν. This is the time scale necessary for the formation of Townsend breakdown. Thus for a high pressure CO_2 laser, with a very fast discharge time ($<\tau_e$), the breakdown mechanism is streamer breakdown. Thus to form a homogeneous discharge in a high pressure pulsed CO_2 laser the formation of streamers must be inhibited. Streamer formation can be inhibited by the creation of a homogeneous background ionization density before the main discharge pulse is applied. This process is known as pre–ionization and has been successfully applied to CO_2,HF,XeCl and many other lasers [60,61,62].

Implicit in the formulation of streamer breakdown theory is that the space charge can develop strong local gradients [59], since it is this feature which causes the discharge current to become filamentary.In the case where the space–charge field is due to a single or just a few primary electron avalanches, strong field gradients clearly exist due to limited diffusive spreading of the individual avalanche patches. As the number of primary avalanches are increased beyond a certain level one would expect adjacent avalanche patches to overlap. Strong overlapping of the secondary ionization generated by the primary avalanches will homogenize the resultant plasma density in the discharge and will also smooth out local gradients of the space field to such an extent that streamer formation is completely inhibited, refer to figure 3.2.

The resultant spatial homogeneity can be achieved [63], only if adjoining avalanches overlap each other in a time which is shorter than the exponentiation time τ of the electrons. Gavrilov et al [64] calculated the pre–ionization density necessary for a stable discharge and the values they obtained were between 10^5 and 10^6 electrons/cm^{-3}. Ohawado and Sekiguchi [65] reported experimental values of 10^6electrons/cm^{-3}.

Different methods can be employed to create a background of electrons in a CO_2 laser. Some of the most common pre–ionization techniques are:

(i) double discharge.
(ii) e–beam.
(iii) UV.
(iv) x–ray pre–ionization.

In these methods the scaling to large laser volumes or high pressures will ultimately be limited by the mass penetration depth of the electron–beam, UV or X–ray photon. The characteristic length scale corresponding to one e–fold attenuation of current density for a 300 keV electron beam in a typical N_2/CO_2 or rare–gas/halogen laser mixture at room temperature and 1 atm is about 20 cm [25]. Therefore homogeneous pumping of the laser gas of mass thickness much greater than 0.2 m/atm would require relativistic electron beams. The effective range for UV pre–ionization in a molecular laser has been found

experimentally to be of the order of 0.1 m/atm [66]. Effective pre–ionization for x–rays at 200 keV is of the order of 50m/atm [67].Since the electrode separation used in this thesis was 1 cm and the maximum operating pressure was 5 atm, UV pre–ionization would be sufficient to ensure a homogeneous discharge. UV pre–ionization was used because it is much more convenient than either e–beam or x–ray pre–ionization.

The UV source used in this thesis was a stripline type device[68]. It consisted of square conducting surfaces on the one side of a PC–board with the ground on the other side, refer to figure 3.3. The last square on the top was connected to the ground at the other side of the PC–board.The equivalent circuit of the stripline is given in figure 3.4. A coaxial transmission line was connected to the other side of the stripline. A high voltage pulse was launched down the transmission line. This pulse caused successive spark discharges between the square conducting surfaces on top of the PC–board. These spark discharges created hot plasmas which served as the source of UV photons. The pre–ionization discharge circuit is shown in figure 3.5

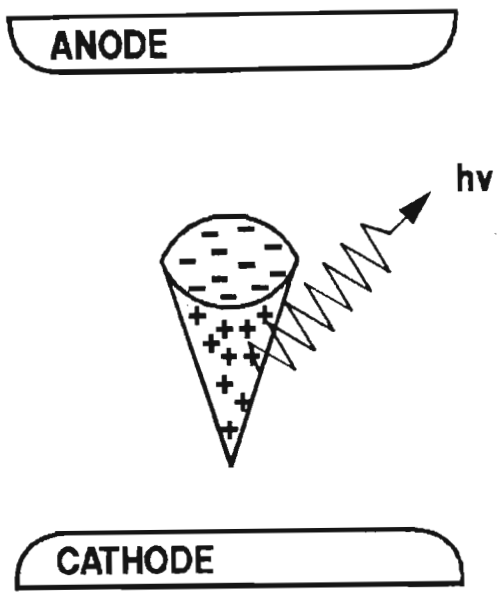

Figure 3.1. Schematic diagram showing streamer development around a single primary electron avalanche [59].

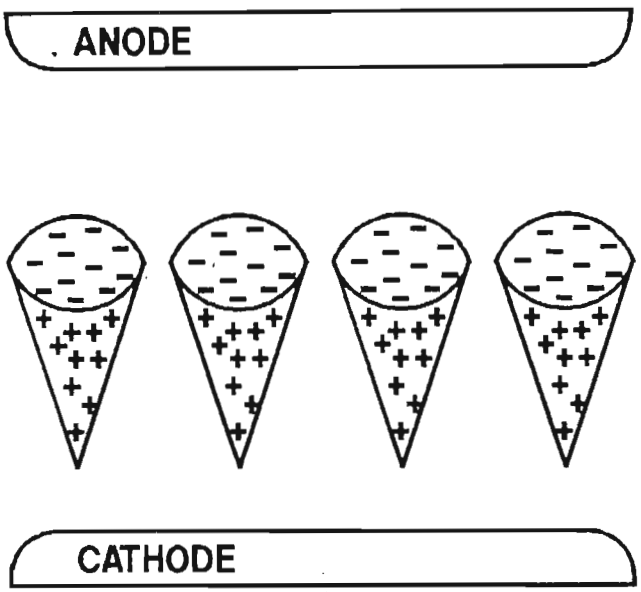

Figure 3.2. Schematic diagram showing one row of simultaneously formed primary electron avalanches[59].

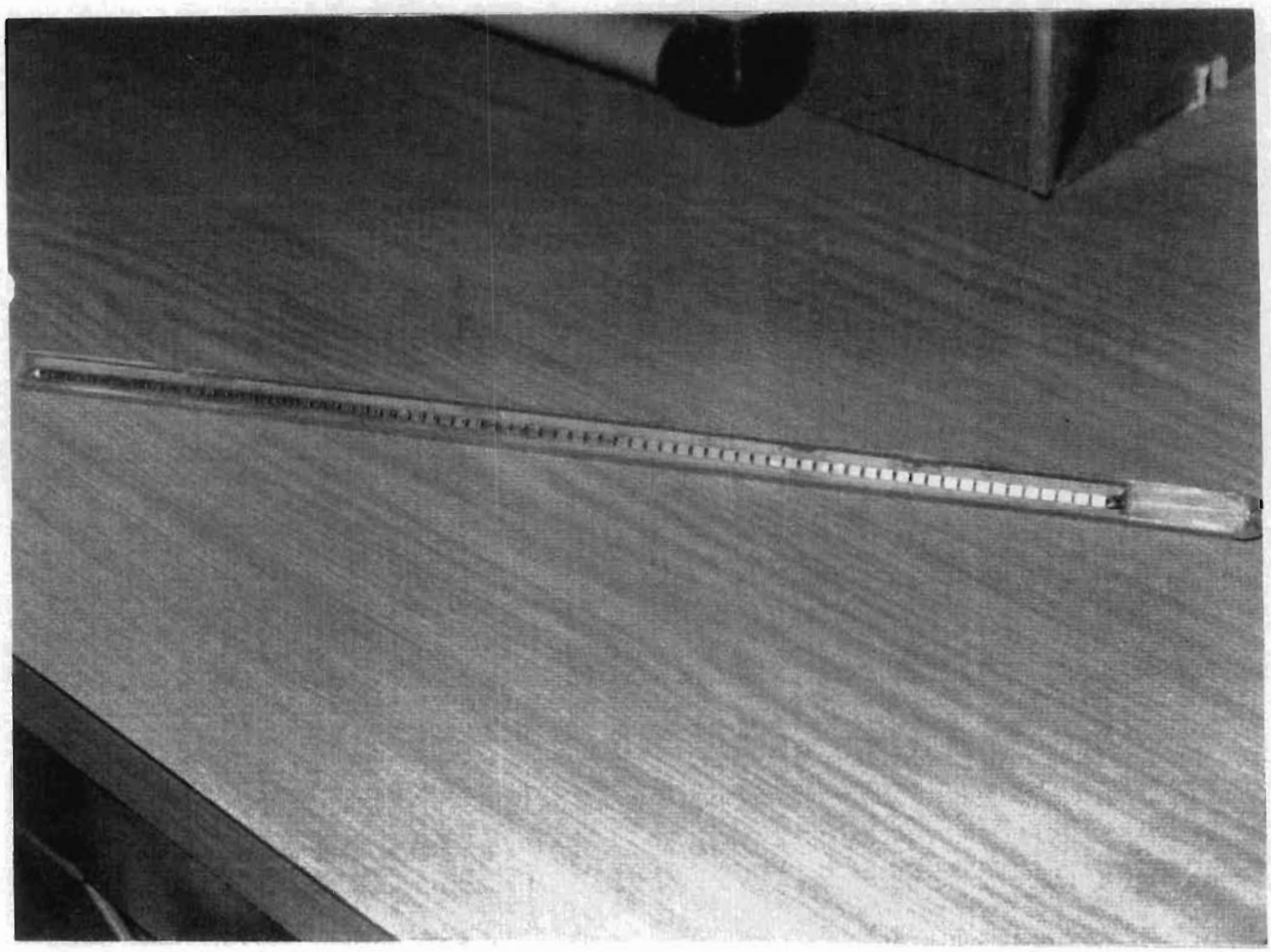

Figure 3.3. A photograph of the stripline pre–ionization device.

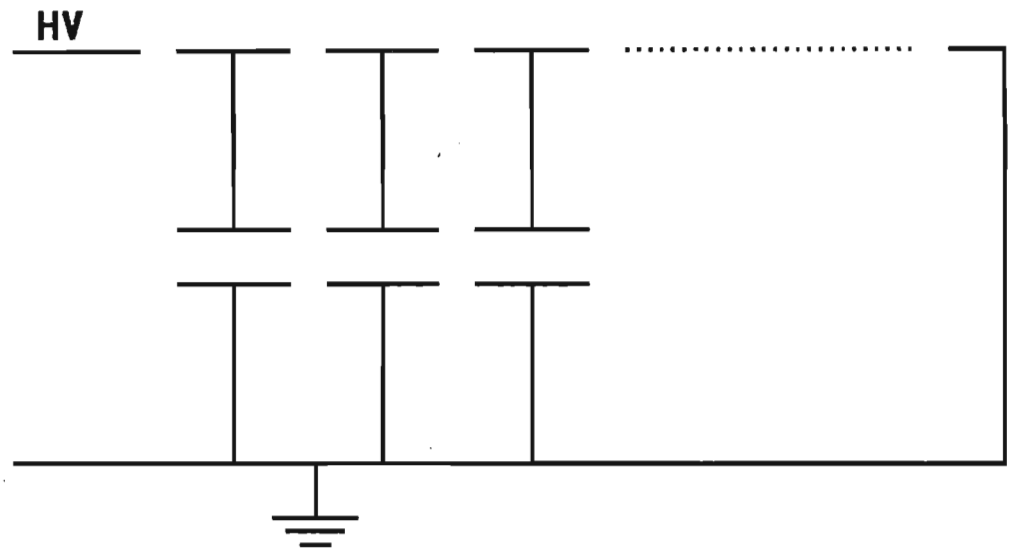

Figure 3.4. The equivalent circuit of the stripline pre–ionization device.

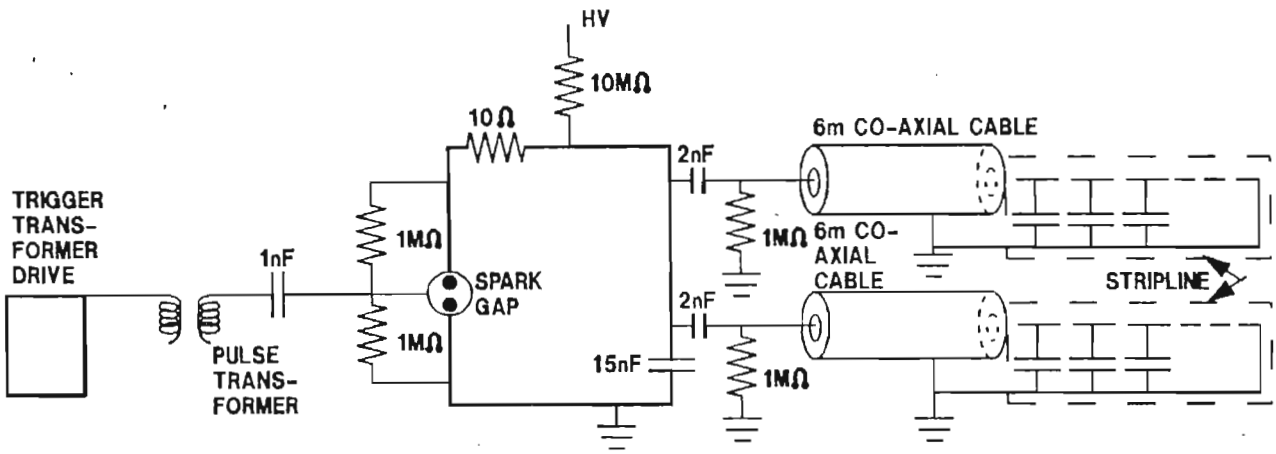

Figure 3.5. The pre–ionization discharge circuit used in this thesis.

3.1.1.2 ELECTRODE DESIGN

In order to obtain a uniform gas discharge it is important to have a very uniform energy loading into the gas between the electrodes. Thus electrodes with a very uniform field distribution are needed. Rogowski's[69] and Chang's[70] electrodes are the electrodes most commonly used in gas discharge lasers. Ernst [71] developed electrodes which used a smaller width for a given discharge width than can be obtained with Chang's electrodes. Since the distance from the UV source to the center of the electrode must be as small as possible, Ernst profile electrodes were used for this laser. The Ernst profile is given by:

$$x=u-k_1\sinh(2u) \qquad 3.2$$

$$y=\pi/2+k_0\cosh(u)-k_2\cosh(3u) \qquad 3.3$$

Where u is the running variable and k_0 is an independent variable that determines the ratio between the electrode gap and the width of the electrodes. k_1 and k_2 can be obtained by iteratively solving the following two equations:

$$k_1=\frac{1}{4}(1-(1-(k_0-9k_2)^2)^{1/2} \qquad 3.4$$

$$k_2=\frac{5}{81}k_0(1-(1-\frac{9}{25}(1-8k_1/k_0^2+64k_1^2/k_0^2)^{1/2}) \qquad 3.5$$

A good approximation is to use:

$$k_1=\frac{1}{8}k_0^2 \qquad 3.6a$$

$$k_2=\frac{1}{90}k_0^3 \qquad 3.6b$$

The value used for k_0 was 0.02. This meant that the field variation $\Delta E/E$ was smaller than $1.0\text{x}10^{-6}$ for $x/y_0<1$ [71]. y_0 is obtained from equation(3.3), thus:

$$y_0=\pi/2+k_0-k_2$$

If an electrode separation of 1 cm is required then a normalization factor f' is given by:

$$f'y_0=0.5$$

Thus:

$$f'=0.5/y_0$$

Thus the real coordinates x' and y' are given by:

$$x'=f'x \qquad 3.7a$$

$$y'=f'y \qquad 3.7b$$

A computer program that calculates and plots the Ernst profiles for a specified k_0 value is given in appendix 2. A plot of the electrode used in

this laser is shown in figure 3.6

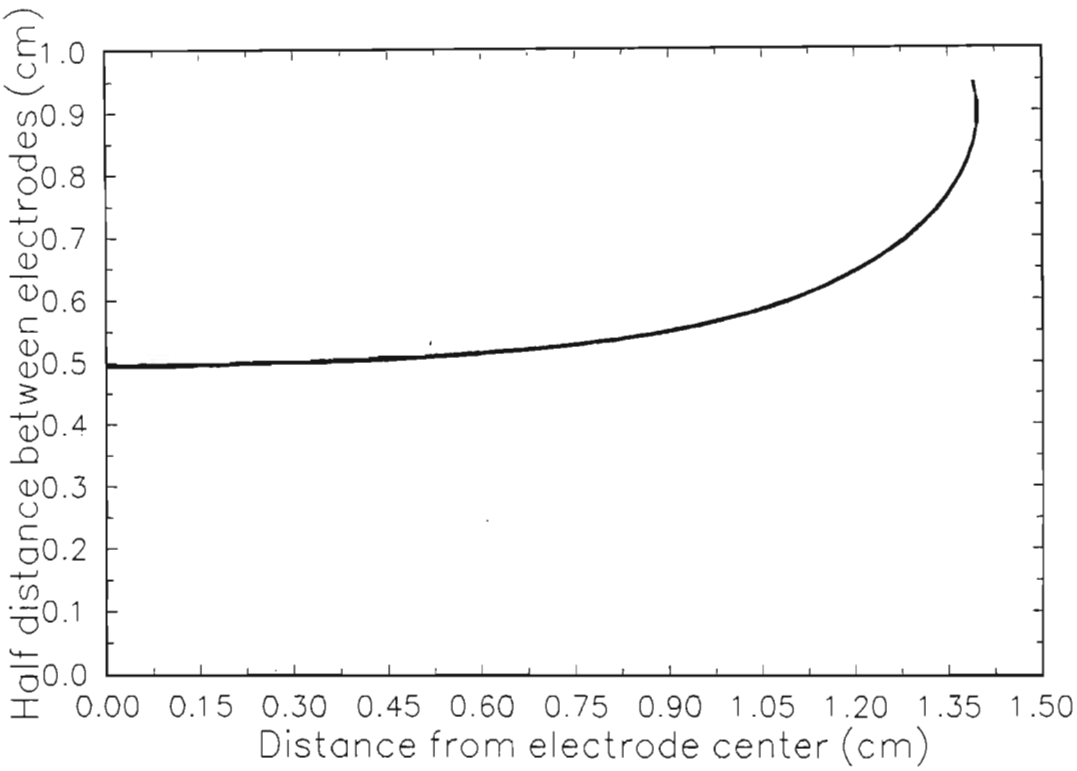

Figure 3.6. The electrode profile used.

3.1.1.3. DISCHARGE CIRCUIT

The most common discharge circuits used to excite a pulsed CO_2 laser are the so called C–C transfer and the LC–inversion circuits.[72]. A C–C transfer circuit was used in this investigation. A typical C–C transfer circuit is shown in figure 3.7. Using Kirchoff's laws the equation controlling the voltage and current in this circuit can be written as:

$$V_0 - \frac{1}{C_s}\int idt - Ri - L\frac{di}{dt} - \frac{1}{C_p}\int idt = 0 \qquad 3.8$$

With:

C_s :Storage capacitance.

L :Inductance of the circuit.

R :Circuit line resistance.

C_p :Peaking capacitor (Discharge gap capacitance).

R_d :Time dependant discharge gap resistance.

In a transient analysis of this circuit specifically relating to the behaviour of the circuit before resistive collapse of the discharge gap, it can be assumed that R_g is very large and the discharge gap can be approximated by an open circuit. In a C–C transfer circuit $C_s >> C_p$. The only resistance in this circuit is thus the line resistance and to a first order approximation the terms $\frac{1}{C_s}\int idt$ and Ri in equation (3.8) were ignorable. Thus equation (3.8) can be simplified to:

$$V_0 - L\frac{di}{dt} - \frac{1}{C_p}\int i\,dt = 0 \qquad 3.9$$

The voltage across the discharge gap, V_d is given by:

$$V_d = \frac{1}{C_p}\int i\,dt \qquad 3.10$$

Equation (3.9) can be re–written as:

$$\frac{d^2 i}{dt^2} = \frac{1}{LC_p} \qquad 3.11$$

Thus:

$$i = K\sin((LC_p)^{-1/2}t) \qquad 3.12$$

K can be solved using the boundary condition:

$$\left.\frac{di}{dt}\right|_{t=0} = \frac{V_0}{L} \qquad 3.13$$

Thus:

$$K = V_0(C_p/L)^{1/2} \qquad 3.14$$

Thus equation (3.12) can be written as:

$$i=V_0(C_p/L)^{1/2}\sin((LC_p)^{-1/2}t) \qquad 3.15$$

The voltage, as a function of time, across the discharge gap can now be calculated using equations (3.10) and (3.15).

$$V_d(t)=V_0[1-\cos((LC_p)^{-1/2}t)] \qquad 3.16$$

The peak voltage is reached when :

$$t=(LC_p)\pi \qquad 3.17$$

Then:

$$V_d=2V_0 \qquad 3.18$$

Thus for a C–C transfer circuit the peak voltage is twice the charge voltage and the pulse rise time is determined by the inductance of the circuit and the capacitance of the peaking capacitor.

Levatter and Lin [56] developed a model where the influence of a finite voltage rise time on the discharge formation was investigated. They found that for a specific mole fraction of free electrons present in a discharge, there exists a minimum breakdown strength say $(E/n)_0$. If the voltage is below $(E/n)_0$ then the net rate of change of free electrons n_e is negative and the free electron density undergoes exponential decay. If the voltage is above $(E/n)_0$ then the rate of change of n_e is positive and the free electron density would undergo exponential

increase. As can be seen from equation (3.17) any real pulse forming network has a finite rise time. During this rise time the applied voltage would stay below the breakdown voltage over a period of time comparable to the rise time. The corresponding field strength during this time ,with $E/n<(E/n)_0$, will thus not increase the number of primary electrons generated by the pre–ionization process. The field will merely cause them to drift away from the cathode towards the anode. If the voltage pulse is such that the electric field strength remains below the threshold value for too long a period of time, then a spatial region lacking free electrons will grow near the cathode surface. This will lead to the development of a nonuniform avalanche discharge or streamer breakdown. It is thus essential to design a pulse forming network with a very fast rise time.Thus to minimize the rise time of the discharge circuit the inductance of the circuit must be kept as low as possible.

As was mentioned in chapter 2, a self–sustained discharge operates at a constant E/p value. The value of V_p is thus a function of electrode spacing, gas pressure and gas mixture. After resistive collapse of the discharge has taken place, the circuit behaviour will be dominated by the discharging of the storage capacitor through the discharge gap. Equation (3.9) can now be simplified by dropping the $\frac{1}{C_p}\int idt$ term. The discharge circuit can now be approximated by a simple RLC circuit.The current as a function of time can now be written as:

$$i(t)=V_0(C_s/L)^{1/2}\sin((C_sL)^{-1/2}t) \qquad 3.19$$

The peak current can thus be written as:

$$i_{max}=V_0(C_s/L)^{1/2} \qquad 3.20$$

The energy input into the plasma can be obtained by multiplying i(t) by V_p and integrating over the time interval of π, thus:

$$E_p(\pi)=2C(V_c-V_p)V_p \qquad 3.21$$

The PFN energy efficiency η is defined as the ratio E_p to the total energy stored in the capacitor $1/2CV_c^2$, thus:

$$\eta=4\frac{V_p}{V_c}(1-\frac{V_p}{V_c}) \qquad 3.22$$

Thus all the energy in the capacitor bank can be transferred into the plasma if $V_p/V_0=0.5$. If $V_p/V_0>0.5$ then the capacitor bank is not completely drained in a half–cycle of current flow. If $V_p/V_0<0.5$ a fraction of the energy that was stored inductively is returned to the capacitor bank and is not available for transfer to the plasma. An equivalent statement of the condition $V_p/V_0=0.5$ is that the impedance of the PFN is matched to the plasma impedance. Thus the maximum energy transfer occurs at a pressure p_{max} at which the quasi–stable discharge voltage V_p is half the capacitor charging voltage.

A further important factor in the design of a CO_2 laser is the

volumetric optical energy extraction. Judd and Wada [10] measured the maximum energy input into a plasma before arcing would begin. They measured these values as a function of the gas pressure in the laser. The values they obtained varied between 160–170 J/l atm for a UV pre–ionized laser.

The discharge circuit used for this laser is shown in figure 3.8 The spark gap used was of the mid plane triggered type. The spark gaps were characterized to determine their operating pressures at different voltage values. The spark gaps were characterized as follows: Pure N_2 at a specific pressure was flowed through the spark gap. HV was then applied across the spark gap. The HV was raised until self breakdown occurred. The spark gap was then operated at 80% of this value. The circuit used in these tests is shown in figure 3.9. The characterization curve (breakdown values) of the two spark gaps used in these tests is shown in figure 3.10.

The correct time delay between the main discharge and pre–ionization pulses was determined in the following way. A RCA silicon photodiode was placed on the optical axis looking into the discharge. The photo diode circuit is shown in figure 3.11. A delay unit was used to trigger the two spark gaps as shown in figure 3.8. Two separate power supplies were used one for charging the main discharge capacitor and the other was used for the pre–ionization circuit. The main discharge capacitor was charged, and the main discharge was then triggered. Because no pre–ionization was present an arc was observed and this was recorded by the photodiode. The trigger pulse was used as a reference signal. The

measured photodiode signal is shown in figure 3.12 and. The pressure in the laser was 2.1 atm and the operating voltage was 27 kV. Because of the electromagnetic noise present this signal was averaged over 64 shots. The pre–ionization time was determined in a similar manner by charging the pre–ionization capacitors and ,without charging the main discharge capacitor, triggering the pre–ionization spark gap, (refer to figure 3.13). The correct time delay was determined by setting the time delay between the pre–ionization pulse and the main discharge, as observed by the photo diode, equal to zero and then increasing the time delay of the main discharge relative the pre–ionization discharge until a stable discharge was obtained. The measured delay value giving a stable discharge was 500 ns. That is,the main discharge must be 500 ns after the pre–ionization pulse as measured by the photo diode.

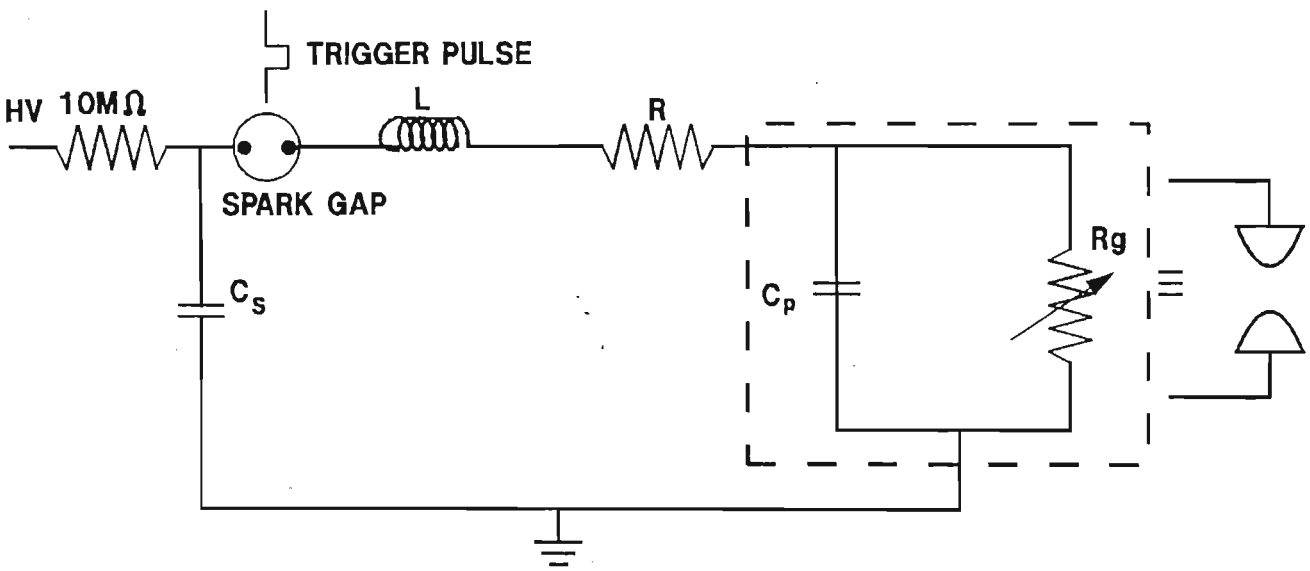

Figure 3.7. A schematic diagram of a typical C–C transfer circuit.

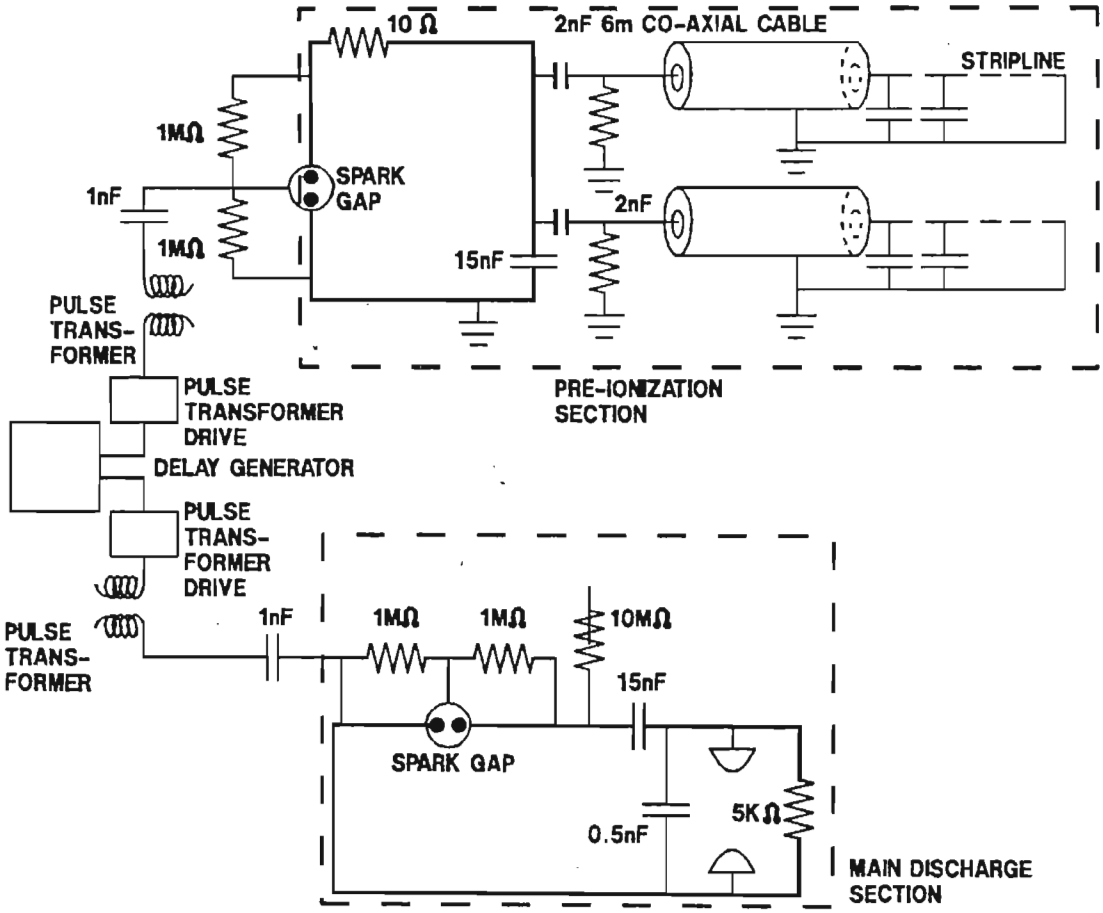

Figure 3.8. The laser discharge circuit used in this research project.

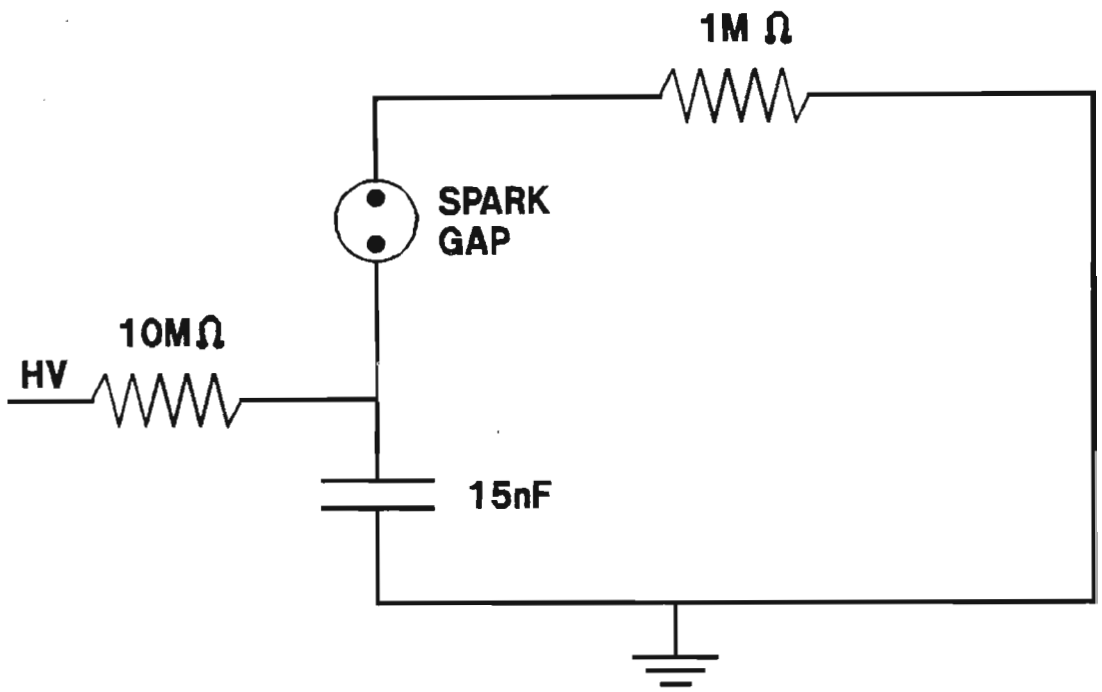

Figure 3.9. The circuit used for characterizing the spark gaps.

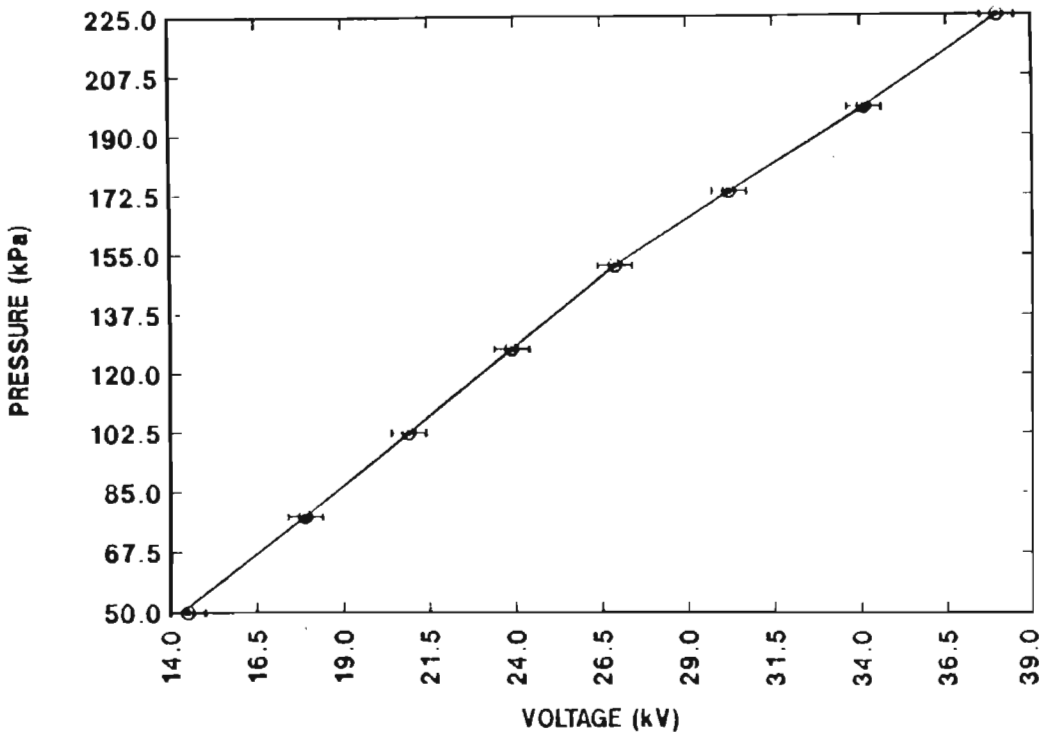

Figure 3.10. The characteristic curve of the spark gaps used in this project.

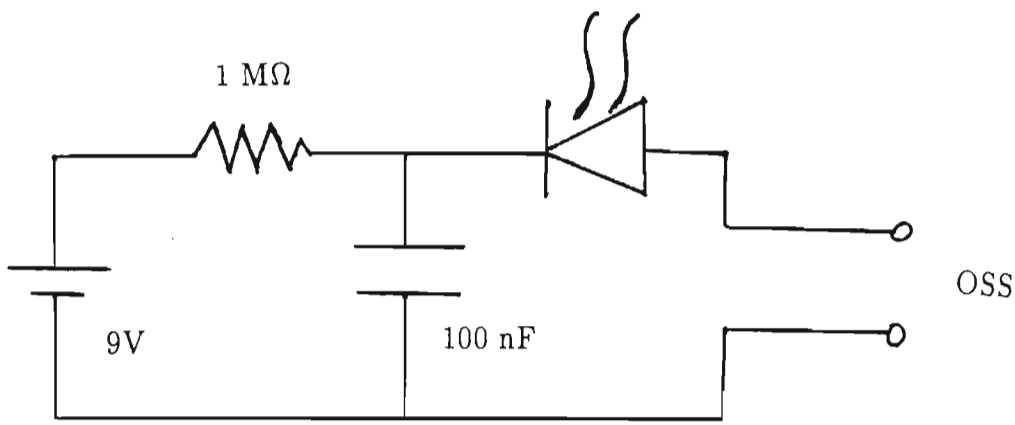

Figure 3.11. The photo diode circuit used.

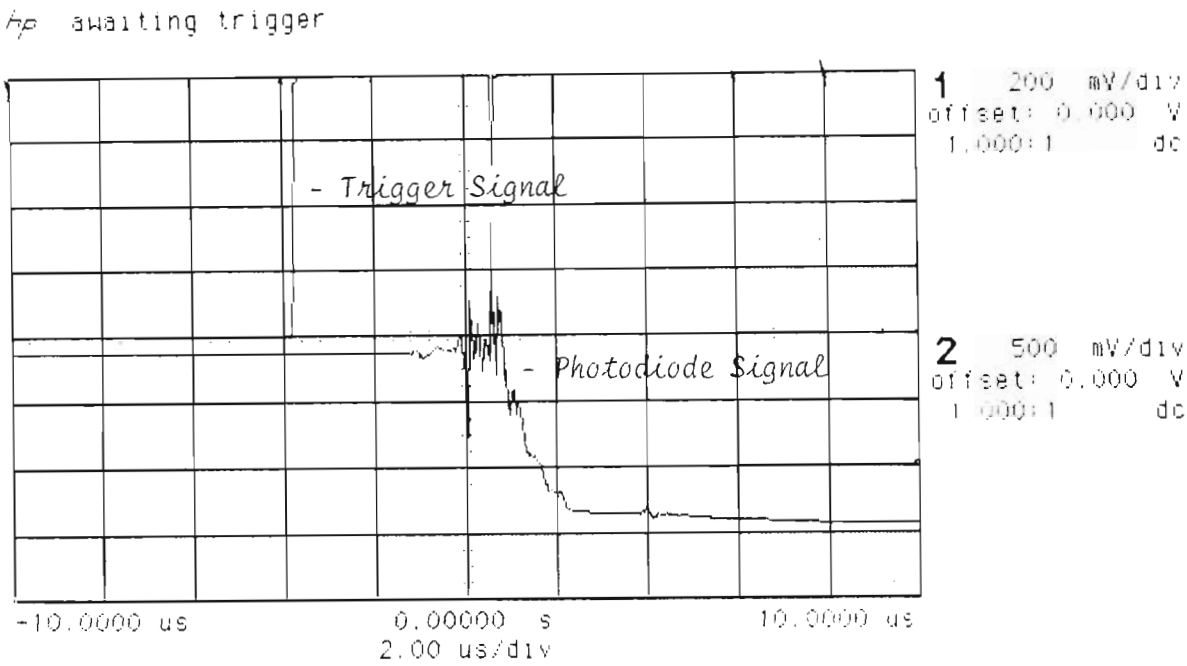

Figure 3.12. The photo diode signal relative to the trigger pulse. This is a photo diode signal of an arc in the main discharge.

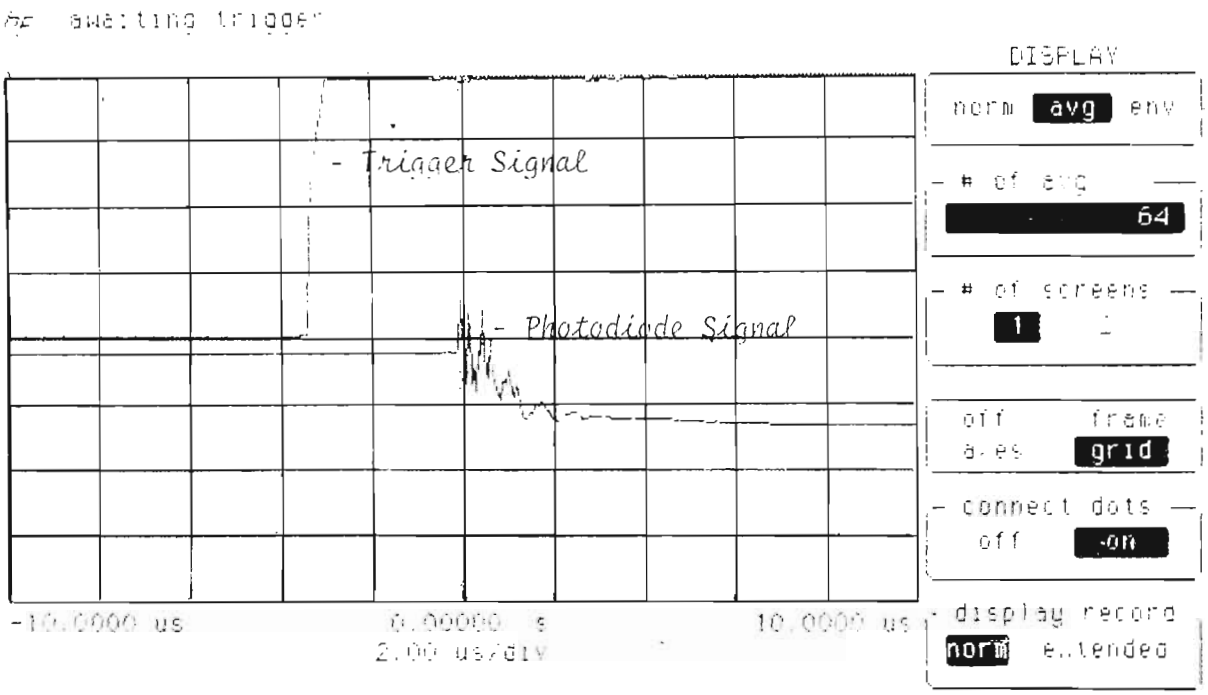

Figure 3.13. The photo diode signal relative to the trigger pulse. This is a photo diode signal of the pre–ionization pulse.

3.1.1.4 MECHANICAL DESIGN OF THE LASER

Because of the limited availability of $C^{18}O_2$ and the high cost factor a closed loop gas flow system had to be designed. The gas flow system is shown in figure 3.14. Gas flows up to 30 l/min could be achieved. The correct gas mixture was obtained by loading the gas fractions by partial pressures.

The laser head design is shown in figure 3.15. The pressure vessel consisted of two concentric PVC tubes. The rated maximum pressure at which these tubes could be operated was 10 atm. The tubes were sealed using o–rings and stainless steel flanges, refer to figure 3.15 and a photograph is shown in figure 3.16.

The resonator was supported on three invar rods, refer to figure 3.16 , and consisted of a 70% ZnSe output coupler with a 10m radius and a 150 l/mm original grating. The resonator design and analysis will be dealt with in chapter 4.

A nitrogen cold trap was incorporated into the gas flow system. The cold trap was used to freeze trap the CO_2 in the gas mixture. This was used to store the isotopic CO_2 when the laser had to be opened for repairs.

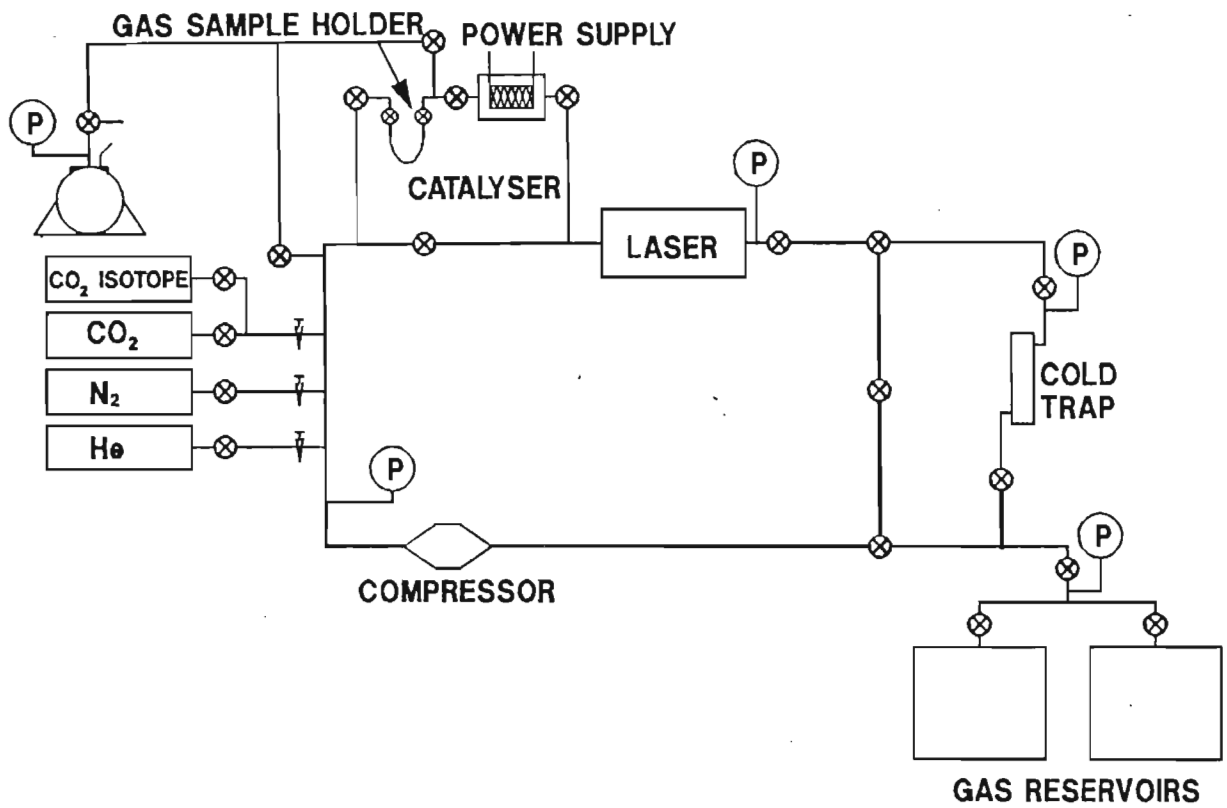

Figure 3.14. A schematic diagram of the closed loop gasflow system.

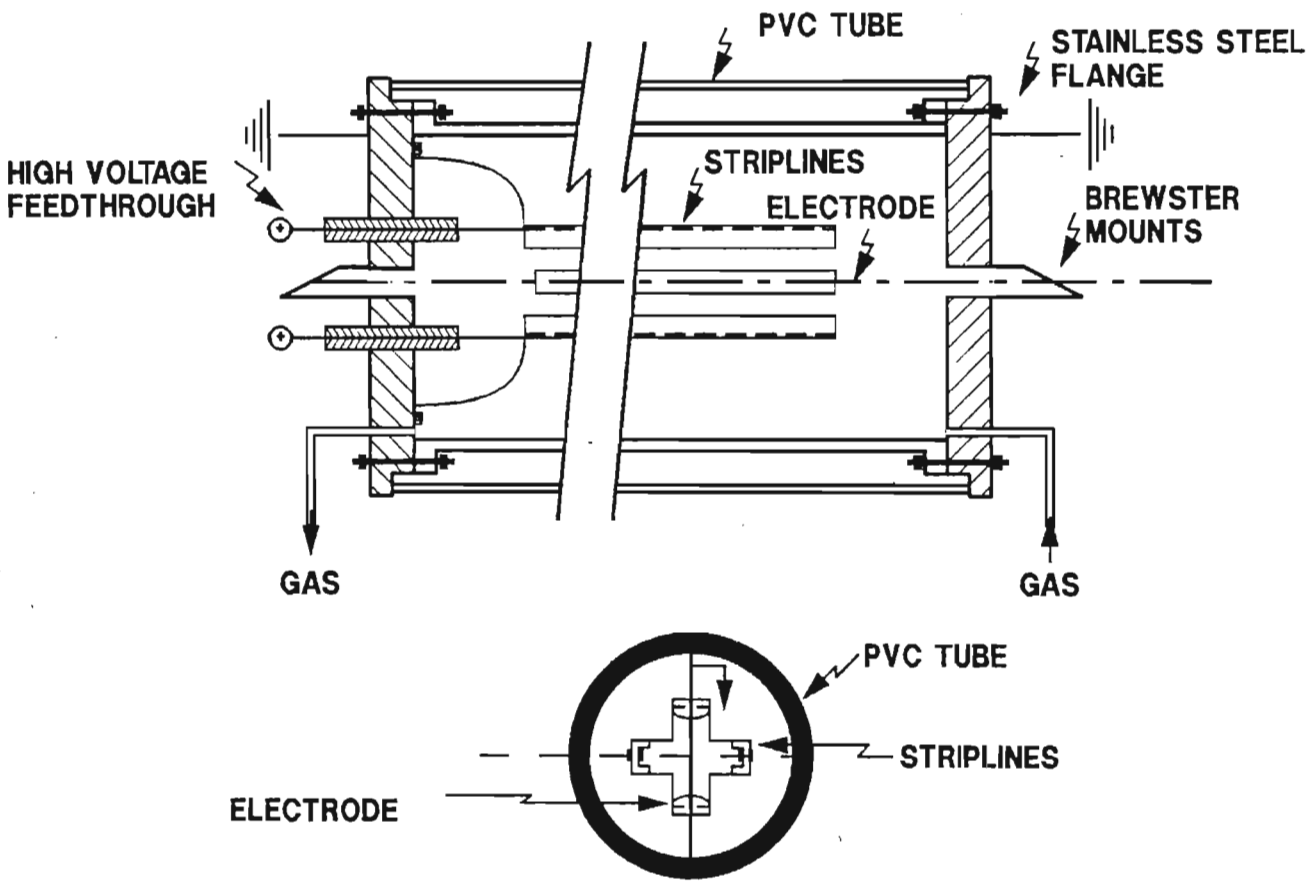

Figure 3.15. A schematic diagram of the laser head.

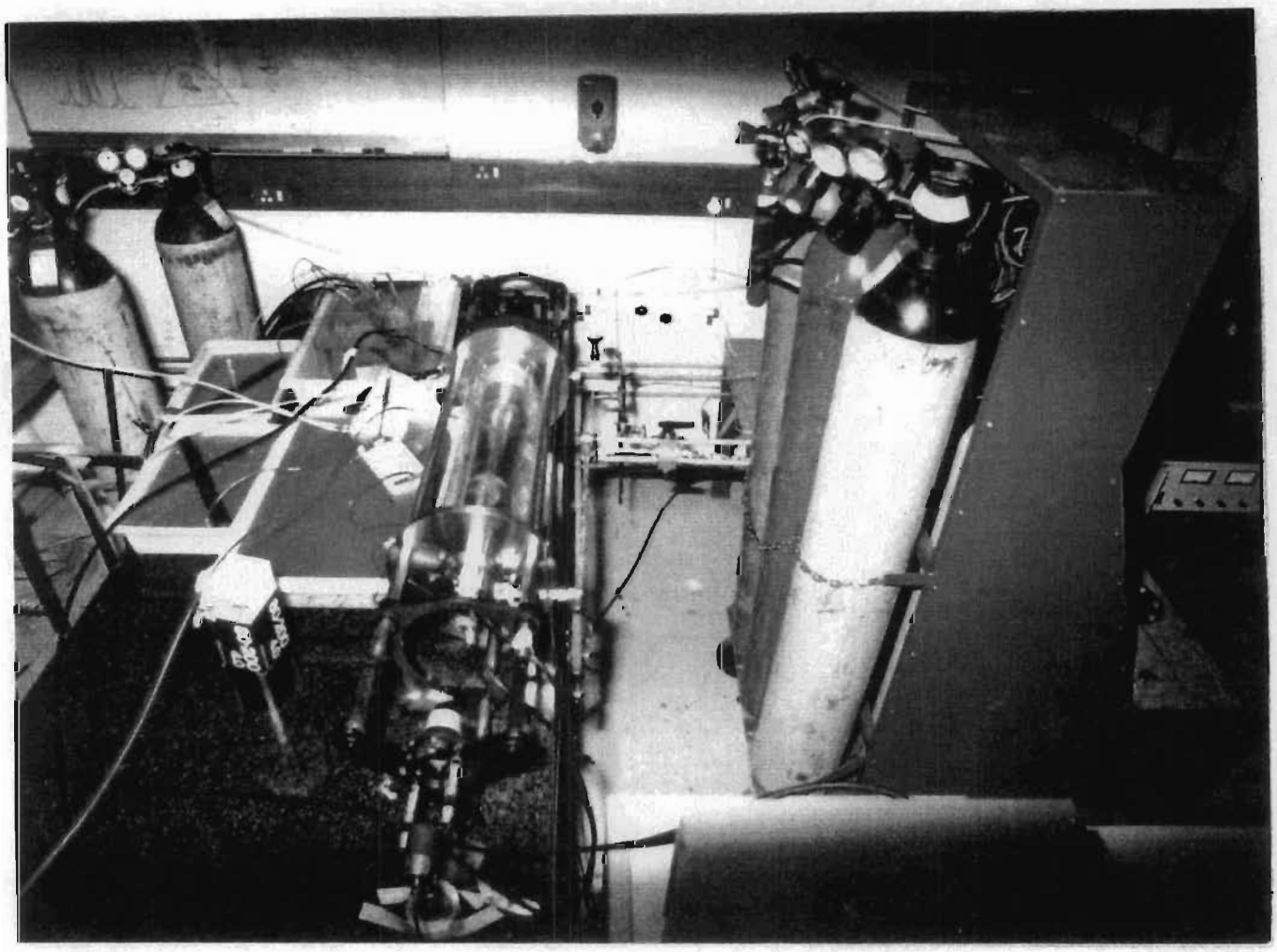

Figure 3.16. A photograph of the laser head, pulse forming network as well as a part of the gas flow section.

3.1.2 WAVELENGTH MEASUREMENT

The CO_2 wavelength was measured using two different techniques. One technique used a Czerny–Turner monochromator. A schematic diagram of this monochromator is shown in figure 3.17. This monochromator was calibrated using the P20 line of a low–pressure cw CO_2 laser. The measured resolution of the monochromator was better than 8 GHz thus better than $8x10^9/(cx100)$ wavenumbers. Thus the resolution of this monochromator was better than 0.27 wavenumbers.

The second method for measuring the wavelength was to use the micrometer readings at the back of the grating. The micrometer was used to adjust the grating angle of incidence. These readings were calibrated in the following manner:

A HeNe laser of a known wavelength ($632.8x10^{-9}$m) was directed down the áxis of the laser onto the grating. The grating was adjusted so that one of the grating orders was directed back along its path into the output aperture of the HeNe laser. The grating equation for the Littrow angle is given by :

$$2d\sin\theta=m\lambda \qquad 3.23$$

d: Separation between grooves.

θ: Grating angle of incidence.

m: Order.

λ: Wavelength of the incident radiation.

The 16th order of HeNe corresponds to $16 \times 632.8 \times 10^{-9}$m=10.125$\mu$m. The 17th order corresponds to 10.758μm. The grating was adjusted until the 16th order of the HeNe returned into the HeNe aperture and the micrometer reading was taken at this position say x_{16}. This was repeated for the 17th order, the micrometer reading was x_{17}. A linear fit between these two points was now done. This can be written as:

$$x_m = x_{16} + \frac{x_{17} - x_{16}}{\lambda_{16} - \lambda_{17}}(\lambda - \lambda_{16}) \qquad 3.24$$

With x_m the micrometer reading. The unknown wavelength λ can now be determined from equation (3.24) if the micrometer reading x_m is known.

The accuracy of this measurement technique was determined by the accuracy of the micrometer reading as well as the resolution of the grating used in the laser. The micrometer used was accurate to within 0.5 micrometer and the calculated resolution of the grating used in the laser was 5 GHz thus approximately 0.15 wavenumbers. Equation (3.24) can be written as:

$$\lambda = \lambda_{16} + \frac{\lambda_{16} - \lambda_{17}}{x_{17} - x_{16}}(x_m - x_{16}) \qquad 3.25$$

The experimental fault can be determined from equation (3.25) by taking the absolute value of its total derivative :

$$\Delta\lambda = \left|\frac{d\lambda}{d\lambda_{16}}\right|\Delta\lambda_{16} + \left|\frac{d\lambda}{d\lambda_{17}}\right|\Delta\lambda_{17} + \left|\frac{d\lambda}{dx_{17}}\right|\Delta x_{17} + \left|\frac{d\lambda}{dx_{16}}\right|\Delta x_{16} + \left|\frac{d\lambda}{dx_{m}}\right|\Delta x_{m} \qquad 3.26$$

Using the above mentioned values of 0.15 wavenumbers for $\Delta\lambda_{16}$ and $\Delta\lambda_{17}$ and 0.25 micron for Δx_{16}, Δx_{17} and Δx_{m} in equation (3.26) an experimental fault of 0.027 micron thus approximately 0.3 wavenumbers was calculated. A problem with this measurement technique was that it could not determine whether mode pulling was taking place.The monochromator was used to determine if mode pulling was taking place but this could also only be measured within the limitations, 0.27 cm^{-1}, of the monochromator. Better measurements of mode pulling would require a high resolution instrument like a Fabry–Perot interferometer.

The energy was measured using a Gentech pyro–electric energy meter. A pyro–electric detector uses the temperature dependence of the electric polarization of ferro–electric materials . A change in temperature causes a change in the electric polarization. The sensitivity of the meter was 2.4V/J. The variation in energy at a specific frequency was less than 10% of its average value at that frequency.

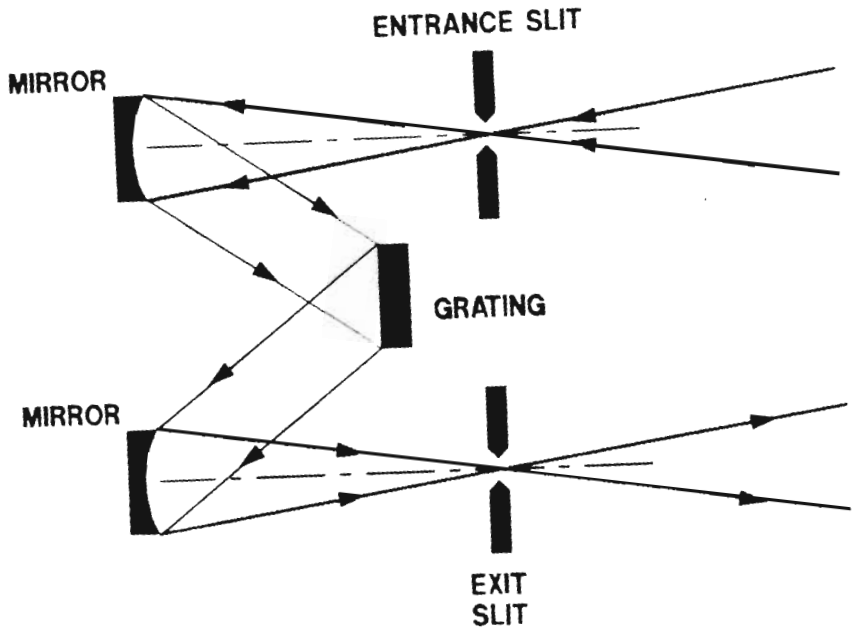

Figure 3.17. A schematic diagram of a Czerny–Turner monochromator.

3.2 RESULTS AND DISCUSSION

The first measurement was done on a 2.1 atm gas mixture of the following composition:1.7atm He,0.2 atm $^{12}C^{16}O_2$ and 0.2 atm N_2. The operating voltage for this test was 30 kV.The energy as a function of wavenumber is shown in figure 3.18. Continuous tunability could not be achieved at any wavelength. The measured half width of the individual lines was found to be approximately 9.7 GHz which is close to the published value of 10.5 GHz for this mixture and pressure.

Figure 3.19 gives two curves. One of $^{12}C^{16}O_2$ and one of $^{12}C^{18}O_2$. The gas mixtures were the same as in the first mixture. The isotope shift can be seen and was measured to be approximately 130 GHz between the two R18 lines. This agrees well with the published [51] value of 128 GHz.

Figure 3.20 gives the measured energy values at different frequencies for the following mixture: 1.7 atm He, 0.2 atm N_2, 0.1 atm $^{12}C^{18}O_2$and 0.1 atm $^{12}C^{16}O_2$. Continuous tuning was possible from the R14 to the R24 line. There was –however– big differences in energy between the on and off line center values. The energy varied from 155 mJ at the peak of the R18 line to 15 mJ at the between line center value.The operating voltage was 31.5 kV.

Figure 3.21 gives the energy values from the R24 to the R32 line for the following mixture: 2.1 atm He, 0.3 atm N_2 O.2 atm $^{12}C^{18}O_2$ and 0.2

atm $^{12}C^{16}O_2$.Continuous tunability was now possible down to the R30 line, again with the big difference in the on and off line center values.The operating voltage was 36 kV. The theoretically calculated gain curve of this mixture is shown in figure 3.22.

The calculations done in chapter 2 have predicted that the optimum isotopic mixture would be a mixture where the CO_2 component consisted of the following isotopes: 25% $^{12}C^{18}O_2$, 50% $^{12}C^{18}O^{16}O$ and 25% $^{12}C^{16}O_2$. Only the single isotope CO_2 gases were available and it was decided to investigate the possibility of manufacturing $^{12}C^{18}O^{16}O$ in the laser discharge.A fraction of the CO_2 is dissociated into CO and O_2 in the gas discharge. A catalyst can thus be used to catalytically recombine the CO and O_2 to form CO_2. This process could be used to manufacture $^{12}C^{18}O^{16}O$. This would happen when the laser is operated with a mixture of $^{12}C^{18}O_2$ and $^{12}C^{16}O_2$ in a closed loop gasflow system which incorporated a catalyst . Isotopic scrambling would occur in the recombination process and after many cycles the equilibrium concentration of 25% $^{12}C^{18}O_2$, 50% $^{12}C^{16}O^{18}O$ and 25% $^{12}C^{16}O_2$ would be reached.

The catalyst used in this process was a platinum mesh since the oxygen in catalysts like $PtSnO_3$ would exchange with the ^{18}O oxygen and after many cycles of operation an equilibrium between the ^{18}O in the gas and that in the catalyst would be reached causing a significant loss of ^{18}O.

The rate of CO production was determined by operating a laser with a

gas mixture consisting of 1.7 atm He, 0.2 atm N_2 and 0.2 atm $^{12}C^{16}O_2$ The laser was operated at 1 Hz at a voltage of 27 KV. Gas samples were taken at 0,1000 and 2000 shots. The gas samples were analyzed on a mass spectrometer. The result of this analysis is shown in figure 3.23. These tests were repeated with a catalyst in the flow system. The catalyst was a platinum wire mesh which was resistively heated by applying a potential difference of 2 V across the mesh and this caused a 30A current . The influence of the catalyst is shown in figure 3.23. As can be seen from these graphs many thousands of shots would be needed to reach the equilibrium concentration.

The laser was operated at 1 Hz and 27 kV for an extended period using a gas mixture consisting of 2.0 atm He, 0.2 atm N_2 ,0.15 atm $^{12}C^{18}O_2$ and 0.15 atm $^{12}C^{16}O_2$. The experiment had to be abandoned at approximately 8000 shots because of the occurrence of severe arcing. It was assumed that this arcing was caused by impurities which were deposited into the gas by the pre–ionization process. No arcing was experienced when the laser was evacuated and the gas was replaced by fresh gas mixture. This experiment was repeated twice with the same results. A gas analysis showed no excessive CO in the mixture which supported the suspicion that impurities in the gas caused the arcing. The experiment had to be abandoned because of the limited amount of $^{12}C^{18}O_2$ available.

Using these experimental and theoretical results the following conclusions could be made:

(i) Continuously tunable operation of a mixed isotope $^{12}C^{18}O_2$ and $^{12}C^{16}O_2$, on the 10μm R branch, was obtained with a big difference between the on and off line center energy values. At 2.7 atm continuous operation was obtained from the R14 to the R30 line.

(ii) The calculated gain curve of the mixture 50% $^{12}C^{16}O_2$ and $^{12}C^{18}O_2$ is shown in figure 3.22. The calculated gain curves for the mixture 50% $^{12}C^{18}O^{16}$, 25% $^{12}C^{16}O_2$ and 25% $^{12}C^{18}O_2$ for 4 and 3 atm respectively are shown in figures 2.7 and 2.8. If figure 2.8 is compared with figure 3.22, it can be seen that the difference between the on and off line center values shown in figure 2.8 is much less than that shown in figure 3.22. Since continuous tunability has been achieved by the curve shown in figure 3.22 it can, with confidence, be said that continuous tunability would be achieved with the equilibrium concentration with less difference between the on and off line center values.

Thus a continuously tunable CO_2 laser could be built at a pressure of approximately 3 atm using isotopic mixtures. As has been mentioned this laser would have many advantages over a 10 atm CO_2 laser. This laser could be operated at about 30% the voltage of a 10 atm laser. This would mean that the requirements on the pulse forming network would be less severe and it would also simplify the pre–ionization techniques. The pressure vessel would be much simpler and it would be much cheaper to pump the 3 atm than the 10 atm gas.

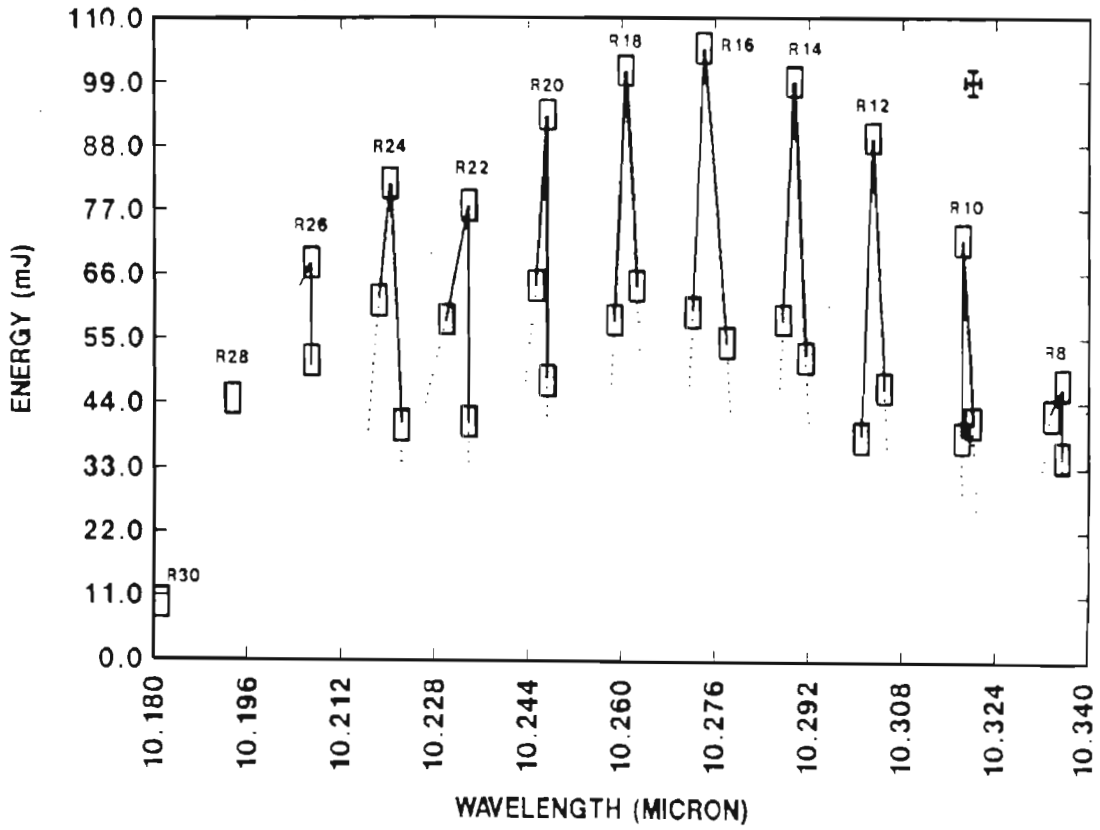

Figure 3.18. The energy as a function of wavelength of the 10μm R branch of CO_2. This was measured at 2.1 atm using $^{12}C^{16}O_2$.

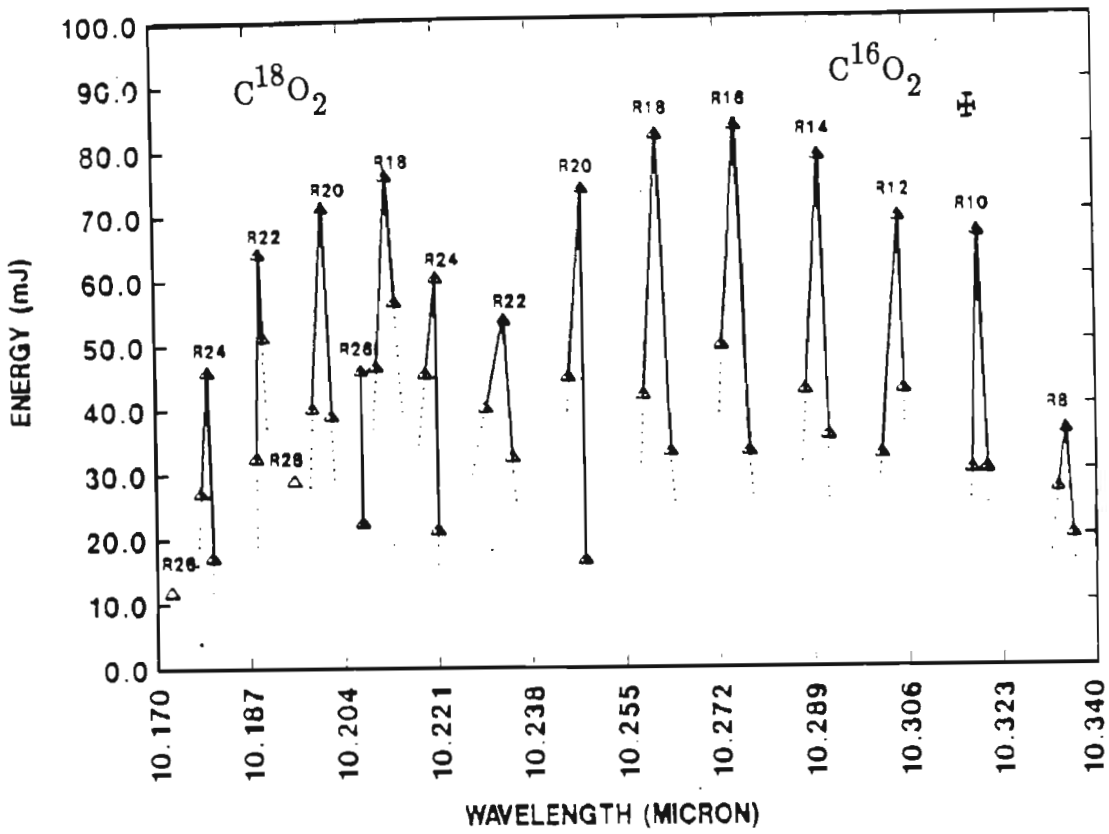

Figure 3.18. The energy as a function of wavelength of the 10μm R branch of $^{12}C^{16}O_2$ and $^{12}C^{18}O_2$ This was measured at 2.1 atm.

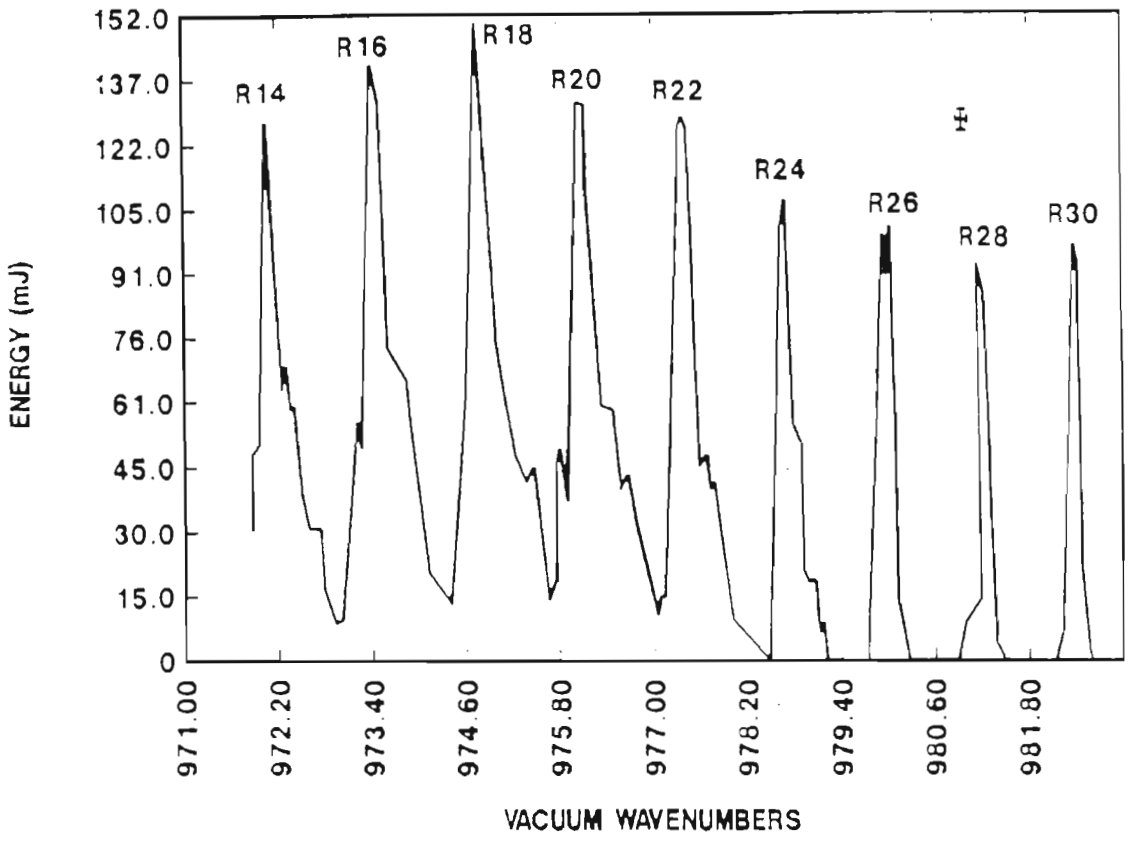

Figure 3.20. The energy as a function of wavelength of the 10μm R branch of an isotopic mixture consisting of 50% $^{12}C^{16}O_2$ and 50% $^{12}C^{18}O_2$. This was measured at 2.1 atm.

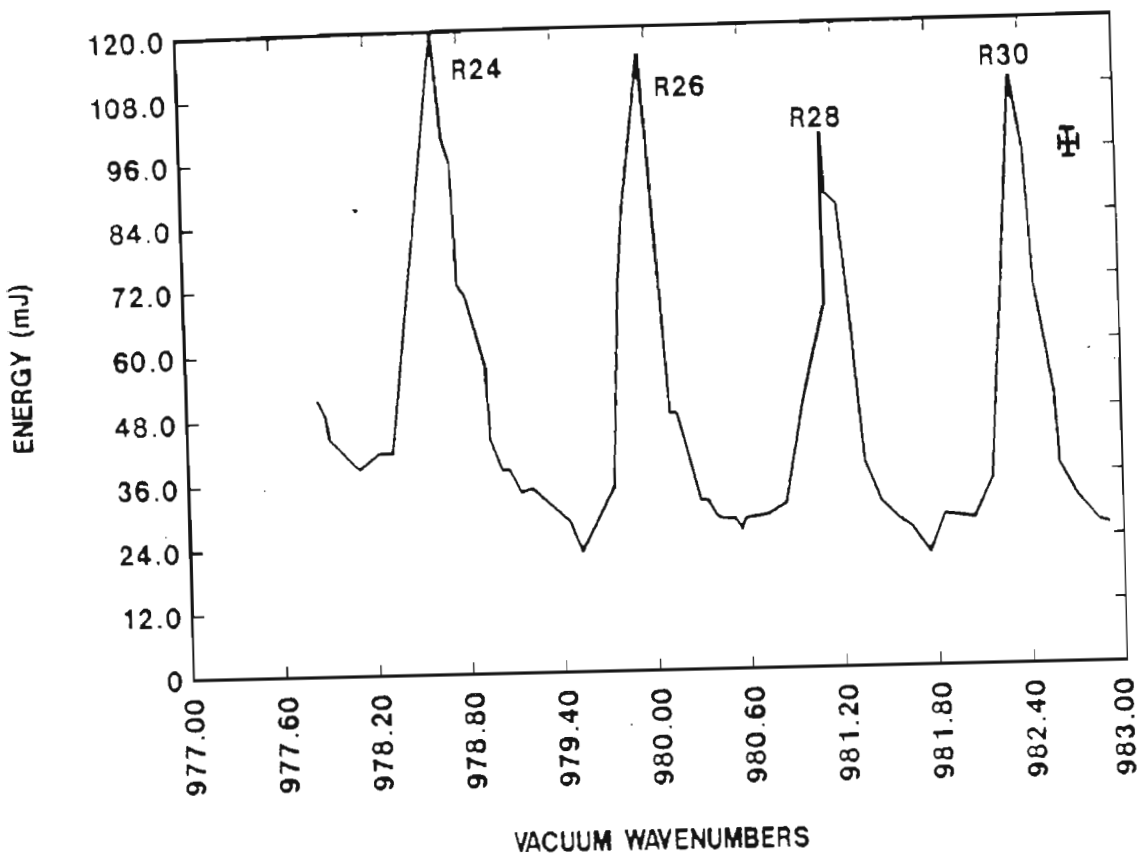

Figure 3.21. The energy as a function of wavelength of the R24 to R28 lines of the 10μm R branch of an isotopic mixture consisting of $50\%\ ^{12}C^{16}O_2$, $50\%\ ^{12}C^{18}O_2$. *This was measured at 2.8 atm .*

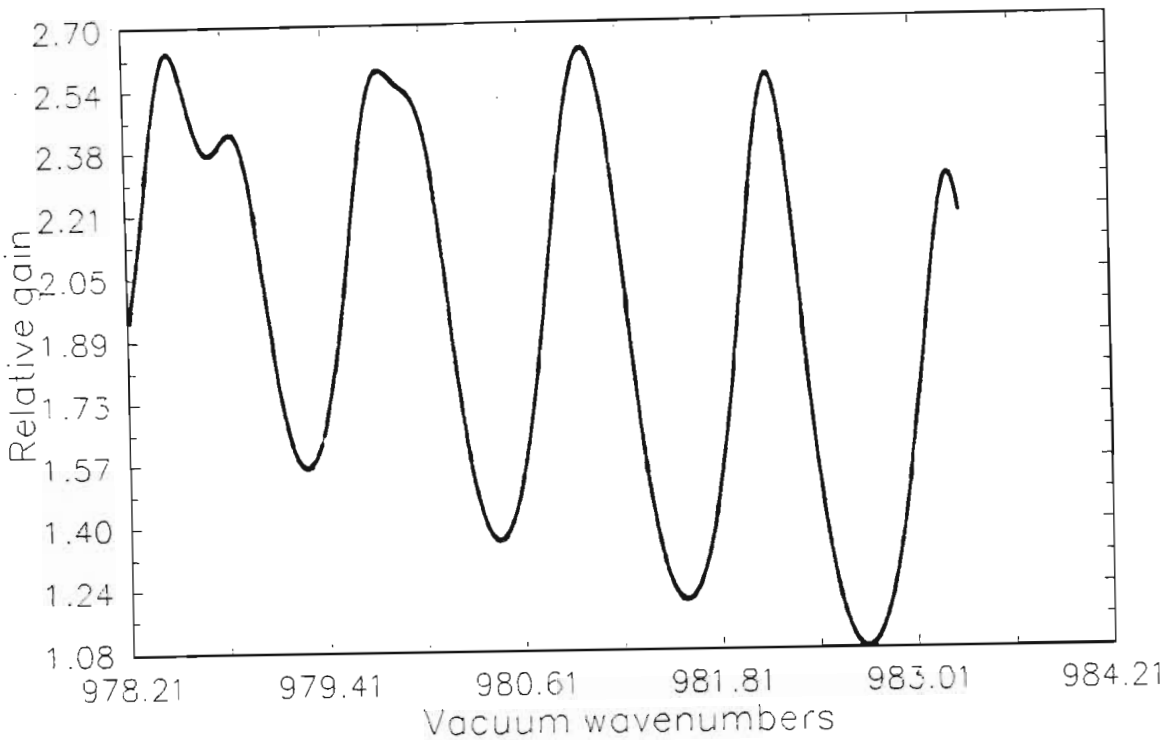

Figure 3.22. The theoretically calculated gain curve of the 10μm R branch of an isotopic mixture consisting of 50% $^{12}C^{18}O_2$ *and 50%* $C^{18}O^{16}O$*. The pressure is 2.8 atm.*

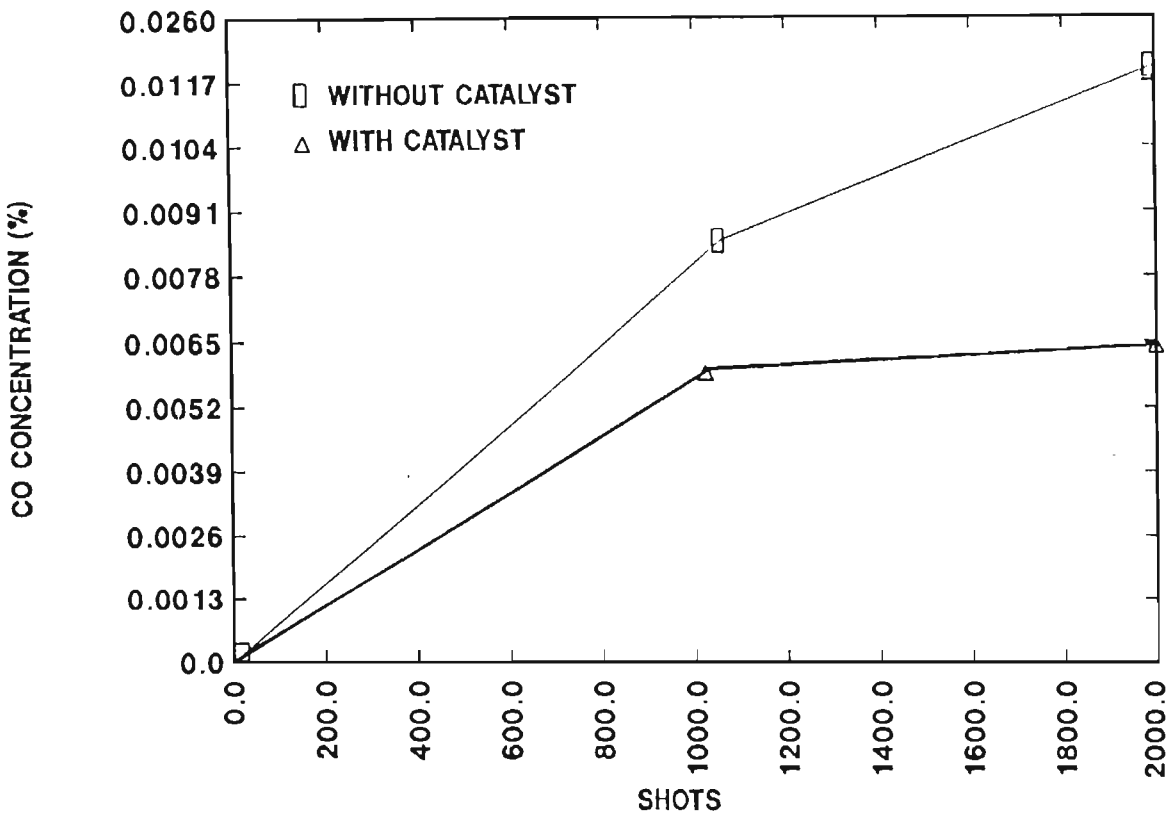

Figure 3.23. CO production as a function of the number of laser shots. Results obtained, with and without, a platinum wire catalyst is shown.

CHAPTER 4

RESONATOR ANALYSIS

4.1 GAUSSIAN OPTICS

In a typical laser resonator the laser beam has a finite transverse dimension (x,y) and propagates in the z direction. An accurate treatment of optical beams and laser resonators must take diffraction and the wave nature of light into account. Ray optics – by which is meant the geometrical laws for optical ray propagation without including diffraction– are not accurate enough to predict observed phenomena. Practical laser beams are almost always well enough collimated that their diffraction properties can be described using a scalar wave equation. If the Maxwell equations are solved using the following assumptions:

(i) The field has a transverse dependence on $r=(x^2+y^2)$.

(ii) The flow of energy is predominantly along a single (e.g. z) direction.

The following solution for the electric field is obtained [30]:

$$E_{l.m}(x,y,z)=_0\frac{\omega_0}{\omega(z)}H_l\left[\sqrt{2}\frac{x}{\omega(z)}\right]H_m\left[\sqrt{2}\frac{y}{\omega(z)}\right]x$$

$$e^{\left[\frac{x^2+y^2}{\omega(z)}-i\frac{k(x^2+y^2)}{2R(z)}-ikz+i(l+m+1)\eta\right]} \qquad 4.1$$

Where H_l is the Hermite polynomial of order l.

$$\omega^2(z) = \omega_0^2\left[1+\frac{z^2}{z_0^2}\right] \qquad 4.2$$

$$R = z\left[1+\frac{z_0^2}{z^2}\right] \qquad 4.3$$

$$\eta(z) = \arctan\,(z/z_0) \qquad 4.4$$

$$z_0 = \frac{\pi\omega_0^2 n}{\lambda} \qquad 4.5$$

ω_0 is the minimum spot size.

Examples of different order Gaussian beams are given in figure(4.1).The zero order Gaussian beam is given by :

$$E_{00}(x,y,z)=E_0\frac{\omega_0}{\omega(z)}e^{-i[kz-\eta(z)]-r^2[1/\omega^2(z)+\frac{ik}{2R(z)}]} \qquad 4.6$$

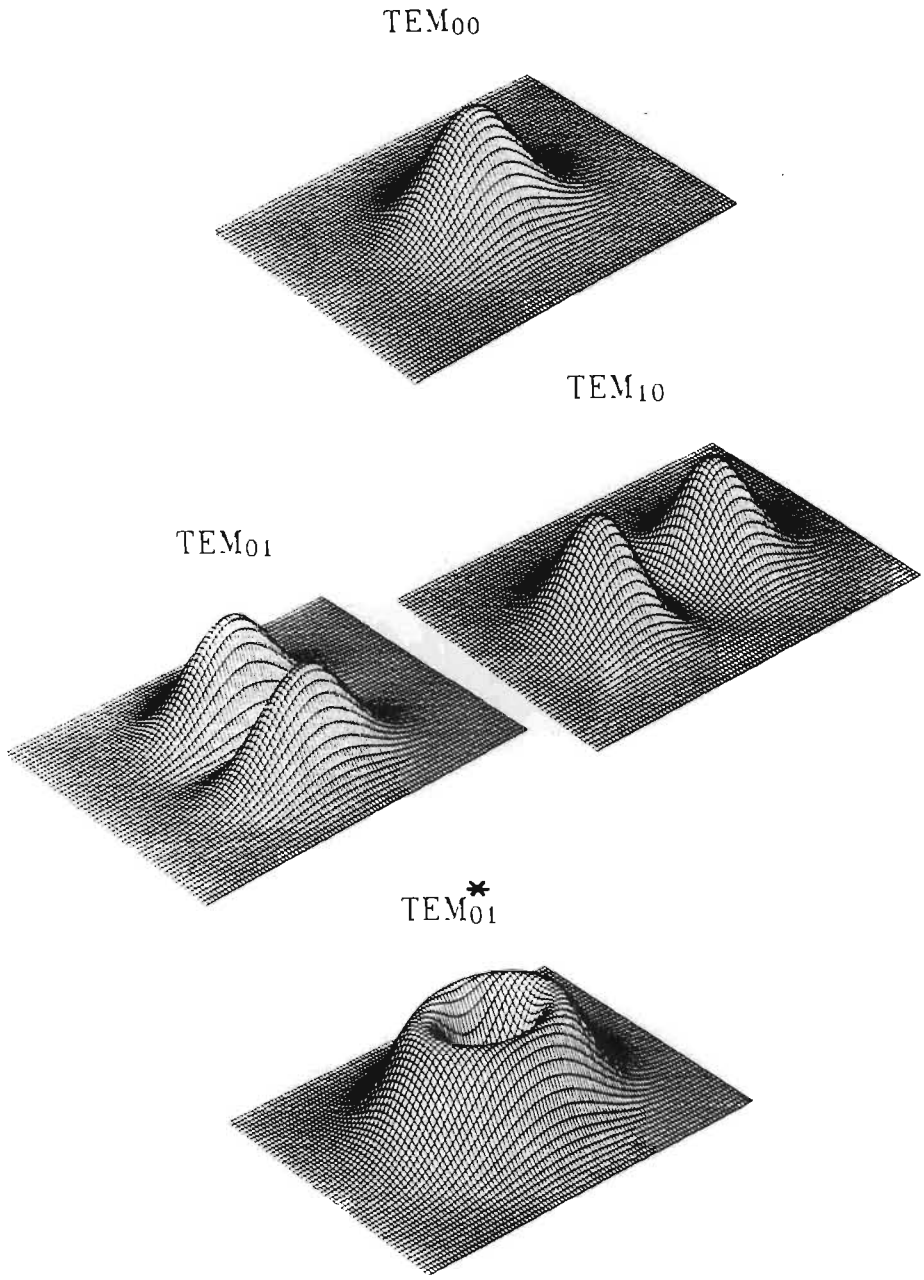

Figure 4.1. The intensity distribution various transverse modes.

4.2 ANALYSIS OF THE OPTICAL RESONATOR

Optical resonators are needed for two related main purposes:

(i) To build up large field intensities at specified (resonance) frequencies.

(ii) To act as spatial and frequency filters responding selectively to fields with prescribed spatial variation and frequency.

A closed cavity with perfectly conducting walls has an infinite number of modes with different frequencies. If we want only one mode to resonate within a fairly wide frequency band, the size of the cavity must then be of the same order of magnitude as the desired wavelength. This is practically impossible to achieve at optical frequencies. This multimode situation is to be avoided in the case of lasers since it will cause the atoms/molecules to emit power into a large number of modes which may differ in their frequencies as well as their spatial characteristics. To a large extent this is overcome by the use of open resonators, which consists of an opposing pair of flat or curved mirrors. In such a resonator the energy of the majority of the modes does not travel at right angles to the mirrors and will thus be lost in a single transversal.

Two different types of modes are usually found in a laser resonator; the so called "transverse" and "longitudinal" modes. The existence of transverse modes can be understood in the following way: Suppose a pulse (or "slab") of radiation makes one complete round trip around an optical cavity. After one complete round trip the transverse field pattern $E^1(x,y)$ within a given "slab" as it arrives back at its starting plane will in general be different from its starting pattern $E^0(x,y)$. This is caused by diffraction, reflection and aperturing effects. After a second round trip the pattern $E(x,y)$ may again be still different. The question can then be asked " Does there exist any transverse patterns say $E_{nm}(x,y)$ such that if the pulse starts off with one of these transverse patterns , it will return one round trip later with exactly the same pattern ?" More precisely it is required that the pulse of radiation must return with exactly the same transverse form , but possibly with a reduced amplitude because of diffraction and other losses in the cavity. If such self–reproducing transverse patterns can be found, it seems reasonable to call them transverse modes of the resonator. If enough laser gain is added within the resonator to just cancel the diffraction losses, it would seem that the resonator could oscillate indefinitely in any one of these transverse modes. It can be shown [30] that such modes do exist if the resonator satisfies the so–called stability criterion:

$$0 \leq (1-l/R_1)(1-l/R_2) < 1 \qquad 4.7$$

Where l is the length of the resonator and R_1 and R_2 are the radii of the two mirrors of the resonator respectively. These transverse modes are the same as the Hermite–Gaussian mode given in equation (4.1) and shown in figure 4.1 These transverse modes were first calculated by Fox and Li [73]. They calculated the iterative round trips of a wave front E(x,y) by using a numerical computation on a digital computer.

The longitudinal modes of a resonator are the so–called axial modes of resonator. These modes are determined by the requirement that the complete round trip phase shift of the resonator must be some multiple of 2π. This makes it possible for a stable standing wave pattern to establish itself along the axis with a transverse field distribution equal to that of the propagating mode.The longitudinal mode whose frequency is located closest to the center of the atomic/molecular transition will see the highest gain and will thus reach oscillation threshold first, before the other modes located further from the atomic/molecular line center. Suppose that the gain or the pump power is turned on still further , beyond the point where the first cavity mode reaches threshold. Will additional modes then also begin oscillating ? The answer to the question depends on whether a homogeneously broadened or an inhomogeneously broadened line is considered.

As was mentioned in section 2.2.2 in an ideally homogeneous laser transition the atomic/molecular lineshape is fixed and

identical for all the atoms/molecules in the laser medium. The magnitude of the gain and the phase shift measured at any given frequency will move up and down as the population inversion ΔN varies; but the lineshape $\chi'(\omega)$ and $\chi''(\omega)$ will remain unchanged– the whole lineshape moves up and down together.

Suppose the midband gain in a homogeneously broadened transition is increased until the axial mode closest to line center just reaches threshold (the gain equals the losses). This mode , say q, can then begin to oscillate whereas all the other modes (q–1,q+1,q+2, etc) are still below threshold and cannot oscillate. Even if the laser is pumped harder the gain profile cannot be pushed further up to cause modes q–1 or q+1 to start oscillating. Such oscillations are not possible on a CW or steady–state basis because the gain of the q th mode would exceed the losses and this mode would grow on successive round trips. It may be possible to push the gain of several modes above the steady–state or threshold value on a transitional basis during initial turn on or in the pulsed operation of a laser. This is what typically happens in a pulsed high pressure CO_2 laser. As was mentioned in section 2.3. the gain of a high pressure CO_2 laser is homogeneously broadened. In a pulsed CO_2 laser the gain is turned on very rapidly using a fast pulse of pumping current. This fast pumping pulse may cause the population difference to go considerably above threshold before the laser oscillation has time to build up from the initial background

noise level [2]. This kind of behaviour is known as gain switching. This may cause several modes to be above threshold so that multimode operation of a pulsed CO_2 laser is possible.

Whereas an homogeneously broadened CW laser will tend to oscillate in only one mode, an inhomogeneously broadened laser can oscillate in many longitudinal modes at the same time, with each mode oscillating almost independently of all the other modes. This is caused by the so called hole burning in the gain curve, the laser "burns a hole" in the gain curve and saturates the gain down to equal loss at each oscillating mode separately.

Another factor that can lead to multimode operation, even in a homogeneously broadened CW laser, is spatial inhomogeneity, and especially spatial hole burning.Suppose a linear standing wave laser is initially oscillating in the q–th axial mode. This leads to a standing wave pattern for the field amplitude or optical intensity along the z axis, with peaks and nulls spaced by one half optical wavelength. The inverted population in the laser will then be saturated in a similar spatially periodic fashion. One of the effects of this saturation will be to produce a spatial inverted population grating or gain grating. The standing wave pattern of the (q+1)–th mode –which squeezes one more half optical wavelength into the cavity length– will have its maximum intensity located just at the points that are left unsaturated by the q–th mode. As a result of this two adjacent axial modes may well be able to oscillate simultaneously, even

with a strongly homogeneous laser medium.

Considerable work has been done on resonators to provide single longitudinal mode continuous tunability for a high pressure CO_2 laser[13–20]. Such a resonator must provide tunability over a broad range as well as a narrow bandwidth. A further requirement is to protect the high resolution elements, the etalon and grating, from damage by the high power density inside the resonator.

The simplest way of tuning a CO_2 laser is to use a grating in the Littrow arrangement[13]. This will give tuning over a broad range but will not realise the narrow bandwidth required for single mode operation. To narrow the bandwidth of this resonator an intra–cavity etalon can be used[15] but this would expose the etalon to the high power density inside the resonator. Another solution could be to use an intra–cavity beam expander[16] to reduce the power density on the etalon and grating and to increase the illuminated area on the grating, thus increasing the resolution of the grating. A problem with using the beam expander is that it introduces more losses in the system thus reducing its effectivity [16]. Because a beam expander at 10.6 μm is rather bulky it increases the length of the resonator and thus increases the diffraction losses, as was found by Deka, Rob and Izatt[16]. Another problem with a beam expander is that it is very difficult to align the system. A way of increasing the effective illuminated area on a grating

without using an intra–cavity beam expander is to use the grating in near grazing incidence. Dyer and Raouf [17] used this configuration and achieved a bandwidth of approximately 0.9 GHz. A disadvantage of this system is the low effective reflectivity of the grating with a standard blaze. A different solution is to use the so called three mirror resonator as shown in figure 4.2, consisting of a partial reflector, a grating and sometimes an etalon. This is also called a MGC (mirror grating combination). Deka, Dyer and Winfield [19] used a MGC without an etalon to achieve single longitudinal mode operation, however this required the use of a short gain length device operated near threshold. This resulted in a low P20 energy output of around 20 mJ per pulse. Deka,Rob and Izatt[16] did a comparative study using an intra–cavity beam expander and a MGC (not single mode). They found that the output of the laser with the MGC was approximately 40% higher than with the beam expander. A MGC resonator with an etalon was thus chosen for this project.

In this thesis a numerical model was developed to describe the behaviour of a MGC with an etalon. The thermal stability of the laser using this resonator was calculated. The model can be used to determine MGC parameters like etalon thickness, reflectivity and sub–resonator length. The first step in the development of this model was to derive an equation for the wavelength selective reflection of the MGC. In this derivation, the wavelength dependent reflection of a blazed diffraction

grating as well as the wavelength dependent transmission of the etalon were used. Using this wavelength dependent reflection a mode discrimination relation was derived and this was used to determine whether a specific resonator would ensure single longitudinal mode operation.

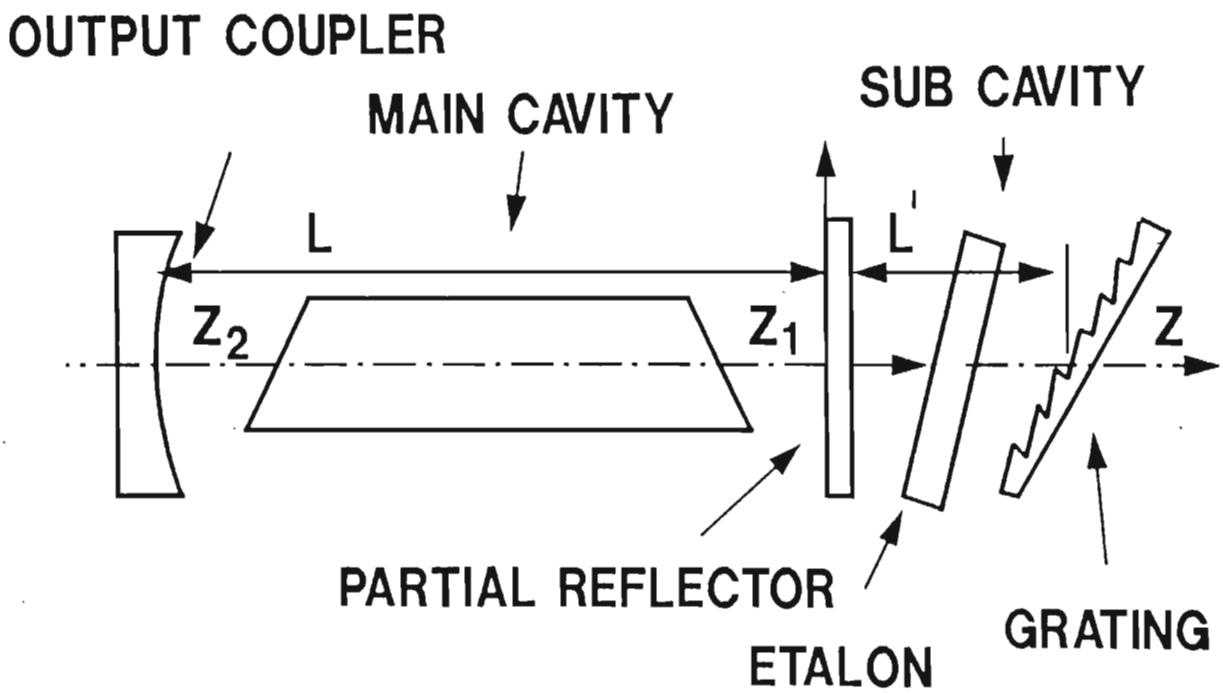

Figure 4.2. A schematic diagram of a three mirror resonator.

4.2.1 WAVELENGTH DEPENDENT REFLECTION OF A MGC WITH AN ETALON.

The wave front inside the resonator has been approximated by a plane wave. Since the region where the derivation takes place is close to the beam waist, and the beam divergence is small, this is not a bad approximation.Let r_1 be the amplitude reflection coefficient of mirror 1 in fig 4.3 and t_1 the amplitude transmission coefficient of mirror one. t_e is the amplitude transmission function of the etalon and will be derived .r_g is the amplitude reflection coefficient of the grating and this will be derived later. Mirror one is a partially reflecting mirror with a anti–reflection coating on the inside and a metallic coating on the outside. The incident medium has a lower index of refraction than the transmitting medium thus the component of the electric field normal to the plane of incidence will undergo a π phase change upon reflection from the grating [74]. E_{1r} in fig 4.3 will also undergo a π phase change. Let the incident field be given by E_0 where:

$$E_0(t)= E_0 e^{i\omega t} \qquad 4.8$$

Here t is the time and $\omega=2\pi f$ is the frequency of the incident radiation. If δ' is the phase shift undergone by a beam after it has moved through an empty sub–resonator then:

$$E_{1r}(t)=E_0 r_1 e^{i\pi} e^{i\omega t} \qquad 4.9$$

$$E_{2r}(t)=E_0 t_1^2 t_e^2 r_g e^{i\pi} e^{i(\omega t+\delta')} \qquad 4.10$$

$$E_{3r}(t)=E_0 t_1^2 t_e^4 r_g^2 r_1 e^{i2\pi} e^{i(\omega t+2\delta')} \qquad 4.11$$

$$E_{4r}(t)=E_0 t_1^2 t_e^6 r_g^3 r_1^2 e^{i3\pi} e^{i(\omega t+3\delta')} \qquad 4.12$$

etc

δ' is given by:

$$\delta' = \frac{4\pi}{\lambda} L' \qquad 4.13$$

L' is the length of the sub–resonator shown, in figure 4.2 and λ is the wavelength of the radiation.The resultant reflected field is given by E_r where:

$$E_r = E_{1r}+E_{2r}+E_{3r}+E_{4r}+.... \qquad 4.14$$

$$=E_0 e^{i\pi} e^{i\omega t}[\ r_1+t_e^2 t_1^2 r_g e^{i\delta}+t_e^4 t_1^2 r_g^2 r_1 e^{i\pi} e^{i2\delta}+t_e^6 t_1^2 r_g^3 r_1^2 e^{i2\pi} e^{i3\delta}+....]$$

$$=E_0 e^{i\omega t}(-1)[r_1+t_1^2 t_e^2 r_g e^{i\delta}[1+t_e^2 r_g r_1 e^{i\pi} e^{i\delta}+(t_e^2 r_g r_1 e^{i\pi} e^{i\delta})^2+....] \qquad 4.15$$

This is a geometric series and can be simplified to :

$$E_r = E_0 e^{i\omega t}(-1)\left[r_1 + t_1^2 t_e^2 r_g e^{i\delta'}\left[\frac{1}{1 - t_e^2 r_g r_1 e^{i\pi} e^{i\delta'}}\right]\right] \qquad 4.16$$

The reflected intensity is given by :

$$I_r = E_r E_r^*$$

$$= E_0^2\left[r_1 + \frac{t_1^2 t_e^2 r_g e^{i\delta'}}{1 + t_e^2 r_g r_1 e^{i\delta'}}\right]\left[r_1 + \frac{t_1^2 t_e^2 r_g e^{-i\delta'}}{1 + t_e^2 r_g r_1 e^{-i\delta'}}\right] \qquad 4.17$$

According to Stoke's relations $t_1^2 = 1 - r_1^2$ thus :

$$I_r = E_0^2\left[\frac{r_1^2 + 2 r_1 t_e^2 r_g e^{-i\delta'} + r_1 t_e^2 r_g e^{i\delta'} + t_e^4 r_g^2}{1 + 2 t_e^2 r_g r_1 \cos\delta' + t_e^4 r_g^2 r_1^2}\right]$$

$$= E_0^2\left[\frac{r_1^2 + 2 r_1 t_e^2 r_g \cos\delta' + t_e^2 r_g^2}{1 + 2 t_e^2 r_g r_1 \cos\delta' + t_e^4 r_g^2 r_1^2}\right] \qquad 4.18$$

$$= E_0^2\left[\frac{R_1 + 2\sqrt{R_1}\sqrt{R_g} T_e \cos\delta' + T_e^2 R_g}{1 + 2 T_e \sqrt{R_g}\sqrt{R_1} \cos\delta' + T_e^2 R_g R_1}\right] \qquad 4.19$$

With:

$R_1 = r_1^2$ the intensity reflection coefficient of mirror 1 in fig 4.3

$R_g = r_g^2$ the intensity reflection coefficient of the grating in fig 4.3

$T_e = t_e^2$ the intensity transmission coefficient of the etalon in fig 4.3

R_g and Te will be derived in the following sections.

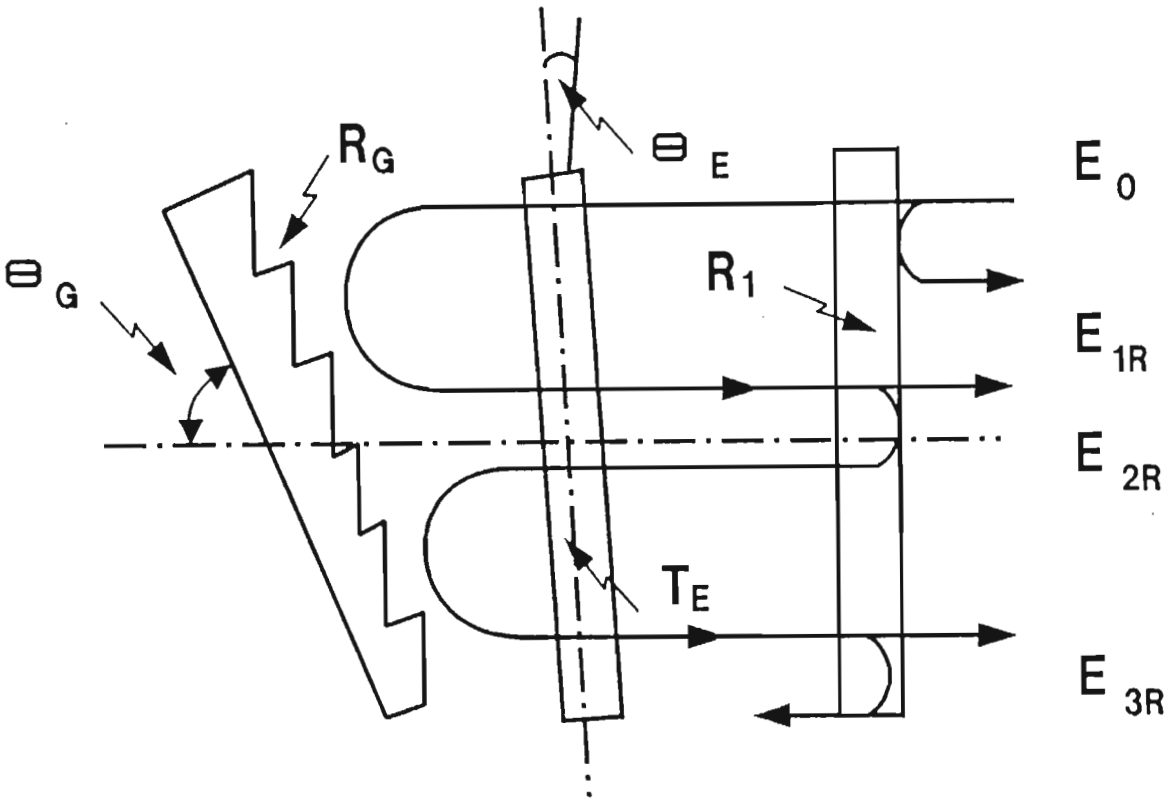

Figure 4.3. The schematic diagram used to calculate the reflectivity of the three mirror resonator.

4.2.2 CALCULATION OF WAVELENGTH DEPENDENT REFLECTION OF A BLAZED GRATING

The reflection from the grating is calculated using the Fraunhofer diffraction integral [74]. The Gaussian beam is again approximated by plane waves as previously. The equations are modified for the case of a blazed grating with blazing angle θ_b.The normalized intensity function of a slit is given by[74]:

$$I^0(p)=\left[\frac{sin(kpa)/2}{kpa/2}\right]^2 \qquad 4.20$$

With:

p= $\sin\theta-\sin\theta_0$, and θ, θ_0, indicated in fig 4.4,k=$2\pi/\lambda$, λ the wavelength of incident radiation.In the case of a blazed grating with blazing angle θ_b, p becomes:

$$p=\sin(\theta)-\sin(\theta_0-\theta_b) \qquad 4.21$$

The normalized intensity function of a grating consisting of N similar equidistant parallel slits is given by[74]:

$$\frac{I}{N^2}=\left[\frac{sin(kap_b/2)}{kap_b/2}\right]^2\left[\frac{sin(Nkdp/2)}{sin(kdp/2)}\right]^2 \qquad 4.22$$

Thus the normalized intensity function for a grating is given by

that of a single slit modulated by the interference function for many slits.The grating equation is given by[74]:

$$d\sin\theta - d\sin\theta_0 = m\lambda \qquad \text{with m an integer} \qquad 4.23$$

For the Littrow case, $\theta = -\theta_0$, the grating equation becomes:

$$2d\sin\theta = m\lambda \qquad 4.24$$

Thus the Littrow angle is given by:

$$\theta_L = \arcsin(m\lambda/(2d)) \qquad 4.25$$

For a typical case of a grating with 135l/mm and λ = 10.2 μm:

$$\theta_L = \arcsin(m*10.2*10^{-6}/(2*1/135000))$$

$$= 43.37^{o}$$

Fig's 4.5 and 4.6 give the reflection of a 150 l/mm grating blazed for 10.6 μm, used in the Littrow arrangement. Zero on the x–axis is equivalent to 10.6 micron. In figure 4.5, the beam diameter used was 1.13cm. In this case the FWHM is approximately 6.0 GHz. Fig 4.6 gives the reflection under the same conditions except that in this case the beam diameter was

0.8cm. In this case the FWHM is approximately 13 GHz. Thus it is clear to see why a intra–cavity beam expander will narrow the bandwidth the resonator. The grating reflectivity curves were calculated using the program given in appendix 3

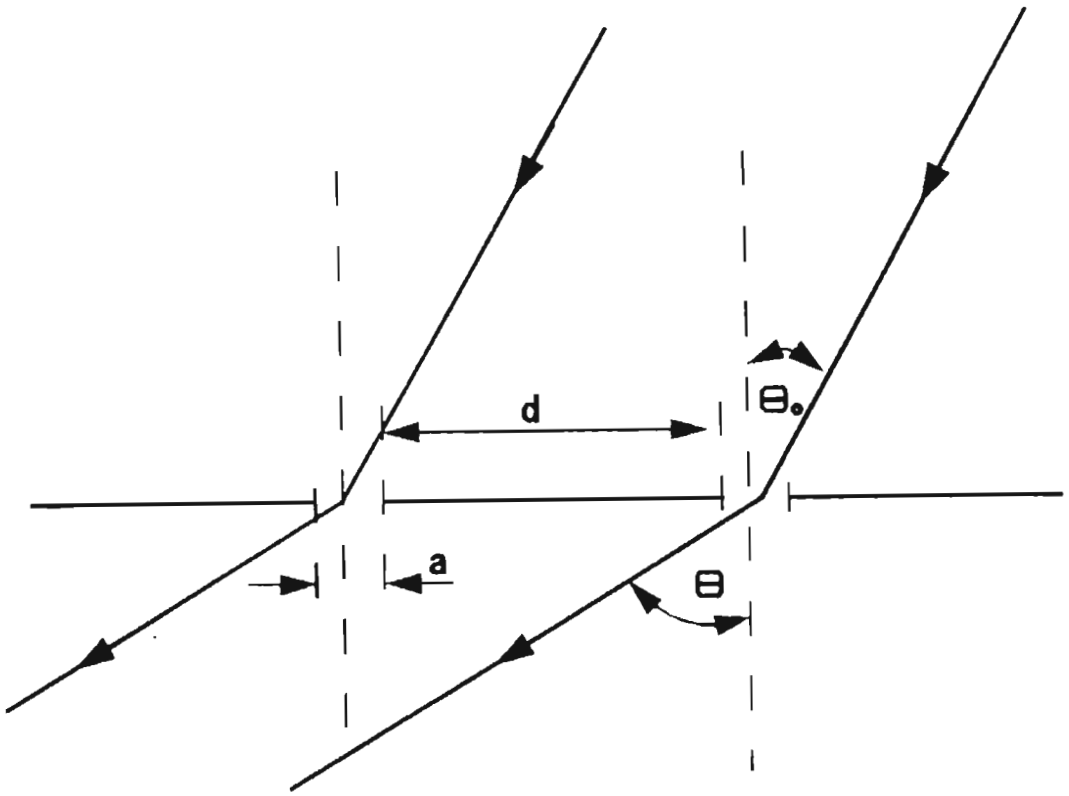

Figure 4.4. A schematic diagram of a part of a transmission grating.

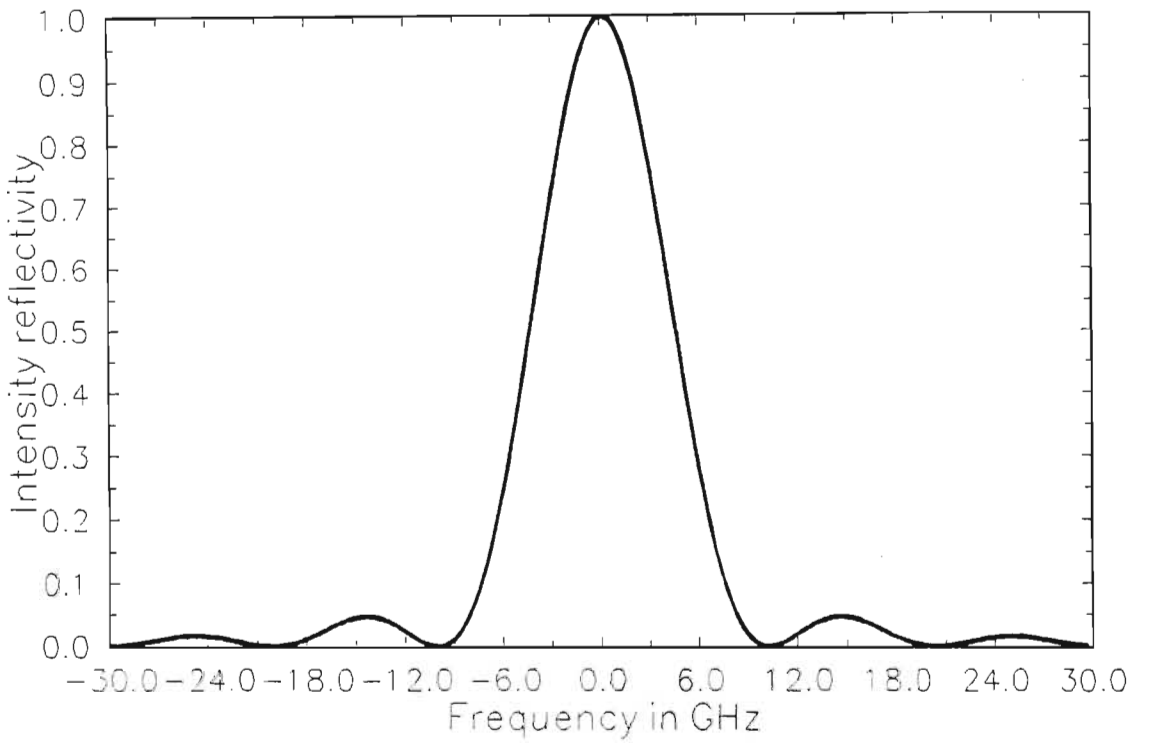

Figure 4.5. The intensity reflection of a 150 l/mm grating in the Littrow arrangement. The beam diameter is 1.13 cm. 0.0 on the x−axis corresponds to 10.6 μm.

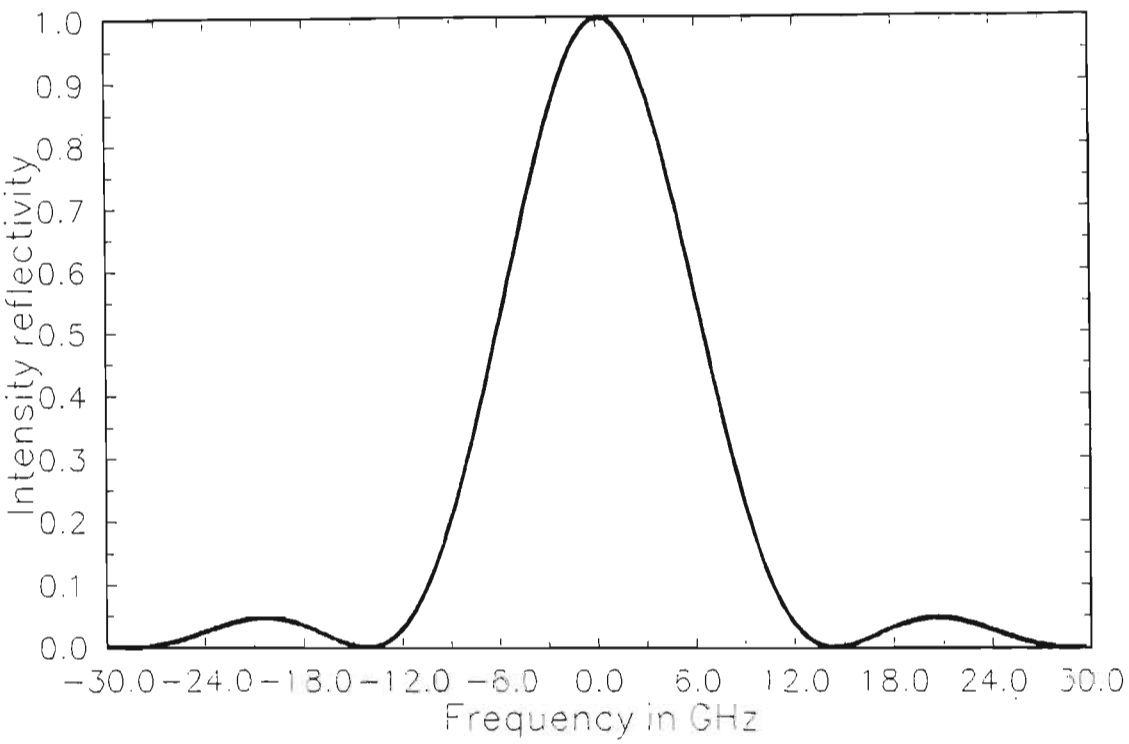

Figure 4.6. The intensity reflection of a 150 l/mm grating in the Littrow arrangement. The beam diameter was 0.8 cm. 0.0 on the x−axis corresponds to 10.6 μm.

4.2.3 CALCULATION OF THE WAVELENGTH DEPENDENT TRANSMISSION OF AN ETALON

Let E_0 be the incident electric field on the etalon, refer to fig 4.7, where $E_o(t)=E_0e^{i\omega t}$.Let δ be the phase difference between two adjacent beams. Let α be the absorption per unit length and r the amplitude reflection coefficient and t the amplitude transmission coefficient. Then:

$$E_{1t}=t^2E_0e^{i\omega t}e^{-\alpha l} \qquad 4.26$$

$$E_{2t}=t^2r^2E_0e^{i(\omega t-\delta)}e^{-3\alpha l} \qquad 4.27$$

$$E_{3t}=t^2r^4E_0e^{i(\omega t-2\delta)}e^{-5\alpha l} \qquad 4.28$$

etc

Thus, if E_t is the total transmitted amplitude then :

$$E_t = E_{1t}+E_{2t}+E_{3t}+ \ldots$$

$$= \frac{t^2E_0e^{-\alpha l}e^{i\omega t}}{1-(re^{-\alpha l})^2e^{i\delta}} \qquad 4.29$$

The total transmitted intensity is, as before :

$$I_t = E_t E_t^* = \frac{t^4 E_0^2}{e^{2\alpha l} + r^4 e^{-2\alpha l} - 2r^2 \cos\delta} \qquad 4.30$$

But $\cos\delta = 1 - 2\sin^2(\delta/2)$, thus :

$$I_t = \frac{t^4 E_0^2}{e^{2\alpha l} + r^4 e^{-2\alpha l} - 2r^2 (1 - 2\sin^2(\delta/2))}$$

$$= \frac{t^4 E_0^2}{(e^{\alpha l} - r^2 e^{-\alpha l})^2 + 4r^2 \sin^2(\delta/2)} \qquad 4.31$$

The phase difference between two adjacent beams is given by :

$$\delta = \frac{4\pi f d \cos\theta'}{v_c} \qquad 4.32$$

Where θ' is given by Snell's law : $n_1 \sin\theta = n_2 \sin\theta'$, f is the frequency of the incident light and v_c is the speed of light in the medium.

The fine tuning of the system will be done with the etalon. Thus the etalon bandwidth as well as the the rate of change of the frequency of maximum intensity transmittance with change in etalon angle θ, are importand and will be derived.The etalon transmission function can be written as :

$$I_t = \frac{E_0^2}{(e^{\alpha l} - Re^{-\alpha l})^2} \cdot \frac{1}{1 + \frac{4R^2}{(e^{\alpha l} - e^{-\alpha l})^2} \sin^2 \delta/2} \qquad 4.33$$

$$\text{Let } F = \frac{4R^2}{(e^{\alpha l} - Re^{-\alpha l})^2} \qquad 4.34$$

Then :

$$I_t = \frac{E_0^2}{(e^{\alpha l} - Re^{-\alpha l})^2} \cdot \frac{1}{1 + F \sin^2 (\delta/2)} \qquad 4.35$$

The maximum transmitted intensity is given by :

$$I_t(\max) = \frac{E_0^2}{(e^{-\alpha l} - Re^{\alpha l})^2} \qquad 4.36$$

$$\text{Thus } I_t / I_{t(\max)} = \frac{1}{1 + F \sin^2 (\delta/2)} \qquad 4.37$$

Thus the relative transmitted intensity is determined by the Airy function. To determine the halfwidth this is set equal to 0.5

Thus :

$$\frac{1}{1 + F \sin^2 (\delta/2)} = 0.5 \qquad 4.38$$

$$=>F\sin^2(\delta/2)=1$$

$$=>\delta/2=\sin^{-1}(\sqrt{1/F}) \qquad 4.39$$

But $F>>1$ Thus $\sin^{-1}(\sqrt{1/F})\approx 1/\sqrt{F}$

$$=>\delta_{(half)}\approx 2/\sqrt{F} \qquad 4.40$$

Thus the halfwidth of the transmitted light is given by :

$$\delta_{FWHM}=4/\sqrt{F} \qquad 4.41$$

The finesse of an etalon is the ratio between the free spectral range and the FWHM of the etalon. The transmission maximum is given by δ_{max} where :

$$F\sin^2(\delta_{max}/2)=0 \qquad 4.42$$

$$=>\delta_{max}/2=m\pi \text{ where } m=1,2,3...$$

Thus the difference between two successive maxima is given by :

$$2(m+1)\pi-2m\pi=2\pi \qquad 4.43$$

Thus the finesse *F*in is given by :

$$Fin = \frac{2\pi}{4/\sqrt{F}}$$

$$= \frac{\pi\sqrt{F}}{2} \qquad 4.44$$

The equation for maximum transmission can be re–written using the frequency of the incident light, equation (4.42) can then be written as :

$$f_{max} = \frac{cm}{2d\cos\theta'} \qquad 4.45$$

But:

$$n'\sin\theta' = n\sin\theta$$

$$=> \sin\theta' = n/n'\sin\theta$$

$$=> \sin^2\theta' = (n/n')\sin^2\theta$$

$$=> (1-\cos^2\theta') = (n/n')^2\sin^2\theta$$

$$=> \cos\theta' = (1-(n/n')^2\sin^2\theta)^{1/2} \qquad 4.46$$

Thus, using equation (4.46) equation (4.44) becomes:

$$f_{max} = \frac{cm}{2d(1-(n/n')^2\sin\theta^2)^{1/2}} \qquad 4.47$$

Differentiating equation (4.47) with respect to θ:

$$\frac{df_{max}}{d\theta} = \frac{cm(n/n')^2 \sin\theta\cos\theta}{(1-(n/n')^2\sin^2\theta)^{3/2}2d} \qquad 4.48$$

Thus:

$$\delta f_{max} = \frac{(n/n')^2 \sin\theta\cos\theta}{(1-(n/n')^2\sin^2\theta)^{3/2}} f_{max}\delta\theta \qquad 4.49$$

Thus changing the etalon angle of incidence by 0.025^{o} with $f_{max}= 2.95x10^{13}$Hz, n=1.5 and n'=2.3 and $\theta = 3.0^{0}$ then f would change by :

$$\delta f = 0.022x2.95x10^{13}\delta\theta$$
$$= 1.62x10^{10}\text{Hz}$$

For an etalon of a certain thickness the free spectral range is always the same, see equation (4.45). The finesse of the etalon can be increased by increasing the reflectivity of the etalon see equation (4.44) .Increasing the finesse will decrease the FWHM of the etalon see equation (4.41). An etalon with a higher finesse will also be slightly more lossy than one with a lower finesse. Since the etalon is used in a passive part of the resonator and only a fraction of the radiation of the main cavity

is passing through it this effect will be much smaller than it would have been were the etalon in the main cavity.

Figures 4.8 and 4.9 are graphs of etalon transmission versus the frequency of the incident radiation. In both cases zero on the x–axis corresponds to 10.6 micron and the units on the x–axis are in GHz. These curves were calculated using the computer program given in appendix 4. The values on the y–axis are relative transmission values. Fig 4.8 is the transmission function for an 11 mm ZnSe etalon with a 80% reflective coating . The finesse of this etalon is 12.3 ,the free spectral range is 5.6×10^9 Hz and the bandwidth is 5.7×10^8Hz. Fig 4.9 is the transmission function of a 19 mm, 80% reflectivity ZnSe etalon. The finesse is 12.12 ,free spectral range is 3.29×10^9 and the bandwidth is 2.7×10^8Hz. The index of refraction of ZnSe is 2.4 and its bulk absorptivity at 10.6 μm is 0.002 cm^{-1}.

If a 0.7 m cavity is used then the intra–mode spacing of the resonator is given by $c/2l = 214$ MHz. Thus approximately 2 cavity modes could fit into the transmission function of the 11 mm etalon and approximately 1 into that of the 19 mm etalon. As can be seen from fig 4.8, if a mode is 214 MHz away from the peak reflectivity of the etalon, then its transmission falls from the 95% peak value to approximately 30% for the 11 mm etalon and approximately 10% for the 19 mm etalon.

The bandwidth of a single mode pulse would of course be

determined by the bandwidth of the resonator. For a 0.7 m long resonator with a 95% reflective mirror and a 75% reflective output coupler the bandwidth would be approximately 14.0 MHz. The free spectral range will be $c/2l$ where l is the length of the resonator. Thus for this resonator the free spectral range would be 214 MHz. The finesse of this resonator is 15.The pulse time and frequency bandwidth are related by a term which can be deduced from Heisenberg's uncertainty relation:

$$\Delta p \Delta x \geq h/2$$

Thus using the term hf/c for the photon momentum and $\Delta x = c\Delta t$ this can be written as:

$$\Delta f \Delta t \geq 1/4\pi \qquad 4.50$$

Thus for a 14 MHz pulse:

$$\Delta t \geq 1/(4\pi \times 14 \times 10^{6}) \geq 5.7\text{ns}$$

Thus the output pulse must be longer than 5.7ns.

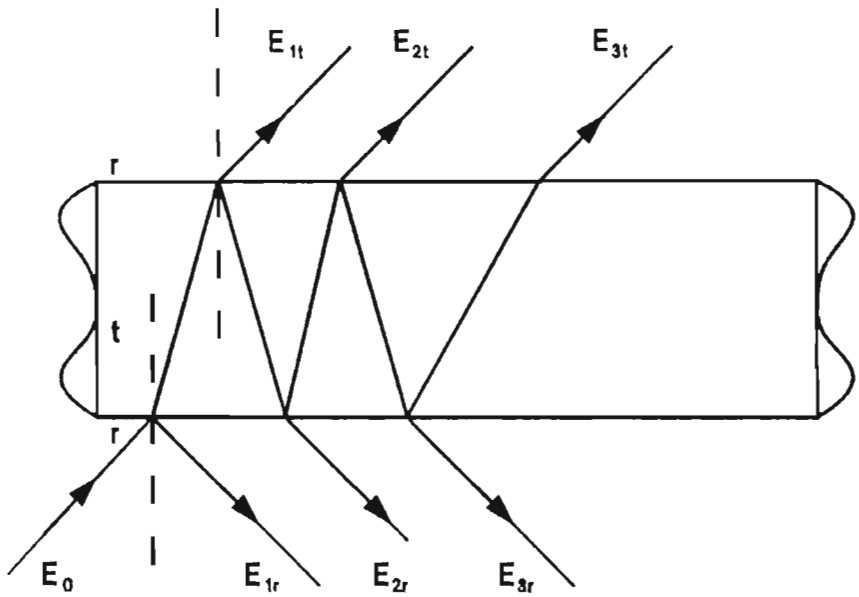

Figure 4.7. Schematic diagram used in the etalon transmission function calculations.

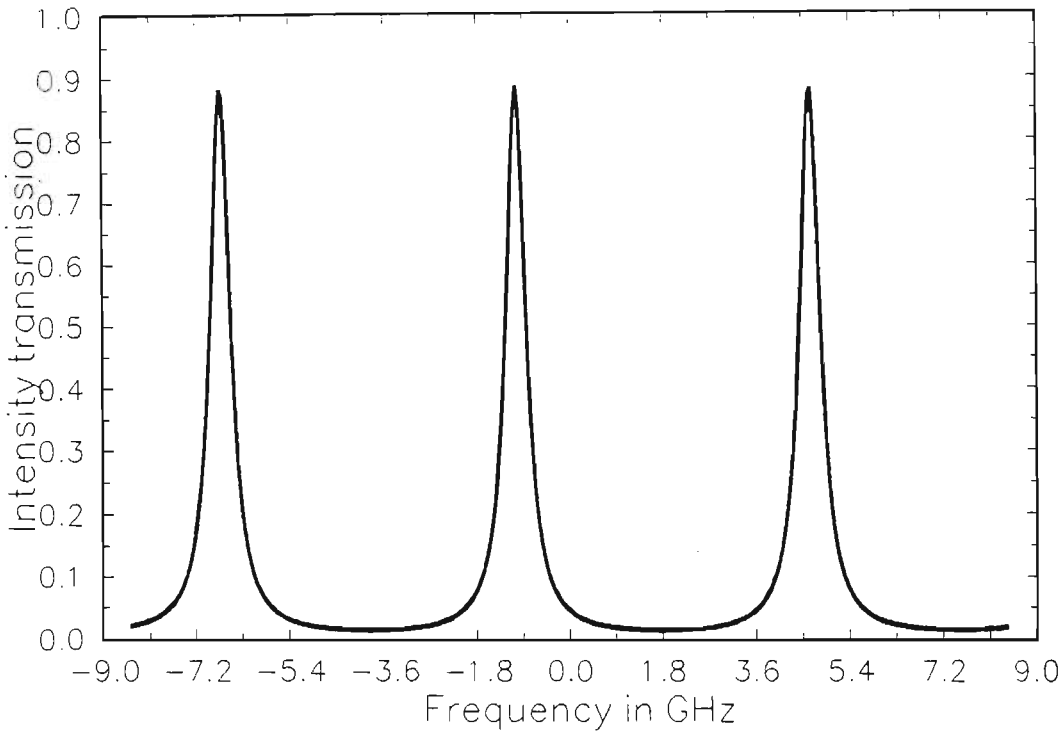

Figure 4.8. The intensity transmission function of an 11mm ZnSe etalon. The reflectivity of this etalon was 80% and its finesse was 12.3. Zero corresponds to 10.6μm.

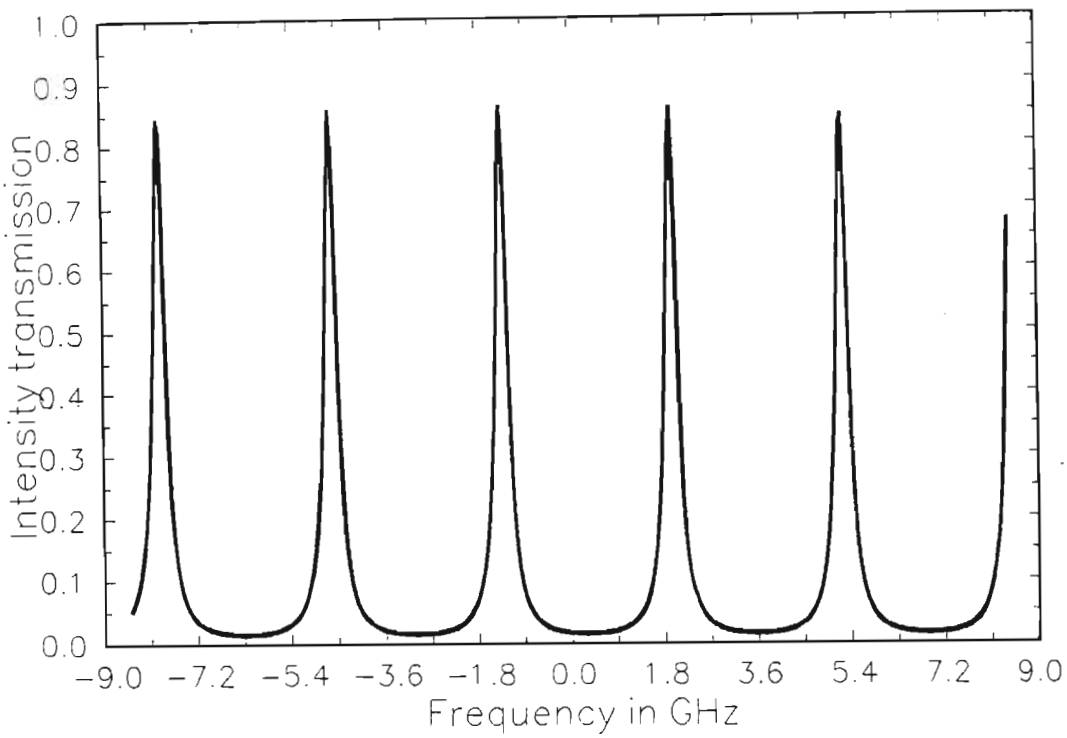

Figure 4.9. The intensity transmission function of a 19mm ZnSe etalon. The reflectivity of this etalon was 80% and its finesse was 12.15. Zero corresponds to 10.6μm

4.2.4 NUMERICAL CALCULATION OF REFLECTION OF DIFFERENT MGC CONFIGURATIONS

In the first example the grating is replaced by a mirror with 90% reflection. This is now basically a Fabry–Perot interferometer operated in anti–resonance Figures 4.10 and 4.11 give the reflected intensity of two different length sub–resonators. Figure 4.10 gives the reflection for a 5 cm sub–resonator and fig 4.11 that for a 10 cm sub–resonator. Zero corresponds to 10.6 micron and the units on the x–axis are in GHz.These curves were calculated using the computer program given in appendix 5. An interesting feature of these graphs is that for the shorter sub–resonator the reflection is close to 1 for a wider frequency interval in other words the free spectral range is greater as would be expected. This means that in a shorter subresonator the etalon can be tuned over a broader frequency range without the etalon peak falling into a null of the sub–resonator causing the resultant reflectivity to be very low.For example in the 5 cm sub–resonator the etalon can be tuned over an approximately 2 GHz range without changing the length of the sub–resonator. By contrast in the 10 cm resonator the etalon can only be tuned over an approximately 1 GHz range without changing the length of the sub–resonator. Of course changing the length of the subresonator by $\lambda/2$ would result in exactly the same graphs. Thus if the etalon transmission peak does not coincide

with the sub–resonator reflected peak a fraction of a wavelength change in the length of the sub–resonator would rectify this problem.

Figures 4.12 gives the reflection of the MGC with a grating but without an etalon.The grating used was a 150 l/mm grating blazed at 52.65^{o} with 99% peak reflection .The laser aperture was 10 mm in diameter. The center wavelength was 10.6μm.The subresonater length was 10 cm. The partially transmitting mirror had a reflectivity of 50%. The reflectivity of the MGC without grating is modulated with the grating reflection, refer to figure 4.12.

Figure 4.13 gives the wavelength dependent reflection of a resonator with a grating and an etalon. The specifications of the resonator (using the terms as defined in figure 4.2) are as follows:

L'	0.1m
R_1	50 %
Etalon Thickness	0.011m
Etalon Reflectivity	80 %
Angle of Incidence	3.05^{o}
Grating lines per mm	150l/mm
Laser Aperture	0.010 m

The grating was used in the Littrow angle. Thus the angle of

incidence was:

$$\theta_L = \arcsin\ (m\lambda/2d)$$

With:

$m = 1$ (First order)

$\lambda = 10.6 \times 10^{-6}$ m

$d = 1/150\ 000$ m

Then:

$$\theta_L = 52.655^{O}$$

The center wavelength in figure 4.13 was 10.6 μm . The etalon used was a ZnSe etalon. The maximum reflectivity peak has a reflectivity of approximately 90 % with three smaller peaks with reflectivities of 80 %, 75 %, and 55 % respectively. The maximum reflectivity caused by the etalon transmission function is modulated by the grating reflectivity function. Away from the grating reflectivity peak the reflectivity is the 50 % reflectivity of the partial reflector. The question was whether this reflective discrimination was enough to ensure single mode operation of the laser if two longitudinal modes happen to fall on two of the reflective peaks shown in figure 4.13. Another question was if the mode discrimination was enough to prevent parasitic oscillations on one of the higher gain lines (eg P20 or R18) if

the grating was tuned to one of the lower gain lines (eg P30 or R30). To answer these questions a mode discrimination analysis was done.

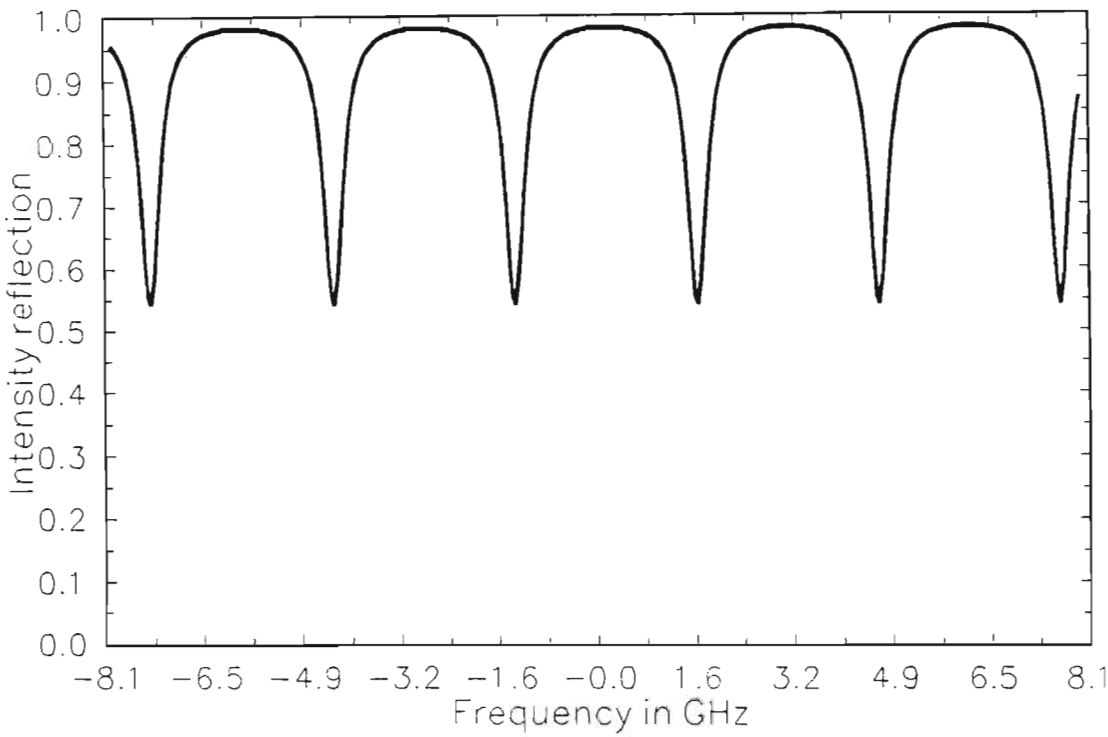

Figure 4.10. *The reflectivity of a 5 cm long sub−resonator. The grating has been replaced by a 90% reflective mirror. The partial reflective mirror had a reflectivity of 50%. Zero on the x−axis corresponds to 10.6μm*

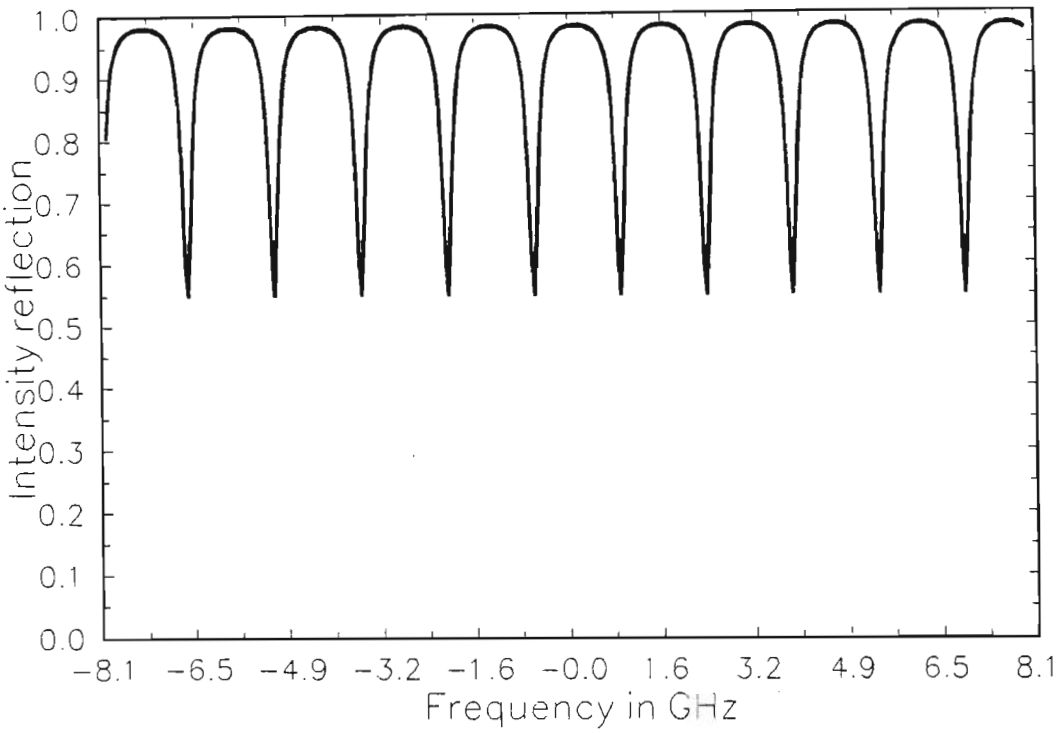

Figure 4.11. The reflectivity of a 10 cm long sub−resonator. The grating has been replaced by a 90% reflective mirror. The partial reflective mirror had a reflectivity of 50%. Zero on the x−axis corresponds to 10.6 μm

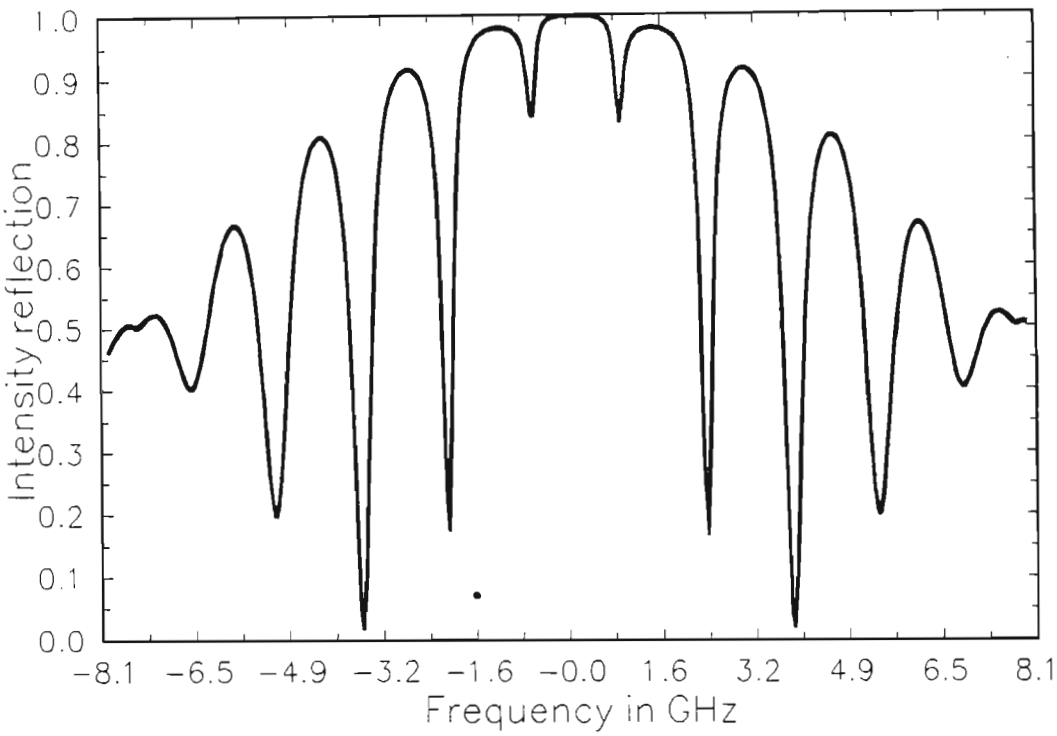

Figure 4.12. The reflectivity of a 10 cm long sub−resonator with a 150l/mm grating. The partial reflective mirror had a reflectivity of 50%.Zero on the x−axis corresponds to 10.6 μm

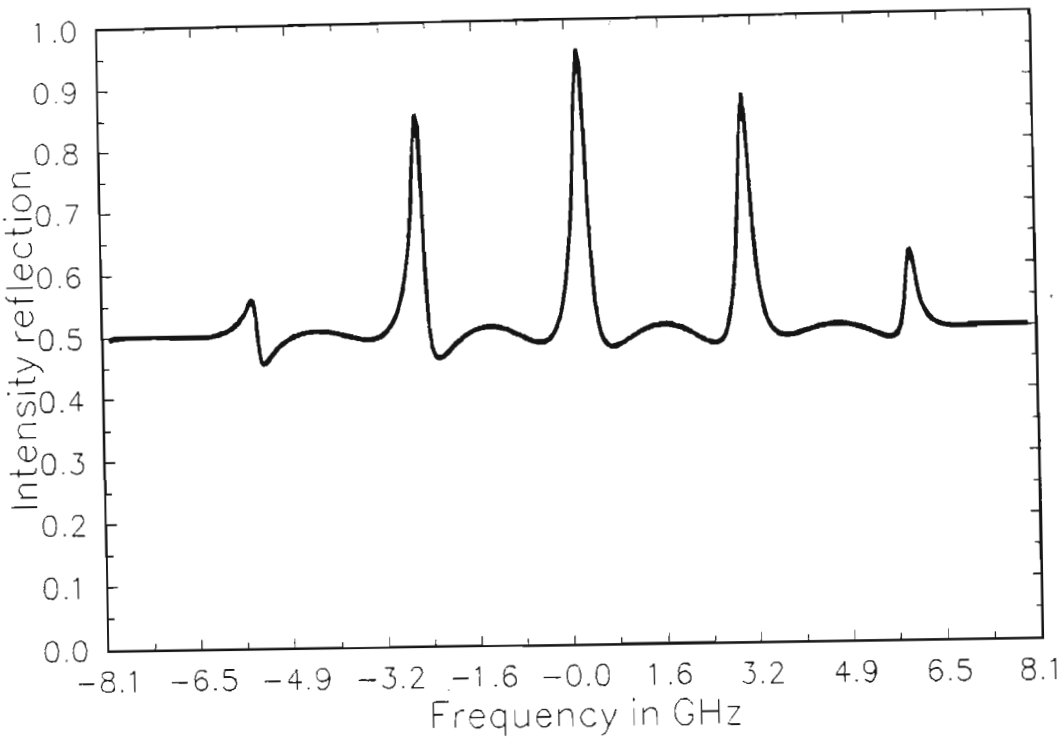

Figure 4.13. The reflectivity of a 10 cm long sub−resonator with a 150l/mm grating and a 11 mm, 80% reflective ZnSe etalon.. The partial reflective mirror had a reflectivity of 50%.Zero on the x−axis corresponds to 10. 6 μm

4.2.5 MODE DISCRIMINATION ANALYSIS.

Consider a mode z with a small signal gain γ_z. According to equation (2.20) the intensity of the mode after it has moved a distance x through the resonator would be:

$$I_z(x)=I_0 e^{\gamma_z x} \qquad 4.51$$

If it is further assumed that the resonator has one mirror with a mode (or frequency) dependent reflectivity R_z and one mode independent mirror R_I (this is the situation in a MGC) and the length of the resonator is l, then after one round trip the intensity of mode z would be given by :

$$I_z(\text{one round trip}) = I_0 R_z R_I I_0 e^{2\gamma_z l} \qquad 4.52$$

Thus after N_r round trips the intensity would be given by:

$$I_z(\text{after } N_r \text{ round trips})=\left[I_0 R_z R_I I_0 e^{2\gamma_z l}\right]^{N_r} \qquad 4.53$$

Consider a mode y with a small signal gain of γ_y and a mode dependent reflective mirror with reflectivity of R_y. It is further assumed that the modes build up from the same background noise I_0 then this mode intensity after one round trip would be

given by:

$$I_y(\text{one round trip}) = I_0 R_y R_I e^{2\gamma_y l} \qquad 4.54$$

After N_r round trips the intensity is given by:

$$I_y(\text{after } N_r \text{ round trips}) = \left[I_0 R_y R_I e^{2\gamma_y l} \right]^{N_r} \qquad 4.55$$

Thus if gain saturation is not taken into account the intensity ratio of the two modes would be given by:

$$\frac{I_z}{I_y} = \left[\frac{R_z}{R_y} e^{2l(\gamma_z - \gamma_y)} \right]^{N_r} \qquad 4.56$$

If the gains of the two modes, that is γ_z and γ_y, are the same then equation (4.56) reduces to:

$$\frac{I_z}{I_y} = \left[\frac{R_z}{R_y} \right]^{N_r} \qquad 4.57$$

Equations (4.56) and (4.57) can now be used to determine whether the mode discrimination of a resonator is good enough to ensure single mode laser action. These equations were applied to determine whether the reflective discrimination,shown in figure 4.13, is good enough to ensure single longitudinal mode laser action. The typical number of round trips in a gain switched

laser is more than 30. The condition used for good mode discrimination was that the one mode must be at least 10 times stronger than the other mode after 30 round trips.

The question is now if reflective discrimination of the resonator, shown in figure 4.13 , is good enough to ensure single mode laser action if one mode happens to fall on the 90 % peak and the other mode on the 80 % peak shown in figure 4.13. In a high pressure CO_2 laser the gain of two neighbouring modes is very nearly the same. Since the gain values are the same (or very nearly the same) the mode discrimination equation reduces to equation (4.57). For this particular resonator the ratio of R_z/R_y is 1.1. Thus after 30 round trips the one mode would be 17.4 times stronger than the other mode. Thus according to the assumption made above– mode discrimination is good enough if the one mode is 10 times stronger than the other– the reflective discrimination of this resonator is good enough to ensure good mode purity. This analysis also shows that the mode discrimination is good enough to ensure single mode action if the one cavity mode falls on the center of the etalon transmission function and the other is 214 MHz away. As was shown in section 4.2.3 if the one mode falls on the transmission peak of the etalon, with a 95% peak transmission, then the transmission of the other closest mode would be 30% and 10% for the 11mm and 19 mm etalons respectively.

The second question is whether the reflective discrimination of

this resonator is good enough to prevent parasitic oscillations from the partial reflector on one of the higher gain lines ,eg P20 or R18,if the grating is tuned to one of the lower gain lines, eg P30 or R30. Table 4.1 gives the mode discrimination for increasing differences in gain between the two lines. It is assumed that the reflection of mode z is 90 % and that of mode y is 50 %. It is further assumed that the gain length of the laser is 0.40m.

Good mode discrimination was obtained for lines with a difference in gain of up to 0.6, refer to table 4.1. If the R30 line is taken as an example, the maximum single mode pulse energy that can be expected on this line can be calculated. For the 10 μm branch the gain of the R30 line is about 0.52 that of the R18 line,as can be seen from figure 2.4. According to table 4.1 single mode action, on the R30 line, will take place without the onset of parasitic oscillations on the R18 line until the difference in gain is 0.6/m, thus:

$$\gamma_{R16}-\gamma_{R30} = 0.6/m \qquad 4.58$$

Thus:

$$1.92\gamma_{R30}-\gamma_{R30}=0.6/m$$

Thus:

$\gamma_{R30} = 0.6/0.92=0.65/m$

If the 50 % partial reflector is changed to a 40 % partial reflector it can be shown, in the same way, that good mode discrimination can be obtained for a difference in gain of 0.9/m. The disadvantage of using a partial reflector with a lower gain is that the etalon and the grating will now be exposed to a higher power density. Using the maximum single mode gain values the pulse energy of a laser can now be calculated to give the maximum expected single mode pulse energies on different CO_2 lines. The maximum expected energies for a specific CO_2 laser will be calculated in the next section.

The same calculation could be made with the isotopic mixture of which the gain curve is shown in figure 2.8. If the frequency of the $C^{16}O_2$ R30 line is used, approximately 982 cm^{-1}, then the on peak value in the vicinity of 982 cm^{-1} is approximately 0.92 times the maximum value. This means that single mode action could be obtained without the onset of parasitic oscillations for a gain value of 6.9/m. This is more than the maximum small signal gain that can be expected for a CO_2 laser. Thus on this

peak single mode action will always be observed without the onset of parasitic oscillations. If the off peak gain is used then its value is approximately 0.69 times the maximum value. This translates to a maximum single mode no parasitic small signal gain value of 1.33/m.

$\lvert a_x - a_y \rvert$	$(I_x/I_y)_{N=1}$	$(I_x/I_y)_{N=30}$
0.1	1.74	1.6×10^7
0.2	1.59	1.1×10^6
0.3	1.45	6.9×10^4
0.4	1.33	5.9×10^3
0.5	1.21	304
0.6	1.11	23
0.7	1.01	1.35

Table 4.1. Mode discrimination of two modes with different reflectivities and different gain values. N equals the number of cavity round trips, I_x and I_y are the intensities of modes x and y respectively and $\alpha_x - \alpha_y$ is the difference in the gain of modes x and y.

4.2.6 CALCULATION OF SINGLE MODE PULSE ENERGIES.

The small signal gain values calculated above can be used to calculate the maximum expected single mode pulse energy and pulse shape. The pulse energy and pulse shape were calculated using the equations derived by Judd [75]. Consider the two level system shown in figure 4.14. Let P_1 and P_2 be the pumping terms of level 1 and 2 respectively. γ_1 and γ_2 are the respective decay rates. n_1 and n_2 are the population densities of level 1 and 2 respectively and σ is the stimulated emission cross section , h is Planck's constant and I is the intensity of the light. The equations describing the respective population densities are:

$$\frac{dn_2}{dt} = P_2 - \gamma_2 n_2 - \frac{\sigma}{h\nu}[n_2 - n_1]I \qquad 4.59$$

$$\frac{dn_1}{dt} = P_1 - \gamma n_1 - \frac{\sigma}{h\nu}[n_2 - n_1]I \qquad 4.60$$

The equation for the photon density is given by [75] :

$$\frac{\partial I}{\partial t} + c\frac{\partial I}{\partial x} = \sigma(n_2 - n_1)I - I/\tau_c \qquad 4.61$$

τ_c is the mean photon lifetime of a photon in the laser resonator and is given by Yariv [30]:

$$\tau_c = \frac{n_0 L}{c(\alpha L - (1 - \sqrt{R_1 R_2}))} \qquad 4.62$$

R_1 and R_2 are the intensity reflection coefficients of the two resonator mirrors, L is the length of the resonator and α is the bulk absorptivity of the active medium. n_0 is the index of refraction of the active medium in the cavity. The above equations are applicable to a two level system. In a CO_2 laser the process can be depicted as in figure 4.15. The equations governing the population of the j th rotational level of the upper vibrational state can now be written as [75]:

$$\frac{dn_j}{dt} = R_j - \gamma_j n_j - \sum_k \Gamma_{jk} n_j + \sum_k \Gamma_{kj} n_k - \sigma_J \frac{I}{h\nu}(n_j - n_j')\delta_{jJ} \qquad 4.63$$

Γ_{jk} is the rate for collisional transitions out of level j to all other levels k within the vibrational band. Γ_{kj} is the rate for collisional transitions of all other levels k to the level j. R_j and γ_j are the pumping and decay rates of the individual rotational levels. Stimulated emission is assumed to occur on the rotational level with quantum number J and is taken into account by the last term in the equation. δ_{jJ} is the Kronecker delta and the primed quantities refer to the lower level. σ_J is the stimulated emission cross–section.By detailed balance, under equilibrium conditions:

$$\Gamma_{jk}=\frac{z_k}{z_j}\Gamma_{kj} \qquad 4.64$$

z_k and z_j are the Boltzmann factors given in equation (2.61). Using equation (4.64), equation (4.63) can now be written as:

$$\frac{dn_j}{dt}=R_j-\gamma_j n_j-\sum_k(n_j z_k-z_j n_k)\frac{\Gamma_{kj}}{z_j}-\sigma_{j\frac{I}{h\nu}}(n_j-n_j')\delta_{jJ} \qquad 4.65$$

It is further assumed that[75]:

$$\frac{\Gamma_{jk}}{z_j}=\frac{1}{\tau_x} \qquad 4.66$$

Where τ_x is the rotational thermalization time. Performing the sum over k the following equation is obtained:

$$\frac{dn_j}{dt}=P_j-\gamma_j n_j\frac{(n_j-z_j n_v)}{\tau_x}-\sigma_{j\frac{I}{h\nu}}(n_j-n_{j\mp1})\delta_{jJ} \qquad 4.67$$

With n_v the total vibrational population of the vibrational level and is thus given by:

$$n_\nu = \sum_j n_j \qquad 4.68$$

By summing each term of this equation over j the total population of the vibrational level is obtained and is given by:

$$\frac{dn_v}{dt}=R-\gamma n_v-\sigma\frac{I}{h\nu}(n_J-n_J') \qquad 4.69$$

Where R and γ are the total pump and decay rates of the vibrational level. If the population difference of the rotational levels (n_J-n_J') is defined as δ' and the population difference of the vibrational levels is defined as Δ, then the difference equations obtained from equations (4.67) and (4.69) can be written as [75]:

$$\frac{d\delta'}{dt}=\frac{(\delta'-z\Delta)}{\tau_x}-2\sigma\frac{I}{h\nu}\delta' \qquad 4.70$$

$$\frac{d\Delta}{dt}=-2\sigma\frac{I}{h\nu}\delta' \qquad 4.71$$

And the optical flux equation can be written as:

$$\frac{\partial I}{\partial t}+c\frac{\partial I}{\partial x}=c\sigma\delta' I(l/l')-\frac{I}{\tau_c} \qquad 4.72$$

With l and l' the gain and resonator lengths respectively. This set of coupled differential equations was numerically solved using a fourth order Runge–Kutta algorithm [76]. The computer program is given in appendix 6. The population inversion at t=0 was calculated using the small signal gain as calculated in section 4.2.5. The population inversion was calculated using

equation(2.21). $$\gamma=\frac{(N_2-N_1 g_2/g_1)\lambda^2 g(\nu_0)}{8\pi n t_{spont}} \qquad 4.73$$

$$g(\nu_0)=\frac{\frac{\Delta\nu}{2\pi}}{(\frac{\Delta\nu}{2})^2} \qquad 4.74$$

$\Delta\nu$ is given by equation (2.56) The thermalization time τ_x is given by Judd[75]

$$\tau_x=(1.6x10^{-7}/(\text{Pressure in torr}))/s$$

The stimulated emission cross–section is given by Judd[75]:

$$\sigma=\frac{\lambda^2 A}{4\pi^2 \Delta\nu} \qquad 4.75$$

With:

$A=0.21/s$

Using the maximum gain values as calculated in section 4.2.5 and given in table 4.2, the maximum expected energy and peak power on the R24–R30 lines were calculated using equations (4.70) to (4.72) The maximum expected energy and peak power are given in table 4.2 The specifications of the laser were as follows:

Gain length	0.4m
Resonator length	0.7m
Back mirror reflectivity	90%
Reflectivity of output coupler	75%
Discharge diameter	0.006m
Pressure	9 Atm

According to the calculations done in section 4.2.5 the maximum gain value that can be obtained with a 3 atm isotopic mixture of line center in the vicinity of 982 cm^{-1} is approximately 1.33/m. If this gain value is used with the resonator above this translates to a maximum energy of 200 mJ. The P20 gain would then be approximately 1.9/m giving an energy of 330 mJ. Wiederhold et al. predicted a maximum CO_2 laser efficiency of 22%. If this factor is used with the above calculated energies an energy loading of the gas of $0.02J/cm^3atm$ is obtained.If a more realistic practical efficiency of 10% is used an energy loading of $0.04J/cm^3atm$ is obtained. This value is well within the arcing limit of 0.16 to 0.17 J/cm^3atm measured for a UV pre–ionized CO_2 laser as measured by Denes and Lowke[41]. Thus a laser could be built using this resonator that would give approximately 200 mJ off line center in the vicinity of $982cm^{-1}$ and 300 mJ on line center. The laser output pulse would be single mode without parasitic oscillations. It was found in chapter 3 that the laser functions well at a voltage of approximately 12 kV/cm.atm. Thus for electrodes with a 0.8 cm gap and width with a laser pressure of 3 atm would mean a charging voltage of

28.8kV.

If the resonator length is 0.4 m an energy loading of $0.12J/cm^3$ would mean that 3.0J is coupled into the gas, thus:

$0.5CV^2=3.0$

With:

V :Charging voltage.

C :Charge capacitor capacitance.

Thus:

$C\approx$ 8nF

Thus a laser using the isotopic mixture at a pressure of 3 atm with the above resonator dimensions with the above capacitor and charging voltage would give approximately 200 mJ in the vicinity of the $C^{16}O_2$, 10μm branch, R30 line.

LASER LINE	ENERGY mJ	POWER MW	GAIN per m
R30	52	0.59	0.65
R28	138	3.74	0.98
R26	228	8.82	1.42
R24	335	17.7	2.10

Table 4.3. Maximum expected single mode energies using a three mirror resonator. The laser specifications are given in section 4.2.6. A single isotope $C^{16}O_2$ mixture was used.

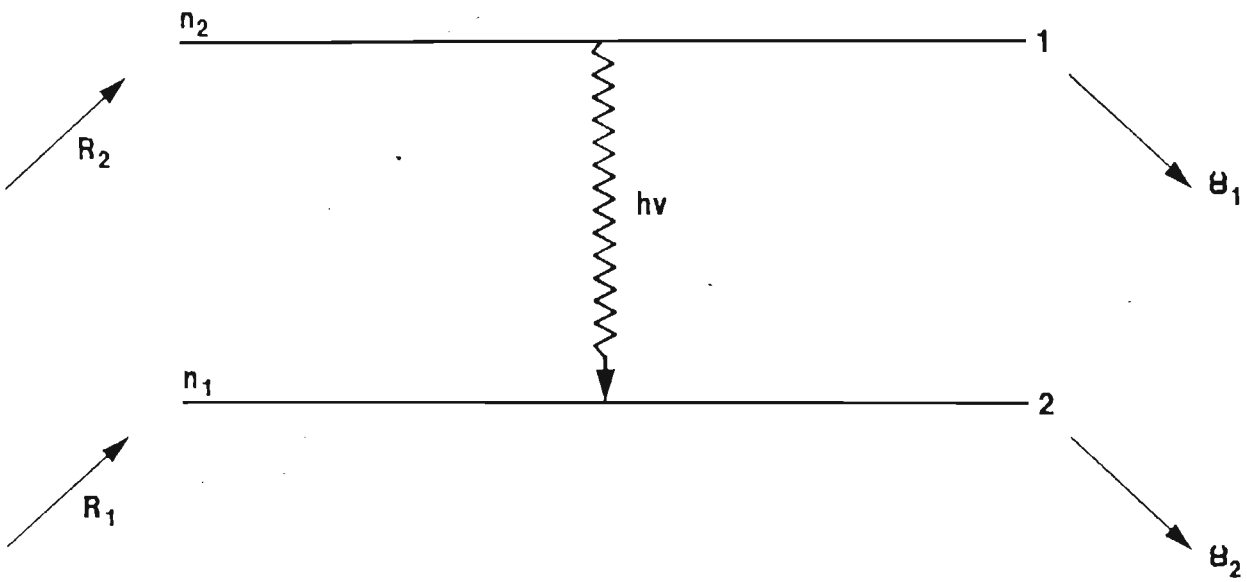

Figure 4.14. The interaction of optical radiation with a two level system. R_1 and R_2 are the pumping rates. γ_1 and γ_2 are the net decay rates.

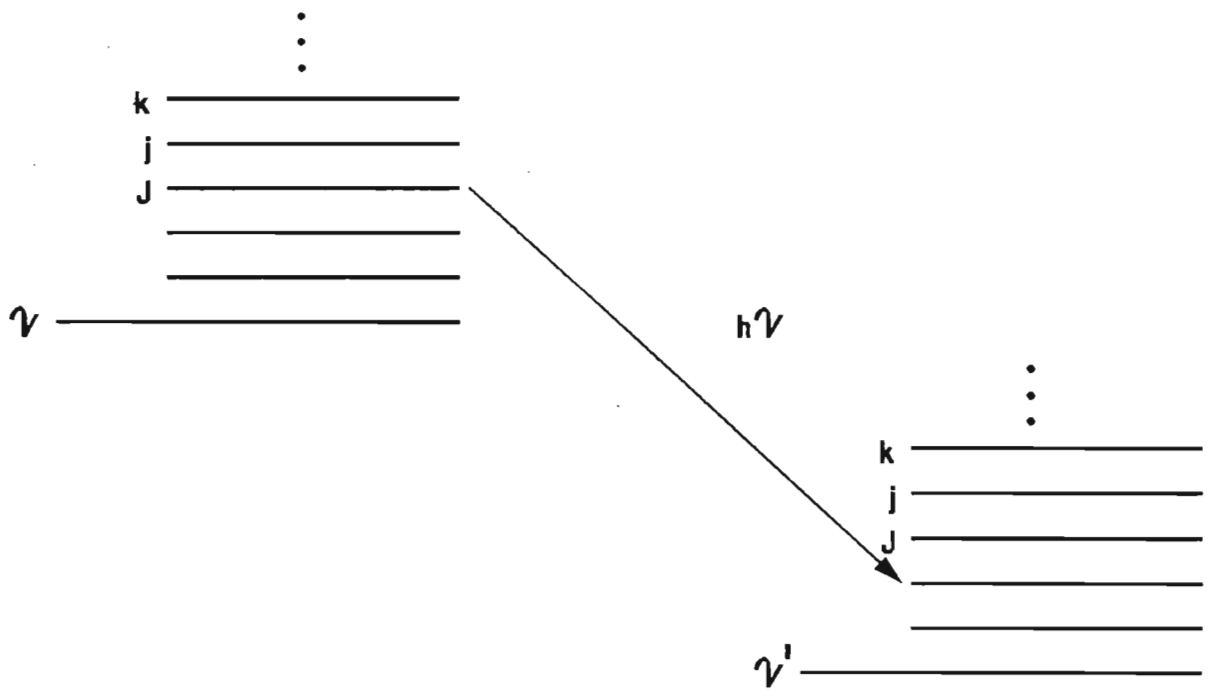

Figure 4.15. The interaction of optical radiation with a two level system. R_1 and R_2 are the pumping rates. γ_1 and γ_2 are the net decay rates.

4.2.7 THERMAL ANALYSIS OF THE RESONATOR.

A thermal analysis of the resonator was done to determine whether the output frequency of the resonator would remain stable if the resonator is used in an area where temperature fluctuations might occur. Consider the three mirror resonator depicted in figure 4.2. As was mentioned in section 4.2.1 the resonance frequencies of the resonator are determined by the requirement that the round trip phase shift be some multiple of 2π. This requirement makes it possible for a standing wave pattern to establish itself along the z–axis. In this instance there is an additional phase shift π at z_2 as was mentioned in section 4.2.2.Because of the sub–cavity plus elements there is another additional phase shift ϕ at z_1. This phase shift is calculated using the complex reflection coefficient given in equation (4.17).This complex reflection coefficient can be written as:

$$r_c=-\frac{1+t_e^2 r_g e^{i\delta}}{1+t_e^2 r_g r_1 e^{i\delta}} \qquad 4.76$$

Writing this equation with a real numerator :

$$r_c=-\frac{1-t_e^2 r_g r_1 e^{-i\delta'}+t_e^2 r_g e^{i\delta}-t_e^4 r_g^2 r_1}{1-t_e^4 r_g^2 r_1^2} \qquad 4.77$$

This can be rewritten as :

$$r_c=\frac{1+(-t_e^2r_gr_1+t_e^2r_g)\cos\delta'+(t_e^2r_gr_1+t_e^2r_g)i\sin\delta'-t_e^4r_g^2r_1}{1-t_e^4r_g^2r_1^2} \qquad 4.78$$

Consider a complex number z. It can be written as:

$$z=x+iy \qquad 4.79$$

The phase ,ϕ, of this complex number can be written as :

$$\phi=\arctan(y/x) \qquad 4.80$$

Thus, using equations (4.78) to (4.80), the phase shift caused by the MGC can be written as:

$$\phi=\arctan\left[\frac{-(t_e^2r_g-t_e^2r_gr_1)\sin\delta'}{-1+t_e^4r_g^2r_1+(t_e^2r_g-t_e^2r_gr_1)\cos\delta'}\right] \qquad 4.81$$

Using equation (4.1), the phase of the (m,n) mode of a Gaussian beam can be written as:

$$\theta_{m.n}=kz+(n+m+1)\arctan(z/z_0) \qquad 4.82$$

z_0 is the Rayleigh range given by equation (4.5). The resonance condition for the (m,n) mode can thus be written as:

$$2(\theta_{m,n}(z_2)-\theta_{m,n}(z_1))+\phi_1+\pi=2\pi q \quad \text{(q:integer)} \qquad 4.83$$

With:

$$(\theta_{m,n}(z_2)-\theta_{m,n}(z_1))=(kz_2-(n+m+1)\arctan(z_2/z_0))-(kz_1-(n+m+1)\arctan(z_1/z_0)) \qquad 4.84$$

Thus the resonance condition equation (4.83) becomes:

$$2\left[k(z_2-z_1)-(n+m+1)\left[\arctan(z_2/z_0)-\arctan(z_1/z_0)\right]\right]-\phi_1+\pi=2\pi q \qquad 4.85$$

For this analysis only the TEM_{00} mode was considered. Thus equation (4.85) reduces to:

$$\left[k(z_2-z_1)-\left[\arctan(z_2/z_0)-\arctan(z_1/z_0)\right]\right]+\phi+\pi=2\pi q \qquad 4.86$$

Furthermore $z_2-z_1=L$ and $z_1=0$, thus $\arctan(z_1/z_0)=0$.

Equation (4.86) can be re-written, using $k=2\pi/\lambda$, as :

$$\lambda=\frac{2\pi L}{\pi(q-1/2)-\phi_1/2+\arctan(L/z_0)} \qquad 4.87$$

If temperature is represented by the variable T then the tempo of change of resonance frequency with a change in temperature is given by:

$$\frac{d\lambda}{dT}=\frac{2\pi\frac{dL}{dT}}{\pi(q-1/2)-\phi_1/2+\arctan(L/z_0)}+$$
$$-2\pi L\left[\frac{1}{2}\frac{d\phi}{dT}+\frac{1/Z_0}{1+(L/Z_0)^2}\frac{dL}{dT}\right]$$
$$\frac{}{[\pi(q-1/2)-\phi/2+\arctan(L/z_0)]^2} \qquad 4.88$$

As shown in equation (4.80), ϕ can be written as:

$$\phi=\arctan(y/x) \qquad 4.89$$

With arctan(y/x) as given by equation (4.82). Thus:

$$\frac{d\phi}{dT}=\left[\frac{1}{1+(y/x)^2}\right]\left[\frac{1}{x}\frac{dy}{dT}-\frac{y}{x^2}\frac{dx}{dT}\right] \qquad 4.90$$

With x,y,dy/dT and dx/dT as given below:

$$x=\frac{r_1-t_e^2r_gr_1+(t_e^2r_gr_1-t_e^2r_gr_1^2)\cos\delta'}{(1-t_e^4r_g^2r_1^2)} \qquad 4.91$$

$$\frac{dx}{dT}=\frac{t_e^2 r_g r_1-t_e^2 r_g r_1^2}{1-t_e^4 r_g^2 r_1^2}\sin\delta'\frac{d\delta}{dT} \qquad 4.92$$

$$y=\frac{-t_e^2 r_g r_1^2-t_e^2 r_g r_1}{1-t_e^4 r_g^2 r_1^2}\sin\delta' \qquad 4.93$$

$$\frac{dy}{dT}=\frac{-t_e^2 r_g r_1^2-t_e^2 r_g r_1}{1-t_e^4 r_g^2 r_1^2}\cos\delta'\frac{d\delta}{dT} \qquad 4.94$$

And $d\delta'/dT$ is given by:

$$\frac{d\delta'}{dT}=\frac{4\pi}{\lambda}\frac{dL'}{dT} \qquad 4.95$$

dL'/dT is given by :

$$\frac{dL'}{dT}=\eta L' \qquad 4.96$$

Where η is the thermal expansion coefficient. To minimize the thermal drift a material with a very low thermal expansion coefficient must be used. An alloy with a very low thermal expansion coefficient is INVAR 36. The thermal expansion coefficient of INVAR 36 is $2.0\text{x}10^{-6}/^{o}\text{C}$ [77]. Thus equation 4.96 can be written as:

$$\frac{dL'}{dT}=2.0\times10^{-6}L' \qquad 4.97$$

Furthermore:

$$f\lambda=c \qquad 4.98$$

Thus:

$$\delta f=-\frac{c}{\lambda^2}\delta\lambda \qquad 4.99$$

Using equations (4.90) to (4.99) the thermal drift of an INVAR 36 resonator of a known length can be calculated. The change in resonance frequency with a change in temperature for different sub–resonator lengths is shown in figure 4.16. Zero in figure 4.16 corresponds to a sub–resonator length of 0.1m and the sub–resonator length was then increased to 0.1 +10 μm. The length of the main resonator was 0.45m. The computer program used for calculating the frequency drift is given in appendix 7. At each new sub–resonator length the change in resonator resonance frequency per degree celsius was calculated. As can be seen the change in resonance frequency per degree celsius varies between 20 MHz to –235 MHz. This change in resonance frequency shows a Fabry–Perot type behaviour with a maximum change in resonance frequency per degree celsius where the sub–cavity is in anti–resonance. By comparison the change in resonance frequency of a resonator without the sub–cavity is

given by:

$$\Delta f = \frac{c}{\lambda} \frac{2}{q} \frac{dL}{dT} L \Delta T \qquad 4.100$$

For a 0.45m resonator supported on INVAR rods, Δf at 10.6μm is approximately 63MHz/^{o}C, thus less than a third of the three mirror resonator.

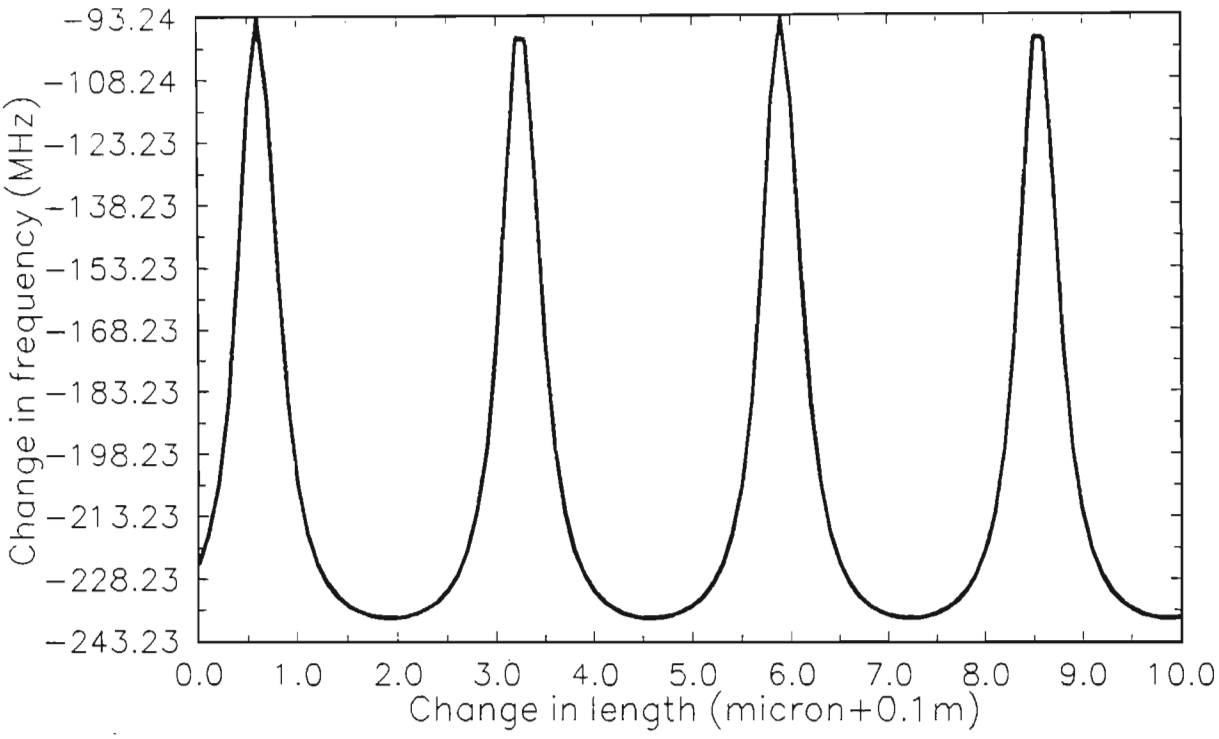

Figure 4.16. The change in resonance frequency with a corresponding change in temperature. Zero on the x−axis corresponds to 0.1 m. The sub−resonator length was then increased by 0.1 micron and the corresponding change in resonance frequency for a 1 Kelvin change in temperature was then calculated.

4.2.8 THE LASER OSCILLATION CONDITION

As was mentioned in section 2.2.4 , the conditions for laser action are that the beam reproduces itself in shape,phase and amplitude. The shape condition determines the transverse modes of the resonator and the phase condition determines the resonance frequencies as was shown in the previous section. The amplitude determines the threshold condition of the laser and this will be dealt with in this section.

Consider figure 4.17. Assume there is a laser medium with a population inversion between the mirrors. It is further assumed that the radiation undergoes a phase change of ϕ_1 and ϕ_2 at mirrors one and two respectively. Approximate the electric field in the cavity with a plane wave. Thus the electric field at the beginning of the trip E_1 is given by:

$$E_1=E_0e^{i\omega t} \qquad 4.101$$

Thus:

$$E_2=E_0e^{i(\omega t-k'l)} \qquad 4.102$$

k is the complex propagation constant as given in equation (2.17).Thus:

$$k' = k\left[1+\frac{\chi'}{2n^2}\right] - ik\frac{\chi''}{2n^2} - i\alpha \qquad 4.103$$

It is further assumed that the reflectivities of mirrors one and two are r_1 and r_2 respectively.Thus:

$$E_3 = E_0 e^{i(\omega t - k' l)} r_1 e^{i\phi_1} \qquad 4.104$$

$$E_4 = E_0 e^{i(\omega t - 2k' l)} r_1 e^{i\phi_1} \qquad 4.105$$

And finally after one complete round trip E_5 is given by:

$$E_5 = E_0 e^{i(\omega t - 2k' l)} r_1 r_2 e^{i(\phi_1 \phi_2)} \qquad 4.106$$

The condition for laser action –threshold condition–requires that:

$$\left|\frac{E_5}{E_1}\right| \geq 1 \qquad 4.107$$

Thus:

$$e^{\frac{-2lk\chi''}{2n^2} - \alpha} r_1 r_2 \geq 1 \qquad 4.108$$

This can be re–written as :

$$\frac{lk\chi''}{n^2}-\alpha-\ln(r_1r_2)\geq 0 \qquad 4.109$$

Using equation (2.20) for the small signal gain (γ) this can be re–written as :

$$l\gamma-\alpha/2+\ln\sqrt{R_1R_2}\geq 0 \qquad 4.110$$

R_1 and R_2 are the intensity reflection coefficients of mirrors one and two respectively. R_1 and R_2 are in general functions of frequency.The laser oscillation condition was numerically calculated using equation (4.110). The specifications of this resonator are the same as the resonator of which the reflectivity is shown in figure 4.13. Figure 4.18 shows the laser oscillation condition of this resonator when a small signal gain of 1.2/m is used with a 75 % output coupler. Figure 4.19 shows the laser oscillation condition of the same resonator with a 75% output coupler with a small signal gain of 0.8/m.

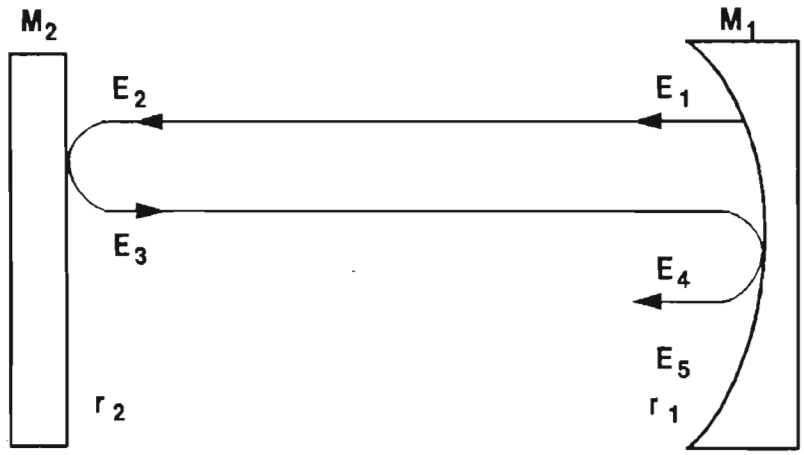

Figure 4.17. The schematic diagram used for deriving the laser oscillation condition.

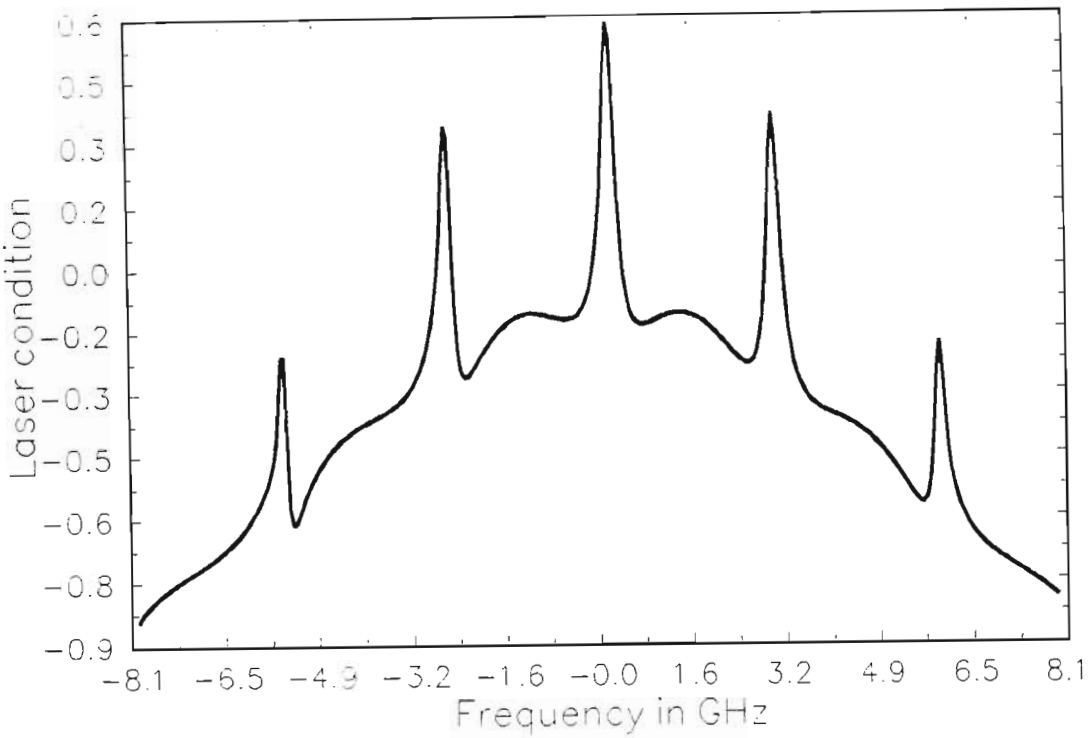

Figure 4.18. The laser condition of a MGC with a 11 mm etalon with 80% reflectivity and a 150 l/mm grating. The small signal gain coefficient was 1.2/ m and the gain length was 0.5m. A 75% reflective output coupler was used.

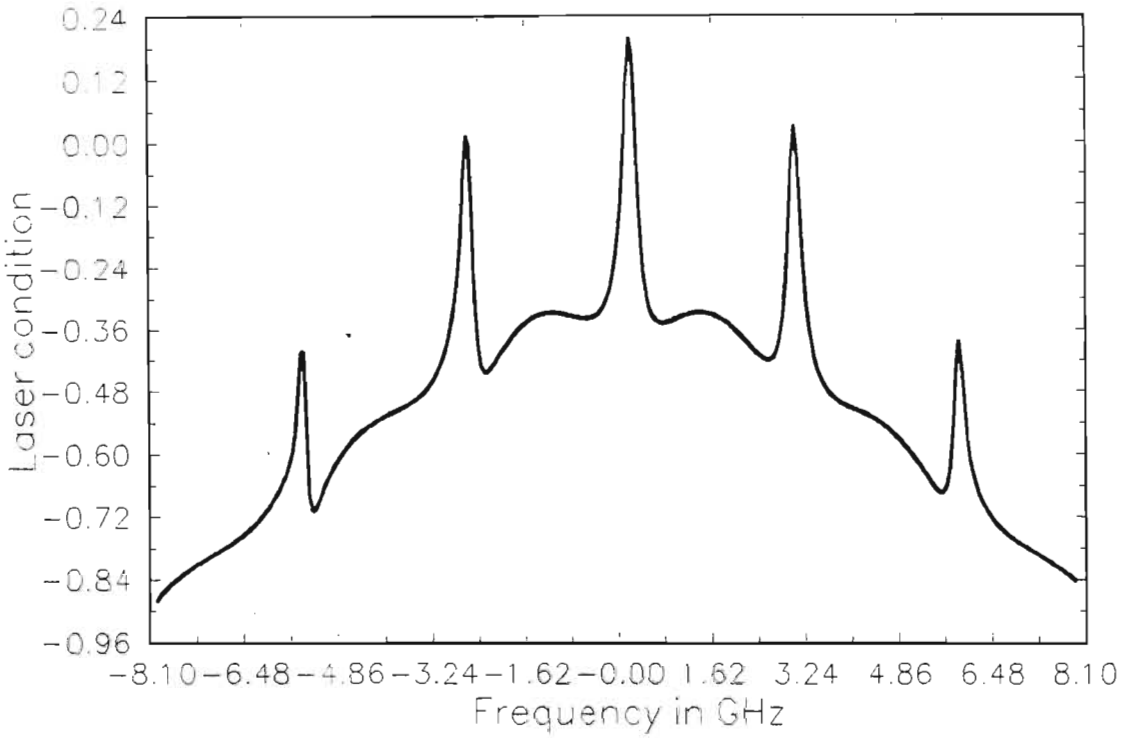

Figure 4.19. The laser condition of a MGC with a 11 mm etalon with 70% reflectivity and a 150 l/mm grating. The small signal gain coefficient was $0.8/m$ *and the gain length was 0.5m. A 75% reflective output coupler was used. Zero corresponds to 10.6 μm.*

4.2.9 DETERMINATION OF OUTPUT COUPLER RADIUS AND REFLECTIVITY.

To ensure that the maximum of the active medium between the electrodes is used and that the resonator satisfied the stability criteria, an appropriate output coupler radius had to be calculated. The spot size must remain relatively constant through the laser, that is :

$$\omega_l = \omega_0$$

According to Yariv [30]

$$\omega_l = \left[1+\frac{l^2}{(lR_2-l^2)}\right]\omega_0 \qquad 4.111$$

Where l is the length of the main resonator.Thus:

$$\omega_0\left[1+\frac{l^2}{(lR_2-l^2)}\right]\approx\omega_0 \qquad 4.112$$

$$=>\frac{l^2}{(lR_2-l^2)}\approx 0$$

$$=> lR_2-l^2 >> l^2$$

$$=>R_2>>2l \qquad 4.113$$

If R_2 is chosen one order larger than l,then:

$$R_2=20l$$

The stability criterion is given by equation (4.7), and can be calculated for this resonator:

$$0\leq(1-l/R_1)(1-l/R_2)\leq 1$$

R_1—>$-\infty$ and $R_2=20l$

Thus the argument in the stability criterion becomes:

$$(1-l/R_1)(1-l/R_2)=(1)(1-1/20)=0.95$$

Thus the stability criterion is satisfied.

Since both radii of the resonator are known the minimum spot size can be calculated. According to Siegman[33] the minimum spot size is given by:

$$\omega_0=\left(\frac{\lambda z_0}{\pi n}\right) \qquad 4.114$$

z_0 is given by:

$$z_0=\frac{l(-R_1-l)(R_2-l)(R_2-R_1-l)}{(R_2-R_1-2l)^2} \qquad 4.115$$

Thus:

$$\lim_{R_1\to-\infty} z_0^2=(lR_2-l^2) \qquad 4.116$$

Thus the minimum spot size, equation (4.114), can be written as :

$$\omega_0=\left[\frac{(lR_2-l^2)^{1/2}\,\lambda}{\pi n}\right]^{1/2} \qquad 4.117$$

For this resonator (l=0.7m, R_2=10m):

ω_0 = 2.9mm

The reflectivity of the output coupler was optimized using the graphs in figures 4.20 and 4.21.The output energy and peak power of the laser were calculated , for different output coupler reflectivities using equations (4.59) to (4.61). Figure 4.20 shows the pulse energy as a function of output coupler reflectivity. Maximum energy per pulse is obtained for a 75% reflective output coupler. Figure 4.21 shows the peak power as a function

of output coupler reflectivity. The maximum peak power is also obtained with a 75% output coupler. It was assumed that the back mirror reflectivity was 90%.

4.2.10 EFFECTIVE SUB–CAVITY INTENSITY.

Consider the three mirror configuration shown in figure 4.3. The total intensity inside the sub–cavity is given by:

$$E_T=E_{1T}+E_{2T}+E_{3T}+... \qquad 4.118$$

Where E_{1T},E_{2T}, etc are the intensities at a specific point inside the sub–cavity. If this point is taken to be just left of the partial reflector then:

$$E_{1T}=E_0 t e^{i\omega t}$$

$$E_{2T}=E_0 t t_e^2 r_g r_1 e^{i(\omega t+2\delta')}$$

$$E_{3T}=E_0 t^4 r_g^2 r_1^2 e^{i(\omega t+4\delta')}$$

These terms form a geometric series and the result is given by:

$$E_T=\frac{E_0 t e^{i\omega t}}{1+t_e^2 r_g r_1 e^{i(\omega t+2\delta')}} \qquad 4.119$$

Consider a lossless etalon, thus $t_e=1$.

The ratio of the field inside the sub–cavity to the incoming

field is given by:

$$t_r = \frac{E_0}{E_T} \qquad 4.120$$

The intensity ratio ,T_r , is given by multiplying t_r by its complex conjugate, thus:

$$T_r = \frac{t^2}{1 - 2 r_g r_1 \cos\delta + r_g^2 r_1^2} \qquad 4.121$$

But $t^2=(1-R)$ and this ratio is a minimum where $\cos\delta=-1$, thus the minimum T_r, thus maximum reflectivity, is given by:

$$T_r = \frac{1 - R_1}{(1 + \sqrt{R_g}\sqrt{R_1})^2} \qquad 4.122$$

Thus for a resonator with a 50% partial reflector and a grating with a reflectivity of 95% the ratio of the intensity on the grating to that inside the main resonator would be 0.17, thus the intensity on the grating would be 17% that inside the main resonator. It must be emphasised that this is only valid when the MGC is adjusted to give maximum reflectivity.

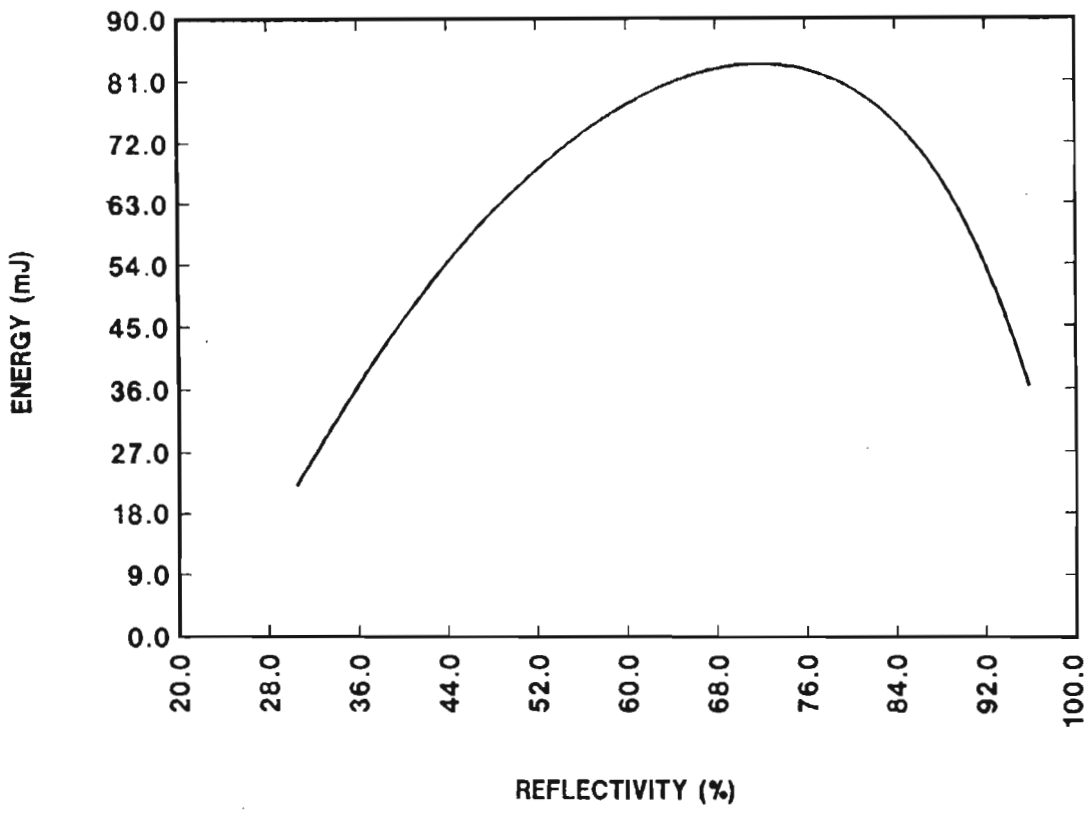

Figure 4.20. Laser output energy as a function of output coupler reflectivities.

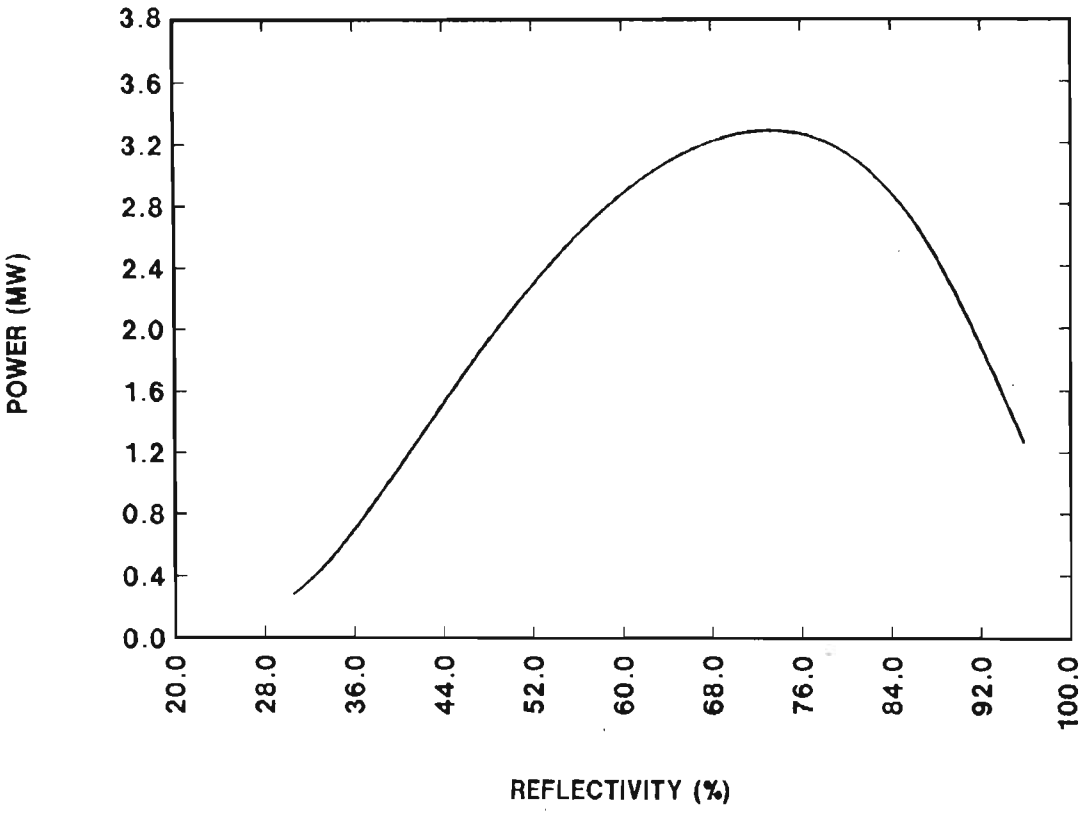

Figure 4.21. Laser peak pulse power as a function of output coupler reflectivities.

CHAPTER 5

TESTING OF A THREE MIRROR RESONATOR.

5.1 EXPERIMENTAL PROCEDURE

5.1.1 LASER AND RESONATOR USED IN THESE TESTS.

The objectives of the resonator tests were to determine if single mode laser action –on one of the lower gain lines– could be obtained with a three mirror resonator and to determine the maximum obtainable single mode laser energy. Of particular interest to this program was the R branch at 10 μm line and thus the tests were done on this branch. These results were compared with the predicted results.

Using the previous analysis a three mirror resonator was designed built and tested. The laser used in the tests was a commercial high pressure laser supplied by Laser Applications (HP 10). This is a discharge excited UV pre–ionized laser. The discharge is excited by a two stage Marx bank with a total capacitance of 30 nF.The standard resonator on this laser was removed and was replaced by the three mirror resonator. The specifications of this resonator are the same as the resonator of which the reflectivity is shown in figure 4.13.The specifications are given below:

Sub–resonator Length 0.1m

R of partial reflective mirror	50%
Main resonator length	0.6m
Gain length	0.4m
Output coupler reflectivity	75%
Output coupler radius	10m
Minimum spot size	2.9mm
Grating	150l/mm
Etalon Thickness (ZnSe)	11mm
Etalon Reflectivity	80%

The resonator was mounted on invar rods. The output coupler was mounted on a piezo–electric drive in order to adjust the length of the main cavity . This ensured that the main resonator axial modes coincide with the mode that was selected by the sub–cavity. The grating angle was adjusted by micrometers. The etalon angle was adjusted by a micrometer and a piezo–electric crystal. The piezo–electric crystal was used for fine adjustments. Pictures of the resonator are shown in figures 5.1 and 5.2. Figure 5.1 shows the sub resonator part and figure 5.2 shows the output coupler mounted on a piezo–electric drive.

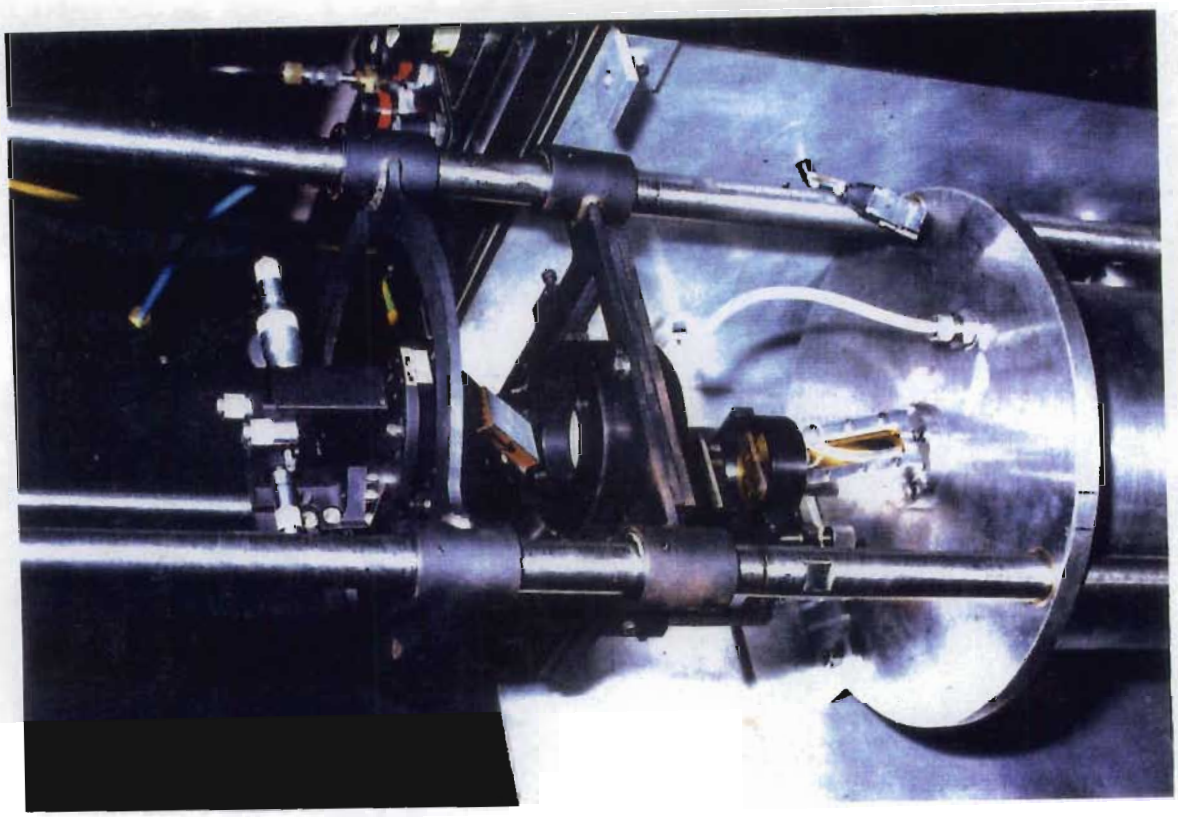

Figure 5.1 A photograph of the resonator used in these tests. The sub–resonator part is shown

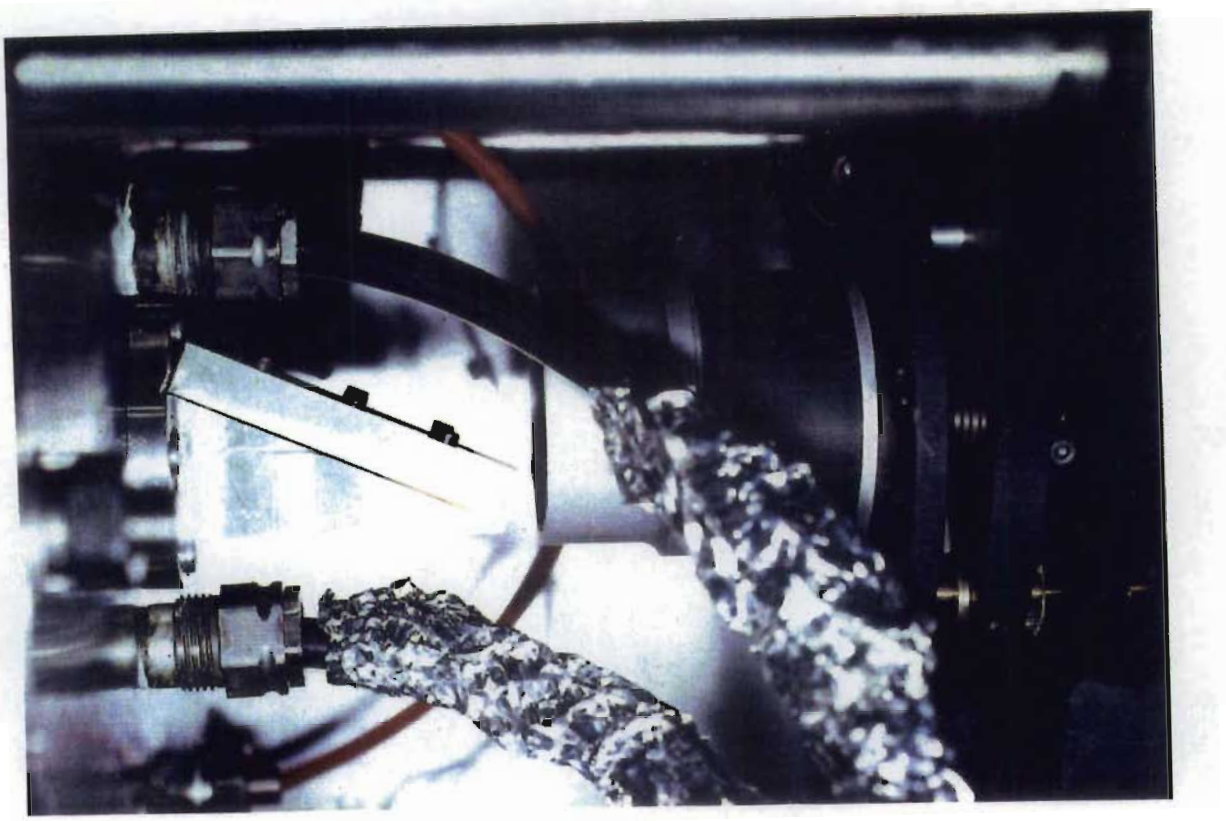

Figure 5.2 A photograph of the resonator used in these tests. The output coupler mounted on a piezo–electric translator is shown.

5.1.2 DETERMINATION OF THE PRESENCE OF MULTI MODE LASER ACTION.

If the laser has multiple modes, which oscillate at the same time, five different scenarios can be sketched [33]:

(i) Uniform amplitude sidebands, all in phase. In this case there is one primary mode–locked pulse per period, with a FWHM pulsewidth given roughly by $\tau_p \approx T/N$, plus N–2 much weaker subsidiary peaks. T is the cavity round trip time and N is the number of modes oscillating at the same time.

(ii) Gaussian–amplitude sidebands,all in phase. Again the result is a train of periodically spaced short pulses, but the pulses now have Gaussian shapes in time, with essentially no subsidiary peaks.

(iii) Random amplitude sidebands all in phase. Periodic pulses are still obtained in this case, but there is an irregular background of sub–pulses between the main pulses.

(iv) Uniform–amplitude sidebands, random phases The signal now consists not of single clean pulses, but of a random set of much weaker impulses–essentially a noise–like signal–with impulses distributed throughout the entire roundtrip period. The signal is still strictly periodic in time that is, it will repeat exactly after one round trip. The "noise spikes" within each period have a

width which is approximately the same as the ideally mode locked situation, ie τ_p=T/N.

(v) Rectangular quasi–FM spectral distribution. In this case the sideband amplitudes are uniform but the sideband phases have been empirically adjusted to give an intensity profile which has reduced peak to peak variation, and which does not go to zero anywhere within the period. This particular result thus represents something close to a quasi–phase modulation or frequency modulation (FM) signal with only a minimal amplitude variation during the round–trip period.

Thus a multimode laser can be characterised by rapid intensity fluctuations(rapid in terms of the cavity round trip time). The most difficult case to detect would be number iv above. In this case the signal would consist of noise like impulses. The half–width of these pulses would be T/N. Thus if an oscilloscope/detector combination is to be able to follow the intensity fluctuations then the combined response time of the oscilloscope and detector must be less than T/N seconds. The resonator used in these tests had a length of 0.5 m and thus the round trip time would be given by:

$T=2*0.5/3.0x10^8=4.7ns$

Thus if 10 modes are oscillating at the same time then the half width of the intensity spikes would be given by:

τ_p=(4.7/10)nS=0.47ns

If the three mirror cavity is used with an etalon the reflectivity for the resonator being tested is given by figure 4.13. As can be seen from this figure it is extremely unlikely that more than three modes can oscillate at the same time. Thus the half–width of the intensity spikes would be given by:

τ_p=(4.7/3)nS=1.57ns

Thus the response time of the oscilloscope/detector must be less than 1.5ns to be able to detect three modes oscillating at the same time.

A more likely scenario is two modes oscillating at the same time.Suppose that two modes are oscillating at the same time. The output field as a function of time can then be written as :

$$E(t)=Re[E_1 e^{i(\omega_1 t+\phi_1)}+E_2 e^{i(\omega_2 t+\phi_2)} \qquad 5.1$$

ϕ_1 and ϕ_2 are the phases of the two axial mode respectively. The output intensity of the laser as a function of time can then be written as:

$$I(t)=|E(t)|^2=E_1^2+E_2^2+2E_1E_2\cos[(\omega_1-\omega_2)t+\phi_1+\phi_2] \qquad 5.2$$

Thus the output intensity of a laser with two axial modes varies sinusoidally with a beat frequency $(\omega_1-\omega_2)$.The depth of the modulation is 100% if the two modes are equal. A change in the relative phases ϕ_1 and ϕ_2 of the two modes will change the time origin for the peak of the mode beating but will not otherwise change the appearance of the mode beats. Thus any two sinusoidal signals are always mode–locked. Mode beating on a laser pulse is thus an indication that at least two modes are oscillating at the same time.

Thus a detector/oscilloscope combination had to be found which had a response time of less than 1.5 ns. If a smooth pulse was then measured when the etalon is in the resonator then it can be said that the laser action is in a single mode. It must be emphasised that this statement can only be made if the etalon is in the resonator. If the etalon is not being used, many modes can be oscillating at the same time making the half–widths of the intensity spikes too small to be followed by the oscilloscope/detector combination. These spikes would then be integrated giving a smooth pulse.

The photondrag mechanism of detection involves the transfer of momentum from the laser photons to the free carriers in a germanium bar, resulting in the dragging of the carriers in the direction of the laser beam propagating in the bar [78,79]. When large peak–power laser pulses are used, the photondrag produces

sufficient longitudinal EMF in a p–type germanium bar for the detection of the incident laser pulses. The fundamental response time of a photondrag detector is the momentum relaxation time of the carriers, approximately $3x10^{-13}$s at room temperature. In practice the speed is limited by the RC time constant of the detector. The detector used in this experiment was a germanium photondrag detector of Edinburgh Instruments (PD–2)with a rated response time better than 1nS[80]. The active diameter of the detector was 11.5mm and its maximum power density was 20 MW/cm^2. The spectral response of the detector was from 9 to 11 μm. The typical sensitivity of the detector was 180 mV/MW. A Tektronix 2440 digital storage oscilloscope was used with the germanium photondrag detector. The sampling rate of the oscilloscope is 500 Ms/s giving it a time resolution of 1ns.Thus the combined response time of this oscilloscope/detector combination would be less than 1.5ns. Thus it can be said that if a smooth laser pulse was measured with this combination and the etalon was in the resonator then the pulse was single longitudinal mode.

The laser line was measured, using a grating monochromator, as was discussed in chapter 4.Energy measurements were made using a Gentech pyro–electric energy meter. A pyro–electric detector uses the temperature dependence of the electric polarization of ferroelectric materials. A change in the temperature causes a change in the electric polarization.

5.1.3 DETERMINATION OF THE ONSET OF PARASITIC OSCILLATION.

The onset of parasitic oscillations was determined in two distinct methods. The first method was to use the grating monochromator to measure the frequency components of the laser radiation. The second method used a photondrag detector. Since the gain and reflectivities of the two modes are different their gain switching time would be different. The photondrag detector shows the intensity as a function of time , thus two distinct pulses would be seen on the photondrag detector.

5.2 EXPERIMENTAL RESULTS

Figure 5.3 shows a photondrag signal of a laser pulse with mode beating. This was measured when the MGC was operated with the etalon removed. The frequency difference between the two modes is 1/(10ns)=100 MHz. The frequency difference between two neighbouring modes in this resonator (length 3.0m) is:

$$\Delta f = c/(2L) = 3 \times 10^8 / (2 \times 1.5) \text{Hz} = 100 \text{MHz}$$

A single longitudinal mode pulse is shown in figure 5.4 . This was measured on the R30 line with the etalon in the MGC. The FWHM of this pulse was 83 nS. The energy of this pulse was 30 mJ as measured by a Gentech pyro–electric detector. The energy could not be increased without causing parasitic oscillations on the P20 branch , lasing from the 50% mirror. Figure 5.5 is a photondrag R30 pulse with the parasitic P20 pulse.The value of 30 mJ obtained was less than the value of 52 mJ predicted in table 4.2. However it could be expected that the practical reflectivity of the grating was less than the 100% used in calculating the MGC reflectivity graph shown in figure 4.13.Using this 100% reflectivity, for the grating peak, the maximum reflectivity peak in figure 4.13 has a reflectivity of 90%. If the MGC maximum reflectivity is lowered to 85% and

this value is used in calculating the laser pulse energy and pulse shape, a pulse with an energy of 34mJ and a FWHM of 87ns is obtained. The calculated pulse is shown in figure 5.6 .This energy and FWHM are close to the measured values.

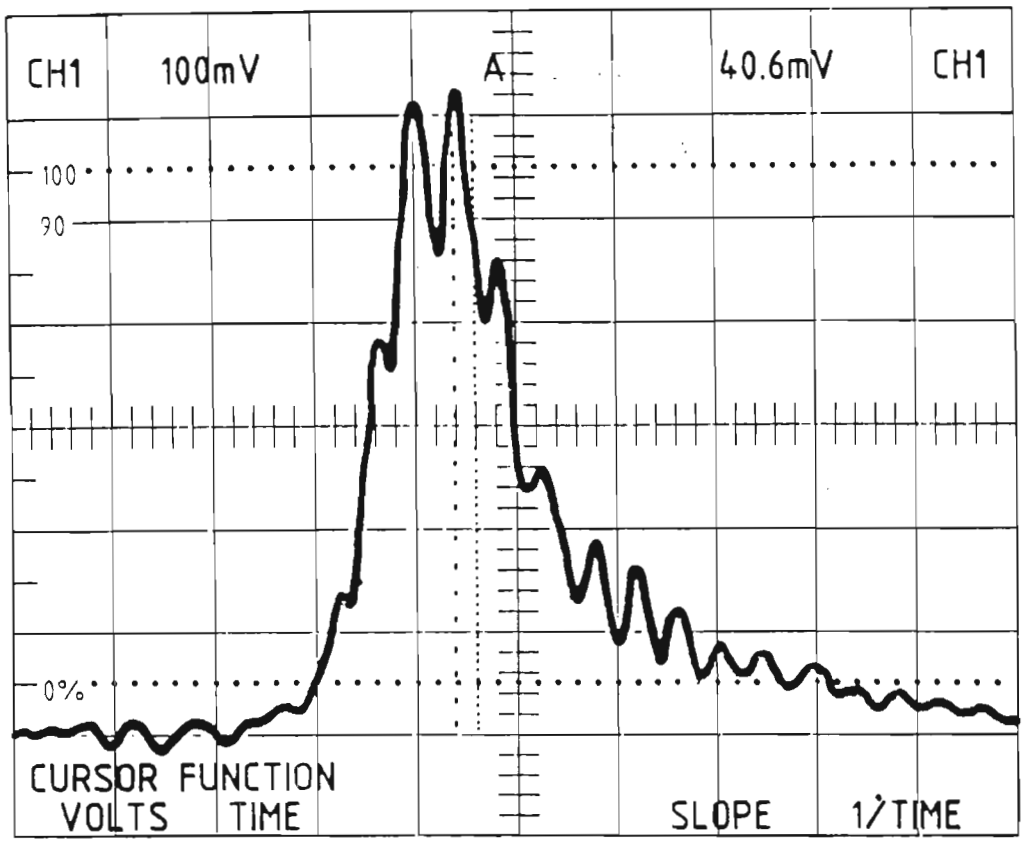

Figure 5.3 A photondrag signal of a laser pulse with mode beating. The time division was 20ns/div.

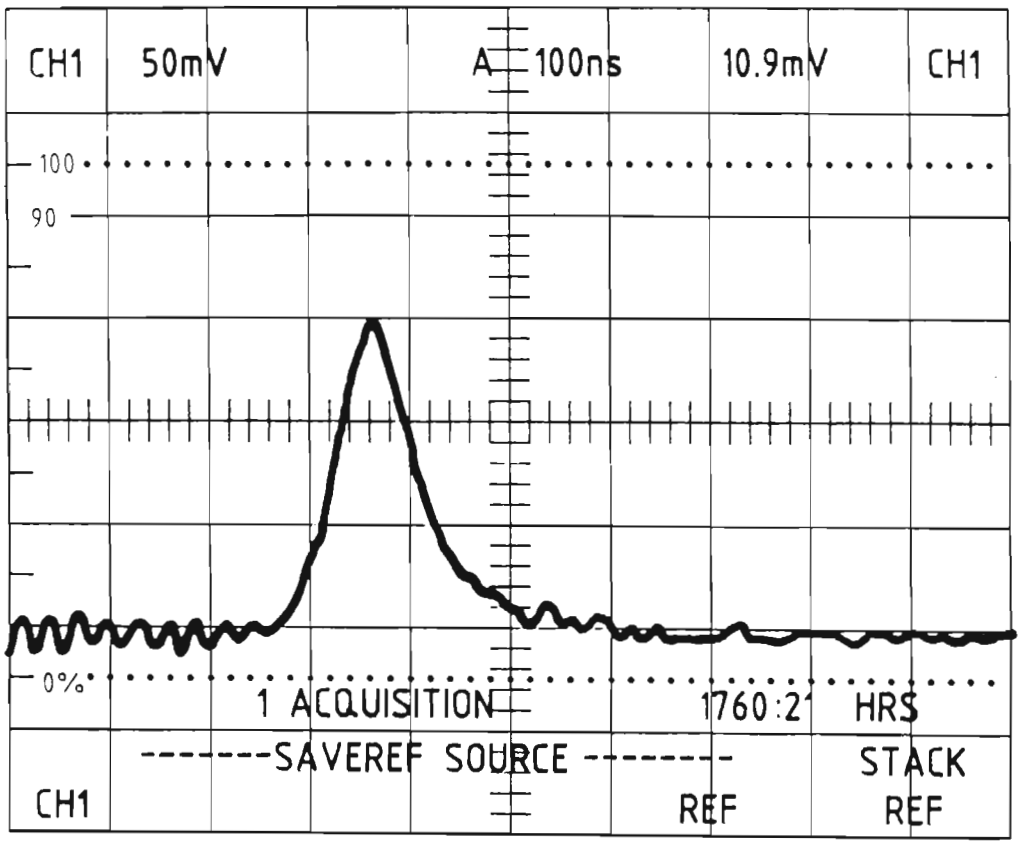

Figure 5.4 A photondrag signal of a single mode pulse. This was measured on the R30 line. The FWHM of this pulse is 83 nS. The energy of this pulse was 30 mJ.

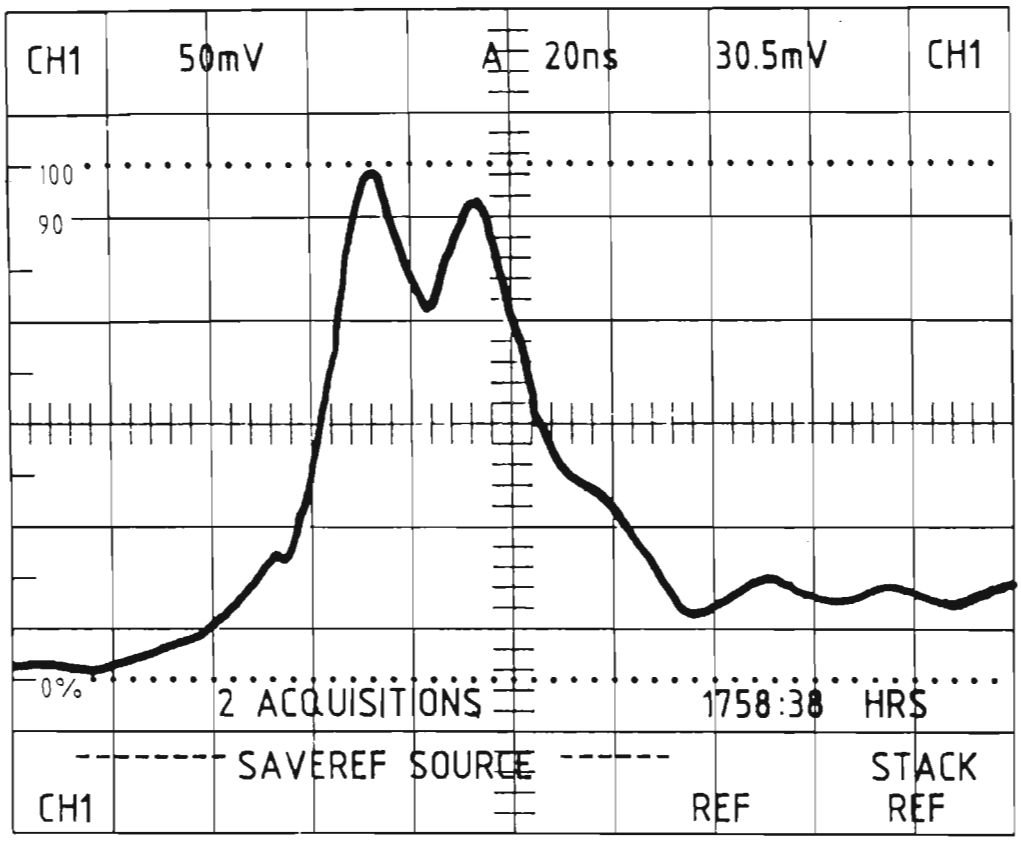

Figure 5.5 A photondrag signal of the R30 pulse with a parasitic P20 pulse.

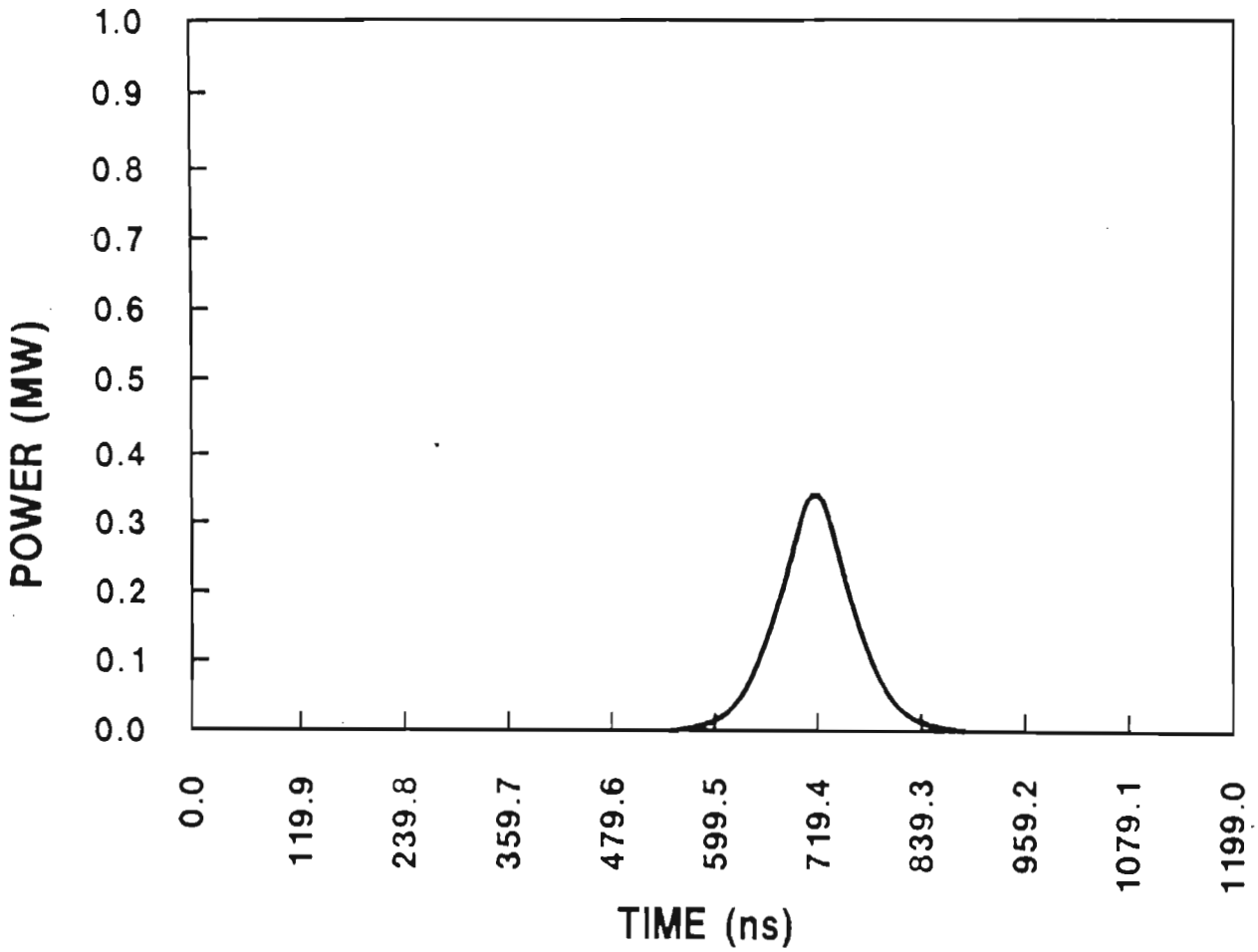

Figure 5.6 The calculated R30 pulse. The FWHM is 87 nS and the energy is 34 mJ

CHAPTER 6

THE USE OF WATER AS A DIELECTRIC MATERIAL IN PULSED POWER DEVICES.

6.1 INTRODUCTION

Capacitors are the basic electrostatic energy storage elements in pulsed power systems. Capacitors are of the weakest elements when the pulsed power system is operated at high repetition rates for extended periods of time [81]. Several factors can influence the life expectancy of a capacitor. Figure 6.1 gives the life expectancy of a capacitor against operating voltage [82]. The life expectancy can be drastically improved by operating at a voltage lower than the rated voltage of the capacitor. Figure 6.2 gives the life expectancy against voltage reversal. Operating at high voltage reversals can reduce the lifetime of the capacitor. The life expectancy against operating temperature is given in figure 6.3. The four main different capacitor types suitable for the use in high power pulsed power supplies are[83]:

(i) Polypropylene or Teflon/Silicon Oil (PPSO)

(ii) Mica

(iii) Ceramic

(iv) Water with metal electrodes.

The basic construction of a PPSO is shown in figure 6.4. It

consists of aluminium foil separated by layers of polypropylene film. The whole capacitor is evacuated and then filled with a dielectric oil eg. silicone oil. Ceramic capacitors have the disadvantage that their capacitance changes with voltage.

The object of this investigation was to determine the feasibility of using water capacitors in high repetition rate pulsed power supplies and to compare it with the other capacitors.

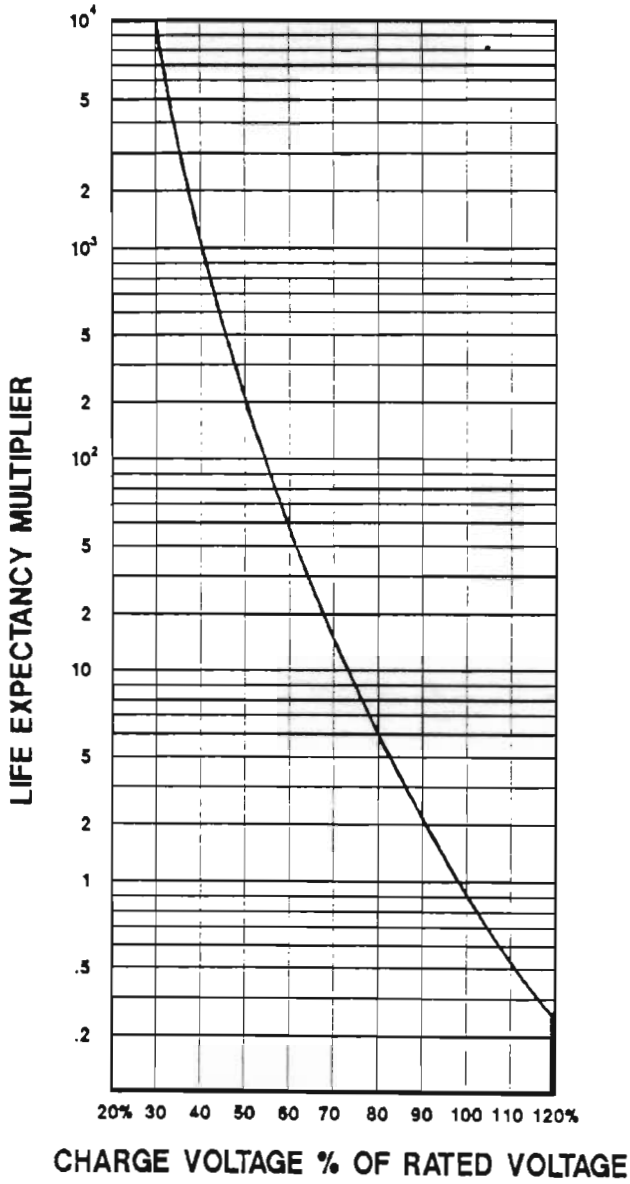

Figure 6.1. Life expectancy as a function of charge voltage for a PPSO capacitor.

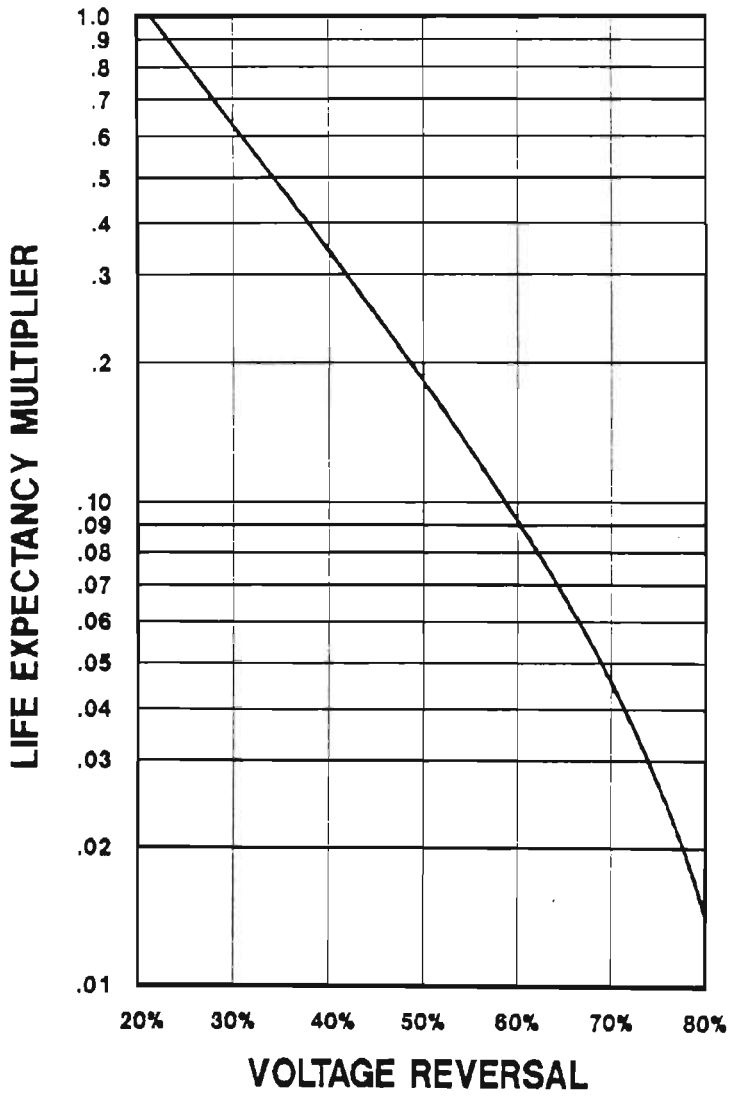

Figure 6.2. Life expectancy as a function of voltage reversal of a PPSO capacitor.

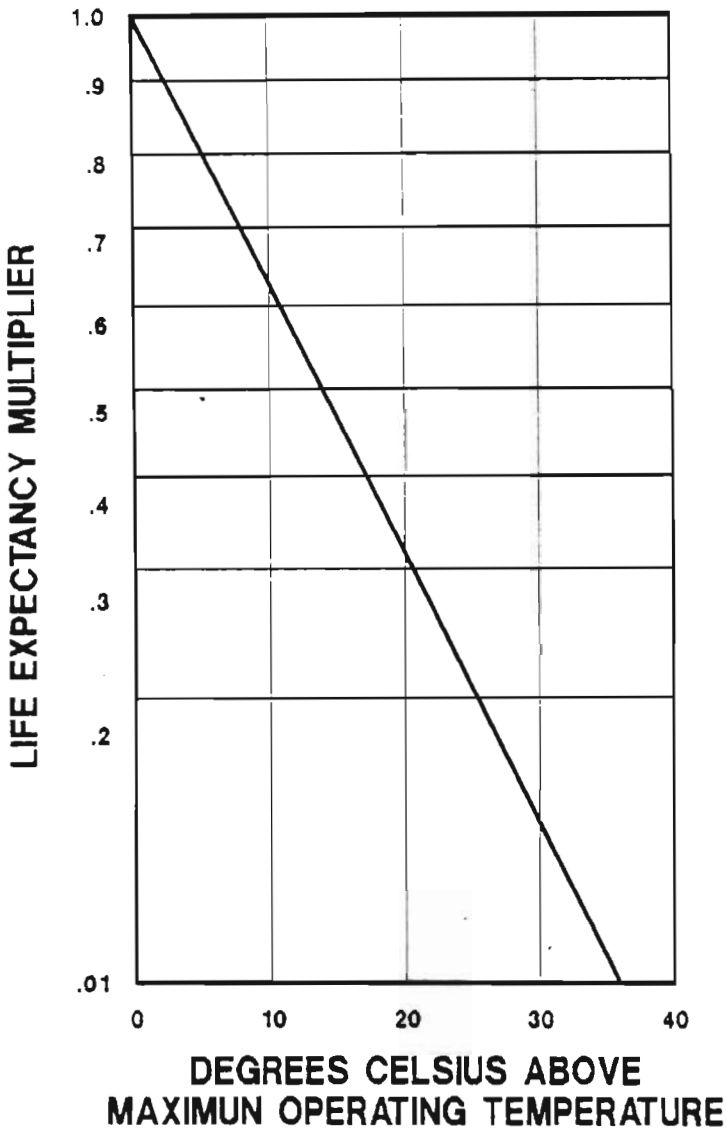

Figure 6.3. Life expectancy as a function of operating temperature of a PPSO capacitor.

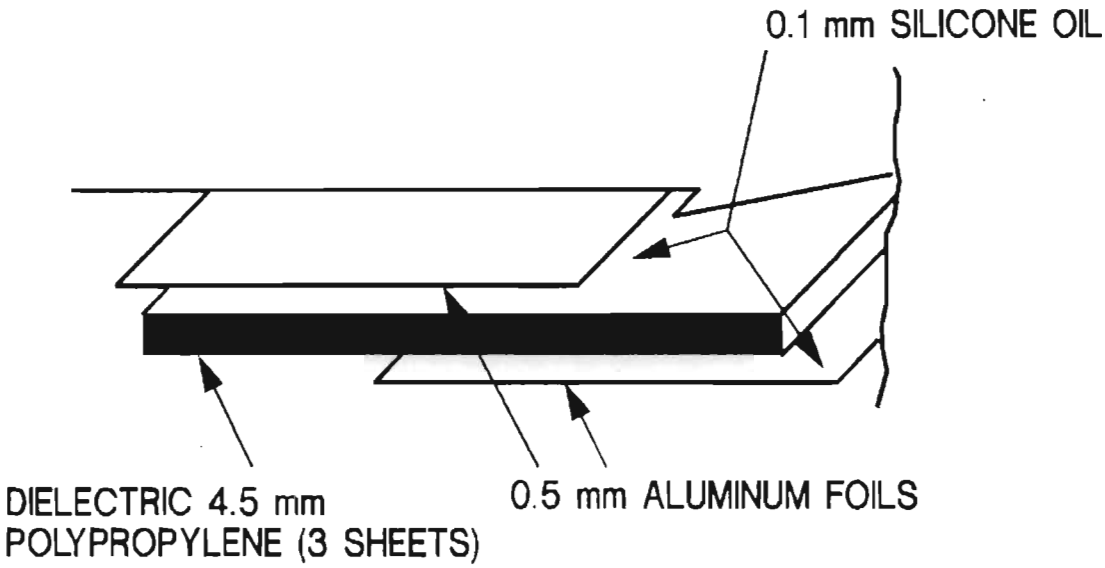

Figure 6.4. The basic construction of a commercial PPSO type capacitor.

6.2 WATER AS A DIELECTRIC MATERIAL.

All chemical bonds are formed by the sharing of electrons between atoms. The sharing is often unequal and some atoms gain electron density at the expense of their neighbours. The electron clouds of the water molecule are shown in figure 6.5. Although the water molecule is not ionic, there is a substantial electron transfer from hydrogen to oxygen, and the molecule has a permanent dipole moment. In the absence of an external electric field, there is no polarization in the water, thus the dipole moment per unit volume in a large–scale sample is zero. However water becomes strongly polarized when an external field is switched on, and the relative permittivity of water at room temperature is approximately 80. The polarization of the atoms or molecules can arise in two ways:

(i)The applied field distorts the charge distribution and so produces an induced dipole moment in each molecule.

(ii)The applied field tends to line up initially random orientated permanent dipole moments of the molecules.

This orientation polarization is important in "polar" substances such as H_2O, HCl,and CH_2OHCH_2OH (ethylene glycol). Booth [84] calculated the dielectric constant of water as well as the saturation of the dielectric constant caused by an applied external electric field. The equation he derived is given by:

$$\epsilon = n^2 + \frac{28N_0\pi(n^2+2)\mu_\nu}{3\sqrt{73}E} L\left[\frac{\sqrt{73}E\mu_\nu(n^2+2)}{6kT}\right] \qquad 6.1$$

Where L(x) is the Langevin function given by:

$$L(x) = \coth(x) - \frac{1}{x} \qquad 6.2$$

And:

n :index of refraction of water (1.33)

N_0 :number density of molecules (molecules/cm^3)

μ_ν :external moment of the molecules (2.1 Debye units)

E :electric field in statvolts.

k is the Boltzmann constant and T is the temperature. Figure 6.6 gives the dielectric constant of water as a function of the electric field. As can be seen the dielectric constant has fallen to half its usual value when the electric field is approximately 5.0 MV/cm.

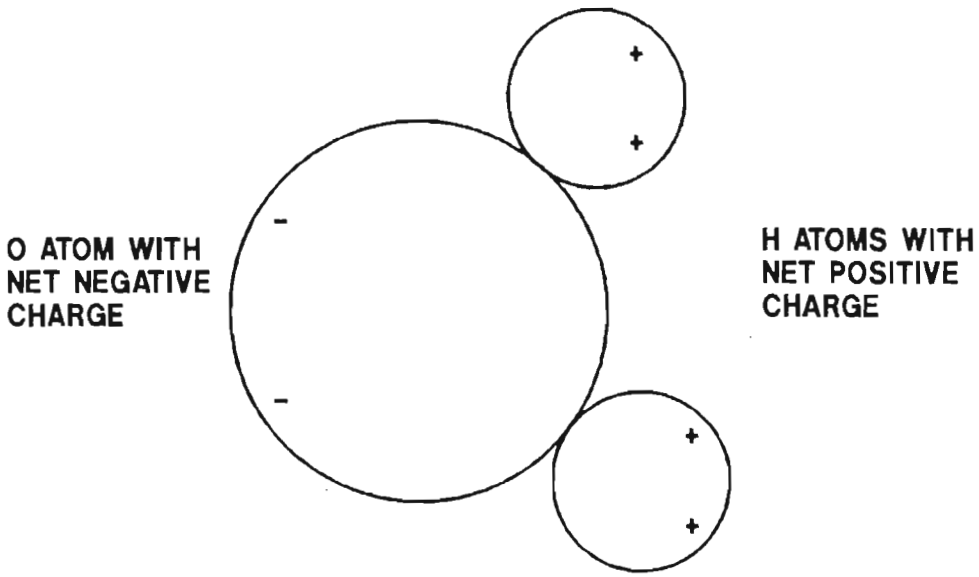

Figure 6.5. The electron cloud configuration of a water molecule.

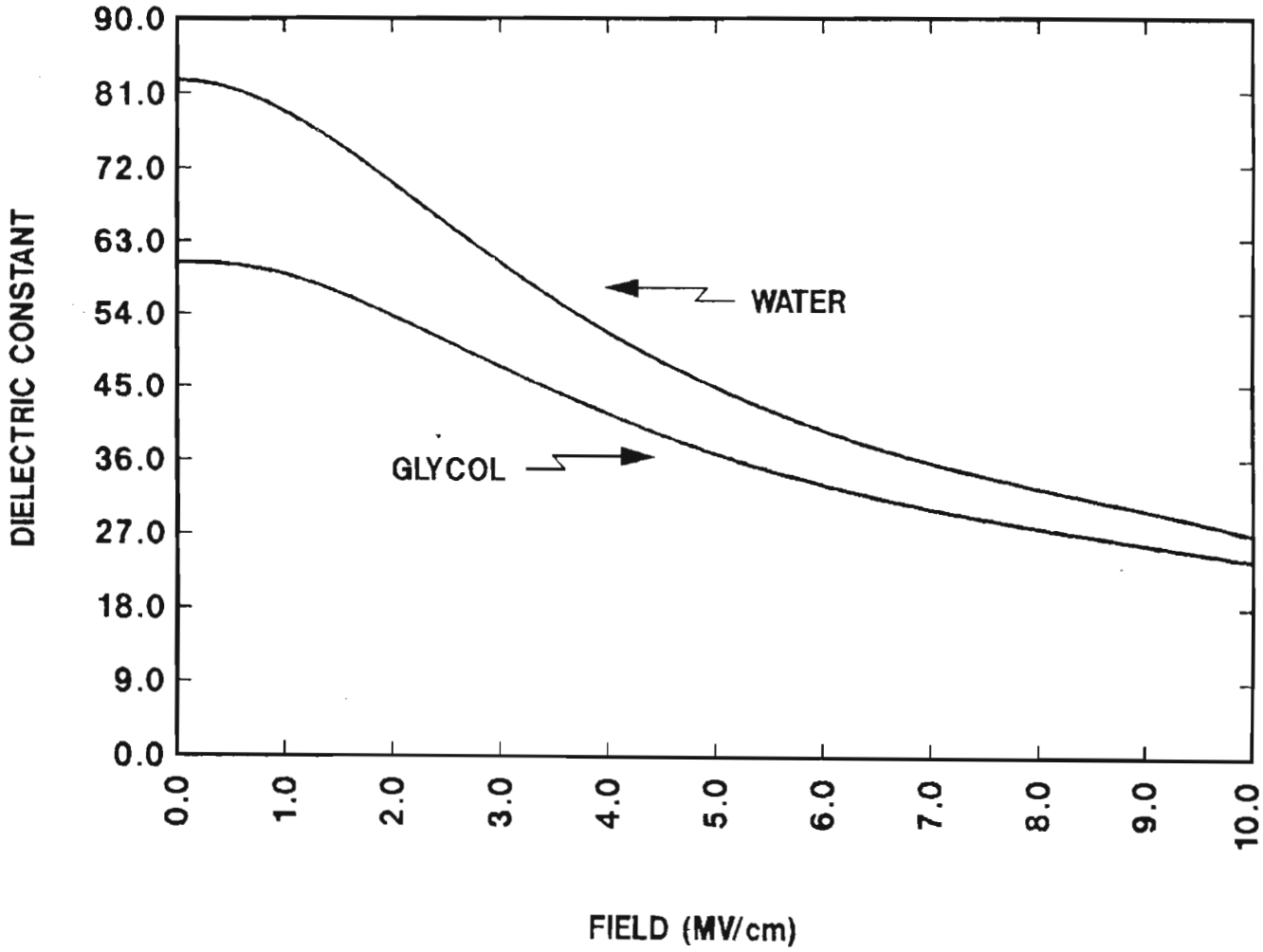

Figure 6.6. The dielectric constant of water at 273 K as a function of the applied electric field.

6.2.1 THE INDUCTANCE AND IMPEDANCE OF A WATER CAPACITOR.

Because of the high dielectric constant of water it is commonly used as the dielectric in high–power pulse forming lines [85,86,87,88]. An idealized water pulse forming line is shown in figure 6.7. This simple system consists of a pulse forming line, a switch S and a load of resistance R. The characteristic impedance of the line is made equal to R. The pulse forming line is initially charged to a voltage V_0. When the switch is closed the voltage across the load instantaneously rises to $V_0/2$ and remains constant for a pulse time t_p, thereafter falling to zero. All the electric energy which was stored as electrical stress in the dielectric filling the PFL is delivered to the load. The advantage of using a dielectric with a high dielectric constant will be explained below.

Consider figure 6.7. The magnetic field in the gap is found by applying Ampere's law. There is no magnetic field outside the transmission line, since a contour integral right around the whole line encloses no current. Applying Ampere's law to the dotted contour gives:

$$\oint \bar{B}.d\bar{l} = \mu\mu_0 I \qquad 6.3$$

Thus:

$$Ba=\mu\mu_0 I \qquad 6.4$$

Thus the magnetic field is given by:

$$B=\frac{\mu\mu_0 I}{a} \qquad 6.5$$

When a closed circuit is formed by connecting the ends of a length l of the line, the magnetic flux is given by:

$$\phi=\int_s \bar{B}.d\bar{s}=Bld \qquad 6.6$$

Using equation (6.5) the magnetic flux can be written as:

$$\phi=\frac{\mu\mu_0 ldI}{a} \qquad 6.7$$

The self–inductance is given by:

$$L=\frac{\phi}{I}=\frac{\mu\mu_0 ld}{a} \qquad 6.8$$

Thus the self–inductance per unit length is given by :

$$L'=\frac{\mu\mu_0 d}{a} \qquad 6.9$$

The characteristic impedance of a transmission line is given

by[89]:

$$Z_0=(L'/C') \qquad 6.10$$

With C' the capacitance per unit length and is given by:

$$C'=\frac{\epsilon\epsilon_0 a}{d} \qquad 6.11$$

Thus the characteristic impedance of this transmission line is given by:

$$Z_0=\left[\frac{\mu\mu_0}{\epsilon\epsilon_0}\right]^{1/2}\frac{d}{a} \qquad 6.12$$

But:

$$[\mu_0/\epsilon_0]^{1/2}\approx 377 \qquad 6.13$$

Assuming $\mu=1$ equation (6.12) can be rewritten as :

$$Z_0=\frac{377d}{\sqrt{\epsilon}a} \qquad 6.14$$

Typical high energy pulse power loads are commonly 10 ohms or less, so that it is clear from equation (6.14) that a high value of ϵ would be desirable to maintain a reasonably shaped transmission line.

Using equation (6.10) the inductance per unit length of water capacitor can be written as:

$$L'=C'Z_0^2 \qquad 6.15$$

If a typical water capacitor with values of 0.005m and 0.1m for d and a respectively is used then the impedance per unit length is given by:

$$Z_0=2.11\ \Omega$$

The capacitance per unit length is given by:

$$C'=\frac{\epsilon\epsilon_0 a}{d}\ 80x8{,}854x10^{-12}x0.1/0.005=\ 14.2nF/m$$

Thus the inductance per unit length is given by:

$$L'=\ 14.2x2.11^2=\ 63.22\ nH/m$$

The length of this configuration of capacitor necessary to give a capacitance of 1 nF is given by:

$$l\ = 1.0x10^{-9}xd/(\epsilon\epsilon_0 a)$$
$$= 0.07m$$

Thus the inductance of this water capacitor is given by:

$$L = L' \times 0.07$$
$$= 4.4\text{nH}$$

Thus the inductance of a this stripline type 1 nF water capacitor is 4.4nH.

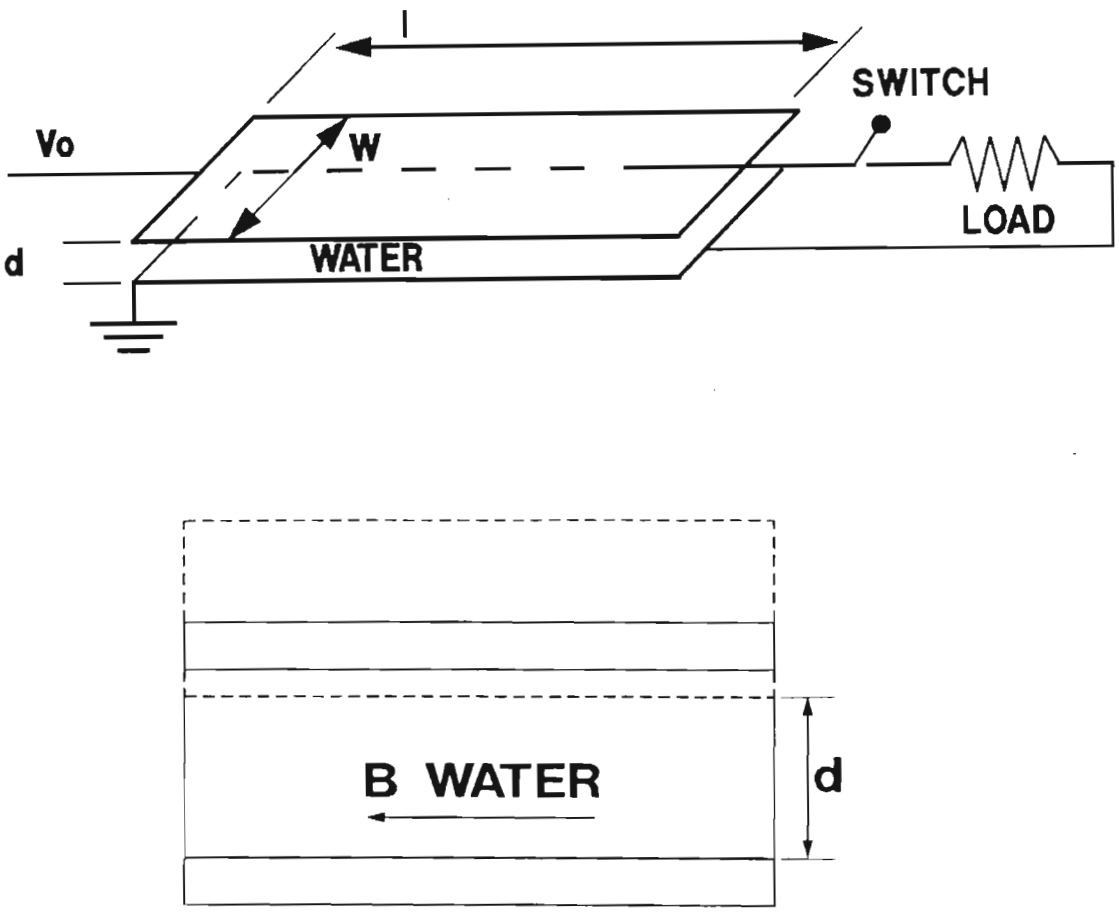

Figure 6.7. An idealized water pulse forming line.

6.3 ELECTRIC BREAKDOWN OF WATER

6.3.1 INTRODUCTION.

The capacitance of a water capacitor is given by equation(6.11). The maximum energy that can be stored in a specific capacitor is given by $0.5CV_{max}^2$, where V_{max} is the maximum electric field that can be applied across the electrodes before electric breakdown would occur. Thus the energy density of a capacitor will be determined by the maximum breakdown strength of the water. The breakdown strength of water is thus an important design parameter. Very few experimental results on the breakdown strength of water for pulse durations of a microsecond and longer have been published. No theoretical model describing the electric breakdown of water under these long pulse durations could be found in the literature. Thus a mathematical model describing the pulse breakdown of water under long pulse durations was developed.

In this model use is made of the so–called "bubble theory" of breakdown. In the "bubble theory" the breakdown mechanism is the formation of a bubble in the liquid dielectric. This bubble is formed by the vaporization of the dielectric by local heating in the strong fields created by asperities on the electrode surface. A bubble so formed will grow and breakdown will occur in the low dielectric strength vapour in the bubble and this rapidly leads to

rupture of the bulk liquid. A review of this subject is given by Sharbough et al. [90]. According to recent literature a gaseous phase is always present in the breakdown streamers [91,92].

Two types of streamers are present, the so–called slow and fast moving streamers. The breakdown process in the two cases is different. In the case of the slow streamer, when voltage is applied to an electrode, a gas bubble will form and grow. As soon as the bubble reaches a critical diameter, a glow discharge, in the bubble, will arise. The electrons generated during this discharge will move to the tip of the streamer and into the liquid forming a space charge layer. The field inside the bubble will thus be weakened and it will be strengthened at the tip of the streamer and the process will repeat itself. During fast streamer breakdown the field at the tip of the streamer becomes high enough to exceed the intrinsic strength of the medium and the molecules will be ionized in the liquid phase. Both processes must be initiated by the formation of a bubble in the liquid. Thus the condition used, in this model, to calculate the minimum electric field necessary to cause a breakdown was the field required to form a bubble in the liquid. The energetic processes considered were:

(i) The energy required to vaporize a unit volume of gas .

(ii) The energy required to move a streamer through

the liquid.

(iii) The energy coupled into the liquid by the electric field and current.

The charge carriers in ultra pure water are positive and negative ions. Since these ions have a low mobility, the formation of space charges have been ignored for the pulsed breakdown of warter.

6.3.2. THEORY

The rate at which energy is coupled into the water can be written as the following equation:

$$E_{avb}J=C_p\rho\frac{dT}{dt}+P_t+P_d+P_Q \qquad 6.16$$

With:

E_{avb}	:Average electric field in the bubble.
J	:Current density.
C_p	:Specific heat capacity of the liquid.
ρ	:Density of the liquid.
$C_p\rho\frac{dT}{dt}$	:Water heating term.
P_t	Thermal conductivity term.
T	:Temperature inside bubble.
T_a	:Ambient temperature.
P_d	:Drag term (to move bubble through the liquid).
P_Q	:Heat of transformation term.

Let $Q=E_{avb}J-P_d-P_Q$ 6.17

Equation (6.16)can be written as:

$$\frac{dT}{dt}=\frac{1}{C_p\rho}Q \qquad 6.18$$

To determine the breakdown strength, E_{max}, of the water it is assumed that enough energy is coupled into the water during a pulse time τ to heat the water from the ambient temperature to the boiling temperature. Thus equation 6.18 has to be solved with the following boundary conditions:

At $t=0, T=T_a$ and at $t=\tau$, $T=T_{boil}$.

Equation (6.18) is a first order homogeneous linear differential equation. It can be solved using the separation of variables, thus:

$$(C_p\rho)(T_b-T_a)=(E_{avb}-P_d-P_q)/\tau \qquad 6.19$$

Thus:

$$E_{avb}J=(C_p\rho(T_b-T_a))/\tau+P_d+P_q \qquad 6.20$$

It was postulated that the breakdown condition for water is the initiation of a low pressure region in the liquid, thus not necessarily a complete phase change in this region, the change of phase term in equation 6.20 , P_q, was thus dropped. It is assumed that the electric breakdown of the liquid is initiated on the surface of the electrode. The interface between the metal

electrode and the liquid forms the so–called electric double layer, refer to figure 6.8. Bockris et al [93] calculated the value of the dielectric constant in the double layer. They predicted a value of 6 for the dielectric constant in the double layer. Since the electric displacement D is continuous across the interface between two different media it can be written that:

$$\epsilon_d E_1(z_1)=\epsilon_b E_2(z_1) \qquad 6.21$$

With ϵ_d and ϵ_b the dielectric constant in the double layer and in the bulk liquid respectively. E_1 is the electric field in the double layer and E_2 is the electric field in the bulk liquid.

Thus:

$$E_2(z_1)=\frac{\epsilon_d}{\epsilon_b}E_1(z_1) \qquad 6.22$$

Since the electric double layer is only a few molecules thick [93] the approximation was made that $E_1(z_1)=E_1(0)=E_c$, where E_c is the electric field at the electrode surface, thus:

$$E_2(z_1)=\frac{\epsilon_d}{\epsilon_b}E_c \qquad 6.23$$

The current density across the interface between two dielectric media is constant and it is assumed that the mobility in the bulk liquid and the double layer is the same. It is further

assumed that the source of charge carriers is the charge injection from the electrode surface[94]. Thus it is assumed that there is no source of charge carriers outside the double layer. Since the current density is constant it can be written that:

$$J_1(z_1)=J_c=J_2(z_1) \qquad 6.24$$

J_1,$J_c$and J_2 are the current densities in the double layer, on the electrode surface and in the bulk liquid respectively, thus:

$$n_c q\mu E_c=n_z q\mu E_2 \qquad 6.25$$

With:

n_c :Density of charge carriers (charge/m^3) at the electrode surface.

n_z :Density of charge carriers in the bulk liquid.

q :Charge of the charge carrier.

μ :Mobility of the charge carriers (m^2/Vs)

Thus using equation (6.23) and equation (6.25) it can be written that:

$$n_c q\mu E_c=n_z q\mu \frac{\epsilon_d}{\epsilon_b} E_c \qquad 6.26$$

Thus:

$$n_z=\frac{\epsilon_b}{\epsilon_d}n_c \qquad 6.27$$

The equations controlling the electric field, in the bulk liquid, can thus be written as:

The Conduction Constitutive Law

$$J=qn_c\mu\frac{\epsilon_b}{\epsilon_d}E(z)+\sigma E \qquad 6.28$$

Where σ is the ohmic conductivity of the liquid.

Gauss' Law

$$\overline{\nabla}.(\epsilon_b\epsilon_0\overline{E})=qn_z \qquad 6.29$$

Irrotational Electric Field

$$\overline{\nabla}XJ\overline{E}=0=>E_{av}d=\int_0^d E(z)dz=V \qquad 6.30$$

With d the electrode separation and V the applied voltage. Since z dependence only has been assumed equation (6.29) can be written as:

$$\frac{\partial}{\partial z}E=\frac{qn_z}{\epsilon_b\epsilon_0} \qquad 6.31$$

Since the charge injection has a quadratic dependence on the electric field and very high field enhancements– at the tip of the asperity– are expected, equation (6.28) is simplified by dropping the linear term

Using equation (6.31),(6.27) and the simplified equation (6.28):

$$E(z)\frac{\partial}{\partial z}(E(z))=\frac{J}{\mu\epsilon_b\epsilon_0} \qquad 6.32$$

Thus integrating equation (6.32) between 0 and z

$$\int_0^z E(z)\frac{\partial E(z)}{\partial z}dz=\int_0^z \frac{J}{\mu\epsilon_b\epsilon_0}dz \qquad 6.33$$

Using the boundary condition:

$$E(0)=\frac{\epsilon_d}{\epsilon_b}E_c \qquad 6.34$$

The electric field as a function of z can then be written as:

$$\frac{1}{2}(E^2(z)-\frac{\epsilon_d^2}{\epsilon_b^2}E_c)=\frac{Jz}{\mu\epsilon_b\epsilon_0} \qquad 6.35$$

Thus:

$$E(z)=\left(\frac{\epsilon_d^2}{\epsilon_b^2}E_c^2+\frac{2J}{\mu\epsilon_b\epsilon_0}z\right)^{1/2} \qquad 6.36$$

It is further assumed that the charge injection is governed by the Fowler–Nordheim equation [94]:

$$J_c=B_1E_c^2e^{-B_2/E_c} \qquad 6.37$$

In the high field limit $E_c>>B_2$ this reduces to [94]:

$$J_c=B_1E_c^2 \qquad 6.38$$

Substituting equation (6.38) into equation (6.36)

$$E(z)=\left[\frac{\epsilon_d^2}{\epsilon_d^2}E_c^2+\frac{2B_1E_c^2z}{\mu\epsilon_b\epsilon_0}\right]^{1/2} \qquad 6.39$$

Using equation (6.30) the average electric field in the liquid can be written as:

$$E_{av}d=V=\int_0^d\left[\frac{\epsilon_d^2}{\epsilon_d^2}E_c^2+\frac{2B_1E_c^2z}{\mu\epsilon_b\epsilon_0}\right]^{1/2}dz \qquad 6.40$$

Thus:

$$E_{av}d=\frac{\epsilon_d}{\epsilon_b}E_c\left[\frac{\mu\epsilon_0\epsilon_d^2}{3B_1\epsilon_b}\left[1+\frac{2B_1 d\epsilon_b}{\mu\epsilon_0\epsilon_d^2}\right]^{3/2}-\left[\frac{\mu\epsilon_0\epsilon_d^2}{3B_1\epsilon_b}\right]\right] \qquad 6.41$$

Let:

$$R=\left[\frac{\mu\epsilon_0\epsilon_d^2}{3B_1\epsilon_b}\left[1+\frac{2B_1 d\epsilon_b}{\mu\epsilon_0\epsilon_d^2}\right]^{3/2}-\left[\frac{\mu\epsilon_0\epsilon_d^2}{3B_1\epsilon_b}\right]\right] \qquad 6.42$$

Then:

$$E_{av}d=\frac{\epsilon_d}{\epsilon_b}E_cR \qquad 6.43$$

Since it is assumed that the breakdown is initiated at a surface roughness a field enhancement factor H, for the field at the electrode surface, was included. The average electric field across the bubble was calculated by making the approximation that the functional form of this dependence on the variable z is the same as the functional dependence of the field if the roughness was a perfect half sphere. Since the bulge is small compared to the electrode it can be assumed that the electric field away from the bulge is uniform in the z–direction. The Poisson equation (in the absence of charge injection) holds at points P and B in figure 6.8, thus:

$$\nabla^2\phi_p=0 \text{ and } \nabla^2\phi_b=0 \qquad 6.44$$

With ϕ_p and ϕ_b the potential functions at points p and b respectively, refer to figure 6.8. The field at point b is uniform and in the z direction and can be written in polar coordinates as follows:

$$E_r=E\cos\theta \qquad 6.45$$

$$E_\theta=Er\sin\theta \qquad 6.46$$

Thus:

$$\frac{\partial\phi}{\partial r}=E\cos\theta \qquad 6.47$$

$$\frac{\partial\phi}{\partial\theta}=Er\sin\theta \qquad 6.48$$

Thus using equation (6.47):

$$\phi=Er\cos\theta+f(\theta)+const \qquad 6.49$$

And using equation (6.48):

$$\phi=Er\cos\theta+f(r)+const_2 \qquad 6.50$$

Thus from equation (6.49) and (6.50):

$$f(r)=f(\theta) \qquad 6.51$$

Since equation (6.51) must be valid for all r and θ:

$$f(r)=f(\theta)=0 \qquad 6.52$$

Thus :

const$\equiv$const$_2$ and its value can be determined using the following boundary condition:

$$\text{At } \theta=\pi/2 \text{ and } r=0,\ \phi=V \qquad 6.53$$

Thus:

$$\phi_p=Er\cos\theta+V \qquad 6.54$$

It seemed reasonable to add the potential function of a half sphere [89] to that of the flat plate (ϕ_p) to give the new potential function,ϕ_b, near the bulge,thus:

$$\phi_b = \phi_p+\phi_{sphere} \qquad 6.55$$

$$=-Er\cos\theta+const(\cos\theta/r^2)+V \qquad 6.56$$

Using the boundary condition:

$$\phi_b(R_s,0)=V=-E_pR_s\cos(0)+const.\cos(0)/R_s^2+V \qquad 6.57$$

Thus:

$$-ER_s=const/R_s^2=0 \qquad 6.58$$

Thus:

$$const=-ER_s^3 \qquad 6.59$$

Thus the potential function close to the bulge is given by:

$$\phi_b=-E(r-R_s^3/r^2)\cos\theta+V \qquad 6.60$$

The components of the electrical field, in spherical coordinates are given by:

$$E_\theta(r,\theta)=-\frac{\partial\phi_b}{\partial\theta}=-E(r-R_s^3/r^2)\sin\theta \qquad 6.61$$

$$E_r(r,\theta)=-\frac{\partial\phi_b}{\partial r}-E(1+2R_s^3/r^3)\cos\theta \qquad 6.62$$

Thus the electric field at the top of the bulge, where $\theta=0$ and $r=R_s$ is given by:

$$E_\theta(R_s,0)=0 \qquad 6.63$$

$$E_r(R_s,0)=3E \qquad 6.64$$

Thus the electric field at the top of the bulge is three times the electric field on top of the flat plate. It is still necessary to show that ϕ_b satisfies the Poisson equation, thus to show that:

$$\nabla^2\phi_b=0 \qquad 6.65$$

Thus to show that:

$$\frac{1}{r}\frac{\partial^2}{\partial r^2}(r\phi_b)+\frac{1}{r^2\sin\theta}\frac{\partial}{\partial\theta}(\sin\theta\frac{\partial\phi_p}{\partial\theta})=0 \qquad 6.66$$

The first term on the left hand side can be written as:

$$\frac{1}{r}\frac{\partial^2}{\partial r^2}(r\phi_b)=\frac{-2E\cos\theta}{r}+\frac{2ER_s^3\cos\theta}{r^4} \qquad 6.67$$

The second term on the left hand side can be written as:

$$\frac{1}{r^2\sin\theta}\frac{\partial}{\partial\theta}(\sin\theta\frac{\partial\phi_p}{\partial\theta})=\frac{2E\cos\theta}{r}\quad\frac{2ER_s^3\cos\theta}{r^4} \qquad 6.68$$

Thus the Poisson equation is satisfied. The approximation is made that the functional dependence of the electric field on the variable z is the same as that of the electric field on z at the top of the bulge , equation (6.62). As was shown the field is enhanced by a factor of three at the top of the bulge. The field

enhancement at the top of the asperity will be much higher than 3, thus equation (6.62) is modified to give a field enhancement of H. This factor will be determined by using experimental breakdown values. Thus equation (6.62) is modified to the following equation:

$$E_{spere}(z)=E_c(1+(H-1)R_s/r^3) \qquad 6.69$$

Where R_s is the radius of curvature of the surface roughness. E_c is the electric field on the flat electrode away from the surface roughness. Thus when $z=R_s$ then:

$$E(R_s)=HE_c \qquad 6.70$$

Thus the charge injection at the tip of the roughness is given by:

$$J=BH^2E_c^2 \qquad 6.71$$

The charge carrier mobility is μ and this can be used to calculate an approximate diameter of the bubble for a specific pulse time τ. The expected breakdown field is in the region of 10 MV/m and thus the approximate bubble diameter can be expressed as:

$$b\approx 10x10^6\mu\tau \qquad 6.72$$

Using the mean value theorem for integrals the average electric field across the bubble can be expressed as:

$$H_{avb}=\frac{1}{b}\left[b\frac{H'R_s^3}{2(R_s+b)^2}+\frac{1}{2}H'R_s\right] \qquad 6.73$$

With:

$$H'=H-1 \qquad 6.74$$

For the calculations in this model the approximation was made that the radius of the surface roughness is in the vicinity of 10μm since this is an easily achievable surface finish:

Using equations (6.70), (6.73) and (6.74) the breakdown equation,equation ,(6.41) can be written as:

$$B_1E_{av}^3H_{avb}\left[\frac{\epsilon_b dH}{\epsilon_d R}\right]^2=C_p\rho(T_b-T_a)/\tau+P_d+P_q \qquad 6.75$$

Thus the breakdown electric field E_{max} can be written as:

$$E_{max}=\left[\frac{\epsilon_d R}{\epsilon_b dH}\right]^{2/3}\left[\frac{C_p\rho\ (T_b-T_a)/\tau+P_d+P_q}{B_1H_{avb}}\right]^{1/3} \qquad 6.76$$

The values used for B_1 and μ were those measured by Zahn et al. [94]. B_1 is approximately $8.7\text{x}10^{-14}C/V^2s$ and the value used for the mobility of the charge carriers is $2.5\text{x}10^{-7}m^2/Vs$. As was

mentioned the dielectric constant in the double layer is approximately 6. Booth[84] derived an equation for the dielectric constant of water as a function of the electric field strength. According to the equation he derived the dielectric constant falls to approximately half its normal value at a field strength of approximately 6 MV/cm Refer to figure 6.6. This value is typical of the expected field strength in the double layer. A value of 3 was thus used for the dielectric constant in the double layer.

An order of magnitude calculation was done to determine the rate at which energy must be supplied to overcome the drag on the streamer. Using the equation for the drag per unit volume on an ellipsoidal body [95]:

$$P_d = C_d \rho \frac{v^2}{2} / \tau \qquad 6.77$$

With:

C_d :Drag coefficient.

v :Velocity of the streamer.

A :Frontal area of the streamer.

The drag coefficient C_d can be written as [95]:

$$C_d = 24/N_r \qquad 6.78$$

With N_r the Reynolds number, and can be calculated using the following equation [95]:

$$N_r = \frac{Dv}{\nu} \qquad 6.79$$

With:

D :Diameter of the streamer.

ν :Kinematic viscosity.

According to the Handbook on Chemistry and Physics [77] the absolute viscosity of water is:

$$\mu = 0.890 \times 10^{-3} Ns/m^2 \qquad 6.80$$

Thus the kinematic viscosity is given by:

$$\nu = \frac{\mu}{\rho} \qquad 6.81$$

$$= 0.890 \times 10^{-6} m^2/s$$

An approximation of the bubble velocity v was made. The velocity of the bubble would be close to that of a slow streamer (a slow streamer is basically a series of bubbles moving

through the liquid). Felici calculated a velocity of approximately 200m/s for a slow moving streamer. To calculate the Reynolds number the diameter of the streamer must be calculated. Since the breakdown process of of the gas in the streamer is a normal gas breakdown its diameter must be larger than the mean free path between collisions. The mean free path between collisions is given by:

$$l = \frac{1}{\sqrt{2}\,\pi\,\sigma^2\,n} \qquad 6.82$$

With σ the collisional cross section of a water molecule ($\approx 3.7 \times 10^{-10}$m) and n the number density of the gas. And can be calculated as follows:

The number of mole of water molecules per unit volume, m_v is given by:

$$m_v = \frac{P}{RT} \qquad 6.83$$

Where P is the pressure = 101 Kpa , R is the specific gas constant = 8.314/0.018 J/kg and T is the temperature = 373 k.

Thus:

$$m_v = \frac{101 \times 10^3}{373 \times 461.9}$$

$=0.586$ mole

Thus:

$n = 0.568 \times 6.022 \times 10^{23}$

$=3.531 \times 10^{23}$ molecules.

Thus:

$$\lambda = \frac{1}{\sqrt{2\pi}(3.72 \times 10^{-10})(3.531 \times 10^{23})}$$

$=8.166$ μm

Thus the minimum diameter of the streamer must be approximately 10μm. And this was used in the Reynolds number calculations. This would give an upper value for the drag coefficient since C_d would decrease with increasing D.

Thus

$$N_r = \frac{10 \times 10^{-6} \times 200}{0.89 \times 10^{-6}}$$

$= \quad 2247$

According to Daugherty and Franzini [95] (p295) C_d for this Reynolds number would be approximately 0.06. Thus the drag would be given by :

$$P_d = C_d \rho \frac{V^2}{2} / \tau$$

$$= 0.06 \times 1000 \times \frac{200^2}{2} / \tau$$

$$= 1.2 \times 10^6 / \tau \ \text{Watt/m}^3$$

This drag term would give the lower limit for the breakdown field strength since the drag coefficient as well as the velocity would increase and as can be seen from equation (6.77) this would cause a larger P_d term. The approximation was made that this drag term is constant and not dependent on the pulse duration. This is not a bad approximation since a longer pulse would obviously cause a higher bubble velocity. It must be emphasised that this is an approximation.The streamer velocity might depend on the pulse duration as well as the applied voltage, but no published experimental results on this could be found. The drag coefficient is also an approximation. Not only does it depend on the velocity of the streamer but also on the shape of it. It is unlikely that the drag coefficient C_d would be larger than the term for an ellipsoid, Thus this drag term would

give the upper limit of the breakdown strength. Using this model and the drag coefficient as calculated above the breakdown strength of water with an ambient temperature of $0^{o}C$ and a 200 μs pulse duration, is approximately 17.7 MV/m. If the C_d value is doubled the breakdown strength increases to 19.47MV/m. When the drag term is dropped this value reduces to 15.0MV/m

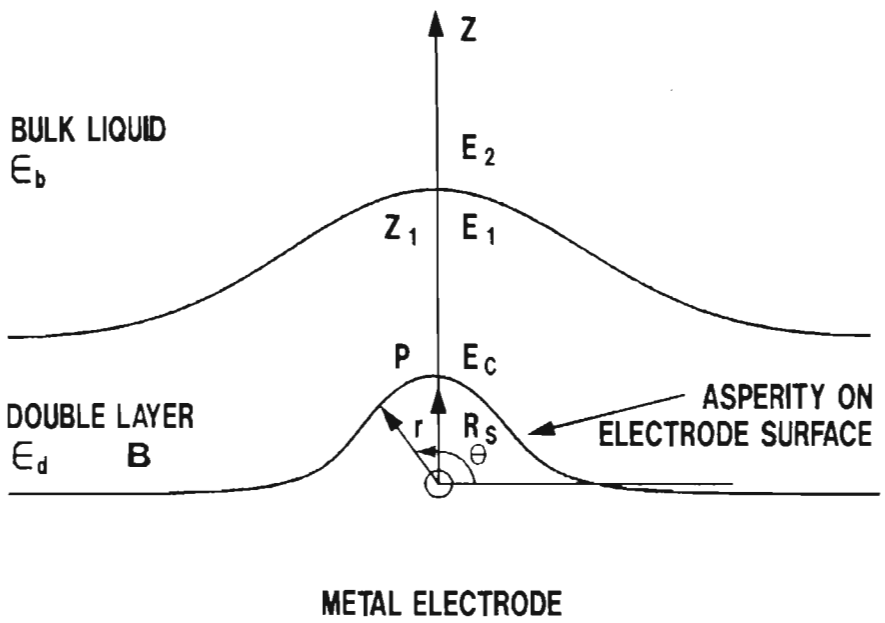

Figure 6.8. A schematic drawing of a surface roughness on top of the electrode surface.

6.3.3 A COMPARISON OF THE BREAKDOWN MODEL WITH PUBLISHED EXPERIMENTAL RESULTS.

Experimental breakdown values measured by Fenneman and Gripshover [97] were used to determine the field enhancement factor H. The breakdown equation, equation (6.76), was set equal to an experimental breakdown value and the field enhancement factor H was determined by solving this equation. A value of 80 was obtained for the field enhancement factor, the total field enhancement at the electrode, equation(6.43) would then be 86. Zahn et al.[94] used a value of 100 in his charge injection calculations. Using experimental breakdown values J C Martin [98]derived an empirical breakdown criterion. The J C Martin[98] breakdown criterion is given by:

$$E_{max} t_{eff}^{1/3} = M/A^{1/10} \qquad 6.84$$

E_{max} is the breakdown strength of the water in MV/cm, t_{eff} is the effective time in microseconds (defined as the duration for which the field exceeds 63% of the value of E_{max}), A is the area of the electrodes in cm^2. M is a constant, values ranging from 0.3 to 0.6 have been reported [99,100]. The value of M used in this comparison is the value of 0.58 measured by Fenneman and Gripshover[97].

The breakdown equation (6.76) does not have any dependence on the electrode area. The field enhancement factor H might have

an area dependence, since it is obviously a statistical factor and the probability of having a surface roughness which causes a different field enhancement will be larger for a larger electrode area. An area dependence similar to the one used by Martin was incorporated into equation (6.76). The factor used was that of 0.108 as published by Fenneman and Gripshover[97].

Figure 6.9 shows the breakdown strength as a function of time, the drag term was ignored for this calculation. The top curve is the breakdown strength as predicted by this model and the bottom curve is the breakdown strength as predicted by the J C Martin breakdown equation. The breakdown values predicted by this model agree well with the J C Martin breakdown criterion for pulse durations of less than 1 μs. Fenneman and Gripshover [97] executed breakdown tests in the 1 to 10 μs regime and found that the value of M used in equation (6.84) was an increasing function of time and they concluded that this suggested a weaker than $t^{1/3}$ dependence on the pulse duration. This weaker than $t^{1/3}$ time dependence is indeed predicted by this model as can be seen in figure 6.9. The experimental measurements of Fenneman and Gripshover are also shown on the graph.

McLeod et al[100] did breakdown tests on different alloys. They used 81cm^2 electrodes which were bead blasted and the water temperature used was 6.3^{o}C. The 10% breakdown probability for 316 stainless steel published by them is 150 kV/cm. This is

slightly higher than the value predicted by this model as is shown in figure 6.9.

Fenneman[101] did breakdown tests on water and water/glycol mixtures for longer pulse durations. He used stainless steel electrodes. He published a value of 13 MV/m for the breakdown probability of 0.1 for water cooled to 0^{o}C. This agrees well with the value predicted by this model as is shown in figure 6.9

A shortcoming of this model is that it does not predict the probabilistic nature of the breakdown process. This may be caused by factors not considered in this model such as the presence of impurities or bubbles in the liquid. According to this model the only source of charge carriers is charge injection. Another source of charge carriers could be field enhanced dissociation[102]. A heating mechanism that was not taken into consideration is that given off by the recombination of excess dissociated hydronium and hydroxyl ions.

The pascal program used for calculating the breakdown strength curve is given in appendix 9.

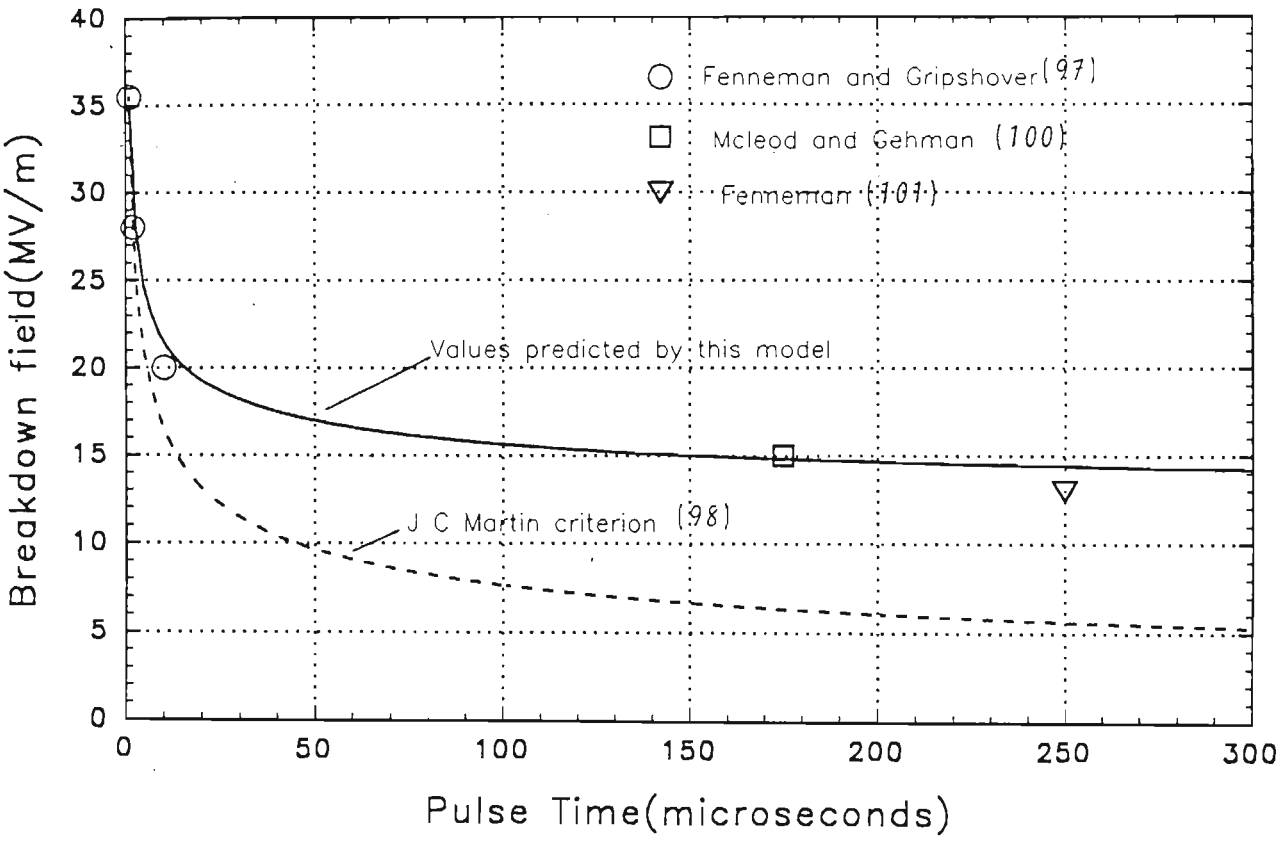

Figure 6.9. This graph gives the breakdown strengths of water with an ambient temperature of $0^{o}C$ as calculated by this model as well as that predicted by the J C Martin breakdown criterion. Also shown are some experimentally measured breakdown values

6.4 THE ESR AND HEATING OF THE WATER IN THE CAPACITOR.

ESR is an acronym used for the equivalent series resistance of a capacitor. By this is meant the value a resistor would have had if the same amount of heat was deposited into the capacitor than would have been deposited into the resistor. Assume that the resistivity of the water is 18 MΩ.cm. The resistivity will be measured in chapter 7. The area of the capacitor is the same as that used in calculating the inductance value in section 6.2.1. Thus the capacitor plate area is 10x7 cm^2. The electrode separation is 0.5 cm.Thus the resistivity of the capacitor is 129.0kΩ. The capacitance of this capacitor is 1nF:

The equivalent series resistance of this capacitor is given by:

$$ESR=P_c/i^2$$

With:

P_c :Power coupled into the water capacitor.

i :Current in the PFN.

The power coupled into the capacitor is given by:

$$P_c=\gamma t_p V_p^2/R_c$$

With:

γ :Pulse repetition rate.

V_p :Voltage of charging pulse (a square pulse has been assumed).

R_c :Resistance of the capacitor.

t_p :Duration of the pulse.

The average current in the circuit is given by:

$$i=CV_p\gamma$$

Thus the ESR is given by:

$$ESR = P_c/i^2 = \frac{t_p}{R_c C^2 \gamma}$$

Thus for a 100 μs charging pulse with a 2 kHz repetition rate and capacitor specifications as given above the ESR value is 0.4MΩ this means that for a 30 kV charging pulse the power dissipated in the water capacitor is 1.4kW. If a 500 nS charging pulse is used the ESR value is 1.9 kΩ with 7.2 watt being dissipated in the capacitor. For a 200 nS pulse the ESR value is 0.4 kΩ and the power dissipated is 1.4 watt.

6.5 A DESIGN PROPOSAL FOR A HIGH REPETITION RATE PULSE POWER CIRCUIT USING WATER CAPACITORS.

As can be seen from the calculated ESR values a water capacitor is not suitable when the charge time is much larger than 1 μs. Thus a water capacitor cannot be used as a storage capacitor as can be seen from the analysis done in section 6.4. A water capacitor would be ideal for the use as the intermediate storage capacitors in a magnetic pulse compression circuit. In a magnetic pulse compression circuit magnetic switches are used to compress a power pulse by a factor of 3 to 10[103]. In this type of circuit the charging capacitors are charged slowly and are then allowed to discharge quickly through the use of a magnetic switch. A magnetic switch is an inductance which can be saturated in a very short time. During the charging time of the charging capacitors the magnetic switch has a much higher inductance than L1, refer to figure 6.10. As a consequence only a small leakage current goes through the switch. This leakage current saturates the magnetic material. The amount of magnetic material determines the time which will elapse before the switch will close. When the magnetic material is saturated the inductance is reduced dramatically and will reach values far below L1. Magnetic switch technology is used commonly in commercial laser systems[103].

A proposed magnetic pulse compression circuit, using water

capacitors for intermediate storage, is shown in figure 6.10. In this circuit a capacitor bank, consisting of ceramic, mica or PPSO capacitors could be charged within 100μs using a suitable power supply.. A saturable inductor could then be used to compress the pulse to about 1μs for the first stage and to about 300nS for the third stage and even shorter if a third stage is used. Since the pulse time on these capacitors is short, water capacitors could be used for these stages.

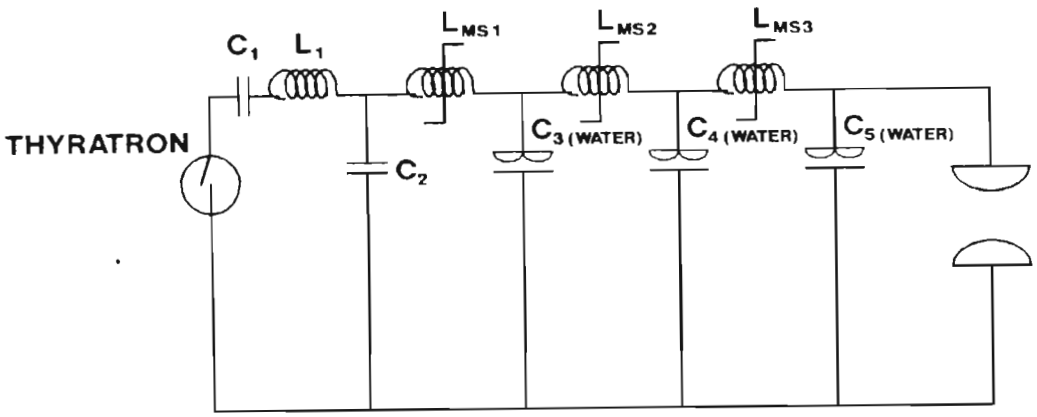

Figure 6.10. A schematic diagram of a multistage magnetic switch circuit using water capacitors as intermediate storage components.

6.6 A COMPARISON BETWEEN A WATER CAPACITOR AND OTHER CAPACITORS.

The comparison between the main capacitor parameters is given in tables 6.1a and 6.1b. The values given in table 6.1 are the best reported values for the individual capacitors. The values quoted for the PPSO, Mica and Ceramic capacitors were those obtained in reference [83]. The inductance value given for water is that calculated in section 6.2.1, its real value might be slightly larger. The ESR value given for water is that calculated in section 6.5 for a 500 nS charging time. The water capacitor is very competitive in all the parameters except its ESR value. The energy density values were calculated using the breakdown strength values as calculated in section 6.3. These breakdown values are shown in figure 6.9. Thus these are the maximum expected values. It would be safe to use values slightly smaller than these values.

Since water seemed to be a viable alternative capacitor for a repetition rate pulsed power supply it was decided to determine experimentally certain factors important in the design of a water capacitor. These were:

(i) Water resistivity measurements as a function of temperature.

(ii) Measurement of the intrinsic time constant (RC time)

of the water capacitor as a function of temperature.

(iii) Measurement of the dielectric constant of water as a function of temperature.

(iv) Investigation of the high voltage high repetition rate behaviour of the water capacitor.

	Inductance nH	Lifetime Shots	Volumetric Efficiency J/m^3
PPSO	150	$>5x10^9$	$3.0x10^3$
Mica	80	$>10x10^9$	$1.0x10^4$
Ceramic	25	$5x10^9$	$2.0x10^4$
Water	5.0	unlimited	$1.4x10^4$

Table 6.1a

	ESR mΩ	Energy Density J/kg	Price $/J
PPSO	0.62	0.15	50.0
Mica	0.65	7.5	600.0
Ceramic	1.54	8.1	40.0
Water	$10.0x10^5$	14.0	20.0

Table 6.1b

Table 6.1a and b. Main capacitor performance parameters. The capacitance of these capacitors was 1nF.

CHAPTER 7

WATER CAPACITOR EXPERIMENTAL MEASUREMENTS.

7.1 WATER PURIFICATION SYSTEM

Water with a very high purity and thus with a high resistivity can be obtained by using the so–called ion exchange method [104]. This is shown in figure 7.1. The left column contains a synthetic cation exchange resin. The exchangeable ion is H^+. The second column is packed with an anion exchange resin in which replaceable OH^- ions are embedded. The two resins can be referred to as HR (cation exchanger) and R'OH (anion exchanger). The following equation can be written to describe what happens when water containing a dissolved salt MX is deionized by passing through the two columns.

1 st $\quad M^+(aq)+HR(s)\text{—>}MR(s)+H^+(aq)$

2 nd $\quad X^-(aq)+R'OH(s)\text{—>}R'X(s)+OH^-(aq)$

The H^+ and OH^- ions produced react with each other to form water:

$$H^+(aq)+OH^-(aq)\text{—>}H_2O$$

The overall reaction can be obtained by adding the three reactions above:

$$M^{+}(aq)+X^{-}(aq)+HR(s)+R'OH(s)\longrightarrow MR(s)+R'X(s)+H_2O$$

Thus there are no ions in the solution at the end of the process. This process is referred to as deionization of the water. The first column can be regenerated by flushing it with a strong solution of hydrochloric acid, which acts as a source of H^{+} ions. The second column can be regenerated by flushing it with sodium hydroxide. The deionization process is shown schematically in figure 7.1.

Because the breakdown model developed in chapter six predicted that electrical breakdown in water is initiated by the formation of a gaseous phase in the liquid, the water in the flow system was deaerated. The stainless dearation column is shown in figure 7.2. The baffles were arranged to give the water a long flow path and to cause cavitation in the water. At a equilibrium temperature T, the percent deaeration of the water is given by the equation [97]:

$$\text{Percent deaeration}=100X\left[1-\frac{p-P_{H_2O}(T)}{760}\right] \qquad 7.1$$

Where p is the pressure in the deaeration column (torr) and

$P_{H_2O}(T)$ is the vapour pressure of the water. The pressure in the deaeration column was maintained by a rotation vacuum pump. The pressure in the deaeration column was measured using a diaphragm type pressure meter. A nitrogen cold trap was placed between the deaeration column and the vacuum pump. This was done to protect the vacuum pump from the water vapour in the deaeration column.The deaeration column was manufactured from stainless steel. All pipes and valves were from hard polyvinyl chloride (PVC). A 60 l/min pump was used.The pump blades were also PVC. A 1 micron filter was installed to remove small particles in the water A NESLAB HP150 chiller was installed to keep the water temperature constant. The water temperature was measured using thermocouples. The water purification system is shown in figure 7.3. The water resistivity could be continuously measured by using a measurement cell . This is shown in figure 7.4. It consisted of a PVC tube with two 2X4cm^2 stainless steel plates 1 cm apart. The resistivity between the two plates was measured using a Philliphs RLC meter. The feed water was standard de–mineralised water with a resistivity of 2 MΩ.cm. Water resistivity measurements for temperatures from 8 to 28 ^oC are shown in figure 7.5.

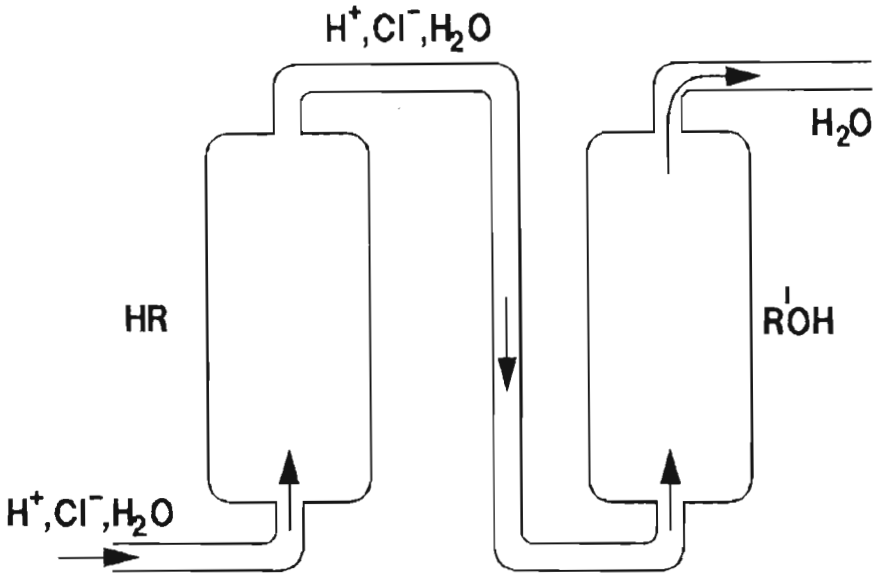

Figure 7.1. A schematic diagram of the de−ionization process.

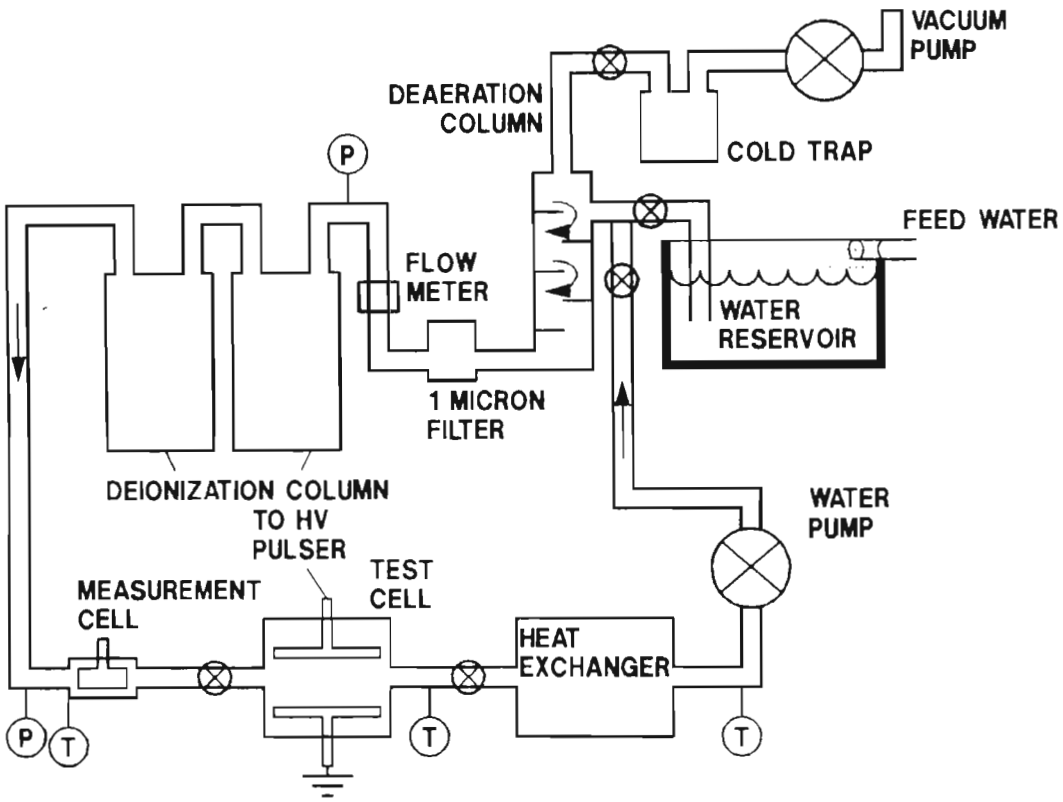

Figure 7.2. A schematic diagram of the water conditioning system.

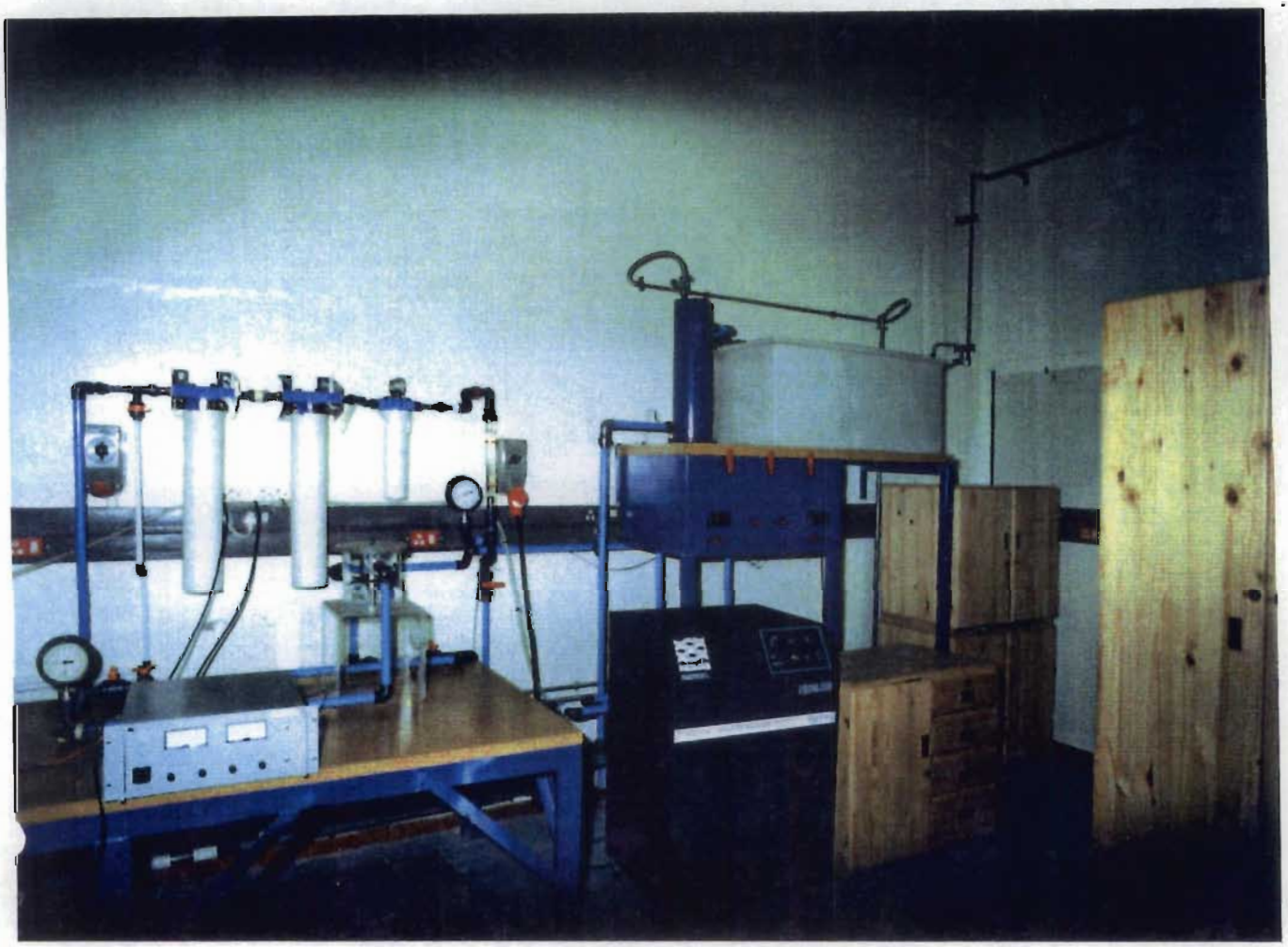

Figure 7.3. A photograph of the water conditioning system.

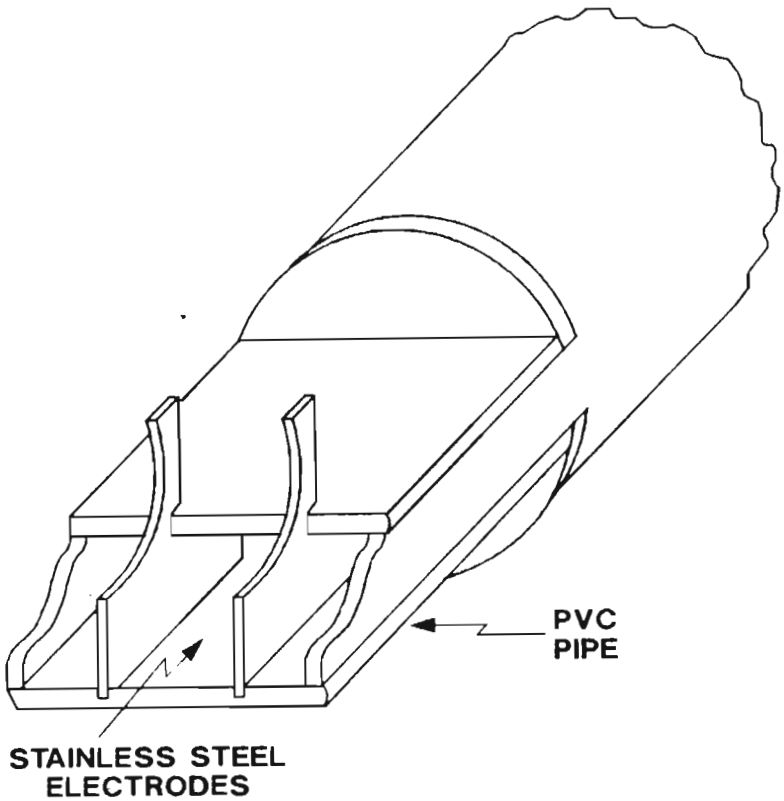

Figure 7.4. A schematic diagram of the water test cell.

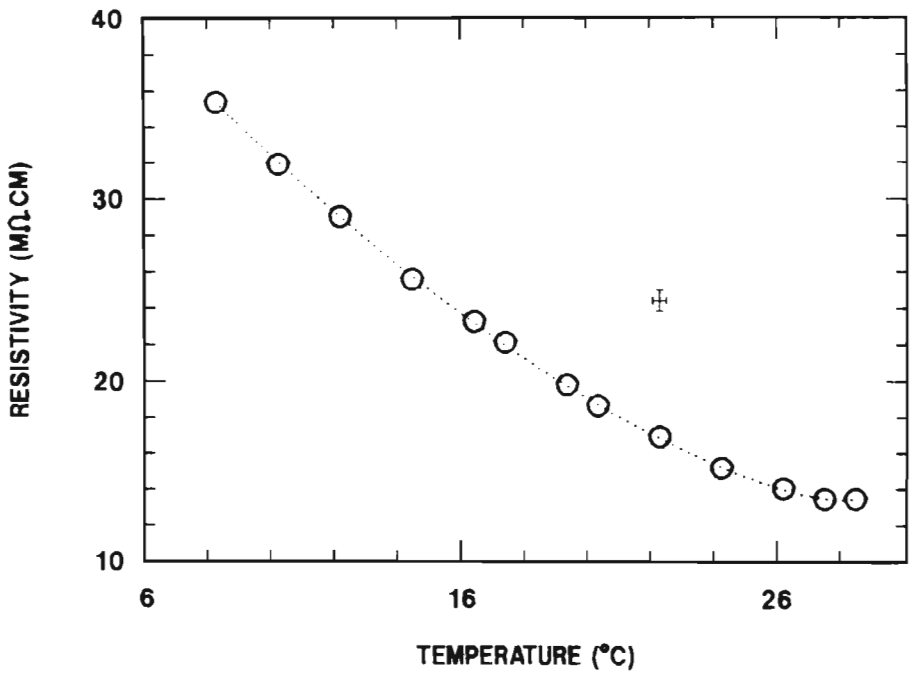

Figure 7.5 Water resistivity measurements as a function of temperature.

7.2 WATER TIME CONSTANT MEASUREMENTS

7.2.1 EXPERIMENTAL METHOD AND RESULTS.

The circuit shown in figure 7.6 was used to measure the intrinsic time constant of water. This time constant is the RC decay time of the water capacitor. As shown in figure 7.6 the water capacitor can be viewed as a capacitor in parallel with a resistance. The value of this resistance is the resistance of the water as measured in the previous section and shown in figure 7.5. Since the impedance of the water is very high a capacitive divider probe was used to measure the test cell voltage. A capacitive divider probe was used to avoid degrading the test cell time constant by the discharging of the capacitor through the resistive divider probe and the oscilloscope. A capacitive divider probe was designed which had a transfer function which was constant, for the discharge time of the test cell. Consider figure 7.7 and using Kirchoff's circuit laws:

Loop 1

$$\frac{1}{C_0}\int i_1 dt+\frac{1}{C_1}\int i_5 dt=\sin(at) \qquad 7.2$$

Taking the Laplace transform this can be written as:

$$\frac{1}{C_0} i_1 + \frac{1}{C_1} i_5 = \frac{a s}{s^2 + a^2} \qquad 7.3$$

Loop 2

$$i_2 R_1 + i_3 R_2 - \frac{1}{C_1} \int i_5 dt = 0 \qquad 7.4$$

Taking the Laplace transform this can be written as:

$$s R_1 i_2 + s R_2 i_3 - \frac{1}{C_1} i_5 = 0 \qquad 7.5$$

Loop 3

$$\frac{1}{C_2} \int i_4 dt - R_2 i_3 = 0 \qquad 7.6$$

Taking the Laplace transform this can be written as:

$$\frac{1}{C_2} i_4 - R_2 s i_3 = 0 \qquad 7.7$$

But:

$$i_5 = i_1 - i_2 \qquad 7.8$$

$$i_4 = i_2 - i_3 \qquad 7.9$$

Thus equation (7.3), (7.5), and (7.7) can be written as:

$$\frac{1}{C_0} i_1+\frac{1}{C_1}(i_1-i_2)=\frac{a s}{s^2+a^2} \qquad 7.10$$

$$sR_1 i_2+sR_2 i_3-1/C_1(i_1-i_2)=0 \qquad 7.11$$

$$\frac{1}{C_2}(i_2-i_3)-R_2 s i_3=0 \qquad 7.12$$

This can be re–written in matrix form as:

$$\begin{bmatrix} \frac{C_1+C_0}{C_0 C_1} & \frac{1}{C_1} & 0 \\ -\frac{1}{C_1} & (sR_1+\frac{1}{C_1}) & sR_2 \\ 0 & \frac{1}{C_2} & -\frac{1}{C_2}+R_2 s \end{bmatrix} \begin{bmatrix} i_1 \\ i_2 \\ i_3 \end{bmatrix} = \begin{bmatrix} \frac{aS}{s^2+a^2} \\ 0 \\ 0 \end{bmatrix} \qquad 7.13$$

Thus using equation(7.13) i_3 can be solved:

$$i_3=\frac{a s C_0 C_1}{(1+R_2 s C_2)((sR_1 C_1+1)(C_1+C_0)-C_0)+sR_2 C_1(C_1+C_0)} \qquad 7.14$$

Thus:

$$i_3=\frac{asC_0}{(s^2+a^2)R_1 R_2 C_2(C_1+C_0)s^2+S((R_1+R_2)(C_1+C_0)+R_2 C_2)+1)} \qquad 7.15$$

Approximate V(t) with:

$$V(t)=\sin(at) \tag{7.16}$$

Thus:

$$V(s)=L(\sin(at))=\frac{a}{s^2+a^2} \tag{7.17}$$

But:

$$V_2(s)=i_3(t)R_2 \tag{7.18}$$

Thus:

$$V(s)=\frac{asC_0R_2}{(s^2+a^2)R_1R_2C_2(C_1+C_0)s^2+S((R_1+R_2)(C_1+C_o)+R_2C_2)+1)} \tag{7.19}$$

Thus:

$$\frac{V_2}{V}=\frac{As}{1+(B+Cs)s} \tag{7.20}$$

With:

$$A=R_2C_o \tag{7.21}$$

$$B=(R_1+R_2)(C_1+C_0)+R_2C_2 \tag{7.22}$$

$$C=R_1R_2C_2(C_0+C_1) \qquad 7.23$$

For the oscilloscope signal to be a true reproduction of the high voltage pulse the ratio $\frac{V_2}{V}$ must be independent of time. This is true if:

$$Bs>>1 \text{ and } Cs^2<<1 \qquad 7.24$$

Then:

$$\frac{V_2}{V}=\frac{As}{Bs}=\frac{A}{B}=\text{constant} \qquad 7.25$$

Thus this probe can be used for times for which $Bs>>1$ and $Cs^2<<1$, thus:

$$|s|>>\frac{1}{(R_1+R_2)(C_1+C_0)+R_2C_2} \qquad 7.26$$

And:

$$|s^2|<<\frac{1}{R_1R_2C_2(C_0+C_1)} \qquad 7.27$$

In this case $s=i\omega=i2\pi/t$. For the values given in figure 7.6 the transfer function is constant for $20\mu s<<t<<35ms$. For these values the ratio V_2/V is approximately $6x10^{-6}$. The oscilloscope

used was a Hewlett–Packard 5421 400 Ms/s digital storage oscilloscope. The charging pulse as well as the RC discharge pulse of the water capacitor are shown in figure 7.8. The water temperature was 28 ^{O}C and the measured resistance of the water was 17.2 MΩ.cm.The time constant was measured as the time the pulse took to decay from its peak value to 1/e of its peak value. In this instance the time constant was approximately 90 μS. Figure 7.9 is a measurement of the time constant of the water at 9^{O}C. In this instance the resistivity of the water was approximately 34 MΩ.cm. The measured time constant was 250 μS. Figure 7.10 gives the measured time constants for water in the temperature range 8^{O}C to 28^{O}C. Using these time constant values and the resistivity measurements of the previous section the dielectric constant of the water as a function of temperature was calculated. This is given in figure 7.11.

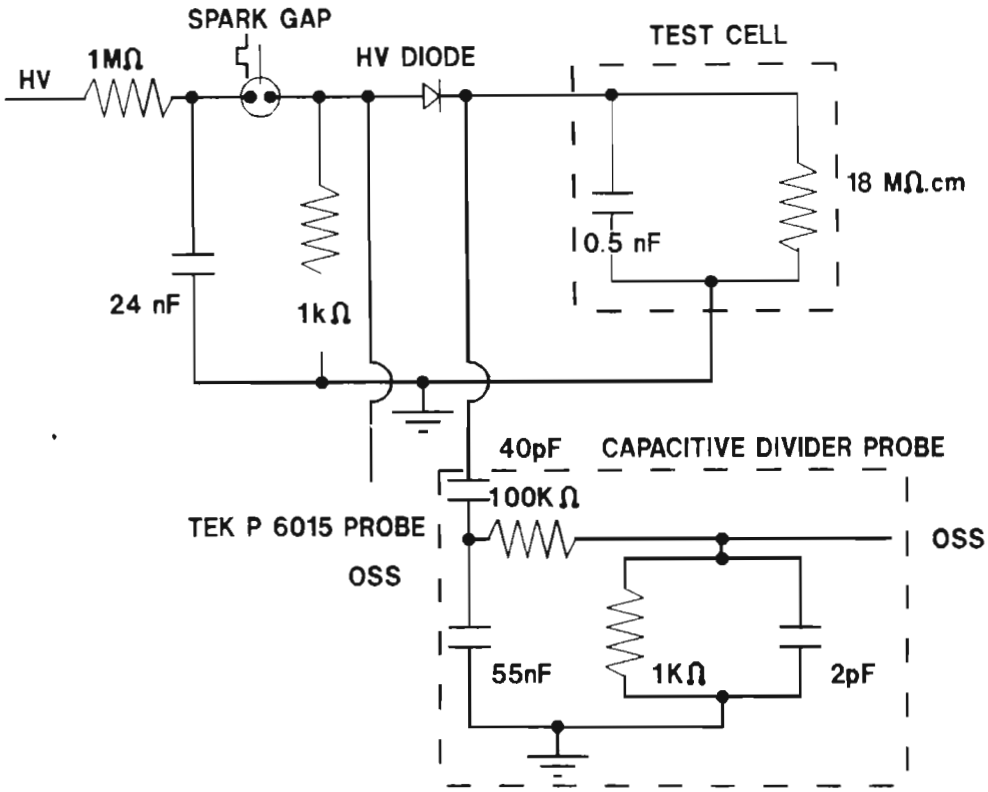

Figure 7.6 The test circuit used for measuring the intrinsic time constant of the water.

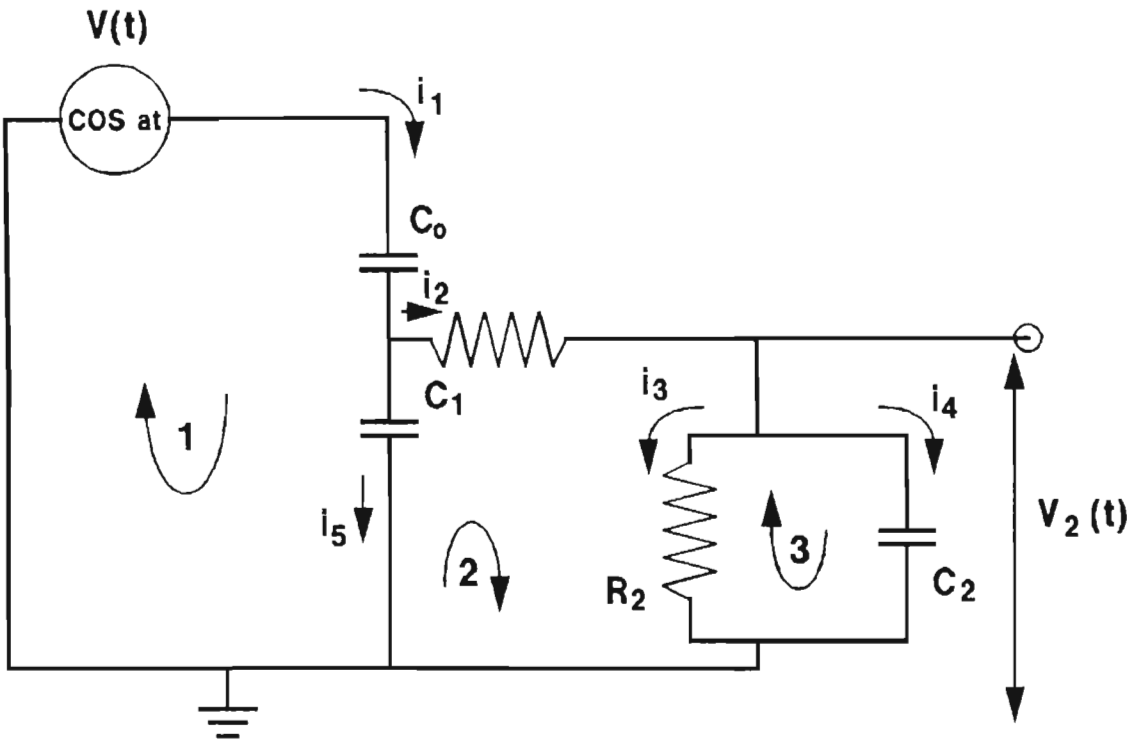

Figure 7.7 A schematic diagram of the circuit used to analyse the capacitive divider probe used in this investigation.

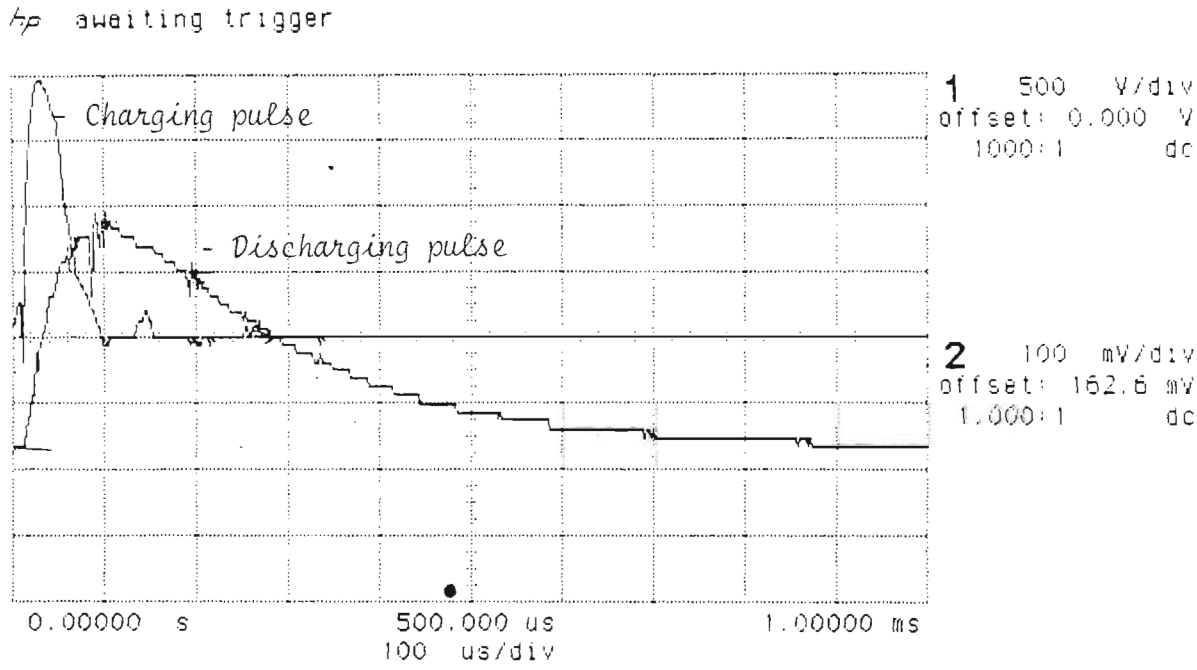

Figure 7.8 The charging as well as the RC discharge pulses of the water capacitor. The water temperature was $28^{o}C$ and the water resistivity was 17.2 MΩ.cm

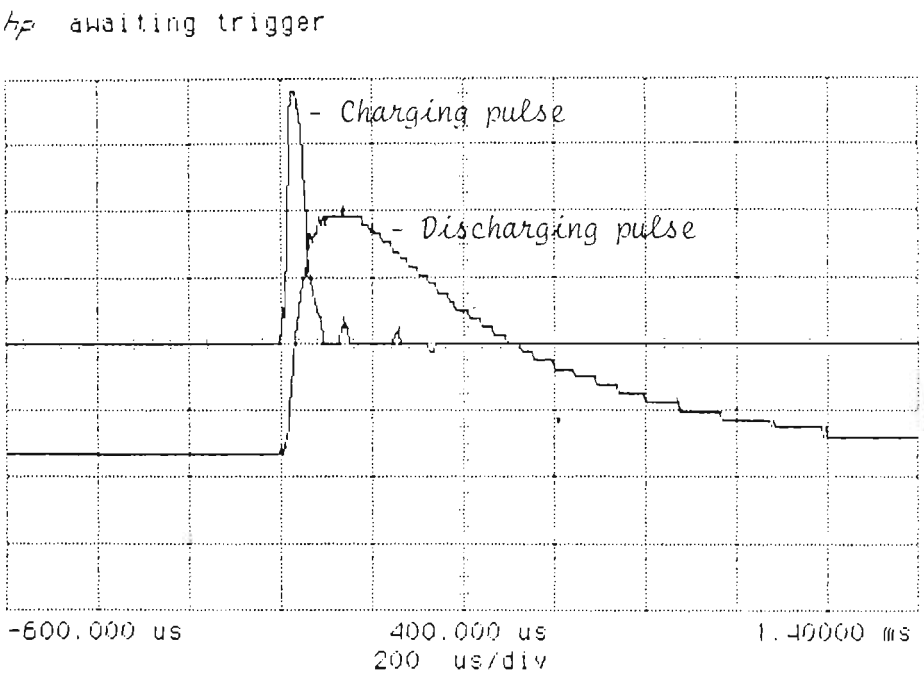

	Sensitivity	Offset	Probe	Coupling
Channel 1	5.00 V/div	0.00000 V	10.00 :1	dc (1M ohm)
Channel 2	100 mV/div	162.600 mV	1.000 :1	dc (1M ohm)

Figure 7.9 The charging as well as the RC discharge pulses of the water capacitor. The water temperature was $9^{o}C$ and the water resistivity was 36.2 MΩ.cm

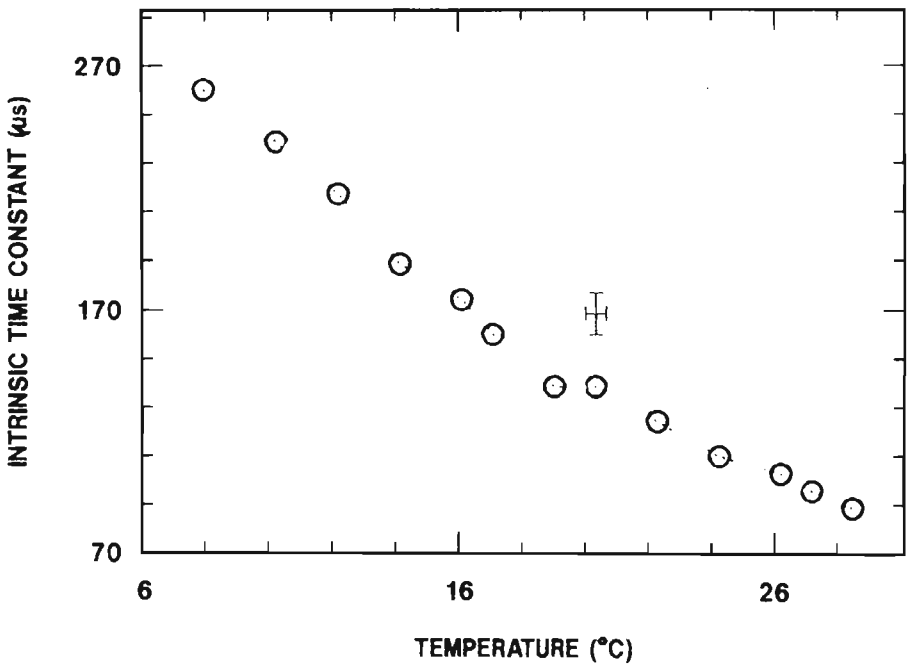

Figure 7.10. The measured time constants of water as a function of temperature

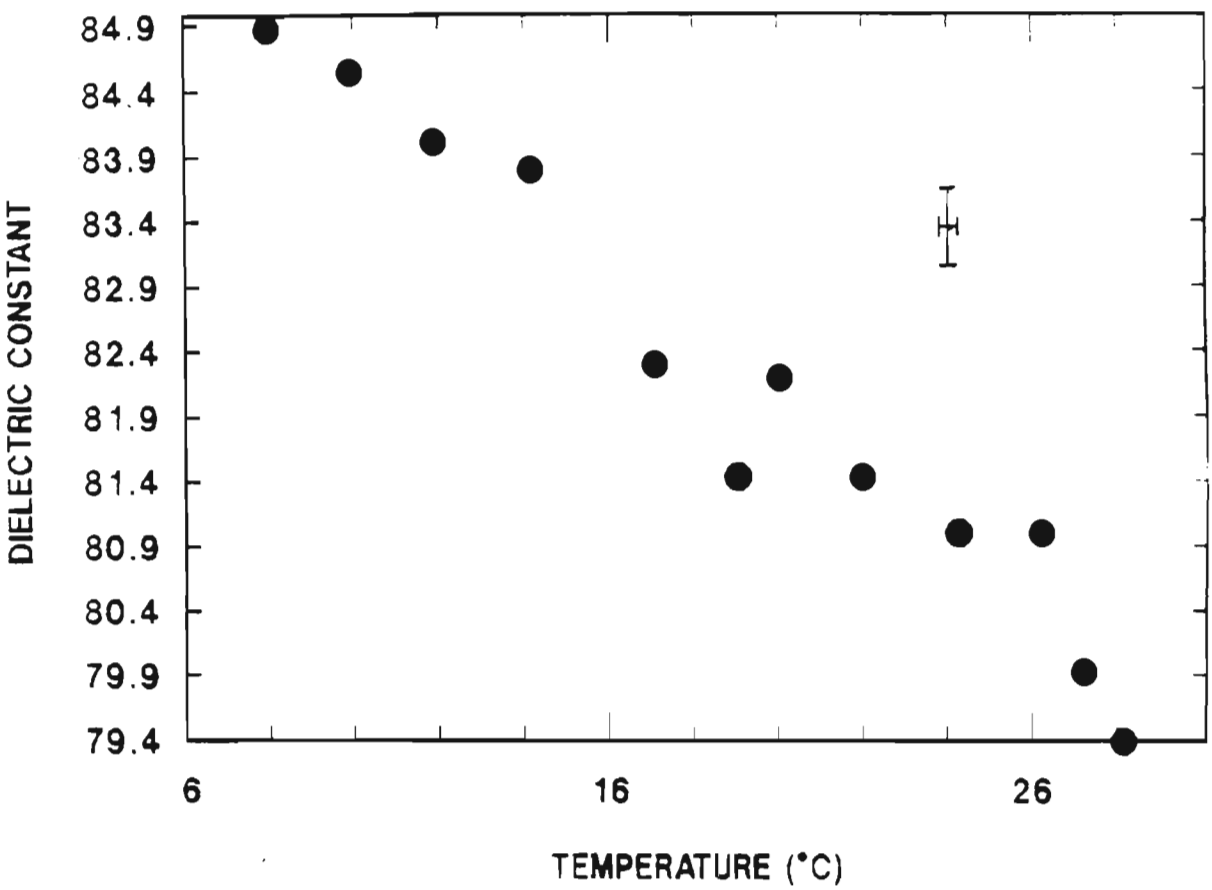

Figure 7.11. The measured diecletric constant of water as a function of temperature

3 HIGH PULSE RATE TESTING OF WATER CAPACITORS.

The purpose of this test was to determine whether a water capacitor would still act as a capacitor at high repetition rates (2000 Hz). Akerlof[105] measured the dielectric constant of water and water/glycol mixtures at 2 MHz for temperatures 20^{o}C and above. He discovered that the data could be accurately expressed using a simple empirical relationship:

$$\epsilon(T,w)=a(w)e^{-b(w)T} \qquad 7.28$$

Where T is the celsius temperature and the empirical constants a(w) and b(w) depend only on the glycol weight fraction w. Fenneman[101] extended these measurements to higher frequencies and lower temperatures and has found that the empirical relationship remains valid to the freezing point of the liquid. He measured ϵ up to 108 MHz and have found that the value was essentially the same as at very low frequencies. They also measured the Debye relaxation time $\tau_d(T,w)$. This is the measure of the time required for the dipoles to re–align in a changing field. They found that although τ_d shows exponential increase with decreasing temperature it remains less than a nanosecond and hence still a small factor. These tests were all done at a very low voltage and the question remained if the capacitor would still act as a capacitor at a high voltage and a high repetition rate.

The circuit used for testing the water capacitor is shown in figure 7.12. The power supply of a copper vapour laser was used. The power supply is able to deliver 20 kV pulses in the range 600–1600 Hz. The laser discharge was simulated by using a copper sulfate resistor. This resistor consisted of two copper plates 1 cm apart in a copper sulfate solution. The resistivity of this resistor could be varied from 1 MΩ to 5 Ω by varying the amount of copper sulfate in the solution. This resistor was used because its inductance is very low. The capacitance of this resistor was measured to be 550 pF. The resistor was impedance matched to the power supply by slowly adding copper sulfate to the solution, the voltage was then measured across the resistor using a Tektronix P6015 probe and a Tektronix 2430 digital storage oscilloscope. The inductance of the circuit was measured to be 800 nH. The experimental procedure was as follows: Kirchoff's laws were used to set up differential equations describing the behaviour of the circuit. These differential equations were then numerically solved and this calculated pulse was then compared with the measured pulse. If the two pulses show the same functional dependence on time as the measured pulse then it was assumed that the capacitor was still acting as a true capacitor. Thus using Kirchoff's law:

For loop 1 in figure 7.12

$$\frac{1}{C_s}\int idt+L_1\frac{di}{dt}+L_2\frac{di_2}{dt}+i_3R_1=V_0 \qquad 7.29$$

This can be written as:

$$\frac{di}{dt} = \frac{1}{L_1}\left[V_0-\left[\frac{1}{C_s}\int idt+L_2\frac{di_2}{dt}+i_4R_1\right]\right] \qquad 7.30$$

For loop 2:

$$L_2\frac{di_2}{dt}+i_3R_1 - \frac{1}{C_w}\int i_1dt=0 \qquad 7.31$$

This can be re–written as:

$$\frac{di_2}{dt} = \frac{1}{L_2}\left[\frac{1}{C_w}\int i_1dt-i_3R_1\right] \qquad 7.32$$

For loop 3:

$$\frac{1}{C_1}\int i_4dt-i_3R_1=0 \qquad 7.33$$

This can be re–written as:

$$i_3=\frac{1}{C_1R_1}\int i_4dt \qquad 7.34$$

Furthermore:

$$i_2=(i-i_1) \qquad 7.35$$

$$i_3=(i-i_1-i_4) \qquad 7.36$$

Equations (7.32), (7.33), (7.34) with equations (7.35) and (7.36) were numerically solved using a simple Euler method. The following values were used:

C_s :6 nF
L_1 :800 nH
C_w :770 pF
L_2 :200 nH
R_1 :50 Ω
C_1 :500 pF

The calculated voltage pulse is shown in figure 7.13. The pulse consists of a main pulse with a FWHM of 112 nS, as well as two subsidiary pulses with a FWHM of approximately 100 nS. The measured pulse is shown in figure 7.14. It consists of a main pulse with a FWHM of approximately 110 nS with two subsidiary pulses, the FWHM of the first peak is approximately 95 nS and that of the third peak also approximately 95 nS. Some smaller spikes are observable on the main pulses. These spikes are caused by stray inductance and capacitance in the test circuit as well as by electromagnetic noise. These tests

were done at 12 kV and the repetition rates varied between 600 Hz and 16 kHz. As can be seen the measured pulse agrees with the calculated pulse and it can thus be said that the capacitor was in fact acting as a capacitor. As an additional test the water capacitor in the test circuit was replaced by a ceramic capacitor with a similar capacitance and an identical pulse shape was measured.

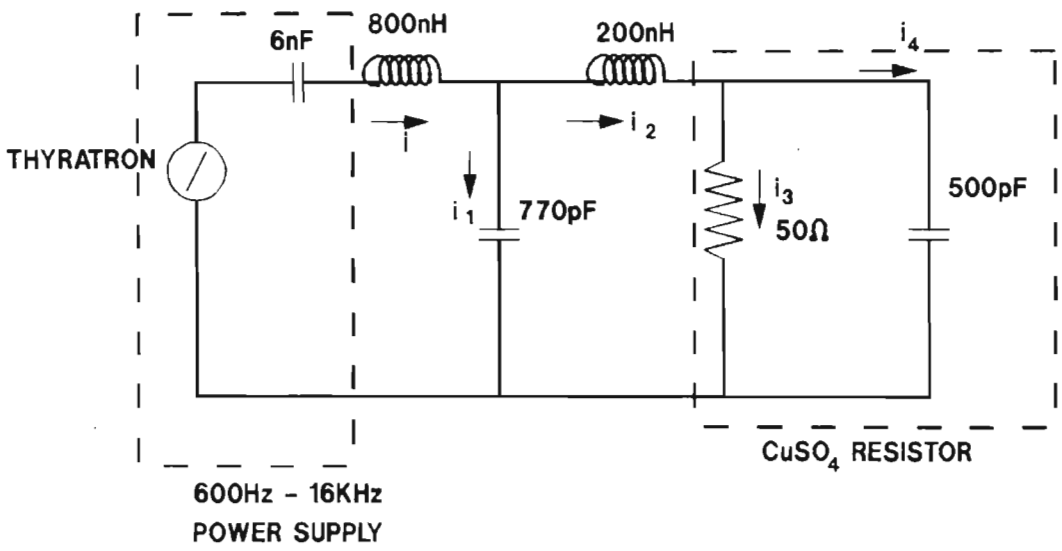

Figure 7.12. A schematic diagram of the circuit used for testing the high repetition rate behaviour of a water capacitor.

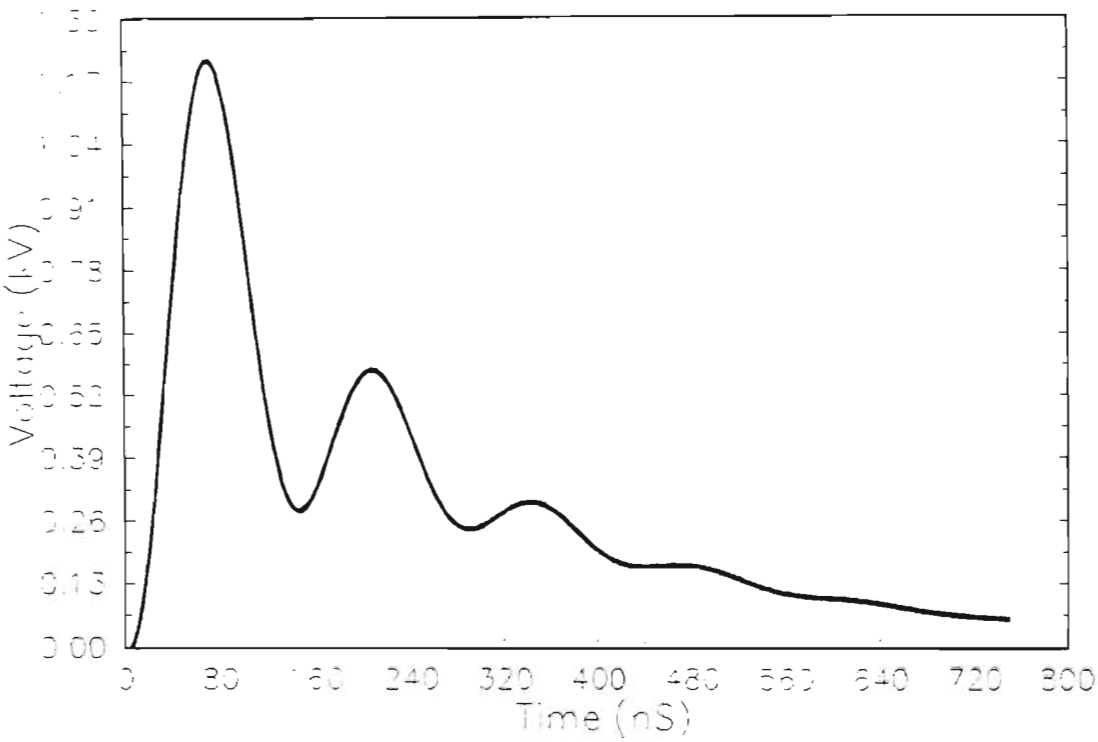

Figure 7.13. The calculated voltage pulse.

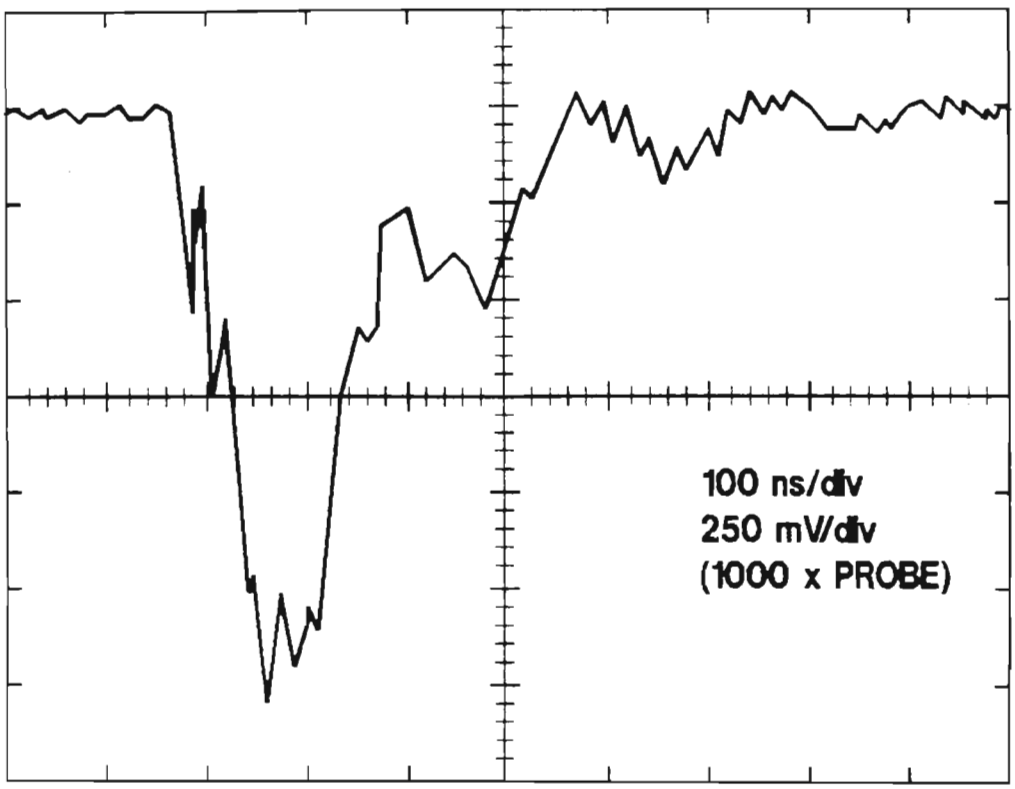

Figure 7.14. The measured high repetition rate pulse.

CHAPTER 8

CONCLUSION

Three factors important for the operation of a continuously tunable CO_2 laser were investigated:

(i) The use of isotopic mixtures to lower the pressure at which continuous tunability could be achieved.

(ii) Design and analysis of a three mirror resonator for such a laser system.

(iii) An investigation into the feasibility of using water capacitors in a high repetition rate power supply for such a laser system.

8.1 THE USE OF ISOTOPIC MIXTURES IN A CO_2 LASER.

The use of isotopic CO_2 mixtures in a high pressure CO_2 laser was investigated both theoretically as well as experimentally. A mathematical model for calculating the small signal gain of any CO_2 isotopic mixture at any pressure was developed. This model indicated that continuous tunability would be possible at 3 atm using a mixture of $25\%C^{16}O_2$,$25\%C^{18}O_2$ and $50\%C^{18}O^{16}O$.

A high pressure CO_2 laser was built and tests were done with a mixture of $50\%C^{18}O_2$ and $50\%C^{16}O_2$. The idea was to use this mixture to produce the isotopic mixture mentioned above. CO_2 is dissociated into CO and O_2 in a gas discharge. Through catalytic recombination isotopic scrambling would take place and after many thousands of shots the equilibrium concentration of $25\%C^{18}O_2$,$25\%C^{16}O_2$ and $50\%C^{16}O^{18}O$ would be reached. Unfortunately the experiment had to be abandoned before the required concentration was reached due to the formation of filamentary arcs in the discharge caused by impurities in the gas. Continuous tunability was observed with the $50\%C^{16}O_2$ and $50\%C^{18}O_2$ mixture at 2.7 atm on the 10 micron R branch from the R14 to the R30 line. This measured curve corresponded to the calculated gain curve and thus predictions made using the calculated gain curves can be made with greater confidence. It can thus be said that continuous tunability on the 10 micron R branch could be expected with the equilibrium concentration. At 3 atm. This agrees well with the experimental results of Gibson, Boyer and Javan[11].

8.2 RESONATOR INVESTIGATION.

An investigation was made into the different types of resonators suitable for the use in a continuously tunable single mode high pressure CO_2 laser. The resonator that was decided upon was the so–called three mirror resonator with a grating and an etalon in the sub–cavity part of the resonator. A mode discrimination analysis for this resonator was done. This predicted that single mode energies in the vicinity of 982 wavenumbers –which is important for the laser isotope separation program as was mentioned in the introduction – ranging from 30 mJ to 200mJ could be achieved. The 30 mJ value is predicted for a single isotope $C^{16}O_2$ laser using a 50% partial reflector and the 200 mJ is predicted for an equilibrium isotopic mixture.

A thermal analysis of the resonator was done and this indicated that the thermal drift of the resonator should not be a problem if the temperature of the resonator is kept constant to within one degree celsius. A three mirror resonator with an etalon and a grating was constructed on a commercial high pressure CO_2 laser. This was done mainly to test the predictions made by the mathematical model. Experimental energy values as well as pulse shapes were measured which agreed well with the experimentally predicted values. The calculations indicate that the etalon and grating would be exposed to much lower power densities than the rest of the components in the resonator. They would be exposed to less than 20% of the intensity inside the resonator.

These factors indicate that the three mirror resonator with a grating and an etalon would be the resonator to use in a high repetition rate continuously tunable single mode CO_2 laser. A future research program could focus on the active control of such a resonator.

8.3 USE OF WATER CAPACITORS.

Finally an investigation was made into the feasibility of using water capacitors in a high repetition rate pulse power supply. Again both a theoretical as well as an experimental investigation was made and the specifications of the water capacitor were compared with that of other capacitor technologies. A mathematical breakdown model was developed which predicted the published experimental results accurately. Experimental measurements of certain dielectric properties of water were carried out, these included the resistivity of the water, its dielectric constant, intrinsic time constant as well as the behaviour of a water capacitor at high repetition rates and high voltages. Finally a design proposal for a high repetition rate pulse power supply using normal capacitors as storage capacitors and water capacitors as the capacitors in the second and third stages of a magnetic pulse compression circuit is given. Although the measurements and calculations indicate that the water capacitors could not be used as storage capacitors they seem to be a viable alternative to use in a pulse power supply of the configuration proposed.

REFERENCES

1. C Wan,U Werling,K Frenk.
   Journal of Applied Physics, 57(3),990,Feb 1985.

2. D J Brink.
   DSc thesis, University of Pretoria, 1979.

3. D J Brink, V Hasson.
   Journal of Applied Physics, 49(4),2250, April 1978.

4. J L Miller, A H Ross, E V George.
   Applied Physics Letters, 26(9),523, May 1975.

5 A M Olbertz, W J Witteman.
   Optics Communications, 30(3),447, Sept 1979.

6. T Carman, P E Dyer.
   Journal of Applied Physics, 49(7),3742, July 1978.

7. C Angelie, R Capitini, P Girard.
   Applied Optics, 26(6),1074, March 1987.

8 G C Stuart, H Houtman, J Meyer.
   Rev. Sci. Instruments, 58(2),261, Feb 1987.

9. I N Knyazen, A A Sarkisian.

Optics Communications, 52(6),421,1985.

10 O P Judd, J Y Wada.
IEEE Journal of Quantum Electronics, Volume QE–10, No 11,12, Jan 1974.

11. R B Gibson, K Boyer, A Javan.
IEEE Journal of Quantum Electronics, Volume QE–15, No 11,1224, Nov 1979.

12. T Shimada et al.
Proccedings of the Conference on Lasers and Electro–optics, FD 2, 1988.

13. T W Carman, P E Dyer.
Optics Communications, 29(2), 218, May 1979.

14. J L Bruneau.
Optics Communications, 41(6), 443, May 1979.

15. P Mathieu, J R Izatt.
IEEE Journal of Quantum Electronics, Volume QE–13, No 6, 465, June 1977.

16. B K Deka, M A Rob, J R Izatt.
Optics Communications, 57(2),111, Feb 1986.

17 P E Dyer, D N Raouf.
Applied Optics, 24(19),3152, 1985.

18 J R Izatt.
SPIE, Volume 666, 15, 1986.

19. B K Deka, P E Dyer, R J Winfield.
Optics Communications, 39(4),225,1981.

20. G J Ernst, J Witteman.
IEEE Journal of Quantum Electronics, Volume QE–7, No10,484, 1971.

21. D B Fenneman, R J Gripshover.
Proceedings of the IEEE Pulsed Power Conference, 302, 1983.

22. V H Gehman, T L Berger.
Proceedings of the IEEE Pulsed Power Conference, 54, 1987.

23. D B Fenneman.
Journal of Applied Physics, 53(12), 8961, December 1982.

24. D B Fenneman, R J Gripshover.
IEEE Transactions on Plasma Science, Volume PS–8,

209, Sept 1980.

25. S C Lin, J I Levatter.
Applied Physics Letters, 34(8), 505, April 1979.

26. W H Long, M J Plummer, E A Stapperts.
Applied Physics Letters 43(8), 735, October 1983.

27. H J Cirkel, W Bette, D Friede, R Muller.
SPIE Conference Proceedings, Pulse Power for Lasers, 50, 1987.

28. H Haken.
Proceedings of the tenth session of the Scottish Universities summer school in physics, 1969, Academic Press.

29 J D Jackson.
Classical Electrodynamics, Second Edition, 1975, John Wiley & Sons.

30 A Yariv.
Quantum Electronics, Third Edition, 1989, John Wiley & Sons.

31 A Einstein.
Phys Zeit, 18, 121, 1917.

32 R K Pathria.
Statistical Mechanics, 1972, Pergamon.

33. A E Siegman.
Lasers, 1986, University Science Books.

34 R Loudon.
The Quantum Theory of Light, Oxford Science Publications, 1979.

35 G Herzberg.
Molecular Spectra and Molecular Structure II, D van Nostrand, 1945.

36. University of Pretoria third year linear algebra notes, 1981.

37. E Merzbacher.
Quantum Mechanics, Second Edition, John Wiley & Sons, 1970.

38 J I Levatter, S C Lin.
J Appl Phys, 51(1), 210, January 1980.

39 C K N Patel, P K Tien, J H McFee.
Appl Phys Lett,14(4),240,1965.

40 W L Nighan, J H Bennet.
Appl Phys Lett,14(8),240,1969.

41 L J Denes, J J Lowke.
Appl Phys Lett, 23(1),130, 1973.

42 G Wiederhold,K H Donnerhacke, G Wanie.
Lasers 75, Optoelectronics Conference Proceedings,38,1975.

43. C Freed.
IEEE Journal of Quantum Electronics, Vol QE–118, No 18, 1220, August 1982.

44. I Wieder, G B Mc Curdy.
Physical Review Letters, 16(13), 565, March 1966.

45. G B Jacobs, H C Bowers.
J Appl Phys, 38(6),2692, May 1967.

46 J C Siddoway.
J Appl Phys, 39, 4854, 1968.

47 C Wills, P A Hackett, J M Parsons.
Rev Sci Instrum, 50(9), 1141, Sept 1979.

48 J Fox, J L Ahl.
J Appl Phys, 61(6),2403, March 1987.

49 R Nordstram.
Photonics Spectra,89, October 1989.

50 R L Abrams.
Appl Phys Lett, 25, 1974.

51 L C Bradley, K L Soohoo, C Freed.
IEEE Journal Of Quantum Electronics, Vol QE–22, No 2, 234, Feb 1986.

52 K G Brown et al.
SPIE, Vol 663, Laser Radar Technology and Applications,136, 1986.

53 L Bhaumik, R Bradford, A R Rault.
Applied Physics Lett.28(1),23,Jan 1976

54 C A Fenstermacher, M J Nutter, W T Leland, K Boyer.
Appl Phys Lett, 20, Jan 1972.

55 N W Harris, F.O'Neill and W T Whitney.

Appl Phys Lett, 25,148,1974.

56 J I Levatter, S C Lin.
J Appl Phys. 51(1), 210, Jan 1980.

57 J S Townsend.
Philos Mag,3,557,1902.

58 L B Loeb.
Basic Processes of Gaseous Electronics, University of California Press, Berkeley,p415,1955.

59 A J Palmer.
Applied Physics Letters, 25(3),138,Aug 1974.

60 H M Lamberton, P R Pearson.
Electron Lett, Vol 7, March 1971.

61 A F Gibson, T A Hall and C B Hatch.
IEEE J Quantum Electron. QE–13,801,1977.

62 J I Levatter and R S Bradford.
Appl Phys Lett. 33,742,1978.

63 V N Karnyushin, R I Soloukin.
Macroscopic and Molecular Processes in Gas Lasers,

Moscow,Atomizdat,1981.

64 P T Gavrilov et al.
J Phys E: Sci Instrum 20,906,1987.

65 Y Ohwadano,T Sekiguchi.
Japan J Appl Phys,19,1493,1980.

66 O R Wood.
Proc IEEE,62, 355,1974.

67 G R White.
NBS Report No 1003 (US GPO, Washington,DC),1952.

68 Private communication with Dr R N Campbell, 1989.

69 W Rogowski.
Arc Elektrotech,12,1,1923.

70 T Y Chang.
Review of Scientific Instr, 44(4),405,1973.

71 G J Ernst.
Optics Communications, 49(4),275,1984.

72 A D Papadopoulos, A A Serafetinides.
IEEE Journal of Quantum Electronics, Vol 26, 169,

Jan 1990.

73 Fox and Li.
I.R.E. Vol 48, 1904, Nov 1960.

74 M Born and E Wolf.
Principles of Optics, Pergamon Press, 1959.

75 O Judd.
High Power Gas Lasers, The Institute of Physics,46, 1975.

76 R L Burden, J D Faires, A C Reynolds.
Numerical Analysis, Second Edition, Prindle,Weber and Schmidt, 1981.

77 R C Weast.
C R C Handbook of Chemistry and Physics, CRC Press, 1985.

78 B S Patel.
Proceedings of the IEEE, 795, June 1973.

79 A F Gibson, M F Kimitt, A C Walker.
Applied Physics Letters, 17(2),75, 15 July 1979.

80 J C Edwards, A C Roddie, P A Smith.
J Phys E, 16, 526,1983.

81 V Valencia ,D K Haskill and R A Cooper.
Proceedings of the Fifteenth IEEE Power Modulator Symposium, 1982.

82 Maxwell Data Sheet, Capacitor Selection Guide, 1990.

83 G Mc Duff.
SPIE vol 1046, Pulse Power for Lasers, 73, 1989.

84 F Booth.
The Journal of Chemical Physics, 19(4), 391, April 1951.

85 J Harrison et al.
Proceedings of the IEEE Conference on Pulsed Power, 304, 1987.

86 J J Ramirez et al.
Proceedings of the IEEE Conference on Pulsed Power, 294, 1987.

87 T L Bergen et al.
Proceedings of the IEEE Conference on Pulsed Power, 263, 1987.

88 J Adams et al.
Proceedings of the IEEE Conference on Pulsed Power, 165, 1987.

89 I S Grant, W R Phillips.
Electromagnetism, John Wiley&Sons Ltd,1976.

90 A H Sharbaugh, J C Devins and S J Rzad.
IEEE Trans.Electr Insul, Vol EI–13,4,249,August,1978.

91 N J Felici.
IEEE Trans on Electrical Insulation, EI–23, 249, 1988.

92 W G Chaband.
Journal of Physics D, 13,1299,1980.

93 J O'M Bockris, M A V Devanathan, K Muller.
Proceedings of the Royal Society,55, 1962.

94 M Zahn, S Voldman, T Takada, D Fennaman.
J Appl Physics,54(1),315,January 1983.

95 L Daughrty , J B Franzini.
Fluid Mechanics with Engineering Applications,

McGraw–Hill, Seventh Edition, 1977.

96 T H Storr, J C Martin.
AWRE Report, SSWA/JCM/758/147, 1978, unpublished.

97 D B Fenneman, R J Gripshover.
IEEE Transactions on Plasma Science, Vol PS–8,209, September 1980.

98 J C Martin.
AWRE Report SSWA/JCM/49,1970, unpublished.

99 I D Smith.
Pulsed Electric Power Dielectric Strength Notes, Vol 1, Notes 1–23, Air Force Weapons Lab.TR 73–167,April 1970.

100 A R McLeod, V H Gehman.
Proceedings of the IEEE Conference on Pulsed Power,57, 1987.

101 D B Fenneman.
J Appl Physics.,53(12),8961,December 1982.

102 G Kortum.
Treatise on Electrochemistry, Elsivier Publishing

Conpany, (1965).

103 D Basting, K Hohla,E Albers,H v Bergmann.
Lasers&Optoelektronik,2/84,128,1984.

104 Masterton and Slowinski.
Chemical Principles,Fourth Edition,W B Saunders Company,1977.

105 G Akerlof.
Journal of American Chem Society,54,4125,1932.

APPENDIX 1

This computer program calculates the small signal gain of an isotopic mixture of CO_2.

```
program Lorentz_1      ;
{-------------------------------------------------------}
{ This program calculates the relative small signal    }
{ gain of different isotopes of CO2                    }
{-------------------------------------------------------}
uses
 dos,crt,gdriver,printer,gkernel,gwindow,gshell;
const
  pi=3.14159;
  c=2.99792458e8;
  nu018=966.956;
  nu016=960.96;
  nu01618=966.2688;
  nu013=914.118;
  B18=34.409;
  BB18=34.740;
  B16=38.71;
  BB16=39.02;
  B1618=36.52;
  BB1618=36.84;
  B13=44.39;
  BB13=44.20;
  k_boltz=1.381e-23;
  h=6.624e-34;
type
  reeks=array[0..600] of real;

var
 druk,nub,nue,inversion,Q,nu_breed,fakt,delta_nu,nu,nu01,verskil:real;
 g,gain,ontaard,g2,gain2,gain3,gain4                          :reeks;
 i,aantal,j,k,tel                          :integer;
 leer                              :text;
 fakt2,nu016f,nu018f,nu013f,nu01618f,lamda,golfgetal:real;
 A1:plotarray;

procedure partition(var Q:real;
                    var ZB,ZO:reeks;
                    var ontaard:reeks;
                    B1,BB1:real;
                    tel:integer);
var
 j     :integer;
 temp:real;
begin
Q:=0.0;
temp:=300;
j:=0;
While (j < 60 ) do begin
 ontaard[j]:=(2*j+1);
 Q:=Q+ontaard[j]*exp((-(h*c*B1)/(k_boltz*Temp))*(j*(j+1)));
 j:=j+tel;
end;
J:=0;
while (j < 62 ) do begin
  ontaard[j]:=(2*J+1);
  ZB[j]:=((ontaard[j])*exp((-(h*c*B1)/(k_boltz*Temp))*(j*(j+1))));
  ZO[j]:=((ontaard[j])*exp((-(h*c*B1)/(k_boltz*Temp))*(j*(j+1))));
  ZB[j]:=ZB[j]/Q;
```

```
  ZO[j]:=ZO[j]/Q;
  {writeln(' ZB[j]= ',ZB[j],' ZO[j]= ',ZO[j]);}
  j:=j+1;
end;
end;


procedure wins(B1,BB1,nu0,nub,nue:real;
               var gain :reeks;
               tel:integer);

var
 i,j   :integer;
 nup,nur,fakt,fakt2,nu,g,g2,antw,tet :real;
 ZB,ZO :reeks;


begin
WRITELN(' nub= ',NUB);
partition(Q,ZB,ZO,ontaard,B1,BB1,tel);
for i:=0 to 500 do begin
  gain[i]:=0.0;
end;
i:=1;
j:=0;
while (j < 60) do begin
  nup:=nu0-(B1/100+BB1/100)*j+(B1/100-BB1/100)*j*j;
  nur:=nu0+2*B1/100+(3*B1/100-BB1/100)*j+(B1/100-BB1/100)*j*j;
  writeln(' j= ',j,' R= ',nuR:10:5);
  nup:=c*(100*nup);
  nur:=c*(100*nur);
  nu:=nub;
  i:=1;
  while(i <500 ) do begin
    fakt:=((ZB[j])-(ZO[j+1]*(1/inversion)));
    fakt2:=((ZB[j])-(ZO[j-1]*(1/inversion)));
    if(j=0) then fakt2:=0.0;
    {writeln(' druk= ',druk,' nu_breed= ',nu_breed,' nu= ',nu);}
    g:=fakt*druk*druk*((nu_breed/(2)))/((sqr(nu-nup)+sqr(nu_breed/2)));
    g2:=fakt2*druk*druk*((nu_breed/(2)))/((sqr(nu-nur)+sqr(nu_breed/2)));
    gain[i]:=gain[i]+g2+g;
    nu:=nu+delta_nu;
    i:=i+1;
  end;
  j:=j+tel;
end;
end;


procedure plotter(a:plotarray; N:integer);
{ Hierdie program plot funksie plus asse                    }
{ program bepaal self die min en max waardes                }

var
 minx,miny,maxx,maxy          :real;
 i                           :integer;
 opskrif                      :string[30];
 antw                         :char;
```

```
 files                              :text;

procedure Asse;

begin
ClearScreen;
SetColorWhite;
SetBackground(0);
DefineHeader(1,opskrif);
DrawBorder;
DrawAxis(8,7,0,0,0,0,0,0,true);
end;

Procedure MinMax(a :PlotArray; N:integer;
                 var minx,maxx,miny,maxy :real);

var
  i:integer;

begin
i:=1;
minx:=A[1,1];
maxx:=A[1,1];
miny:=A[1,2];
maxy:=A[1,2];
for i:=1 to n do begin;
  if ( A[i,1] > maxx ) Then begin
      Maxx:=A[i,1];
  end;
  if ( A[i,1] < minx ) Then begin
      minx:=A[i,1];
  end;
end;
for i:=1 to n do begin
   if( A[i,2] > maxy ) then begin
      maxy:= A[i,2];
    end;
    if ( A[i,2] < miny ) then begin
      miny:=A[i,2];
    end;
end;
end;

begin
MinMax(a,n,minx,maxx,miny,maxy);
writeln(' minx= ',minx,' maxx= ',maxx);
writeln(' miny= ',miny,' maxy= ',maxy);
initgraphic;
DefineWindow(1,0,0,Xmaxglb,YmaxGlb);
DefineWorld(1,minx,miny,maxx,maxy);
SelectWorld(1);
SelectWindow(1);
Asse;
Drawpolygon(A,1,n,0,0,0);
repeat until KeyPressed;
LeaveGraphic;
end;
```

```
begin
assign(leer,'lorentz4.dat');
rewrite(leer);
writeln(' Druk in atmosfeer ?');
readln(druk);
nu_breed:=6.0e9*druk;
ontaard[0]:=1.0;
aantal:=60;
inversion:=1.7;
nu018f:=c*(100*nu018);
nu016f:=c*(100*nu016);
nu013f:=c*(100*nu013);
nu01618f:=c*(100*nu01618);
nub:=3.0e8/10.177e-6;
nue:=3.0e8/10.23e-6;
delta_nu:=(nue-nub)/500;
tel:=2;
WRITELN(' nub= ',nub);
wins(B18,BB18,nu018,nub,nue,gain,tel);
wins(B16,BB16,nu016,nub,nue,gain2,tel);
{wins(B13,BB13,nu013,gain3,tel);}
tel:=1;
{wins(B1618,BB1618,nu01618,nub,nue,gain4,tel);}
nu:=nub;
for i:=1 to 499 do begin
   gain[i]:=0.6*gain2[i]+0.4*gain[i];
   writeln('nu = ',(nu-nu018f)/1.0e9,' gain= ',gain[i]*0.13e12);
   lamda:=(c/nu);
   golfgetal:=1/(lamda*100);
   writeln(leer,golfgetal,' ',gain[i]*0.13e12);
   A1[i,1]:=golfgetal;
   A1[i,2]:=gain[i]*0.13e12;
   nu:=nub+i*delta_nu;
end;
writeln(' Verskil= ',verskil);
plotter(a1,i);
close(leer);
end.
```

APPENDIX 2

This computer program calculates the electrode profile.

```
    program Ernst;
{-----------------------------------------------}
{ This program calculates the electrode profiele}
{ using the method of Ernst                     }
{-----------------------------------------------}
uses

 dos,crt,gdriver,printer,gkernel,gwindow,gshell;

const
 pi=3.1415;
var
u,k1,k2,k0,x,y:real;
ai:plotarray;
files       :text;
i,tel,j:integer;

function cosh(x:real):real;
begin
cosh:=(exp(x)+-exp(-x))/2.0;
end;

function sinh(x:real):real;
begin
sinh:=(exp(x)+exp(-x))/2.0;
end;



procedure plotter(a:plotarray; N:integer);
{ Hierdie program plot funksie plus asse                    }
{ program bepaal self die min en max waardes                }

var
 minx,miny,maxx,maxy            :real;
 i                             :integer;
 opskrif                        :string[30];
 antw                           :char;
 files                          :text;

procedure Asse;

begin
ClearScreen;
SetColorWhite;
SetBackground(0);
DefineHeader(1,opskrif);
DrawBorder;
DrawAxis(8,7,0,0,0,0,0,0,true);
end;

Procedure MinMax(a :PlotArray; N:integer;
                 var minx,maxx,miny,maxy :real);

var
  i:integer;

begin
i:=1;
minx:=A[1,1];
maxx:=A[1,1];
miny:=A[1,2];
maxy:=A[1,2];
for i:=1 to n do begin;
```

```
  if ( A[i,1] > maxx ) Then begin
      Maxx:=A[i,1];
  end;
  if ( A[i,1] < minx ) Then begin
      minx:=A[i,1];
  end;
end;
for i:=1 to n do begin
   if( A[i,2] > maxy ) then begin
      maxy:= A[i,2];
    end;
    if ( A[i,2] < miny ) then begin
      miny:=A[i,2];
    end;
end;
end;

begin
MinMax(a,n,minx,maxx,miny,maxy);
writeln(' minx= ',minx,' maxx= ',maxx);
writeln(' miny= ',miny,' maxy= ',maxy);
initgraphic;
DefineWindow(1,0,0,Xmaxglb,YmaxGlb);
DefineWorld(1,minx,miny,maxx,maxy);
SelectWorld(1);
SelectWindow(1);
Asse;
Drawpolygon(A,1,n,0,0,0);
repeat until KeyPressed;
LeaveGraphic;
end;



begin
assign(files,'Ernst.dat');
rewrite(files);
u:=0.0 ;
k0:=0.02;
k1:=k0*k0/8;
k2:=k0*k0*k0/90;
i:=1;
while (u<5.1) do begin
 x:=u-k1*sinh(2*u);
 y:=pi/2+k0*cosh(u)-k2*cosh(3*u);
 u:=u+0.1;
 writeln('x= ',x/(pi/2+k0),' y= ',y/(pi/2+k0));
 ai[i,1]:=x*0.314;
 ai[i,2]:=y*0.314;
 writeln(files,ai[i,1],' ',ai[i,2]);
 i:=i+1;
end;
i:=i-1;
plotter(ai,i);
close(files);
end.
```

APPENDIX 3

This computer program calculates the wavelength dependent reflection of a grating.

```
program grating;
uses
 dos,crt,gdriver,printer,gkernel,gwindow,gshell;

const
  pi=3.141592654;
  c=3.0e8;

var
  lamda,lengte,area,k,f_ruimte,a,b    :real;
  fakt1,fakt2,fakt3,fakt4,alpha,beta  :real;
  n,I_theta,theta,l_mm,lamda1,nu      :real;
  f,min,maks,midpt,littrow        :real;
  theta_r,theta_i,aperture,max    :real;
  files                               :text;
  nu_uit,midpt1                       :real;
  Tel,Np,i :integer;
  A1:plotarray;

procedure plotter(a:plotarray; N:integer);
{ Hierdie program plot funksie plus asse                    }
{ program bepaal self die min en max waardes                }

var
 minx,miny,maxx,maxy            :real;
 i                             :integer;
 opskrif                        :string[30];
 antw                           :char;
 files                          :text;

procedure Asse;

begin
ClearScreen;
SetColorWhite;
SetBackground(0);
DefineHeader(1,opskrif);
DrawBorder;
DrawAxis(8,7,0,0,0,0,0,0,true);
end;

Procedure MinMax(a :PlotArray; N:integer;
                 var minx,maxx,miny,maxy :real);

var
  i:integer;

begin
i:=1;
minx:=A[1,1];
maxx:=A[1,1];
miny:=A[1,2];
maxy:=A[1,2];
for i:=1 to n do begin;
  if ( A[i,1] > maxx ) Then begin
      Maxx:=A[i,1];
  end;
  if ( A[i,1] < minx ) Then begin
      minx:=A[i,1];
  end;
end;
for i:=1 to n do begin
   if( A[i,2] > maxy ) then begin
      maxy:= A[i,2];
```

```
    end;
    if ( A[i,2] < miny ) then begin
      miny:=A[i,2];
    end;
end;
end;

begin
MinMax(a,n,minx,maxx,miny,maxy);
writeln(' minx= ',minx,' maxx= ',maxx);
writeln(' miny= ',miny,' maxy= ',maxy);
initgraphic;
DefineWindow(1,0,0,Xmaxglb,YmaxGlb);
DefineWorld(1,minx,miny,maxx,maxy);
SelectWorld(1);
SelectWindow(1);
Asse;
Drawpolygon(A,1,n,0,0,0);
repeat until KeyPressed;
LeaveGraphic;
end;

begin
assign(files,'grating2.dat');
rewrite(files);
writeln(' Aperture of Laser ? ');
readln(aperture);
writeln(' Hoeveel lyne/mm ');
readln(l_mm);
writeln(' littrow ');
readln(littrow);
littrow:=(pi/180.0)*littrow;
writeln(' Theta i ');
readln(theta_i);
theta_i:=(3.14159/180.0)*theta_i;
lengte:=aperture/(cos(theta_i));
writeln(' Lengte= ',lengte);
writeln(' Theta r ');
readln(theta_r);
writeln(' Midpt van grafiek ?');
readln(midpt);
midpt1:=c/(midpt*1.0e-6);
max:=midpt1+30.0e9;
min:=midpt1-30.0e9;
theta_r:=(3.14159/180.0)*theta_r;
N:=trunc(lengte*L_mm*1000);
writeln(' N= ',n);
f_ruimte:=1/(l_mm*1000.0);
a:=f_ruimte;
b:=a/2.0;
f:=min;
tel:=1;
  i:=1;
lamda:=min;
while ( f < max) do begin
  lamda:=c/f;
  k:=(2*pi)/lamda;
  beta:=((K*b))*sin(theta_i-littrow-0.0001);
  alpha:=((K*a/2.0))*(sin(theta_i)-sin(theta_r));
  fakt1:= (sin(beta))/(beta);
  fakt1:=fakt1*fakt1;
  fakt2:=(sin(N*alpha))/(N*sin(alpha));
  fakt2:=fakt2*fakt2;
  fakt3:=(fakt1*fakt2);
```

```
    nu:=(c/lamda-c/(10.6e-6))/1.0e9;
    lamda1:=(lamda-10.1738e-6)*1.0e9;
    {writeln(' Lamda= ',lamda,' R= ',fakt3);}
    nu_uit:=(f-midpt1)/1.0e9;
    A1[i,1]:=NU_uit;
    A1[i,2]:=fakt3;
    writeln(files,nu_uit,' ',fakt3);
    f:=f+0.25e9;
    tel:=tel+1;
    i:=i+1;
  end;
  writeln(' Tel= ',tel,' maks= ',max,' min= ',min);
  writeln(' midpt= ',midpt);
  np:=tel-1;
  plotter(a1,np);
  close(files);
  end.
```

APPENDIX 4

This computer program calculates the wavelength dependent transmission of an etalon.

```
program etalon;
{ Hierdie program bereken die transmissie funksie van 'n    }
{ etalon                                                    }
uses printer;
var
 files                                              :text;
 alpha,beta,R,T,dikte,nu,n_aksent,n,theta,theta_aks   :real;
 Trans,c,pi,min,maks,gamma,a,Deel,antw,nu_nuut,lamda        :real;
 I:integer;
 deler,hoek,lamda_0,nu_uit,nu_0,midptn,half,fin,f,freespek:real;
{-----------------------------------------------------------}
{ Hierdie funksie doen magsverheffing                       }
{-----------------------------------------------------------}
function mag(x,y:real):real;
begin
mag:=exp(y*ln(x));
end;
{-----------------------------------------------------------}


{-----------------------------------------------------------}
{ Hierdie funksie bereken die bgsin van 'n hoek             }
{-----------------------------------------------------------}
function bg_sin(x:real):real;
begin
 bg_sin:=x+(1.0/2.0)*((mag(x,3.0))/3.0)+(1.0/2.0)*(3.0/4.0)*((mag(x,5.0))/5.0
end;

begin
writeln(' Etalon data ');
writeln(' ZnSe ');
c:=3.0e8;
assign(files,'ETALON2.DAT');
rewrite(files);
writeln('Middelpunt van grafiek in mikron  ');
readln(midptn);
midptn:=c/(midptn*1e-6);
min:=midptn-12.0e9;
writeln(' Hoek ');
readln(theta);
writeln(' Invalshoek = ',theta:10:5,'Grade');
theta:=theta*(3.141592/180.0);
nu:=min;
maks:=midptn+5.0e9;
nu_0:=(maks+min)/2.0;
writeln(' min= ',min,' maks= ',maks);
writeln(' 1 om voort te gaan ');
readln(antw);
c:=3.0e8;
pi:=3.1415;
alpha:= 0.2;
n:=1.0;
n_aksent:=2.4;
WRITELN(' DIKTE ?');
READLN(DIKTE);
writeln(' Dikte= ',Dikte:10:5,'meter');
WRITELN(' R ?');
READLN(R);
writeln(' Reflektiwiteit = ',R:10:5);
A:=0.04;
T:=1-(R+0.004);
i:=0;
hoek:=bg_sin(n/n_aksent);
writeln(' arg= ',n/n_aksent:10:5,' hoek= ',hoek:10:5);
```

```
while (nu < maks) do begin;
 theta_aks:=bg_sin((n/n_aksent)*sin(theta));
 gamma:=(2.0*pi*n_aksent*dikte*nu*cos(theta_aks))/(c);
 beta:=(dikte*alpha)/(cos(theta_aks));
 deler:=(exp(beta)-R*exp(-beta));
 F:=(4.0*R*R)/(deler*deler);
 half:=C/(SQRT(F)*PI*N_AKSENT*DIKTE*COS(THETA_AKS));
 Fin:=(3.14159*(sqrt(F)))/2.0;
 Trans:=((1-A)*T*T);
 Deel:=(exp(beta)-R*exp(-beta));
 Deel:=Deel*Deel;
 Deel:=Deel+4.0*R*R*sin(gamma)*sin(gamma);
 Trans:=Trans/Deel;
 nu_uit:=(nu-nu_0)/1.0e9;
 lamda:=((c/nu)*1.0e6-10.2)*1000.0;
 i:=i+1;
 freespek:=Half*fin;
 writeln('nu_uit= ',nu_uit:10:5,' trans= ',trans,' I= ',i);
 writeln(files,nu_uit,'  ',Trans,' ',i);
 nu:=nu+0.05e+9;
end;
writeln(' Halfwydte = ',half,'Hz   Finesse= ',Fin:10:5);
writeln(' Vry Spektraalwydte = ',freespek);
writeln('1 om terug te keer');
readln(antw);
close(files);
end.
```

APPENDIX 5

This computer program calculates the wavelength dependent reflection of a three mirror resonator with an etalon and a grating.

```
program mgc;
uses
 dos,crt,gdriver,printer,gkernel,gwindow,gshell;

const
 pi=3.14159;
 c=3.0e8;
var
 maks,R1,R2,Te,lamda,lengte,kos,Ir,delta:real;
 n,antw:integer;
 bo,onder,lamda1,littrow:real;
 dikte,Re,theta,lengte_g,l_mm:real;
 f,f_uit,min,max,midpt,midpt1,logir :real;
 theta_i,theta_r,blaze              :real;
 files :text;
 A1:plotarray;
 i:integer;

procedure plotter(a:plotarray; N:integer);
{ Hierdie program plot funksie plus asse                    }
{ program bepaal self die min en max waardes                }

var
 minx,miny,maxx,maxy            :real;
 i                             :integer;
 opskrif                        :string[30];
 antw                           :char;
 files                          :text;

procedure Asse;

begin
ClearScreen;
SetColorWhite;
SetBackground(0);
DefineHeader(1,opskrif);
DrawBorder;
DrawAxis(8,7,0,0,0,0,0,0,true);
end;

Procedure MinMax(a :PlotArray; N:integer;
                 var minx,maxx,miny,maxy :real);

var
  i:integer;

begin
i:=1;
minx:=A[1,1];
maxx:=A[1,1];
miny:=A[1,2];
maxy:=A[1,2];
for i:=1 to n do begin;
  if ( A[i,1] > maxx ) Then begin
      Maxx:=A[i,1];
  end;
  if ( A[i,1] < minx ) Then begin
      minx:=A[i,1];
  end;
end;
for i:=1 to n do begin
   if( A[i,2] > maxy ) then begin
      maxy:= A[i,2];
    end;
```

```
    if ( A[i,2] < miny ) then begin
      miny:=A[i,2];
    end;
end;
end;

begin
MinMax(a,n,minx,maxx,miny,maxy);
writeln(' minx= ',minx,' maxx= ',maxx);
writeln(' miny= ',miny,' maxy= ',maxy);
initgraphic;
DefineWindow(1,0,0,Xmaxglb,YmaxGlb);
DefineWorld(1,minx,miny,maxx,maxy);
SelectWorld(1);
SelectWindow(1);
Asse;
Drawpolygon(A,1,n,0,0,0);
repeat until KeyPressed;
LeaveGraphic;
end;


{-------------------------------------------------------------}
{ Hierdie prosedure bereken die transmissie van 'n Etalon     }
{-------------------------------------------------------------}
procedure etalon(var Trans :real;
                 lamda,dikte,R,theta:real);
var
 files                                          :text;
 alpha,beta,T,nu,n_aksent,n,theta_aks   :real;
 min,maks,gamma,a,Deel,antw,nu_nuut        :real;
 I:integer;
 deler,hoek,lamda_0,nu_uit,nu_0,midptn,half,fin,f,freespek:real;
{-------------------------------------------------------------}
{ Hierdie funksie doen magsverheffing                         }
{-------------------------------------------------------------}
function mag(x,y:real):real;
begin
mag:=exp(y*ln(x));
end;
{-------------------------------------------------------------}


{-------------------------------------------------------------}
{ Hierdie funksie bereken die bgsin van 'n hoek               }
{-------------------------------------------------------------}
function bg_sin(x:real):real;
begin
 bg_sin:=x+(1.0/2.0)*((mag(x,3.0))/3.0)+(1.0/2.0)*(3.0/4.0)*((mag(x,5.0))/5.0
end;

begin
{writeln(' Etalon data ');}
{writeln(' ZnSe ');          }
{assign(files,'ETALON.DAT');}
{rewrite(files);             }
theta:=theta*(3.141592/180.0);
alpha:= 0.2;
n:=1.5;
n_aksent:=2.4;
A:=0.04;
T:=1-(R+0.004);
i:=0;
nu:=c/lamda;
```

```
hoek:=bg_sin(n/n_aksent);
theta_aks:=bg_sin((n/n_aksent)*sin(theta));
gamma:=(4.0*pi*n_aksent*dikte*nu*cos(theta_aks))/(c);
beta:=(dikte*alpha)/(cos(theta_aks));
deler:=(exp(beta)-R*exp(-beta));
F:=(4.0*R*R)/(deler*deler);
half:=C/(SQRT(F)*PI*N_AKSENT*DIKTE*COS(THETA_AKS));
Fin:=(3.14159*(sqrt(F)))/2.0;
Trans:=((1-A)*T*T);
Deel:=(exp(beta)-R*exp(-beta));
Deel:=Deel*Deel;
Deel:=Deel+4.0*R*R*sin(gamma)*sin(gamma);
Trans:=Trans/Deel;
nu_uit:=(nu-nu_0)/1.0e9;
lamda:=((c/nu)*1.0e6-10.2)*1000.0;
freespek:=Half*fin;
{ writeln(files,nu_uit,'  ',Trans,' ',i);}
{close(files);                          }
end;

{-------------------------------------------------------------}


{-------------------------------------------------------------}
{ Hierdie prosedure bereken die refleksie vanaf 'n Rooster    }
{ Hierdie rooster sit op die Littrow hoek                     }
{-------------------------------------------------------------}

procedure grating(var R2 :real;
                  lamda,lengte,L_mm,theta_i,theta_r,blaze:real);

var
  area,k,f_ruimte,a,b                  :real;
  fakt1,fakt2,fakt3,fakt4,alpha,beta   :real;
  n,I_theta,theta,lamda1,nu            :real;
  f,min,maks,midpt,tel                 :real;
  {files                                :text;}

begin
{assign(files,'grating.dat');}
{rewrite(files);              }
area:=lengte*lengte;
k:=(2*pi)/lamda;
writeln(' K= ',k);
N:=trunc(lengte*L_mm*1000);
f_ruimte:=1/(l_mm*1000.0);
a:=f_ruimte;
b:=a/2.0;
beta:=((k*b))*sin(theta_i-blaze-0.0001);
alpha:=((k*a/2))*(sin(theta_i)-sin(theta_r));
fakt1:= (sin(beta))/(beta);
fakt1:=fakt1*fakt1;
fakt2:=(sin(N*alpha))/(N*sin(alpha));
fakt2:=fakt2*fakt2;
fakt3:=(fakt1*fakt2);
writeln(' fakt3= ',fakt3);
R2:=fakt3;
end;

{-------------------------------------------------------------}
begin
assign(files,'MGC2.dat');
rewrite(files);
{-------------------------------------------------------}
```

```
{ Sub - Cavity input data                                    }
writeln(' Sub - Cavity Mirror Reflection ? ');
readln(R1);
writeln(' Length of sub Cavity ');
readln(lengte);
{-------------------------------------------------------------}
{Etalon invoer data                                           }
  writeln('-----------------------------------------------');
  writeln('Etalon data ');
  WRITELN(' DIKTE ?');
  READLN(DIKTE);
  WRITELN(' R van Etalon?');
   READLN(Re);
  writeln(' Hoek waarteen Etalon staan ?');
  readln(theta);
  writeln('-----------------------------------------------');
{-------------------------------------------------------------}
{ Grating invoer data                                         }
  writeln('-----------------------------------------------');
  writeln(' Grating invoer data');
  writeln(' Laser aperture ');
  readln(lengte_g);
  writeln(' Hoeveel lyne/mm ');
  readln(l_mm);
  writeln(' Hoek waarteen Rooster staan  ? ');
  readln(theta_i);
  theta_i:=(3.14159/180.0)*theta_i;
  Lengte_g:=lengte_g/cos(theta_i);
  writeln(' Refleksie hoek ');
  readln(theta_r);
  theta_r:=(3.14159/180.0)*theta_r;
  writeln(' Blazing angle ');
  readln(blaze);
  blaze:=(3.14159/180)*blaze;
  writeln('-----------------------------------------------');
  writeln(' Is hierdie n grazing incedence opstelling ? ');
  writeln(' 2 indien ja ');
  readln(antw);
  writeln(' Midpt ? ');
 readln(midpt);
 min:=c/(midpt*1.0e-6)-8.0e9;
 max:=c/(midpt*1.0e-6)+8.0e9;
 f:=min;
 i:=1;
while (f < max) do begin
 lamda:=c/f;
 etalon(Te,lamda,dikte,Re,theta);
 Te:=1.0;
 grating(R2,lamda,lengte_g,l_mm,theta_i,Theta_r,blaze);
 delta:=((4*pi)/(lamda))*lengte;
 bo:=(R1+R2*Te*Te+2*sqrt(R1*R2)*Te*cos(delta));
 onder:=(1+Te*Te*R2*R1+2*Te*sqrt(R2*R1)*cos(delta));
 if (antw = 2) then begin
    bo:=(R1+R2*R2*Te*Te+2*R2*sqrt(R1)*Te*cos(delta));
    onder:=(1+Te*Te*R2*R2*R1+2*R2*Te*sqrt(R2)*cos(delta));
 end;
 Ir:=bo/onder;
 writeln(' lamda= ',lamda,' Ir= ',Ir);
 logiR:=ln(Ir*0.8);
 writeln('logir = ',logir);
 lamda1:=(lamda-10.1738e-6)*1.0e8;
 midpt1:=c/(midpt*1.0e-6);
 f_uit:=(f-midpt1)*1.0e-9;
 writeln(files,f_uit,' ',Ir);
```

```
 a1[i,1]:=f_uit;
 a1[i,2]:=Ir;
 i:=i+1;
 kos:=cos(delta);
 writeln(' cos= ',kos);
 f:=f+0.05e9;
end;
plotter(a1,i-1);
close(files);
end.
```

APPENDIX 6

This computer program calculates the wavelength dependent laser oscillation condition for a three mirror resonator with an etalon and a grating.

```
program L_Condition;
uses Crt;
const
 pi=3.14159;
 c=3.0e8;
var
 maks,R1,R2,Te,lamda,lengte,kos,Ir,delta:real;
 n:integer;
 bo,onder,lamda1,littrow:real;
 dikte,Re,theta,lengte_g,l_mm,r_out:real;
 f,f_uit,min,max,midpt,midpt1 :real;
 grens_on,grens_bo,midpt3:real;
 logir,L_hoof,absorbsie,S_gain,total     :real;
 files :text;

{-------------------------------------------------------------}
{ Hierdie prosedure bereken die transmissie van 'n Etalon     }
{-------------------------------------------------------------}
procedure etalon(var Trans :real;
                 lamda,dikte,R,theta:real);
var
 files                                              :text;
 alpha,beta,T,nu,n_aksent,n,theta_aks   :real;
 min,maks,gamma,a,Deel,antw,nu_nuut        :real;
 I:integer;
 deler,hoek,lamda_0,nu_uit,nu_0,midptn,half,fin,f,freespek:real;
{-------------------------------------------------------------}
{ Hierdie funksie doen magsverheffing                         }
{-------------------------------------------------------------}
function mag(x,y:real):real;
begin
mag:=exp(y*ln(x));
end;
{-------------------------------------------------------------}


{-------------------------------------------------------------}
{ Hierdie funksie bereken die bgsin van 'n hoek               }
{-------------------------------------------------------------}
function bg_sin(x:real):real;
begin
 bg_sin:=x+(1.0/2.0)*((mag(x,3.0))/3.0)+(1.0/2.0)*(3.0/4.0)*((mag(x,5.0))/5.0
end;

begin
{writeln(' Etalon data ');}
{writeln(' ZnSe ');          }
{assign(files,'ETALON.DAT');}
{rewrite(files);              }
theta:=theta*(3.141592/180.0);
alpha:= 0.2;
n:=1.5;
n_aksent:=2.4;
A:=0.04;
T:=1-(R+0.004);
i:=0;
nu:=c/lamda;
hoek:=bg_sin(n/n_aksent);
theta_aks:=bg_sin((n/n_aksent)*sin(theta));
gamma:=(4.0*pi*n_aksent*dikte*nu*cos(theta_aks))/(c);
beta:=(dikte*alpha)/(cos(theta_aks));
deler:=(exp(beta)-R*exp(-beta));
F:=(4.0*R*R)/(deler*deler);
half:=C/(SQRT(F)*PI*N_AKSENT*DIKTE*COS(THETA_AKS));
```

```
Fin:=(3.14159*(sqrt(F)))/2.0;
Trans:=((1-A)*T*T);
Deel:=(exp(beta)-R*exp(-beta));
Deel:=Deel*Deel;
Deel:=Deel+4.0*R*R*sin(gamma)*sin(gamma);
Trans:=Trans/Deel;
nu_uit:=(nu-nu_0)/1.0e9;
lamda:=((c/nu)*1.0e6-10.2)*1000.0;
freespek:=Half*fin;
{ writeln(files,nu_uit,'  ',Trans,' ',i);}
{close(files);                          }
end;

{-------------------------------------------------------------}


{-------------------------------------------------------------}
{ Hierdie prosedure bereken die refleksie vanaf 'n Rooster    }
{ Hierdie rooster sit op die Littrow hoek                     }
{-------------------------------------------------------------}

procedure grating(var R2 :real;
                  lamda,lengte,L_mm,littrow:real);

var
  area,k,f_ruimte,a,b                  :real;
  fakt1,fakt2,fakt3,fakt4,alpha,beta   :real;
  n,I_theta,theta,lamda1,nu            :real;
  f,min,maks,midpt,tel                 :real;
  {files                                :text;}

begin
{assign(files,'grating.dat');}
{rewrite(files);              }
area:=lengte*lengte;
k:=(2*pi)/lamda;
writeln(' K= ',k);
N:=trunc(lengte*L_mm*1000);
f_ruimte:=1/(l_mm*1000.0);
a:=f_ruimte;
b:=a/2.0;
beta:=((k*b))*sin(0.00001);
alpha:=((k*a))*sin(littrow);
fakt1:= (sin(beta))/(beta);
fakt1:=fakt1*fakt1;
fakt2:=(sin(N*alpha))/(N*sin(alpha));
fakt2:=fakt2*fakt2;
fakt3:=(fakt1*fakt2);
writeln(' fakt3= ',fakt3);
R2:=fakt3;
end;

{-------------------------------------------------------------}
begin
clrscr;
assign(files,'L_CONDIT.dat');
rewrite(files);
writeln(' Refleksie van 1 ste MGC spieel ? ');
readln(R1);
writeln(' Lengte van cavity ');
readln(lengte);
{-------------------------------------------------------------}
{Etalon invoer data                                           }
  writeln('-----------------------------------------------');
```

```
  writeln('Etalon data ');
  WRITELN(' DIKTE ?');
  READLN(DIKTE);
  WRITELN(' R van Etalon?');
   READLN(Re);
  writeln(' Hoek waarteen Etalon staan ?');
  readln(theta);
  writeln('-----------------------------------------');
{-------------------------------------------------------}
{ Grating invoer data                                   }
  writeln('-----------------------------------------');
  writeln(' Grating invoer data');
  writeln(' lengte  van grating ');
  readln(lengte_g);
  writeln(' Hoeveel lyne/mm ');
  readln(l_mm);
  writeln(' Hoek waarteen Rooster staan  ? ');
  readln(littrow);
  littrow:=(3.14159/180.0)*littrow;
  writeln('-----------------------------------------');
  writeln(' Midpt in mikron? ');
 readln(midpt);
 writeln(' Refleksie van output coupler ');
 readln(R_out);
 writeln(' Lengte van hoof resonator ');
 readln(L_hoof);
 writeln(' Absorbsie ');
 readln(absorbsie);
 writeln(' Small signal gain ');
 readln(S_gain);
 min:=c/(midpt*1.0e-6)-8.0e9;
 max:=c/(midpt*1.0e-6)+8.0e9;
f:=min;
while (f < max) do begin
 lamda:=c/f;
 etalon(Te,lamda,dikte,Re,theta);
 grating(R2,lamda,lengte_g,l_mm,littrow);
 delta:=((4*pi)/(lamda))*lengte;
 bo:=(R1+R_out*Te*Te+2*sqrt(R1*R_out)*Te*cos(delta));
 onder:=(1+Te*Te*R2*R1+2*Te*sqrt(R_out*R1)*cos(delta));
 Ir:=bo/onder;
 writeln(' lamda= ',lamda,' Ir= ',Ir);
 logiR:=ln(Ir*R2);
 total:=exp(S_gain*L_hoof+logir)-1;
 writeln('logir = ',logir);
 lamda1:=(lamda-10.1738e-6)*1.0e8;
 midpt1:=c/(midpt*1.0e-6);
 f_uit:=(f-midpt1)*1.0e-9;
 writeln(files,f_uit,' ',total);
 kos:=cos(delta);
 writeln(' cos= ',kos);
 f:=f+0.05e9;;
end;
close(files);
end.
```

APPENDIX 7

This program calculates the laser pulse shape and energy solving the CO_2 rate equations using a Runge–Kutta method.

```
program l_puls;
{+$}
{-------------------------------------------------------}
{ Program determines laser pulse shape and energy       }
{ taking therm lization of rotational bands into        }
{ account                                               }
const
c=3.0e8;
pi=3.14159;
h=6.626e-34;
type
  reeks=array[1..2600] of real;
var
 gain,druk,delta_nu,length,width,volume,R1,R2,tc,energy:real;
 length2,sigma,tx,delta_t,lamda,f,toets,toets2,toets3,stop,max  :real;
 delta,gdelta,Int,int_uit                                :reeks;
 i,j                                                    :integer;
 tyd,uit,z:real;
 k1,k2,k3,k4,l1,l2,l3,l4,m1,m2,m3,m4 :real;
 leer                                  :text;

{-------------------------------------------------------------}
function dr_dt(delta,Gdelta,I :real):real;

begin
  dr_dt:=-(delta-z*gdelta)/Tx-((2*sigma*I*delta)/(h*f));
end;
{-------------------------------------------------------------}


{-------------------------------------------------------------}
function dv_dt(delta,Gdelta,I:real):real;
var
  t1,t2,t3:real;

begin
  dv_dt:=-2*sigma*I*delta/(h*f);
end;
{-------------------------------------------------------------}


{-------------------------------------------------------------}
function di_dt(delta,Gdelta,I :real):real;

begin
  di_dt:=(c*sigma*delta*I*(length2/length))-I/Tc;
end;
{-------------------------------------------------------------}


{-------------------------------------------------------------}
{ Hoofprogram                                                 }
{-------------------------------------------------------------}
begin
assign(leer,'l_puls.dat');
rewrite(leer);
lamda:=10.6e-6;
z:=0.07;{Boltzmann faktor}
f:=c/lamda;
Writeln(' Small signal gain ?');
readln(gain);
writeln(' Pressure in atmospheres ?');
readln(druk);
delta_nu:=6.0e9*druk;
```

```
writeln(' Length of resonator in meter ?');
readln(length);
writeln(' Width of resonator in meter ?');
readln(width);
writeln(' Gain length in meter ?');
readln(length2);
volume:=        width*width;
{volume:=1.0;    }
delta[1]:=(gain*4*pi*pi*delta_nu)/(lamda*lamda*0.21);
gdelta[1]:=delta[1]/0.07;
int[1]:=0.01;
R1:=0.85;
{R2:=0.70;}
writeln(' Output Coupler ?');
readln(R2);
tc:=length/(c*(1-(sqrt(R1*R2))));
sigma:=(lamda*lamda*0.21)/(4*pi*pi*delta_nu);
writeln(' sigma= ',sigma,' delta= ',delta[1]);
writeln(' tc= ',tc,' sigma= ',sigma);readln(stop);
tx:=1.16e-6/(druk*760.0);
{tx:=150e-12;}
i:=1;
delta_t:=6.0e-10;
energy:=0.0;
tyd:=0.0;
max:=0.0;
While (i < 2600) do begin
   {toets:=(dr[i]-0.7*dv[i]/tx)*delta_t; }
   k1:=delta_t*dr_dt(delta[i],gdelta[i],Int[i]);
   l1:=delta_t*dv_dt(delta[i],gdelta[i],Int[i]);
   m1:=delta_t*di_dt(delta[i],gdelta[i],Int[i]);

   k2:=delta_t*dr_dt(delta[i]+k1/2,gdelta[i]+l1/2,Int[i]+m1/2);
   l2:=delta_t*dv_dt(delta[i]+k1/2,gdelta[i]+l1/2,Int[i]+m1/2);
   m2:=delta_t*di_dt(delta[i]+k1/2,gdelta[i]+l1/2,Int[i]+m1/2);

   k3:=delta_t*dr_dt(delta[i]+k2/2,gdelta[i]+l2/2,Int[i]+m2/2);
   l3:=delta_t*dv_dt(delta[i]+k2/2,gdelta[i]+l2/2,Int[i]+m2/2);
   m3:=delta_t*di_dt(delta[i]+k2/2,gdelta[i]+l2/2,Int[i]+m2/2);

   k4:=delta_t*dr_dt(delta[i]+k3/2,gdelta[i]+l3/2,Int[i]+m3/3);
   l4:=delta_t*dv_dt(delta[i]+k3/2,gdelta[i]+l3/2,Int[i]+m3/3);
   m4:=delta_t*di_dt(delta[i]+k3/2,gdelta[i]+l3/2,Int[i]+m3/2);

   delta[i+1]:=delta[i]+(k1+2*k2+2*k3+k4)/6;
   gdelta[I+1]:=gdelta[i]+(l1+2*l2+2*l3+l4)/6;
   int[i+1]:=Int[i]+(m1+2*m2+2*m3+m4)/6;

   {dr[i+1]:=dr[i]-((dr[i]-0.07*dv[i])/tx)*delta_t-(2*sigma*int[i]/(h*f))*del
   {dv[i+1]:=dv[i]-(2*sigma*dr[i]*int[i]/(h*f))*delta_t; }
   {toets2:=(2*sigma*dr[i]*int[i]/(h*f));}
  { toets3:=((dr[i]-0.07*dv[i])/tx)-(2*sigma*int[i]/(h*f));}
  { toets:=(c*sigma*dr[i]-1/tc);}
  { int[i+1]:=int[i]+(c*sigma*dr[i]*int[i]-int[i]/tc)*delta_t;}
   int_uit[i]:=(1-R2)*int[i+1]*volume;
   if (int_uit[i]>max)then begin;
     max:=int_uit[i];
   end;
   energy:=energy+int_uit[i]*delta_t;
   i:=i+1;
   tyd:=tyd+delta_t;
end;
writeln('i= ',i,' Energie= ',energy*1000:10:5,' mJ');
writeln(' Maksimum Drywing = ',Max/1.0e6:10:5,' MW');
```

```
writeln('tyd= ',tyd*1.0e9,' nS ');
j:=1;
i:=1;
tyd:=delta_t;
while (j < 2000) do begin
   uit:=int_uit[j];
   writeln(leer,tyd*1.0e9,' ',uit/1.0e6);
   i:=i+1;
   j:=j+4;
   tyd:=tyd+delta_t*4;
end;
close(leer);
end.
```

APPENDIX 8

This computer program calculates the thermal frequency drift of a three mirror resonator.

```
program MGC_Tol;
uses
 dos,crt,gdriver,printer,gkernel,gwindow,gshell;

{-------------------------------------------------------}
{ This program calculates the change in resonance frequency}
{ with a change in temperature                          }
{-------------------------------------------------------}
const
 Pi=3.1415;
 c=3.0e8;
type
  reeks=array[1..400] of real;

var
DnuDT,Rg,R1,Te,Lamda,L_S,Einde,Delta,Deler,DyDT,DxDT:real;
y,x,arg,ls1,Phi,DPhiDT,Arg2,arg3,arg4,DlamdaDT    :real;
Dls,n,a,L_H,delta_nu,z0,arg5,omega0,delta_lam     :real;
DL_SDT,DL_HDT,DdeltaDT,Temp0,Temp,delta_t         :real;
onder,eerste,tweede,nu0,nu,frekw,totaal,delta_lam2:real;
dlamda_dt2:real;
Lamda_v                                          :reeks;
i,j                                               :integer;
leer                                             :text;
ai                                               :plotarray;
L_H1,L_S1 :real;

procedure plotter(a:plotarray; N:integer);
{ Hierdie program plot funksie plus asse                }
{ program bepaal self die min en max waardes            }

var
 minx,miny,maxx,maxy            :real;
 i                             :integer;
 opskrif                        :string[30];
 antw                           :char;
 files                          :text;

procedure Asse;

begin
ClearScreen;
SetColorWhite;
SetBackground(0);
DefineHeader(1,opskrif);
DrawBorder;
DrawAxis(8,7,0,0,0,0,0,0,true);
end;

Procedure MinMax(a :PlotArray; N:integer;
                 var minx,maxx,miny,maxy :real);

var
  i:integer;

begin
i:=1;
minx:=A[1,1];
maxx:=A[1,1];
miny:=A[1,2];
maxy:=A[1,2];
for i:=1 to n do begin;
  if ( A[i,1] > maxx ) Then begin
      Maxx:=A[i,1];
```

```
  end;
  if ( A[i,1] < minx ) Then begin
      minx:=A[i,1];
  end;
end;
for i:=1 to n do begin
   if( A[i,2] > maxy ) then begin
      maxy:= A[i,2];
    end;
    if ( A[i,2] < miny ) then begin
      miny:=A[i,2];
    end;
end;
end;

begin
MinMax(a,n,minx,maxx,miny,maxy);
writeln(' minx= ',minx,' maxx= ',maxx);
writeln(' miny= ',miny,' maxy= ',maxy);
initgraphic;
DefineWindow(1,0,0,Xmaxglb,YmaxGlb);
DefineWorld(1,minx,miny,maxx,maxy);
SelectWorld(1);
SelectWindow(1);
Asse;
Drawpolygon(A,1,n,0,0,0);
repeat until KeyPressed;
LeaveGraphic;
end;
```

```
begin
assign(leer,'MGC_TOL.DAT');
rewrite(leer);
writeln(' Rg ? ');
readln(Rg);
writeln(' R1 ? ');
readln(R1);
Te:=1;
writeln(' Lamda ? in micron ');
readln(Lamda);
lamda:=Lamda*1.0e-6;
NU0:=c/lamda;
i:=1;
lamda_v[i]:=lamda;
{writeln('Length of Sub-resonator');}
{readln(L_S);                      }
{writeln(' Length of main resonator ?');}
{readln(L_H);                           }
L_S1:=0.1;
L_H1:=0.45;
n:=trunc((2*L_H1)/lamda);
writeln('n= ',n,' L_H= ',L_H,' lamda= ',lamda);
writeln(' Minimum spot size ? ');
readln(omega0);
writeln('lamda 1= ',lamda_v[i]);
writeln(' Temperature ?');
readln(Temp0);
temp:=temp0;
delta_t:=0.5;
einde:=temp+0.5;
Z0:=(pi*omega0*omega0*1.0)/lamda;
```

```
Dls:=0.04e-6;
NU:=0.0;
totaal:=0.0;
While (L_S1 < 0.10001) do begin
i:=1;
totaal:=0.0;
temp:=temp0;
L_S:=L_S1;
L_H:=L_H1;
While (Temp < einde ) do begin
  delta:=((4*Pi)/lamda_v[i])*L_S;
  deler:=(1-Rg*Rg*R1*R1*Te*Te*Te*Te);
  DL_SDt:=2.0e-6*L_S;
  L_S:=L_S+DL_SDT*delta_T;
  DL_HDT:=2.0e-6*L_H;
  L_H:=L_H+DL_HDT*delta_t;
  DdeltaDt:=(4*pi/lamda_v[i])*dL_SdT;
  DyDT:=(((-Te*Te*Rg*R1*R1)-(Te*Te*Rg*R1))/(Deler))*cos(delta)*DdeltadT;
  DxDT:=((Te*Te*Rg*R1-Te*Te*Rg*R1)/(deler))*sin(Delta)*Ddeltadt;
  y:=-((Te*Te*Rg*R1+Te*Te*Rg*R1)/(Deler))*sin(Delta);
  x:=((R1-Te*Te*Te*Te*Rg*R1+(Te*Te*Rg*R1-Te*Te*Rg*R1*R1))/(deler))*cos(delta)
  Phi:=ArcTan(y/x);
  {phi:=0.0;      }
  DphiDT:=(1/(1+(y/x)*(y/x)))*((1/x)*DyDT-(y/(x*x))*DxDT);
  {dphidt:=0.0; }
  onder:=pi*(n-0.5)-phi/2;
  eerste:=(2*pi*dL_HdT)/onder;
  tweede:=(-2*pi*L_H)*(-0.5*dphidt+(1/Z0)/(1+L_H*L_H/(Z0*Z0))*dL_Hdt);
  tweede:=tweede/(onder*onder);
  dlamdadt:=eerste+tweede;
  delta_lam2:=dlamdadt*delta_t;
  Lamda_v[i+1]:=(pi*(L_H))/(pi*(n-0.5)-phi/2.0);
  dlamda_dt2:=(lamda_v[i+1]-lamda_v[i])/delta_t;
  {DlamdaDls:=Lamda_v[i+1]-Lamda_v[i];}
  delta_lam:=(lamda_v[I+1]-lamda_v[i]);
  Delta_nu:=(-Delta_lam2*c)/(lamda_v[i+1]*lamda_v[i+1]);
  DnuDT:=(-c/(lamda_v[i+1]*lamda_v[i+1]))*DlamdaDT;
  {delta_nu:=c*(1/lamda_v[i+1]-1/lamda_v[i]); }
  Temp:=Temp+delta_t;
  totaal:=totaal+delta_nu;
  {writeln('totaal = ',totaal);}
end;
ai[j,1]:=L_S1/L_H1;
ai[j,2]:=totaal/1.0e6;
totaal:=totaal/1.0e6;
writeln(' L_S/L_H= ',(L_S1-0.1)*10000,' Totaal = ',totaal);
j:=j+1;
writeln(leer,(L_S1-0.1)*1000000,' ',Totaal);
L_S1:=L_S1+0.0000005;
end;
{plotter(ai,j);}
close(leer);
end.
```

APPENDIX 9

This program calculates the time dependent breakdown strength of water.

```
    program break;
uses
 dos,crt,gdriver,printer,gkernel,gwindow,gshell;
const
pi=3.14159;
k=1.381e-16;
var
Ta,Tb,tau,ro,Cp,ed,db,e0,n,d,l,Emax,fakt1,fakt2,fakt3,tel:real;
B1,H,R,Q,nu,eb,fakt4,E_JC,frac,Rs,b,H_aks,k1,epsilon,Emax1,antw:real;
ai:plotarray;
j:integer;
leer:text;


begin
frac:=0.0;
T:=T+273.0;
Estat:=E/300;
n:=frac*(1.43)+(1-frac)*1.33;          { Brekings indeks van water };
nu:=Frac*1.35e-18+(1-frac)*2.1e-18;     { Debye eenhede dipool moment van wat
N0:=3.3e22; { Molekules per kubieke cm water }
x:=(sqrt(73)*Estat*nu*(n*n+2))/(6*k*T);
y:=(28*N0*pi*(n*n+2)*nu)/(3*sqrt(73)*Estat);
if ( x > 100 ) then begin
     z:=1.0-1/x;
end
else begin
     z:=coth(x)-1/x;
end;
epsilon:=n*n+y*z;
end;

begin
assign(leer,'BREAK.DAT');
rewrite(leer);
Writeln('Begin Temp ?');
readln(Ta);
writeln(' Kookpunt ?');
readln(Tb);
Writeln('Pulstyd ?');
readln(tau);
writeln('Epsilon bulk ?');
readln(EB);
WRITELN('Etalon fraction ?');
readln(frac);
n:=0.20;
d:=0.01;
nu:=2.66e-7;
e0:=8.854e-12;
ed:=6.0;
eb:=80.2;
epsilon:=eb;
B1:=2.414e-14;
Rs:=10.0e-6;
H:=140.9;
l:=2.0e-9;
Cp:=((100-FRAC)/100)*4200.0+(FRAC/100)*2300;
ro:=1000.0;
{tau:=1.0e-6;}
j:=1;
Emax1:=36.0e6;
While (tau < 300.63e-6) do begin
  b:=(nu*Emax1*tau)+Rs;
  {b:=200*tau;}
```

```
    H_aks:=(1+((3*H-1)*Rs*b+6*(H-1)*Rs*Rs*b)/(b*b+2*Rs*b+Rs*Rs));
    K1:=H-1;
    writeln('H_aks=',H_aks);
    H_aks:=(b-((k1*Rs*Rs*Rs)/((Rs+b)*(Rs+b)*2))+(k1*Rs/2))/b;
    writeln(' H_aks=',H_aks);
    fakt1:=(nu*e0*ed*ed)/(3*B1*eb);
    fakt2:=(1+(2*B1*d*eb)/(nu*e0*ed*ed));
    fakt2:=exp((3/2)*ln(fakt2));
    R:=fakt1*fakt2-fakt1;
    writeln('R=',R);
    Q:=(Cp*(Tb-Ta)/(tau*B1))+1.200e6/(tau-6*B1)+2.256e9/(tau*B1);
    Q:=Q/(H*H*H_aks);
    fakt3:=((ed*R)/(eb*d));
    fakt3:=exp((2/3)*ln(fakt3));
    fakt4:=exp((1/3)*ln(q));
    Emax:=fakt3*fakt4/1.55;
    Emax1:=Emax;
    ed:=ed*(epsilon/eb);
    writeln(' Emax= ',Emax/1.0e6:10:5,' MV/m   Tau= ',tau);
    E_JC:=(0.55/(exp(1/3*ln(tau*1.0e6))))/1.55;
    ai[j,2]:=Emax/1.0e6;
    ai[j,1]:=tau*1.0e6;
    E_JC:=E_JC*100;
    Writeln(' E_JC=',E_JC:10:5,' MV/m ');
    WRITELN(LEER,tAU*1.0E6,' ',Emax/1.0e6,' ',E_JC);
    tel:=Tel+1;
    tau:=tau+5.0e-6;
    j:=j+1;
end;
plotter(ai,j-1);
close(leer);
end.
```

APPENDIX 10

This computer program calculates the pulse of a RLC circuit.

```
program discharge;
{N+}
uses
 dos,crt,gdriver,printer,gkernel,gwindow,gshell;

type
  reeks=array[1..1000] of real;
var
 ai:plotarray;
 i,i1,i2        : reeks;
 L2,di2dt,L,C,R1,V0,Vc,delta_t,Vr,Vc1,tyd,tyd1,E_op_n :real;
 int4,Vc2,c2,Vcr,R2,drdt,Vr2,druk,d,n0,dryf_s,i3:real;
 int1,int2,int3,int,aaa,area,Vg,N_elek,el,Vc22,i_int,dryf1,K,aantal:real;
 Energie,Ener2,Eta,I22,didt,afstand,elek_t,recom,recom2:real;
 j           :integer;
 files       :text;



procedure plotter(a:plotarray; N:integer);
{ Hierdie program plot funksie plus asse                    }
{ program bepaal self die min en max waardes                }

var
 minx,miny,maxx,maxy           :real;
 i                            :integer;
 opskrif                       :string[30];
 antw                          :char;
 files                         :text;

procedure Asse;

begin
ClearScreen;
SetColorWhite;
SetBackground(0);
DefineHeader(1,opskrif);
DrawBorder;
DrawAxis(8,7,0,0,0,0,0,0,true);
end;

Procedure MinMax(a :PlotArray; N:integer;
                 var minx,maxx,miny,maxy :real);

var
  i:integer;

begin
i:=1;
minx:=A[1,1];
maxx:=A[1,1];
miny:=A[1,2];
maxy:=A[1,2];
for i:=1 to n do begin;
  if ( A[i,1] > maxx ) Then begin
      Maxx:=A[i,1];
  end;
  if ( A[i,1] < minx ) Then begin
      minx:=A[i,1];
  end;
end;
for i:=1 to n do begin
   if( A[i,2] > maxy ) then begin
```

```
      maxy:= A[i,2];
    end;
    if ( A[i,2] < miny ) then begin
      miny:=A[i,2];
    end;
  end;
  end;

  begin
  MinMax(a,n,minx,maxx,miny,maxy);
  writeln(' minx= ',minx,' maxx= ',maxx);
  writeln(' miny= ',miny,' maxy= ',maxy);
  initgraphic;
  DefineWindow(1,0,0,Xmaxglb,YmaxGlb);
  DefineWorld(1,minx,miny,maxx,maxy);
  SelectWorld(1);
  SelectWindow(1);
  Asse;
  Drawpolygon(A,1,n,0,0,0);
  repeat until KeyPressed;
  LeaveGraphic;
  end;


  begin
  assign(files,'rlc.dat');
  rewrite(files);
  i[1]:=0.0;
  i1[1]:=0.0;
  i2[1]:=0.0;
  L:=800.0e-9;    { Henry}
  L2:=350.0e-9;
  C:=6.0e-9;      { Farad}
  C2:=0.770e-9;
  V0:=1.0e3;    { Volt }
  Vc2:=0.0;
  R1:=2.0;
  R2:=40.0;
  Vc:=0;
  tyd:=0.0;
  delta_t:=2.5e-9; {sekondes}
  tyd:=delta_t;
  AI[1,1]:=DELTA_T;
  AI[1,2]:=0.0;
  int:=0.0;
  int2:=0.0;
  int3:=0.0;
  Int4:=0.0;
  di2dt:=0.0;
  for j:=2 to 300 do begin
   Int:=Int+(I[j-1]*delta_t);
   Int2:=Int2+(I1[j-1]*delta_t);
   Int3:=Int3+(V0-(+R1*I[j-1]+R2*I2[j-1]+1/C*Int))*delta_t;
   int4:=Int4+((1/C2)*int2-i2[j-1]*R2)*delta_t;
   I[j]:=(1/L)*(Int3);
   {I2[j]:=((1/(C2*R2)*Int2))-(L2/R2)*di2dt;}
   i2[j]:=(1/L2)*(int4);
   {di2dt:=(i2[j]-i2[j-1])/delta_t;}
   di2dt:=0.0;
   i1[j]:=i[j]-i2[j];
   Vc:=V0-(1/C)*int;
   Vc2:=(1/C2)*Int2;
   Vc1:=i2[j]*R2;
```

```
 {energie:=(Vc2*(i[j]-il[j]));}
 writeln(' Vc = ',Vc);
 TYD:=TYD+DELTA_T;
 AI[J,1]:=TYD;
 AI[J,2]:=Vc2;
 writeln(files,tyd*1.0e9,'   ',Vc2/1.0e3);
end;
plotter(ai,j);
close(files);
end.
```